Surface Tension and Adsorption Kinetics of Volatile Organic Amphiphiles in Aqueous Solution

by

Abdolhamid Firooz

A thesis
presented to the University of Waterloo
in fulfilment of the
thesis requirement for the degree of
Doctor of Philosophy
in
Chemical Engineering

Waterloo, Ontario, Canada, 2011

I hereby declare that I am the sole author of this thesis. This is a true copy of the thesis, including any required final revisions, as accepted by my examiners.

I understand that my thesis may be made electronically available to the public.

Abstract

Amphiphiles that possess a dual character, hydrophobic and hydrophilic, are employed in many chemical, pharmaceutical and biological applications. Amphiphile molecules that include a hydrophilic head and a hydrophobic tail can easily adsorb at a liquid/vapour interface, to reach to a minimum free energy and hence a most thermodynamically stable state. Surface tension is a key parameter for understanding such behavior of an amphiphile, or a surfactant. This thesis represents a comprehensive study on adsorption and surface tension of slightly volatile, organic amphiphiles in aqueous solution.

Although for a vapor-liquid interface, adsorption from both liquid and vapor phases should be considered, they have been almost always considered exclusive of one another. When a volatile surfactant is dissolved in the liquid phase, it also applies a finite partial pressure in the vapor phase. Recently, dynamic surface tension experiments showed that adsorption from both sides of a vapor/liquid interface must be studied simultaneously. It is noted that surface tension phenomena are often dynamic, in particular when the surface under consideration is perturbed. With the newly discovered importance of adsorption from both sides of a vapor/liquid interface, one may have to ask the question: how dynamic surface tension is influenced and responding to the surface perturbation and environment changes, and whether both sides of the interface play a role in surface tension responses.

In this research, axisymmetric drop shape analysis-profile (ADSA-P) is used for surface tension measurement. The experiments are performed in a closed chamber where the effects of surfactant concentrations of both liquid and vapor phases on the surface tension can be studied. The partial vapor pressure of surfactant is controlled with an environment solution containing the same surfactant as the sample solution. The environment solution is to facilitate adsorption from the vapor side of the interface by creating a surfactant vapor phase. The effects of surface perturbation, environment condition (i.e., temperature and pressure) and carbon chain length on the surface tension and adsorption kinetics are studied in detail.

The surface tension response of 1-octanol aqueous solution to surface area perturbation is investigated. Upon surface compression, the surface tension decreases followed by a gradual increase back to the value prior to compression. On surface expansion, two categories of surface tension response are observed: First, when the change in surface area is smaller than 5%, the behavior similar to that of conventional surfactants is observed. The surface tension increases followed by a gradual decrease back to the value prior to expansion. Second, when the change in surface area is greater than 5%, and the drop concentration is sufficiently larger than the environment concentration, the surface tension initially slightly increases, but after a time delay, it sharply decreases, followed by a gradual increase back to the value prior to expansion. Previous studies showed that at steady-state condition a network of hydrogen bonding between surfactant and water molecules near the surface is

created. The unique surface tension response after large expansion might be related to the momentarily destruction of this hydrogen bonding network and gradually making a new one.

The effect of temperature on the surface tension and adsorption kinetics of 1-octanol,1-hexanol and 1-butanol aqueous solutions is studied. The steady-state surface tension is found to decrease upon an increase in temperature, and a linear relationship is observed between them. The modified Langmuir equation of state and the modified kinetic transfer equation are used to model the experimental data of the steady-state and dynamic (time-dependent) surface tension, respectively. The equilibrium constants and adsorption rate constants are evaluated through a minimization procedure for temperatures ranging from 10 °C to 35 °C. From the steady-state modelling, the equilibrium constants for adsorption from vapor phase and liquid phase are found to increase with temperature. From the dynamic modelling, the adsorption rate constants for adsorption from vapor phase and liquid phase are found to increase with temperature too.

The influence of carbon dioxide pressure on the surface tension and adsorption kinetics of the aforementioned surfactant aqueous solutions is investigated. To consider the effect of adsorption/desorption of the two species (surfactant and carbon dioxide) from both sides of a vapor/liquid interface on the surface tension, the modified Langmuir equation of state and the modified kinetic transfer equation are derived. The steady-state and dynamic surface tension data are modelled using the modified Langmuir equation of state and the modified kinetic transfer equation, respectively. The equilibrium constants and adsorption rate constants of surfactant and carbon dioxide are evaluated through a minimization procedure for CO_2 pressures ranging from 0 to 690 KPa. From the steady-state modelling, the equilibrium parameters for surfactant and carbon dioxide adsorption from vapor phase and liquid phase are found unchanged for different pressures of carbon dioxide. From the dynamic modelling, the adsorption rate constants for surfactant and carbon dioxide are found to decrease with carbon dioxide pressure.

The role of carbon chain length of amphiphiles in aqueous solution is also studied. It is illustrated that the equilibrium constants for adsorption from both sides of a vapor/liquid interface increase from 1-butanol to 1-octanol. The modelling results show that the ratio of the equilibrium constant for adsorption from vapor phase to the equilibrium constant for adsorption from liquid phase declines from 260 to 26 as the chain length is increased from 1-butanol to 1-octanol. Therefore, the contribution to adsorption from liquid phase augments as the chain length is increased. The adsorption kinetics for this group of short carbon chain surfactants is modelled using a kinetic transfer equation. The modelling results show that the adsorption rate constants from vapor phase and liquid phase (k_a^g and k_a^l) increase from 1-butanol to 1-octanol. Steady-state and dynamic modelling also reveals that the maximum surface concentration increases with carbon chain length. These results may be due to the higher hydrophobicity character of a surfactant molecule at longer

carbon chain length.

Acknowledgements

I would like to express my profound and sincere gratitude to my supervisor, Professor Pu Chen for his careful guidance, encouragement and continuous support throughout this research.

I take the opportunity to show my deepest appreciation to the thesis committee members, Professors Hind Al-Abadleh, Thomas A. Duever, Russell Thompson, and Boxin Zhao for their valuable comments.

I would like to express my profound gratitude to my lovely wife Mitra for her love and companionship. She has been my strongest supporter, and my best friend. To my beautiful daughters Katayoun, Kiana, and Kimia , I express my deepest appreciation for their inspiration and the joy, happiness, faith and love they have added to my life.

I would like to thank all Interfacial Engineering Group for their encourage and support during this research.

Dedication

To my lovely wife Mitra,

Our wonderful daughters Katayoun, Kiana and Kimia

and

In the memory of the first supporter in my life, my beautiful mother

In the memory of my first teacher, my father

Contents

List of Tables

List of Figures

List of symbols

A	Interfacial area (m^2)
A_f	Frequency factor or pre-exponential factor ($m^3/mol.s$)
A_{fr}	Non-ideality parameter of the Frumkin isotherm (dimensionless)
a_2	Activity of solute (mol/mol)
a	Constant
b	Constant
C	Concentration of the component in the bulk liquid solution (mol/m^3)
C_i^{α}	Concentration of the i^{th} component in α phase (mol/m^3)
C_i^{β}	Concentration of the i^{th} component in β phase (mol/m^3)
C_i	Bulk concentration of the i^{th}component in α phase (mol/m^3)
$C_i^{'}$	Bulk concentration of the i^{th} component in β phase (mol/m^3)
C_{drop}	Concentration of surfactant in the drop solution (mol/m^3)
C_{env}	Concentration of surfactant in the environment solution (mol/m^3)
ΔC	Concentration difference between drop and environment solutions (mol/m^3)
E	Energy barrier (j/mol)
F_d	Net force in the Du Nouy ring method (N)
F	Dimensionless parameter
f	Correction factor for the drop weight method (dimensionless)
f_2	Solute activity coefficient (dimensionless)
g	Gravity constant (m^2/s)
h	Capillary rise (m)

H Henry's constant

K Constant (s)

K_a Equilibrium adsorption constant for adsorption from vapor and liquid phases (m^3/mol)

K_b Constant

K_1 Equilibrium adsorption constant for adsorption from the vapor phase for species 1 (m^3/mol)

K_2 Equilibrium adsorption constant for adsorption from the liquid phase for species 1 (m^3/mol)

K_3 Equilibrium adsorption constant for adsorption from the vapor phase for species 2 (m^3/mol)

K_4 Equilibrium adsorption constant for adsorption from the liquid phase for species 2 (m^3/mol)

$K_1^{'}$ Equilibrium adsorption constant for adsorption from the vapor phase (m^3/mol)

$K_2^{'}$ Equilibrium adsorption constant for adsorption from the liquid phase (m^3/mol)

K_F Frumkin equilibrium adsorption constant (m^3/mol)

K_H Henry equilibrium adsorption constant (m)

K_L Langmuir equilibrium adsorption constant (m^3/mol)

$K_L^{'}$ Modified Langmuir isotherm equilibrium adsorption constant (m^3/mol)

$K_V^{'}$ Modified Langmuir isotherm equilibrium adsorption constant $(1/atm)$

k_a^g Adsorption rate constant for adsorption from the gas phase $(m^3/mol.s)$

k_a^l Adsorption rate constant for adsorption from the liquid phase $(m^3/mol.s)$

k_d^g Desorption rate constant for desorption to the gas phase $(m^3/mol.s)$

k_d^l Desorption rate constant for desorption to the liquid phase $(m^3/mol.s)$

M Molecular weight (g/mol)

m Mass of the drop in the drop weight method (kg)

N_i Number of moles in the i^{th} component (mol)

n_i^t Total number of moles of the i^{th} component in all regions (mol)

n_i^α Number of moles of the i^{th} component in α regions (mol)

n_i^β Number of moles of the i^{th} component in β regions (mol)

n_i^s Number of moles of the i^{th} component in surface (mol)

n_i Total number of moles of the i^{th} component in phase α of the idealized system (mol)

$n_i^{'}$ Total number of moles in the i^{th} component in phase β of the idealized system (mol)

n_i^x Gibb's surface excess of the i^{th} component (mol)

P Pressure (Pa)

P_1 Partial pressure of species 1 (Pa)

P_2 Partial pressure of species 2 (Pa)

P_w Perimeter of the plate in the Wilhelmy plate method (m)

ΔP Pressure difference across the curved interface (Pa)

r Capillary radius $(m\ )$

r_1 Constant

r_2 Constant

R_1 Principal radius of curvature (m)

R_2 Principal radius of curvature (m)

R Universal gas constant $(j/mol.k)$

R_d Radius of the ring in the Du Nouy ring method (m)

r_a^g Adsorption rate from the gas phase $(mol/m^2.s)$

r_a^l Adsorption rate from the liquid phase $(mol/m^2.s)$

r_d^g Desorption rate to the gas phase $(mol/m^2.s)$

r_d^l Desorption rate to the gas phase $(mol/m^2.s)$

S Entropy of the system (j/k)

S_1 Number of occupied adsorption sites per unit area for species 1

S_2 Number of occupied adsorption sites per unit area for species 2

S_{m1} Total number of adsorption sites if all occupied by species 1

S_{m2} Total number of adsorption sites if all occupied by species 2

ΔS Change in surface area (m^2)

T Bulk absolute temperature (k)

t	time (s)
t_{95}	The time required reaching to the 95% of the steady-state value (s)
Δt	Time delay (s)
U	Internal energy of the system (j)
V	Volume of the system (m^3)
V^{α}	Volume in α phase (m^3)
V^{β}	Volume in β phase (m^3)
V'^{α}	Volume added to phase α (m^3)
V'^{β}	Volume added to phase β (m^3)
W	Total force in the Du Nouy ring method and Wilhelmy plate method (N)
W_{ring}	Net weight of the ring in the Du Nouy ring method (N)
W_{plate}	Net weight of the plate in the Wilhelmy plate method (N)
X_2	Mole fraction of solute (mol/mol)

Greek symbols

β	Correlation factor in the Du Nouy ring method (dimensionless)
γ	Surface tension $(N/m, mN/m)$
γ_{avr}	Average surface tension $(N/m, mN/m)$
$\Delta\gamma$	Surface tension changes $(N/m, mN/m)$
γ_0	Surface tension of pure solvent $(N/m, mN/m)$
Θ	Contact angle $(^{\circ})$
$\Delta\rho$ (kg/m^3)	Density difference between gas and liquid in the capillary rise method
Γ	Surface excess of component (mol/m^2)
Γ_w	Surface concentration of solvent (mol/m^2)
Γ_{∞}	Maximum surface concentration of the component (mol/m^2)
Γ_{min}	Minimum surface concentration of the component (mol/m^2)

Γ_i	Surface concentration of the i^{th} component (mol/m^2)
Γ_1	Solvent surface concentration (mol/m^2)
Γ_2	Solute surface concentration (mol/m^2)
μ_1	Chemical potential of the solvent (j/mol)
μ_2	Chemical potential of the solute (j/mol)
μ_i	Chemical potential of the i^{th} component (j/mol)

Chapter 1

Introduction

1.1 Overview of the Research

An interface is a physical boundary in which the properties vary from one phase to another, over a distance of molecular dimension. Surface or interfacial tension of the vapor-liquid interface of alcohol in aqueous solution has long been considered as one of the most intriguing surface phenomena [1, 2, 3]. Surface tension is crucial to the understanding of many important processes, including self-assembly of biomolecules [4], modification of membranes [5], coating and wetting [6]. Also, in physiology, the natural pulmonary surfactant, made up of a complex mixture of lipids and proteins, plays a key role in respiration by modulating the surface tension and stabilizing the lungs for proper breathing [7, 8]. The organic or inorganic chemicals tending to adsorb at the interface and modify the surface properties may be classified as surface-active-agents, or surfactants. In many cases, surfactants alter or even control the surface properties and the surface tension of a particular system. In a freshly formed interface, the surfactant is adsorbed toward the interface to achieve a thermodynamically more stable state [9, 10]. The result is a reduction in the free energy of the system and therefore a decrease in surface tension [11].

A common goal of most surfactant applications is to select surfactants that could effectively reduce the surface tension to a desired value within a desired time. An optimum use of surfactant cannot be achieved without a clear understanding of their interfacial behavior including the dynamic and steady-state surface tension and adsorption kinetics.

Although for a vapor-liquid interface, adsorption from both liquid and vapor phases should be considered, they have been almost always considered exclusive of one another [12, 13, 14, 15, 16, 17, 18, 19, 20, 21, 22]. For example, in Langmuir or Frumkin isotherms only adsorption from the liquid phase has been considered [23, 24]. When a volatile surfactant is dissolved in the liquid phase, it also exerts a finite partial pressure in the vapor phase.

Recently, dynamic surface tension experiments showed that adsorption from both sides of a vapor/liquid interface must be considered simultaneously [25]. It is noted that surface tension phenomena are often dynamic, i.e., time dependent, in particular when the surface under consideration is perturbed. With the newly discovered importance of adsorption from both sides of a vapor/liquid interface, one may have to ask the question: how dynamic surface tension is influenced and responding to the surface perturbation and environment changes, and whether both sides of the interface play a role in surface tension responses.

Environment conditions are crucial in many application of surfactants, i.e., in the lung, temperature and pressure can change the surface tension of pulmonary surfactant, which in turn plays a key role in proper breathing. In plastic foaming and in coating, efficiency of the operations can be affected by surface tension, and hence by temperature and pressure. This is due to the fact that a change in the environment conditions will cause a change in molecular driving forces at the interface and consequently dynamic and equilibrium surface tension.

In this research, the effect of surface perturbation and environment conditions are investigated on the dynamic and steady-state surface tension of several alcohols, i.e., 1-octanol, 1-hexanol, and 1-butanol aqueous solutions. The experiments are performed in a novel experimental condition where the effect of adsorption/desorption of both phases are considered simultaneously. 1-octanol, 1-hexanol and 1-butanol have many different applications. They are used as ingredients in foods, wines, flavors, perfumes and as substitutes for gasoline and diesel fuel [102, 103, 104, 105]. Recent studies have been shown that essential tremors can be treated if 1-octanol, 1-hexanol or 1-butanol is used as the prescription drug [26]. Essential tremor is a disorder in which the hands, and sometimes the head, shake involuntarily. 1-hexanol is also used as the promoter of mRNA release in the presence of Ttgv protein [27]. In all cases, temperature and pressure can change the surface tension, hence the efficiency of the operation [27, 28, 29, 30, 31].

The kinetics of surfactant adsorption is usually monitored through the measurement of time-dependent or dynamic surface tension (DST). This data can be used to determine the key kinetic parameters that characterize the adsorption and ascertain the molecular mechanisms involved in the process. Previous studies showed that the dynamic adsorption behavior of normal alcohols with short carbon chains is controlled by the transfer of surfactant molecules from the subsurface to the surface [14, 32]. When an interface is formed between two bulk phases, physical properties like the density vary rapidly and continuously from one bulk to another. However, because the interface region is very thin, the influence of the interface is limited and does not extend beyond several molecule diameters in each side of the interface. The subsurface is a name for the position, in the neighbourhood of the surface, in which the variation of physical properties is started. Previous studies also showed that the diffusion from the bulk to the subsurface is very fast compared to the transfer of molecules from the subsurface to the surface.

Our experiments will be performed in a closed chamber where the drop is hanging from a capillary and dynamic surface tension can be affected by adsorption from both sides of the interface. A simple schematic of the system under study is shown in Figure 1.1.

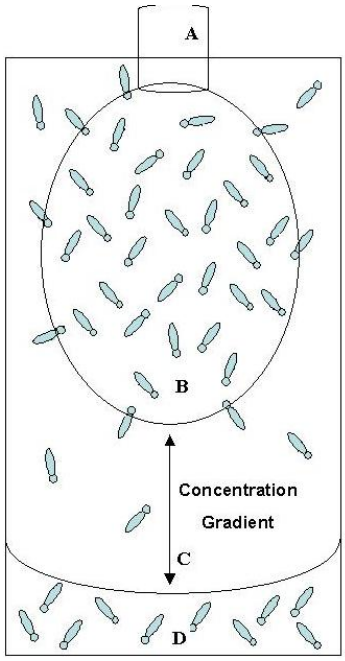

Figure 1.1: A simple schematic of the surfactant distribution in the system; (A) Capillary tip for drop formation, (B) liquid or drop solution, (C) the distance between drop and environment solutions, (D) environment solution.

In this research, the new modified Langmuir equation of state and the new modified kinetic transfer equation are developed to model the experimental data of the steady-state and dynamic (time-dependent) surface tension, respectively. In these equations the effect of adsorption/desorption of more than one specious from both sides of a vapor/liquid interface on the surface tension is studied. The equilibrium constants and adsorption rate constants are evaluated through non-linear regression for temperatures ranging from 10 to 35 °C and carbon dioxide pressure ranging from 0 to 690 KPa.

1.2 Research Objectives

This research is focused on the comprehensive investigation on the effects of environment conditions (i.e., temperature and carbon dioxide pressure) and surface perturbation on the surface tension of aqueous alcohol solutions. The objectives can be classified as follows:

1. Examine the effect of adsorption/desorption from both sides of the vapor/liquid interface on the surface tension of several aqueous alcohol solutions i.e., 1-octanol, 1-hexanol and 1-butanol.

2. Probe the effect of surface perturbation, i.e., compression or expansion, on the surface tension of volatile organic amphiphiles in aqueous solutions.

3. Investigate the effect of environment temperature on the dynamic and steady state surface tension of the three volatile alcohols in aqueous solution.

4. Inspect the effect of carbon dioxide pressure on the dynamic and steady state surface tension of volatile alcohols in aqueous solution. The experiments are repeated for three different surfactants: 1-octanol, 1-hexanol and 1-butanol.

5. Model the experimental results of the steady-state and dynamic surface tension at different temperatures using the modified Langmuir equation of state and the modified kinetic transfer equation.

6. Develop a new modified Langmuir isotherm, a new modified Langmuir equation of state and a new kinetic transfer equation for a condition where the effect of adsorption/desorption of more than one species from both sides of a vapor/liquid interface on the surface tension is considered.

7. Model the experimental results of the steady-state and dynamic surface tension at different carbon dioxide pressures using the new modified Langmuir equation of state and the new modified kinetic transfer equation, respectively.

8. Investigate the effect of carbon chain length on the surface tension and adsorption kinetics at different temperatures and different carbon dioxide pressures.

1.3 Thesis Outline

The materials presented in this thesis address the objectives outlined in the preceding section. The thesis is organized in the following manner: In chapter 2 the theoretical background and literature review of research applicable to the current work, including relevant experimental methods, are presented. In Chapter 3 the materials and experimental methods including the sample preparation and surface tension measurements are described. In

Chapter 4 the results from the experimental investigation are presented and discussed. The section includes the surface tension experiments for three different systems. In this section the effect of adsorption/desorption from both sides of a vapor/liquid interface on the surface tension of alcohol solutions is investigated. In chapter 5 the effect of surface perturbation on the surface tension of 1-octanol aqueous solutions is examined and discussed. In chapter 6 using an experimental design the effects of other experimental factors, such as the volume of the environment solution, the distance between the sample drop and the environment solution, the area of the environment solution, the saturation time and the effect of the drop and environment concentrations on the surface tension of a volatile alcohol in aqueous solutions is investigated. In chapter 7 the effect of temperature on the dynamic and steady state surface tension of volatile alcohols in aqueous solutions is probed and discussed. In this chapter the experimental results are correlated using the modified Langmuir adsorption equations for temperature ranging from 10 to 35 °C. In chapter 8 the effect of carbon dioxide pressure on the dynamic and steady state surface tension of volatile alcohols in aqueous solutions is inspected. In this chapter the theoretical framework for both the steady-state and dynamic analysis is developed and the experimental results are correlated using the new equations for pressure ranging from 0 to 690 KPa. In chapter 9 the role of carbon chain length on the surface tension and adsorption kinetics of a group of short carbon chain surfactants are investigated. Finally, in Chapter 10 the conclusions from the research are stated and some recommendations are given for future research directions.

Chapter 2

Theoretical Background and Literature Review

In this chapter physical chemistry of surfaces and theoretical concepts behind adsorption at an interface will be introduced. The discussion will address the thermodynamics of adsorption, the concepts of dynamic and equilibrium adsorption and various surface tension measurement techniques. Also, the literature on surface tension and some of the applications will be reviewed.

2.1 Physical Chemistry of Surfaces

The properties of a surface or interface are affected by physical or chemical changes in either of the two phases involved. These two phases can be in any two of the three states of solid, liquid and gas. If one of these two contacting phases is gas, the interface is called "surface". Interface or surface is a physical boundary separating two distinguishable bulk phases over a distance of molecular dimension. The exchange phenomenon between these two immiscible phases is controlled by the interface. The prerequisite for the existence of a stable interface is a positive value of free energy of formation. Otherwise, complete dispersion of one phase in another takes place.

2.2 Adsorption at an Interface

2.2.1 Basic Thermodynamics

For a 3-D system, the relation postulated by J.W. Gibbs between the internal energy of a simple bulk system, and various modes of energy transfer between the system and the surroundings (Figure 2.1) is:

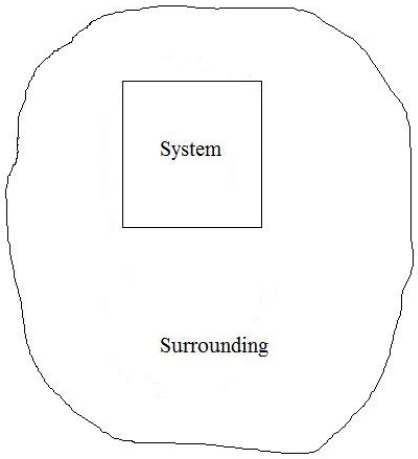

Figure 2.1: System and surrounding

$$dU = TdS - PdV + \sum_{i=1}^{n} \mu_i dN_i \tag{2.1}$$

Where dU is the change in internal energy of the system, TdS is the amount of heat transfer, $-PdV$ is the mechanical work and $\sum_{i=1}^{n} \mu_i dN_i$ is the chemical work. T, P, S, and V are the bulk temperature, pressure, entropy, and volume of the system respectively. μ_i and N_i are chemical potential and number of moles of the ith component of the system respectively. Based on equation (2.1) the following functional relationship can be written:

$$U = U(S, V, N_i) \tag{2.2}$$

Where S, V and Ni are independent extensive properties of the system. With differentiation of equation (2.2) the following equation can be written:

$$DU = \frac{\partial U}{\partial S} dS + \frac{\partial U}{\partial V} dV + \frac{\partial U}{\partial N_i} dN_i \tag{2.3}$$

Comparing equations (2.1) and (2.3) the intensive parameters T, P and $\mu_i$can be written as:

$$\frac{\partial U}{\partial S} = [T]_{V,N_i} \tag{2.4}$$

$$\frac{\partial U}{\partial V} = [-P]_{S,N_i} \tag{2.5}$$

$$\frac{\partial U}{\partial N_i} = [\mu_i]_{S,V,N_{j\neq i}} \tag{2.6}$$

With integrating the functional equation (2.1), the 3-D Euler equation can be written as:

$$U = TS - PV + \sum_{i=1}^{n} \mu_i N_i + C \tag{2.7}$$

Differentiating equation (2.7) and subtracting to equation (2.1) yields:

$$SdT - VdP + \sum_{i=1}^{n} N_i d\mu_i = 0 \tag{2.8}$$

The equation (2.8) is known as Gibbs-Duhem relation among changes in intensive parameters.

2.2.2 Surface Thermodynamics

In complete analogy to that of 3-D situations, the fundamental equation for 2-D systems, i.e., interfaces, can be written as:

$$dU = TdS + \gamma dA + \sum_{i=1}^{n} \mu_i dN_i \tag{2.9}$$

Where γdA is the work done in generating an interfacial area increment dA and γ is the interfacial tension. The functional relationship based on equation (2.9) is:

$$U = U(S, A, N_{i)} \tag{2.10}$$

Associated intensive parameters can be defined as:

$$\frac{\partial U}{\partial T} = [T]_{A,N_i} \tag{2.11}$$

$$\frac{\partial U}{\partial A} = [\gamma]_{S,N_i} \tag{2.12}$$

$$\frac{\partial U}{\partial N_i} = [\mu_i]_{S,A,N_{j\neq i}} \tag{2.13}$$

Integrating equation (2.9), the 2-D Euler equation can be written as:

$$U = TS + \gamma A + \sum_{i=1}^{n} \mu_i N_i + C \tag{2.14}$$

Differentiating equation (2.14) and subtracting equation (2.9) yields:

$$SdT + Ad\gamma + \sum_{i=1}^{n} N_i d\mu_i = 0 \tag{2.15}$$

Equation (2.15) is the 2-D Gibbs-Duhem relation among changes in intensive parameters at the interface.

2.2.3 The Gibbs Adsorption Equation

In the Gibbs treatment, a column containing two bulk phases α and β is considered. They are separated by a surface region (Figure 2.2A) [11]. Gibbs realized that the actual surface region is inhomogeneous and hard to define. Thus, he considered an idealized column along with the two phases α and β separated by a mathematical plane $GG^{'}$, parallel to $AA^{'}$ and $BB^{'}$(Figure 2.2B). This plane is not only homogeneous, but also arbitrary. In the actual system, the bulk concentration of the i^{th} component in α and β phases are C_i and $C_i^{'}$, respectively, and assume n_i^t stands for the total number of moles of the i^{th} component in all three regions. In the idealized system, the chemical composition of α and β phases are assumed to remain constant right up to the dividing surface.

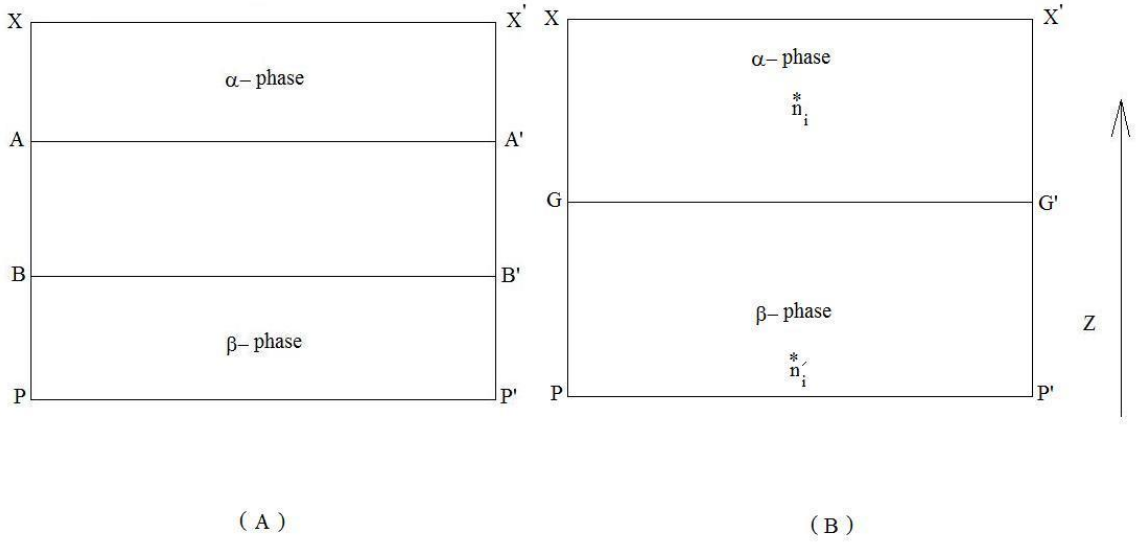

Figure 2.2: The phase column in the real (A) and ideal (B) systems

If n_i^* and $n_i^{*'}$ stand for the total number of moles of the i^{th} component of the two phases of the idealized system, the Gibbs surface excess of the i^{th} component, n_i^x can be defined as:

$$n_i^x = n_i^t - n_i^* - n_i^{*'} \tag{2.16}$$

For a real system the total number of moles n_i^t remains constant. However, the value of $n_i^* + n_i^{*'}$ of the idealized system may change depending upon of the dividing plane at

the different positions perpendicular to the Z direction. By numerical calculation, it can be shown that n_i^x may be greater, equal or less than zero, depending upon the position of the plane GG' [35]. In constant temperature, equation (2.15) can be reduced to:

$$d\gamma + \Sigma\Gamma_i d\mu_i = 0 \tag{2.17}$$

Where the surface concentration equals to:

$$\Gamma_i = \frac{n_i}{A} \tag{2.18}$$

For two component systems, such as binary solutions equation (2.17) can be written as:

$$d\gamma + \Gamma_1 d\mu_1 + \Gamma_2 d\mu_2 = 0 \tag{2.19}$$

Where Γ_1 and Γ_2 are the solvent and solute surface concentrations, respectively, and μ_1 and μ_2 are the chemical potential of solvent and solute respectively. From the aforementioned discussion it can be inferred that if we choose the arbitrary plane GG' properly, it is possible to set the number of excess molecules of the solvent at the interface n_1^x equal to zero ($\Gamma_1 = 0$), so that:

$$\Gamma_2 = -\left[\frac{d\gamma}{d\mu_2}\right]_T \tag{2.20}$$

At equilibrium, chemical potential is uniform throughout the interface, and two adjacent bulk phases

$$\mu_2 = \mu_2^0 + RTln(a_2) \tag{2.21}$$

$$\mu_2 = \mu_2^0 + RTln(f_2 x_2) \tag{2.22}$$

Where μ_2^0 is the reference chemical potential, (a_2 is the activity of solute, f_2 is the solute activity coefficient, x_2 is the mole fraction of solute, R is the universal gas constant, and T is the absolute temperature. For premicellar dilute solutions ($C \ll CMC$)

$$f_2 \cong 1 \tag{2.23}$$

and

$$x_2 \cong C_2 \tag{2.24}$$

Where C_2 is the concentration of the solute in the liquid phase. By substituting equation (2.22) into equation (2.20) the simplest form of the Gibbs adsorption equation [34], which relates the changes in the surface excess accumulation to surface tension, is derived.

$$\Gamma_2 = -\frac{1}{RT}\left[\frac{d\gamma}{d(lnC_2)}\right] \tag{2.25}$$

Based on the Gibbs adsorption equation (2.25), if a solute adsorbs at the interface it will result a decrease in surface tension, and if it desorbs from the interface it will result an increase in surface tension.

2.2.4 Adsorption Isotherm

Adsorption isotherm is the equilibrium relation between the concentration of the component at the bulk liquid solution and the amount adsorbed at the interface [24]. Henry′s law isotherm (or Henry isotherm) is a linear relation between the concentration of the component in the bulk liquid solution (C) and the surface excess (Γ). The constant for this linear relation is the equilibrium adsorption constant K_H which has the dimension of length. It is an empirical value representing the surface activity. The Henry isotherm is valid for dilute solution where interactions between species at the surface are negligible.

$$\Gamma = K_H C \tag{2.26}$$

The most commonly used isotherm is the Langmuir isotherm:

$$\frac{\Gamma}{\Gamma_\infty} = \frac{K_L C}{1 + K_L C} \tag{2.27}$$

In this non-linear isotherm, Γ_∞ is the maximum surface concentration and K_L is the Langmuir equilibrium adsorption constant. Γ_∞ is the theoretical limit of Γ , and it cannot normally be reached. In this equation, it is assumed that there are no interactions or intermolecular forces between surface molecules and the adsorption of a new single molecule in an empty site does not depend on the occupancy of the neighboring sites [24]. The last point is the main limitation of this equation, because many species interact with each other at the interface. This interaction may be due to the electrostatics effects, hydrogen bonding or Van der Waals forces.

The Frumkin isotherm attempts to consider solute-solvent interactions at a non-ideal surface, and has been used for non-ionic surfactants [23]. The general form of this equation presented in the following form:

$$C = \frac{1}{K_F}\frac{\Gamma}{\Gamma_\infty - \Gamma} exp\left[A_{fr}\frac{\Gamma}{\Gamma_\infty}\right] \tag{2.28}$$

Where K_F is the Frumkin equilibrium adsorption constant, and A_{fr} is the measure of the non-ideality of the surface, and it serves as the influence of molecular interactions at the interface on the surface concentration. If $A_{fr} = 0$, the surface is ideal and there is no interaction between molecules at the surface, and the Frumkin equation reduces to the Langmuir equation.

Recently, Andrew et al., showed that the adsorption from both sides of a vapor/liquid interface must be considered simultaneously [25]. He modified the Langmuir adsorption equation for this situation:

$$\frac{\Gamma}{\Gamma_\infty} = \frac{K_1^{'}P + K_2 C_{drop}}{1 + K_1^{'}P + K_2 C_{drop}} \tag{2.29}$$

Where Γ_∞ is the maximum surface concentration, P is the surfactant partial pressure at the vapor phase, and K_1 and K_2 are the equilibrium constants for adsorption from the vapor and liquid phase, respectively. C_{drop} is the concentration of surfactant in the liquid (drop) phase. Equation (2.29) can be simplified if the partial pressure of surfactant in the vapor phase is related to the concentration of surfactant in the environment solution (C_{env}) through Henry′s law ($P = HC_{env}$) [36]:

$$\frac{\Gamma}{\Gamma_\infty} = \frac{K_1^{'}HC_{env} + K_2 C_{drop}}{1 + K_1^{'}HC_{env} + K_2 C_{drop}} \tag{2.30}$$

2.2.5 Surface Equation of State

The Gibbs adsorption equation and the proper isotherm equation $\Gamma(C)$ can be used to drive the surface equation of state $\gamma(C)$. The purpose of the equation of state is to relate the surface tension directly to the concentration in the bulk and eliminate the surface concentration . It should be noted that the following equations of state can be applied for premicellar dilute solution ($C \ll CMC$), so that the Gibbs adsorption equation (2.25) was derived based on this assumption.

If the Henry isotherm (2.26) combines with the Gibbs adsorption equation (2.25), a simple linear Henry′s equation of state can be derived as follows:

$$\Gamma = \gamma_0 - RTK_H C \tag{2.31}$$

Where γ_0 and γ are the surface tensions of the pure solvent and solution, respectively. The Szyszkowski equation of state can be derived with Combining the Gibbs adsorption equation (2.25) with the Langmuir isotherm (2.27):

$$\Gamma = \gamma_0 - RT\Gamma_\infty ln(1 + K_L C) \tag{2.32}$$

The corresponding Frumkin equation of state based on the Gibbs adsorption equation (2.25) and the Frumkin isotherm (2.28) is [24]:

$$\Gamma = \gamma_0 + RT\Gamma_\infty ln\left(1 - \frac{\Gamma}{\Gamma_\infty}\right) + \frac{1}{2}RTA_f\Gamma_\infty\left(\frac{\Gamma}{\Gamma_\infty}\right)^2 \tag{2.33}$$

This equation is a nonlinear equation and it cannot be solved analytically. However, numerical solution can be derived.

The modified Langmuir equation of state can be derived with combining modified Langmuir isotherm (2.29) and the Gibbs adsorption equation (2.25) [36].

$$\Gamma = \gamma_0 - RT\Gamma_\infty ln(1 + K_1^{'} HC_{env} + K_2 C_{drop}) \tag{2.34}$$

Equation (2.34) can be used to predict the surface tension response to change in drop and environment concentrations [25].

2.3 Mechanisms of Surfactant Adsorption

When a new surfactant surface is created, the steady state surface tension is not attained instantly. A finite time is required to reach to the steady-state between the concentration of the surfactant at the surface and the bulk surfactant concentration [23]. Time dependent surface tension is called the dynamic surface tension. It is dependent on the type of the surfactant and its concentration at the surface. There are three steps for the adsorption of a soluble surfactant from a liquid bulk phase to the interface (Figure 2.3). The first step is the diffusion of the surfactant molecules from the bulk phase to the subsurface. The second step is the transfer of surfactant molecules between subsurface and the surface layer. The third step is the rearrangement of surfactant molecules at the interface to reach to an equilibrium state. The adsorption kinetics is characterized based on rate-limiting step. If the characteristic time for the first step is much greater than that of second and third steps, the adsorption dynamics is said to be diffusion controlled. The adsorption dynamics is transfer controlled when the characteristic time of the second step is much greater than that of first and third steps. Similarly, the adsorption dynamics is rearrangement controlled

when the characteristic time for the third step is much greater than that of the both first and second steps. Besides, the adsorption dynamics is mixed diffusion-transfer controlled when the characteristic time for both first and second steps are comparable and much greater than that of third step. It was shown that for small molecules, rearrangement is generally a fast process and characteristic time for this step is much smaller than that of the other steps. Thus, it has little effect on the overall adsorption time [37]. Also, Previous studies showed that the adsorption kinetics of normal alcohols with short carbon chain is transfer controlled [14, 38]. In this case, the bulk surfactant concentration is always uniform and equal to its initial value at the bulk solution, and adsorption does not significantly deplete the solution.

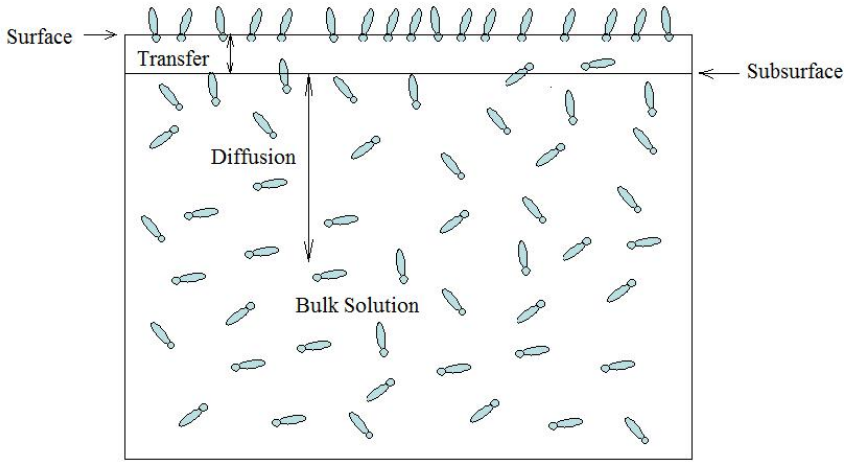

Figure 2.3: A Schematic diagram of the adsorption mechanism. Surfactants are represented using cartoon.

2.4 Experimental Methods for Surface Tension Measurements

During the past century, a wide variety of methods have been developed for measuring the surface tension of a liquid solution at the liquid/vapor interface [10]. They may be

categorized into four different classes according to the fundamental that the measurement is based on: (i) force methods, (ii) shape methods, (iii) pressure methods, and (iv) other methods. In the force methods, the surface tension of a solution is determined based on the amount of force required to detach a ring or plate from a liquid surface. The Du Nouy ring method and the Wilhelmy plate method can be classified in this category. In the shape methods, the surface tension is determined based on the shape of a liquid drop or a bubble formed inside the solution. The drop methods can be divided into two different categories: pendant or sessile drop methods. In the pendant drop method, the drop is hanging from a capillary tube, but in the sessile drop method, the drop is formed on a flat surface. The maximum bubble pressure method can be classified as the pressure methods. In this method, the maximum pressure required to release a bubble in a liquid solution is measured. Other methods such as the capillary rise method, and the drop weight methods are categorized as the other methods. In the next section, a brief introduction for the aforementioned methods is presented.

2.4.1 Du Nouy Ring Method

In this method, the capillary force on a platinum ring at the liquid/vapor surface is measured. The maximum force required to disconnect the ring from the liquid surface is proportional to the contact angle, surface tension, and wetted perimeter of the ring. The apparatus consists of a liquid container and a ring attached to a sensitive force measurement device (figure 2.4). The container can be moved upward and downward in a controlled manner. Initially, it is positioned so that the ring is submerged just below the surface. It is moved slowly downward and meanwhile the force exerted on the ring is measured, until the ring becomes detached from the liquid. The force exerted on the ring at detachment is approximately equal to the surface tension multiplied by the perimeter of the ring.

$$W - W_{ring} = F_d = 4\pi R_d \gamma \tag{2.35}$$

Where W, F_d and W_{ring} are the total force, the net force and the net weight of the ring, respectively. R_d is the radius of the ring, and γ is the liquid surface tension. In practice, this force has to be corrected because the surface tension does not completely act in the vertical direction and also because some of the liquid remains adhered to the ring after it has become detached.

$$F_d = 4\pi R_d \gamma \beta \tag{2.36}$$

In this equation, β is a correction factor that depends on the dimensions of the ring and the density of the liquid. Since a fresh interface is formed as the ring is pulled upward,

this method can be applicable in systems with very short adsorption time. Therefore, the method is not recommended for dynamic surface tension measurements. Furthermore, surfactant adsorption on the wetted portion of the ring can considerably affect the measured surface tension.

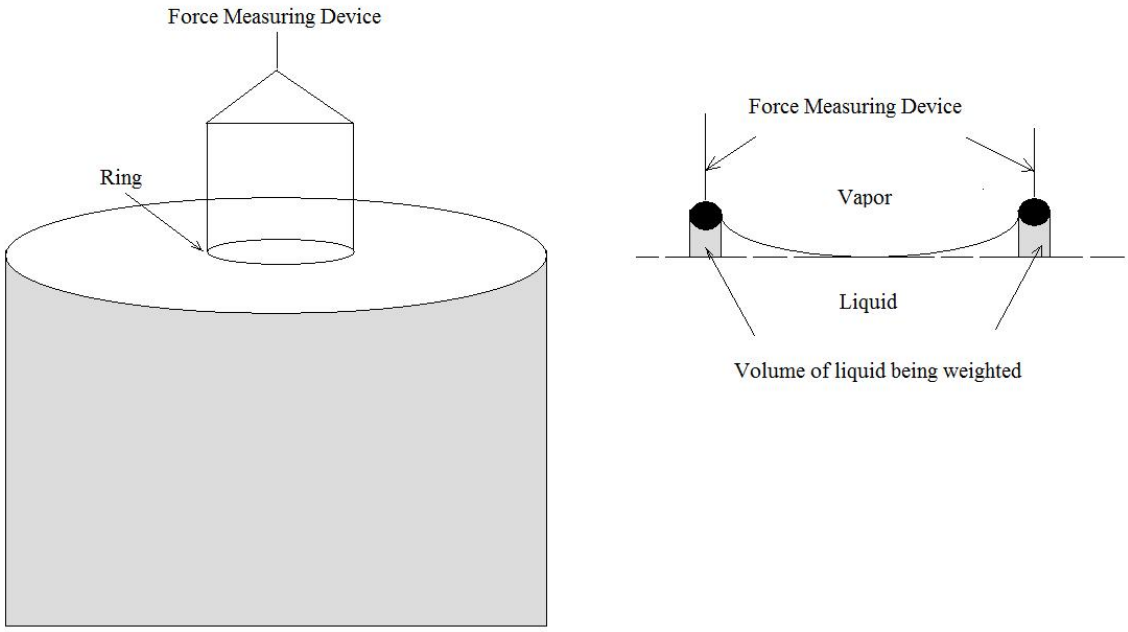

Figure 2.4: Du Nouy ring method for measuring the surface tension of a liquid. The force on the ring is measured as the container holding the liquid is lowered.

2.4.2 Wilhelmy Plate Method

Similar to Du Nouy ring, the wilhelmy plate method is based on a force measurement. However, in this case the force acting on a rectangular plate. Initially, the container is positioned so that the liquid just comes into contact with the plate, and the bottom of the plate is parallel to the surface of the bulk liquid. The force acting on the plate is related to the weight of the plate (W_{plate}), the perimeter of the plate (P_w), the contact angle between liquid and plate (θ), and the liquid surface tension(γ) (Figure 2.5). The plate is usually made up of platinum which has been roughened so that the contact angle becomes close to zero(i.e., complete wetting). If the contact angle remains constant and the plate is kept steady, then reliable results can be attained for dynamic or steady-state surface tension on most systems.

$$W - W_{plate} = F_d = \gamma P_w cos(\theta) \tag{2.37}$$

This method is not accurate for the slow adsorption rate surfactant solutions. Also, Surfactant adhesion to the wetted portion of the plate is another source of error for the measured surface tension.

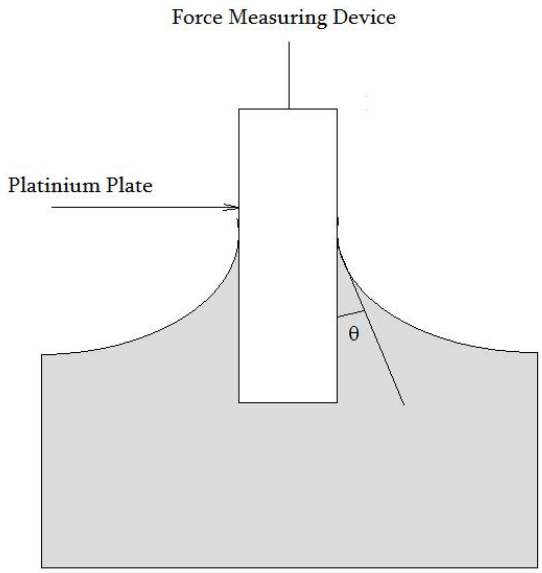

Figure 2.5: Wilhelmy plate method for measuring the surface tension of a liquid. The force on the ring is measured as the container holding the liquid is lowered. θ is the contact angle between liquid and plate.

2.4.3 Drop and Bubble Shape Method

In this approach, the surface tension of a solution is obtained based on the shape of a liquid drop (or bubble formed inside the solution). To measure the surface tension of a liquid using shape analysis two methods can be used: pendant drop method and sessile drop method. In the pendant drop method, the drop is hanging from a capillary, while in sessile drop method, the drop is formed on a flat surface. In both cases, the shape of the drop is dictated by the combination of gravity force and surface tension. Surface tension tends to make the drop more spherical, whereas the gravity force tends to elongate the pendant drop or spread the sessile drop. The drop shape method has numerous advantages

compare to other methods. (i) In this method, only small amount of liquid is required; (ii) Both liquid/vapour and liquid/liquid interfacial tension can be determined by this method; (iii) It is applicable for a wide variety of materials ranging from organic liquid to molten melts and from pure solvent to concentrated surfactant solutions; (iv) In this method, the dynamic surface tension as well as the steady-state surface tension can be determined using an automated image analysis apparatus; (v) There is no limitation of the magnitude of the surface or interfacial tension of the material under study; (vi) It is applicable for different range of pressures and temperatures; (vii) The drop shape method is one of the most accurate methods for measuring the surface tension. Due to the fact that image capturing starts a few seconds after the drop formation, this method is most suitable for the systems changing little during the first few seconds after drop is made.

2.4.4 Maximum Bubble Pressure Method

The maximum bubble pressure method has been used to measure the static and dynamic surface tension of liquids. A detailed review of this method and the apparatus design is given by Mysles [38]. The apparatus consists of vertical tube whose tip is immersed below the surface of liquid under study (figure 2.6). When gas is pumped into the tube, the pressure inside the tube increases and the bubble start to form. The pressure increases as the bubble grows until it reaches to a maximum value when the bubble is hemispherical. In this condition, surface tension acts in the vertical direction. Any further bubble growth, causes a decrease in the pressure. After bubble detaches from the tip and transfer to the surface of liquid, another bubble starts to form and the whole process is repeated. For measuring the dynamic surface tension, the pressure in the capillary is remained constant and the interval between released bubbles is measured. By changing the pressure, the change in surface tension versus time can be determined from the appropriate equation.

2.4.5 Capillary Rise Method

If a capillary tube is dipped into a container of water, the liquid climbs up the tube and forms a curved surface (Figure 2.7). The surface tension is proportional to the height of rise (h). By applying the Laplace equation of capillary, and by assuming that the contact angle on the top of liquid is zero, the following equation can be obtained (Laplace equation of capillarity will be discussed in the next chapter).

$$\Delta\rho g h = \frac{2\gamma}{r} \tag{2.38}$$

Where $\Delta\rho$ is the density difference between gas and liquid, g is the gravity constant and γ is the surface tension of the liquid.

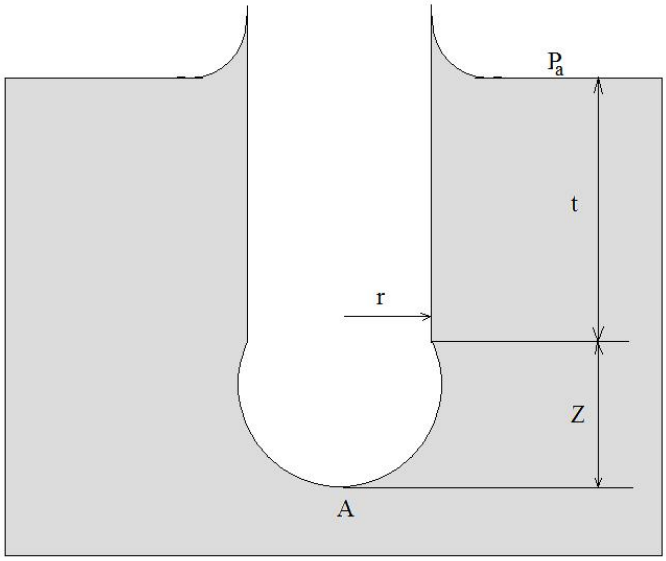

Figure 2.6: Maximum bubble pressure method for measuring the surface tension of liquids.

2.4.6 Drop Weight Method

A pendant drop will become unstable and detach from its supporting tip if it grows too large. The weight of the detached portion is related to the surface tension of the liquid by:

$$W = mg = 2\pi r\gamma f \tag{2.39}$$

Where m is the mass of the drop, g is the gravity constant, and r is the capillary tip radius. When a drop reaches the point of instability only a portion of the drop falls and about 40% of the liquid remain attached to the tip. Correction factor f accounts for this fact. Harkins et al. presented the empirical values of the correction factor [39]. Drop weight method typically involves weighting the accumulated liquid from a large number of drops to determine the average weight per drop.

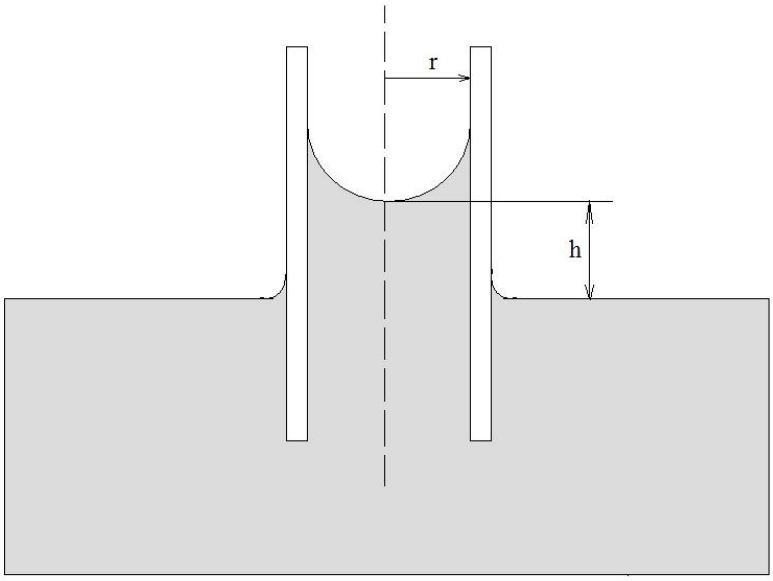

Figure 2.7: Capillary rise method for measuring the surface tension of liquids.

Chapter 3

Materials and Experimental Methods

3.1 Materials and Sample Preparation

The chemicals 1-octanol, 1-hexanol, and 1-butanol with purity greater than 99%, was purchased from Sigma-Aldrich (Oakville, Ontario, Canada). The molecular weight, vapor pressure [40, 41, 42, 43], water solubility [44, 45], and specific gravity of these chemicals are listed in Table 3.1. The water is purified by an ultra-pure water system (Millipore Ltd., Mississauga, Ontario, Canada), with resistivity of 18.2 MΩ. Six different concentrations: 0.2, 0.4, 0.6, 0.8, 1 and 2.92 mM, are prepared for 1-octanol aqueous solutions, eight different concentrations: 1, 2, 5, 6, 9, 10, 25 and 30 mM, are prepared for 1-hexanol aqueous solutions, and four different concentrations: 20, 60, 100, and 400 mM are prepared for 1-butanol. They are used for both sample drop and environment solution concentrations. The sample with the highest concentration is prepared as the stock solution and lower concentration samples are made by diluting the stock solution.

Table 3.1: Molecular weight, vapour pressure, water solubility and specific gravity data of chemicals under study.

Chemicals	Molecular Weight	Vapor Pressure	Water Solubility	Specific Gravity
	(g/mol)	$mmHg$	mol/m^3	g/cm^3
1-octanol	130.23	0.083 (25 °C)	4.15 (25 °C)	0.824 (25 °C)
1-hexanol	102.17	0.863 (25 °C)	57.83 (25 °C)	0.814 (25 °C)
1-butanol	74.10	5.020 (20 °C)	1058.44 (20 °C)	0.810 (20 °C)

3.2 Surface Tension Measurements

Different methods have been used for measuring surface tension [46, 47]. Among them, Axisymmetric Drop Shape Analysis-Profile (ADSA-P) is one of the most accurate methods and has been widely used [17, 48, 49, 50]. In this method, the drop is hanging from a capillary, and combination of gravity force and surface tension dictate the shape of the drop. Surface tension tends to make the drop more spherical, whereas the gravity force tends to elongate the pendant drop. The theoretical shape of the pendant drop is given by the Laplace equation of capillarity. In this equation the pressure difference across the curved interface ΔP is related to the surface tension γ and the two radii of curvature of the interface R_1 and R_2 [50]:

$$\Delta P = \gamma \left(\frac{1}{R_1} + \frac{1}{R_2} \right) \tag{3.1}$$

The ADSA-P program compares the experimental drop profile (Figure3.1A) to the theoretical solution of equation 3.1. An objective function, which shows the deviation of the experimental drop profile from the theoretical one as a sum of squares of the normal distance between the experimental points an the theoretical curve (from equation 3.1) is minimized numerically [49]. The surface tension is the fitting parameter for this calculation. The program requires a manual input of the cut-off coordinates of the capillary tube location at the hanging point of the drop, the magnitude of the local gravitational constant, and the density difference across the interface. The output of the ADSA-P program is the surface tension, the surface area of interface, and the radius of curvature of the pendant drop.

Figure (3.1B) shows an experimental setup of ADSA-P used in our work: a vibration-isolated workstation is used to prevent vibration during surface tension measurements. To illuminate the sample (e.g., a pendant drop), a fiber optic light source filtered by a diffuser is employed. The sample solution drop is formed by means of a motorized syringe pump attached to a Hamilton gas-tight syringe. The experiments are performed in a closed chamber (environment chamber) where the effects of chemical concentrations of both liquid and vapor phases on the surface tension could be studied. The vapor phase pressure is controlled with an environment solution of a prescribed chemical concentration. The tip of the syringe supporting the sample drop is positioned inside a clear quartz cuvette containing a relatively large volume of the environment solution. In order to minimize the vapor leakage, a laboratory film is used to seal the chamber. The chamber is fixed on a stage that could finely adjust its position in three directions. The drop images are captured by a high-speed camera and microscope system. Using this system the profile of the drop is displayed on a monochromatic monitor, and the image files are transmitted to a computer.

An ADSA-P program is used to analyze the images and implement the numerical procedure that yields output, including surface tension, surface area and volume of the sample.

Before each set of experiments, the gas-tight syringe is cleaned by a Branson B5510 ultrasonic cleaner and repeated rinsing with purified water, THF, and finally dried with pressurized air. Afterwards, about 0.3 ml of chemical aqueous solution with a specified concentration is drawn into the syringe, and the sample pendant drop is formed at the syringe tip. 1 ml of the environment solution is added to the bottom of the cuvette, and the chamber is sealed. At normal operation, the distance between the environment solution and the sample drop is about 1 cm, and the system is allowed to equilibrate for 15 min until a constant vapor pressure is achieved in the closed chamber. The temperature of the chamber is controlled using a RTE 111 NesLab circulating bath. The pressure of the chamber is controlled using Teledyne ISCO model 260D syringe pump with an ISCO pump controller series D. Image capturing is started immediately after the drop is formed, and continued with specific time intervals until surface tension reaches to a steady-state value. The change in drop surface area is made with the motorized syringe pump (ORIEL, model 18709)

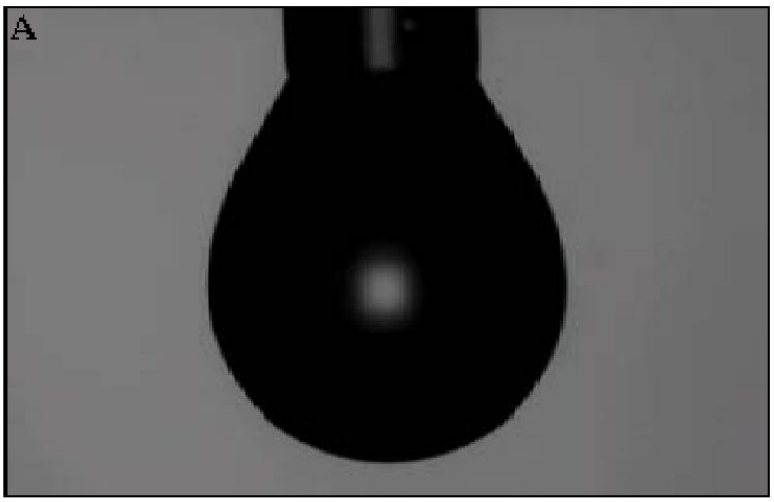

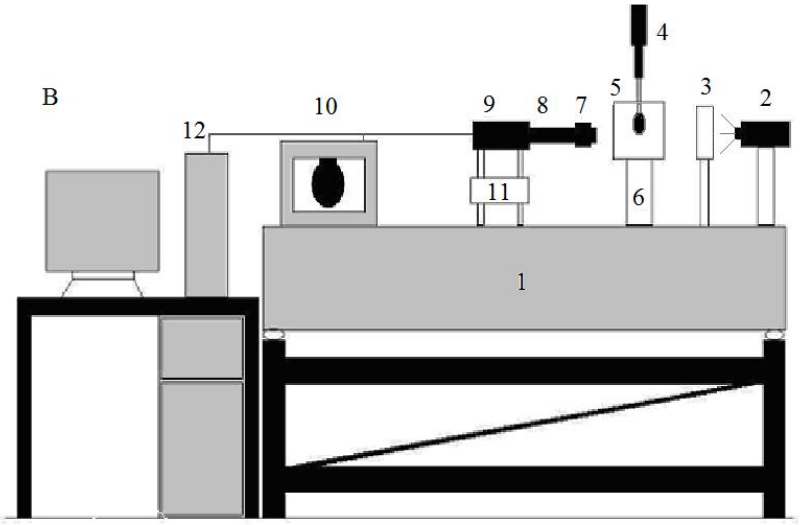

Figure 3.1: (A) Sample pendant drop image, captured by the high speed camera, was used by the ADSA-P program for surface tension determination. (B) Schematic of an ADSA-P experimental setup; (1) Vibration-isolated workstation, (2) optical light source, (3) light diffuser, (4) motorized syringe pump and gas-tight syringe, (5) environment chamber, (6) stage, (7) microscope, (8) lens, (9) high speed camera, (10) monochromatic monitor, (11) stage, and (12) computer system.

Chapter 4

Effect of Liquid and Vapor Phase Adsorption on the Surface Tension of 1-octanol, 1-hexanol and 1-butanol Aqueous Solutions

4.1 Introduction

This chapter presents the experimental investigation of dynamic surface tension of aqueous solutions containing slightly volatile organic amphiphiles at the vapor/liquid surface. Axisymmetric Drop Shape Analysis-Profile (ADSA-P) technique is used due to high accuracy and sample environment control abilities of the method. An amphiphile is a chemical compound that shows both hydrophobic and hydrophilic properties. The hydrophobic part of the molecule usually consists of a non-polar hydrocarbon chain, but the hydrophilic part includes a polar function group attached to the hydrocarbon end. Hydrophilic head and hydrophobic tail of amphiphiles allows them to form interactions with adjacent water molecules through the formation of the hydrogen bonds between the polar groups. Without this interaction the water solubility of these compounds would be minimal. In this chapter, the dynamic surface tension results of three organic compounds (1-octanol, 1-hexanol and 1-butanol) measured by the ADSA-P technique are presented and the effect of adsorption from vapor and liquid phase are investigated. Then, the surface tension behavior of these short chain alcohols are compared with the surface tension behavior of some traditional surfactants

4.2 Dynamic Surface Tension

The dynamic surface tension results are organized in three sections according to the different surfactant studies. Data from 1-octanol aqueous solutions with different concentrations are presented in section 4.3, and data from 1-hexanol aqueous solutions with various concentrations are introduced in section 4.4. In section 4.5 dynamic surface tension results from 1-butanol aqueous solutions with various concentrations are presented. In order to show the differences between the surface tension behavior for these volatile organic amphiphiles and traditional surfactants, results from some traditional surfactants are mentioned in section 4.5.

The experimental procedure for the surface tension measurements was explained in detail in the third chapter. Briefly, a pendant drop of an aqueous solution (drop solution) was formed inside a clear quartz cuvette, containing 1 ml of the same aqueous solution (environment solution) as the pendant drop. When the sample drop and environment solutions have different concentrations, molecular exchange across the vapor/liquid surface causes a change in the surface tension of the drop. Based on the definition of concentration difference (equation 4.1), three distinct concentration difference can be investigated: positive if the sample drop concentration is greater than environment concentration, negative if the environment concentration is greater than sample drop concentration, and zero if the two are equal.

$$\Delta C = C_{drop} - C_{env} \tag{4.1}$$

To facilitate the investigation of various concentration differences, four different concentrations for 1-octanol, four different concentrations for 1-hexanol and four different concentration for 1-butanlol are used in preparation of drop and environment solutions.

4.3 1-octanol Dynamic Surface Tension

The Dynamic Surface Tension (DST) profiles for 1-octanol systems at four sample drop solution concentrations and four environment solution concentrations are illustrated in Figure 4.1. In this figure the surface tension gradually changes until a steady-state surface tension is achieved between the surface and the two bulk phases. When concentration difference (equation 4.1) is positive, the surface tension increases as surfactant molecules desorbs from the interface. For the negative concentration difference, the surface tension decreases as surfactant molecules adsorbs at the interface. For the zero concentration difference, the surface tension remains constant, because there is no driving force to transfer molecules from the bulks to the surface or vice versa. However, some small changes in surface tension

profiles can be observed in such a condition at the beginning of the experiments (i.e. when $C_{drop} = C_{env} = 1mol/m^3$. These variations may be related to experimental errors or more likely due to the change in surface area when the drop is formed and will be discussed in detail in chapter 5. Interesting results for each environment solution concentration are observed. At a specific environment solution concentration the same steady-state surface tension is achieved by the entire sample drop solution concentrations; regardless of the concentration of the sample drop solution. In Figure 4.1, when the environment solution concentration is 0.2 mM, each profile converge towards a surface tension about 64mN/m. Similar results are observed in the other environment solution concentrations. When the environment solution concentration is 0.6 mM, 1mM and 2.92 mM the steady-state surface tension converge towards the values about 56, 53 and 37 mN/m, respectively. These results show that the steady-state surface tension are dictated by the environment solution concentrations, regardless of the drop solution concentrations. To investigate whether this results only valid for 1-octanol system, aqueous solutions of 1-hexanol and 1-butanol are also examined.

4.4 1-hexanol Dynamic Surface Tension

The Dynamic Surface Tension (DST) profiles for 1-hexanol systems at four sample drop solution concentrations and four environment solution concentrations are illustrated in Figure 4.2. Similar to 1-octanol system, the surface tension increases when concentration difference between drop and environment solutions (equation 4.1) is positive. For the negative concentration difference, the surface tension decreases as surfactant molecules adsorbs at the interface. For the zero concentration difference, the surface tension remains constant. In figure 4.2 similar to 4.1 the same steady-state surface tension is achieved when concentration of the environment solution is unchanged; regardless of the concentration of the drop solution. In Figure 4.2, when the environment solution concentration is 2 mM, all profiles converge towards an identical steady-state surface tension about 58 mN/m. Very similar results are observed in the other environment solution concentrations. When the environment solution concentration is 5 mM, 9mM and 30 mM the steady-state surface tension regardless of the drop concentrations converge towards the identical values about 56, 53 and 35 mN/m, respectively. This shows that also for 1-hexanol aqueous solutions the steady-state surface tension are dictated by the environment solution concentrations, regardless of the drop solution concentrations. To inspect whether this results are also valid for 1-butanol system, the effect of drop and environment concentrations on the dynamic

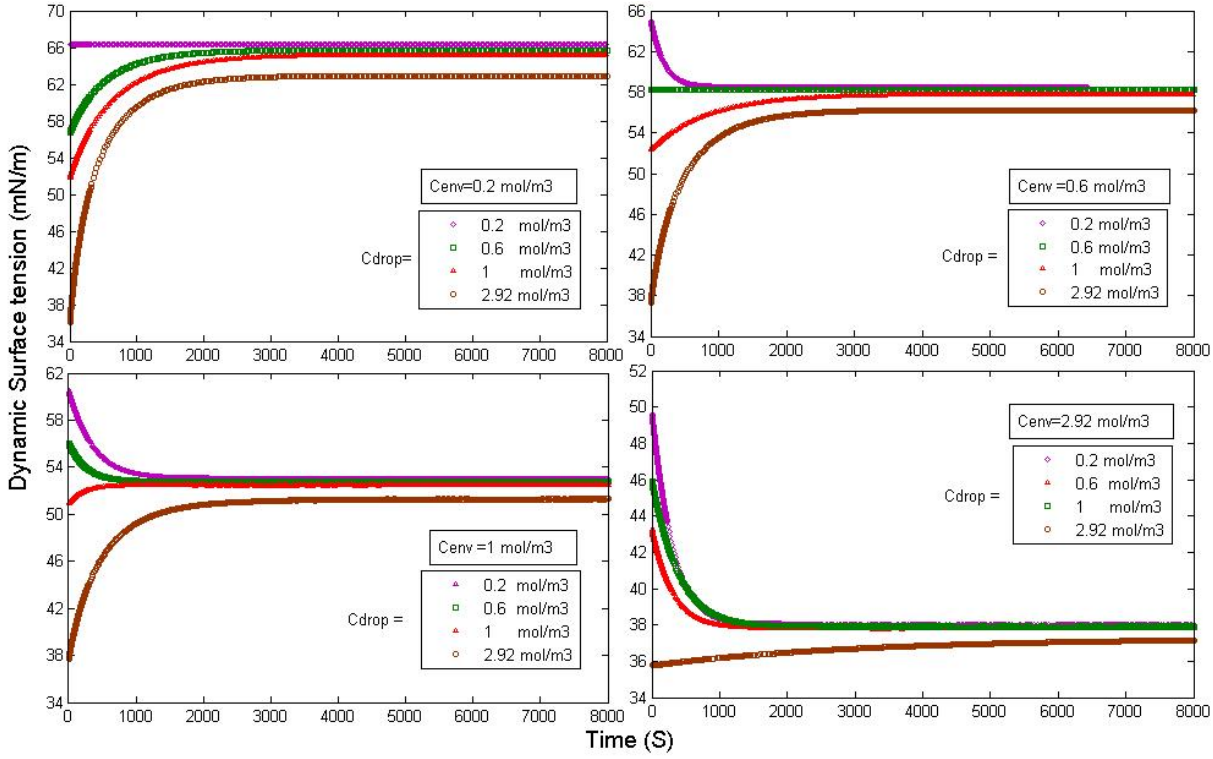

Figure 4.1: Dynamic surface tension profiles of aqueous 1-octanol solutions. Drop solution concentrations are illustrated in the legend of each graph. The environment solution concentration are presented in each graph.

surface tension of 1-butanol aqueous solution is investigated on the next section.

4.5 1-butanol Dynamic Surface Tension

The Dynamic Surface Tension (DST) results for 1-butanol systems at four sample drop solution concentrations and four environment solution concentrations are illustrated in Figure 4.3. In this figure similar to Figures 4.1 and 4.2 the surface tension gradually changes until a steady-state surface tension is achieved between the surface and the two bulk phases. The results follow the same trends as figures 4.1 and 4.2 which the steady-state

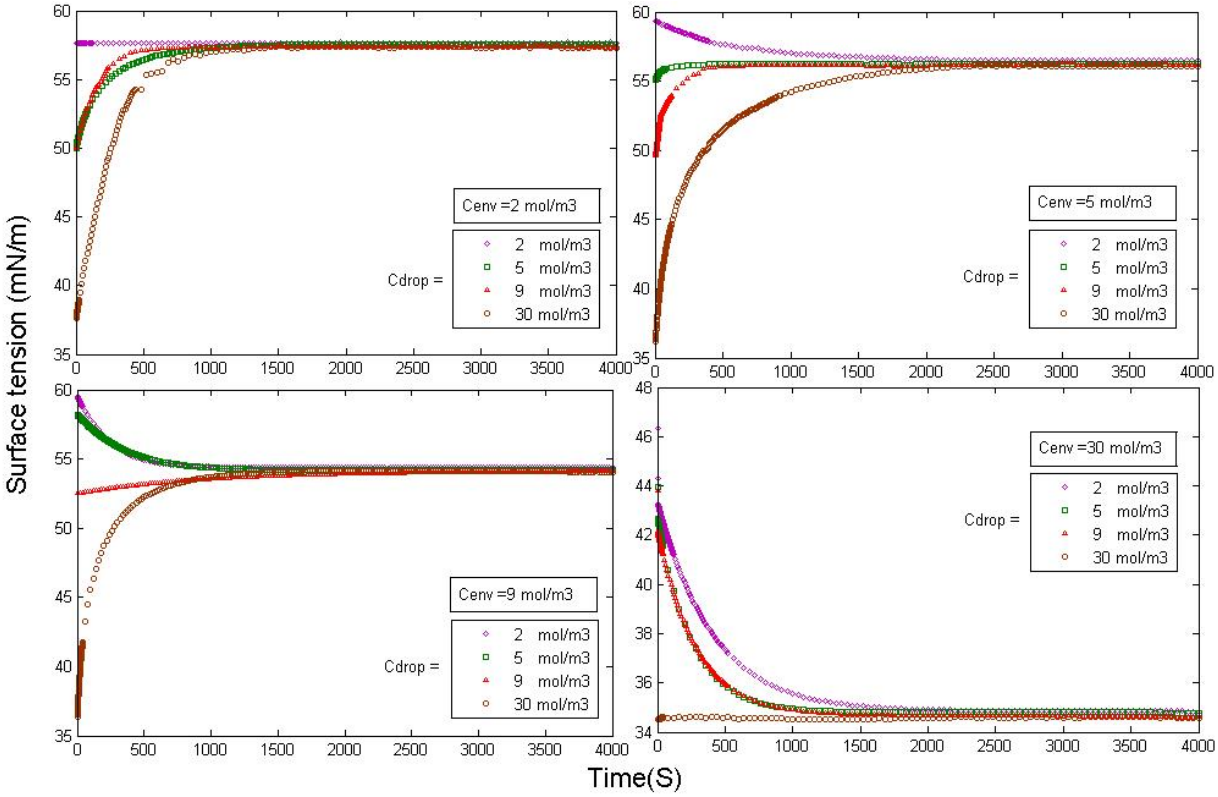

Figure 4.2: Dynamic surface tension profiles of aqueous 1-hexanol solutions. Drop solution concentrations are illustrated in the legend of each graph. The environment solution concentration are presented in each graph.

surface tension for different drop concentrations and the same environment concentration is almost identical. Figure 4.3 shows that when the environment solution concentration is 20 mM, all profiles converge towards an identical steady-state surface tension about 60 mN/m. Very similar results are observed in the other environment solution concentrations. When the environment solution concentration is 60 mM, 100mM and 400 mM the steady-state surface tension of different profiles related to different drop concentrations converge towards the identical values about 51, 48 and 38 mN/m, respectively. These results show that also for 1-butanol aqueous solutions the steady-state surface tension are dictated by the environment solution concentrations, regardless of the drop solution concentrations.

These results for 1-octanol, 1-hexanol and 1-butanol are in stark contrast to the surface tension behavior of conventional surfactants such as aqueous octaethelene glycol monododecyl ether ($C_{12}E_8$) and aqueous Igepal CO-720 (Figure 4.4) [75]. The results show that

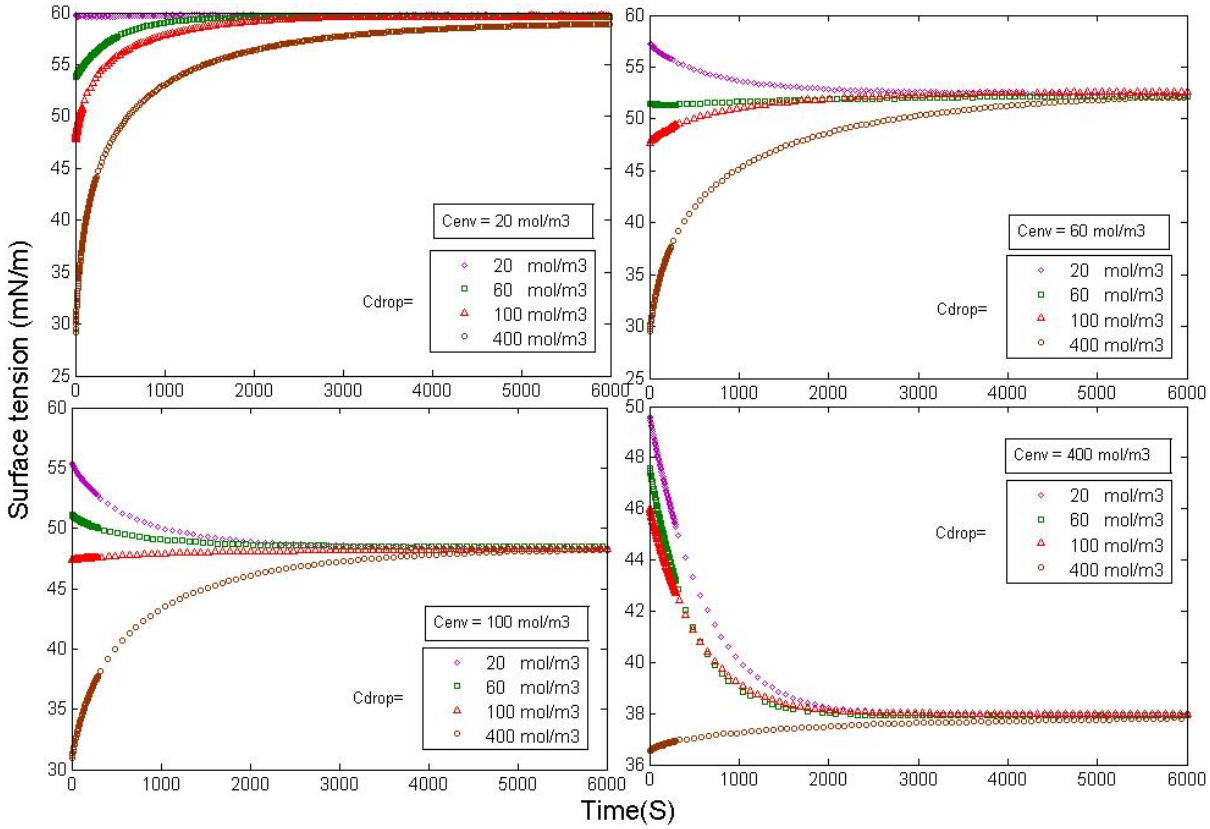

Figure 4.3: Dynamic surface tension profiles of aqueous 1-butanol solutions. Drop solution concentrations are illustrated in the legend of each graph. The environment solution concentration are presented in each graph.

when 1-octanol, 1-hexanol or 1-butanol is dissolved in water, it presents a finite partial pressure in the vapor phase, and the surface tension of the solution can be affected by surfactant adsorption from both sides of the vapor/liquid interface.These results also show that at the steady-state, the effect of adsorption from the vapor side is more important than that from the liquid side. The results contradict with the surface tension behavior of conventional surfactants in which the effect of adsorption from the liquid side is more important than that from the vapor side. The unusual behavior of surface tension for this group of short carbon chain amphiphiles may be related to a gradually formed network of hydrogen bonding in the liquid side which hinder the adsorption from liquid phase. This phenomenon will be discussed in more detail in chapters 5 and 10. In order to investigate if the surface tension behavior of this group of short carbon chain surfactants (1-octanol, 1-hexanol and 1-butanol) can be affected by other factors, the effect of different parameters

such as surface perturbation and environment conditions on the dynamic and steady-state surface tension is studied in the next chapters.

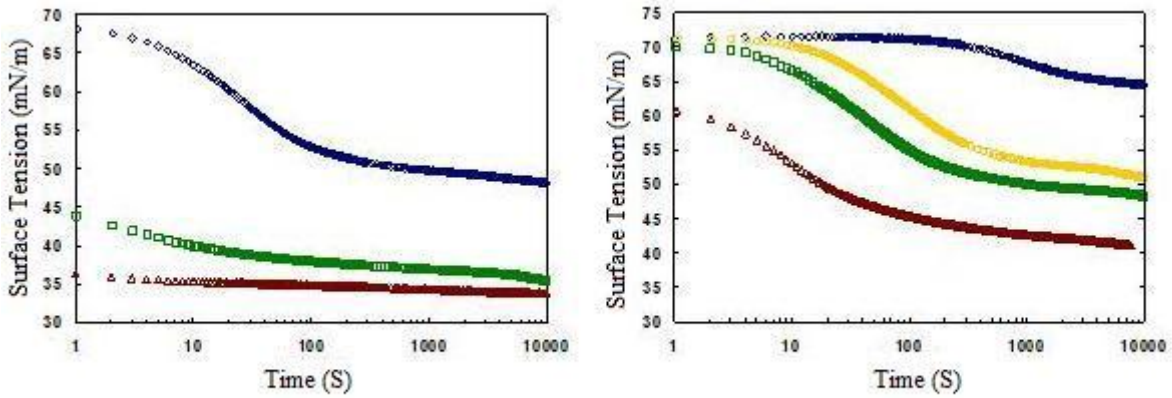

Figure 4.4: Dynamic surface tension profile of some traditional surfactant systems. Environment solution is pure water for both cases. (A) Aqueous solutions of octaethylene glycol monododecyl ether ($C_{12}E_8$) at drop concentrations of 0.008 mol/m^3 (blue), 0.04 mol/m^3 (green), 0.093 mol/m^3 (brown). (B) Aqueous solutions of Igepal CO-720 at drop concentrations of 0.00123 mol/m^3 (blue), 0.00657 mol/m^3 (yellow), 0.00985 mol/m^3 (green), 0.0246 mol/m^3 (brown).

Chapter 5

Effect of Surface Perturbation on the Surface Tension of 1-octanol Aqueous Solutions

In this chapter, the dynamic surface tension response to a change in drop surface area (i.e., surface compression and expansion) is examined. Between this group of short carbon chain amphiphiles (1-octanol, 1-hexanol and 1-butanol), 1-octanol has the longest chain and the minimum energy barrier for adsorption (based on modelling results in chapter 7). 1-octanol is chosen for surface perturbation experiments as small change in surface area (especially when the drop is expanded) may break the hydrogen bonding network at the surface, and make a significant change in the dynamic surface tension. In section 5.1 the dynamic surface tension response to a change in surface area for 1-octanol aqueous solutions is addressed. The concentration difference between sample drop and environment solution (equation 4.1) may be positive, negative or zero. This experiment is repeated for different drop and environment concentrations explained in section 3.1. In section 5.2 , for an unexpected surface tension response to surface expansion, using Buckingham Π theorem, a dimensionless parameter is derived and a regression model is developed and fitted to the experimental results. Using the regression equation, the surface tension response can be predicted based on the molecular weight of the organic compound, liquid and vapor phase concentrations and the amount of change in surface area.

5.1 Surface Tension Response of 1-octanol Solutions to the Surface Expansion and Compression

In this section, in order to explain the dynamic surface tension behavior, the effect of surface expansion and compression on the surface tension of an alcohol solution, 1- octanol, is studied. After a primary steady state surface tension is attained, the surface area is either compressed or expanded (using a stepping motor connected to the syringe containing the sample drop), and the response of the surface tension is investigated through continuous measurement of its value. Three cases are subjected to a sudden change in surface area, first when the sample drop concentration is higher than the environment concentration, second when they are the same, and third when the sample drop concentration is lower than the environment concentration. In most cases, the dynamic surface tension decreases in response to compression, and increases in response to expansion.

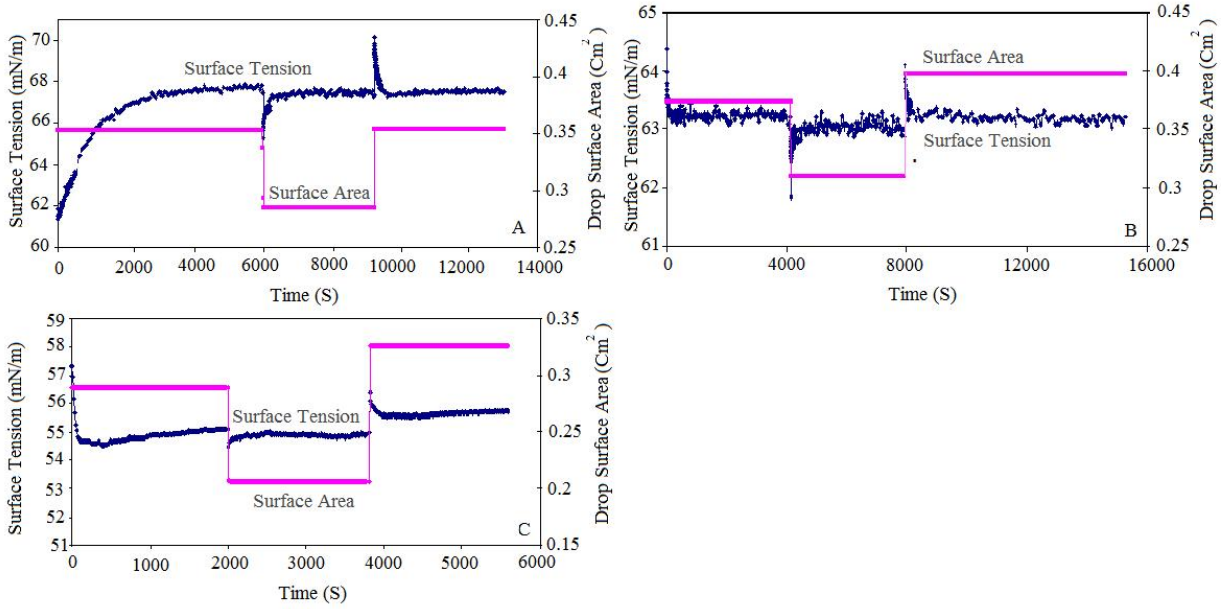

Figure 5.1: Effect of changes in surface area on the dynamic surface tension of 1-octanol solutions. (A)$\Delta C = C_{drop} - C_{env}$ is positive, $C_{drop} = 1mM$ and $C_{env} = 0.2mM$ (B)$\Delta C = 0, C_{drop} = C_{env} = 0.4mM(C)\Delta C$ is negative, $C_{drop} = 0.6mM$ and $C_{env} = 0.8mM$.

Figure 5.1A shows the dynamic surface tension response to changes in surface area when the sample drop concentration ($C_{drop} = 1mM$) is higher than the environment concentration ($C_{env} = 0.2mM$). Figure 5.1B shows the dynamic surface tension re-

sponse to changes in surface area when the sample drop and environment concentrations ($C_{drop} = C_{env} = 0.4mM$) are equal. Figures 5.1C shows the surface tension response to changes in surface area when the sample drop concentration ($C_{drop} = 0.6mM$) is lower than the environment concentration ($C_{env} = 0.8mM$). The observed surface tension results are usual behavior of surfactant solutions and can be explained as follows: As the surface area is reduced, the concentration of the surfactant increases at the surface, and consequently the surface tension decreases. With desorption of surface surfactant molecules to the bulk phase, the surface tension gradually increases back almost to the value prior to compression [13]. The reverse happens as the surface area is expanded (Figure 5.1 A,B,C). Figure 5.1 shows that the primary and secondary steady-state surface tensions are almost identical and the steady-state surface tension is not affected by the surface perturbation. Figure 5.2 shows the effect of different changes in surface area on the dynamic surface tension of 1-octanol solutions. In this experiments the same environment solution concentration ($C_{env} = 1mM$) and different sample drop concentrations ($C_{drop} = 0.2mM, 0.4mM, 0.6mM$) are used. In chapter 4 it was shown that the steady-state surface tension of 1-octanol, 1-hexanol and 1-butanol solutions is not affected by the liquid phase concentration. Figures 5.1 and 5.2 show that the steady-state surface tension of 1-octanol solutions is only dictated by the adsorption/desorption from the vapor phase, regardless of the concentration, and the surface area of the liquid phase and also regardless of the history of the surface perturbation.

An extremely interesting and unexpected surface tension response is observed in the expansion experiments when the change in surface area of the sample drop is greater than 5% and the sample drop concentration is sufficiently greater than environment concentration (Figures 5.3, 5.4 and Table 5.1). In this case as the surface area is increased, the surface tension slightly increases immediately, but after a certain time (time delay) it sharply decreases, followed by a gradual increase back to the value prior to expansion. These results contradict with aforementioned results in expansion experiments when the drop concentration is lower than or equal to the environment concentration (Figures 5.1B,C, and 5.2). Also, they contradict with the surface tension response when the drop concentration is not that much higher than the environment concentration, or change in sample drop area is smaller than 5% (Figure 5.1A).

Table 5.1 summarizes these interesting results of surface expansion experiments. In this case, when the drop is expanded, the surface area increases and the number of surfactant molecules at the surface decreases, causing a sudden increase in the surface tension. When considering the principle of mass transfer, due to the concentration difference between the liquid phase and the surface, a driving force is established causing a number of surfactant molecules adsorb to the surface from the liquid bulk phase. If the higher change in surface area is used, the higher number of vacant places at the surface is created; consequently more surfactant molecules adsorb to the surface to occupy these places and more reduction

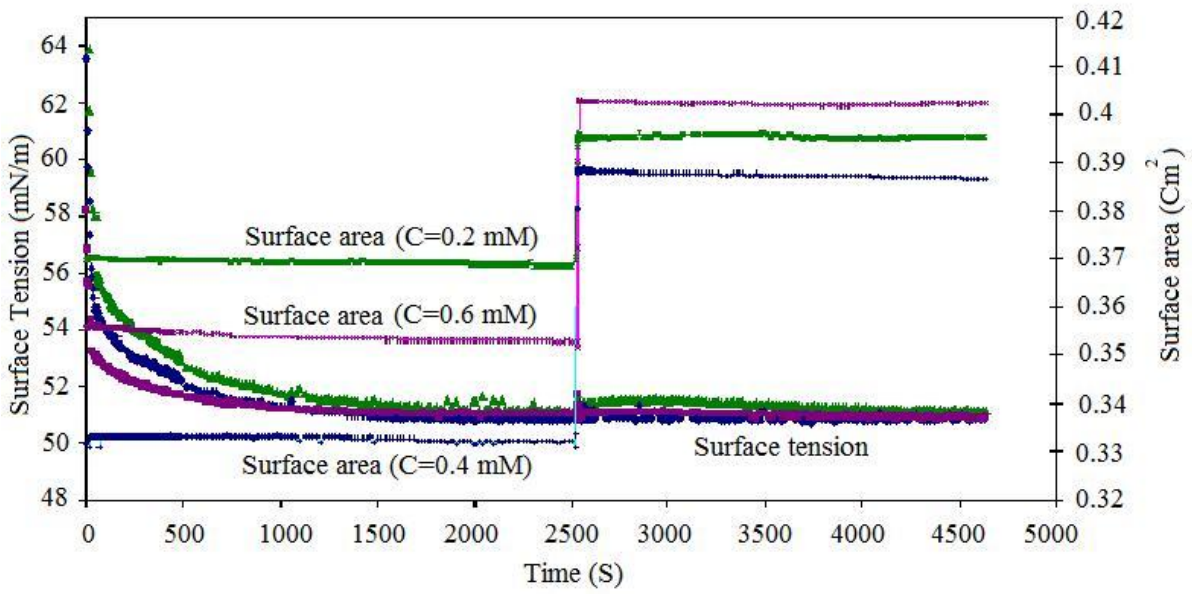

Figure 5.2: Effect of changes in surface area on the dynamic surface tension of 1-octanol solutions. Green ($C_{drop} = 0.2mM$), Blue ($C_{drop} = 0.4mM$), and Purple ($C_{drop} = 0.6mM$). The concentration of the environment solution Cenv. = 1 mM in all three experiments.

in surface tension is observed. This process continues until there is no vacant position at the surface to occupy with the adsorbed surfactant molecules. At this point, the lowest surface tension is achieved due to the highest surface concentration. After reaching the minimum, desorption to the vapor phase takes place and surface tension gradually increases back to the value prior to expansion (Figure 5.3, and 5.4).

The molecular dynamic simulation of 1-octanol and ethanol solutions shows that at the steady-sate conditions a network of hydrogen bonding between surfactant and water molecules near the surface is created [51, 52, 53, 54, 55, 56, 57]. This network can make a barrier just beneath the surface that may be responsible for diminishing the adsorption from liquid phase to the surface at the steady-state conditions. This unusual behavior of dynamic surface tension after large expansion may be the consequences of the destruction of this barrier.

5.2 Dimensionless Parameter

In order to find a meaningful dimensionless parameter to describe the surface tension response to changes in surface area, the Buckingham Π theorem is employed. The parameters

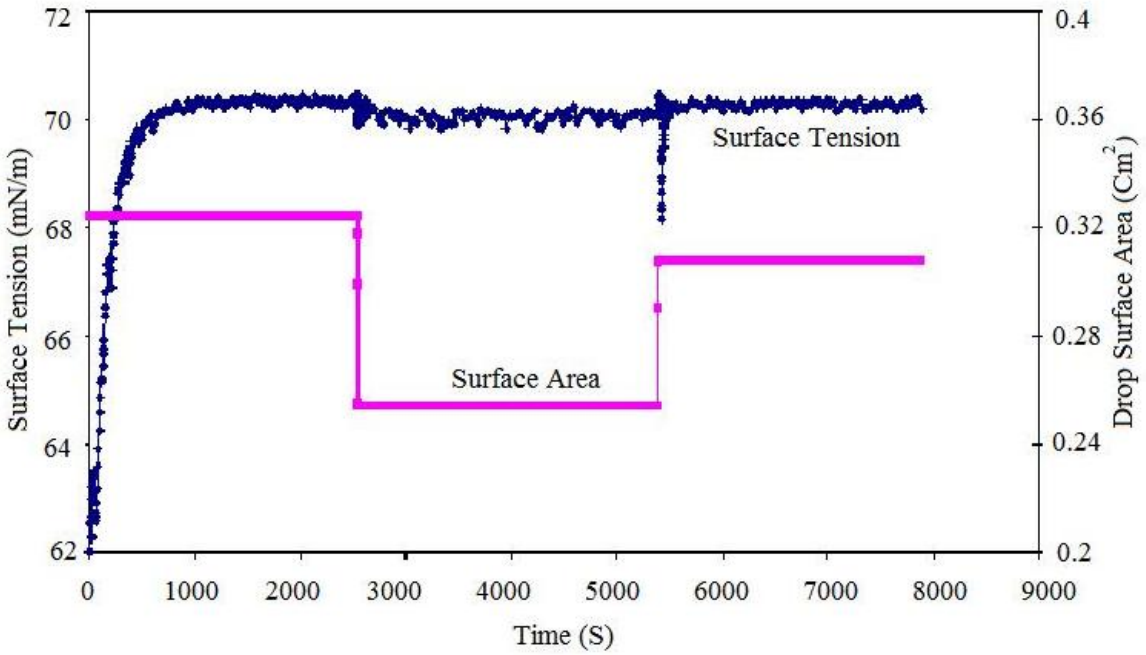

Figure 5.3: Sharp decrease in surface tension in response to increase in surface area when the drop concentration is much greater than the environment concentration ($C_{drop} = 0.8mM$and $C_{env} = 0$(water)).

involved in the expansion experiments are: the amount of reduction in surface tension after expansion ($\Delta\gamma$), the response time delay (Δt), the molecular weight (M), the concentration difference between drop and environment solutions (ΔC) and the change in surface area (ΔS). Time delay is the time interval after which the surface tension responds to the increase in surface area by exhibiting a sharp decrease.

The dimensionless parameter F can be derived:

$$F = \frac{\Delta\gamma(\Delta t)^2}{(M\Delta C)(\Delta C)^{3/2}} \tag{5.1}$$

Figure 5.5 represents a relation between response time versus dimensionless parameter F. Based on the experimental data, a best-fit regression model for this profile can be derived as:

$$\Delta t = KF^{0.4904} \simeq KF^{0.5} \tag{5.2}$$

Table 5.1: Surface tension response to changes in surface area in the expansion experiments (C_{drop} = concentration of the drop solution, C_{env} = concentration of the environment solution, ΔS = changes in surface area, $\Delta\gamma$ = decrease in surface tension, Δt = time delay, and F = dimensionless parameter).

C_{drop}	C_{env}	ΔS	$\Delta\gamma$	Δt	$F \times 10^{-8}$
mol/mL $\times 10^7$	mol/mL $\times 10^7$	m^2	mN/m	Sec	
29.2	0	0.070	27.0	5	0.954
29.2	0	0.045	14.3	1	0.039
29.2	0	0.035	24.8	7	4.384
29.2	8	0.025	8.4	19	20.685
29.2	8	0.021	6.8	25	36.696
29.2	8	0.107	12.7	9	0.767
10	0	0.138	11.9	8	1.133
10	0	0.066	5.3	22	11.556
10	0	0.051	13.7	7	4.469
10	0	0.069	5.4	6.5	0.957
8	0	0.088	7.7	10	2.807
8	0	0.070	5.4	7	1.098
8	0	0.026	2.1	19	13.997
8	0	0.059	1.9	30	11.516
8	0	0.064	0.7	24	2.390
8	0	0.056	1.4	8	0.636
8	0	0.038	2.0	3	0.229
6	0	0.066	0.8	61	22.595
6	0	0.034	1.3	7	1.366
6	0	0.058	1.6	3	0.132
4	0	0.045	2.5	31	19.200
4	0	0.041	2.5	30	20.750
2	0	0.104	2.2	49	12.133

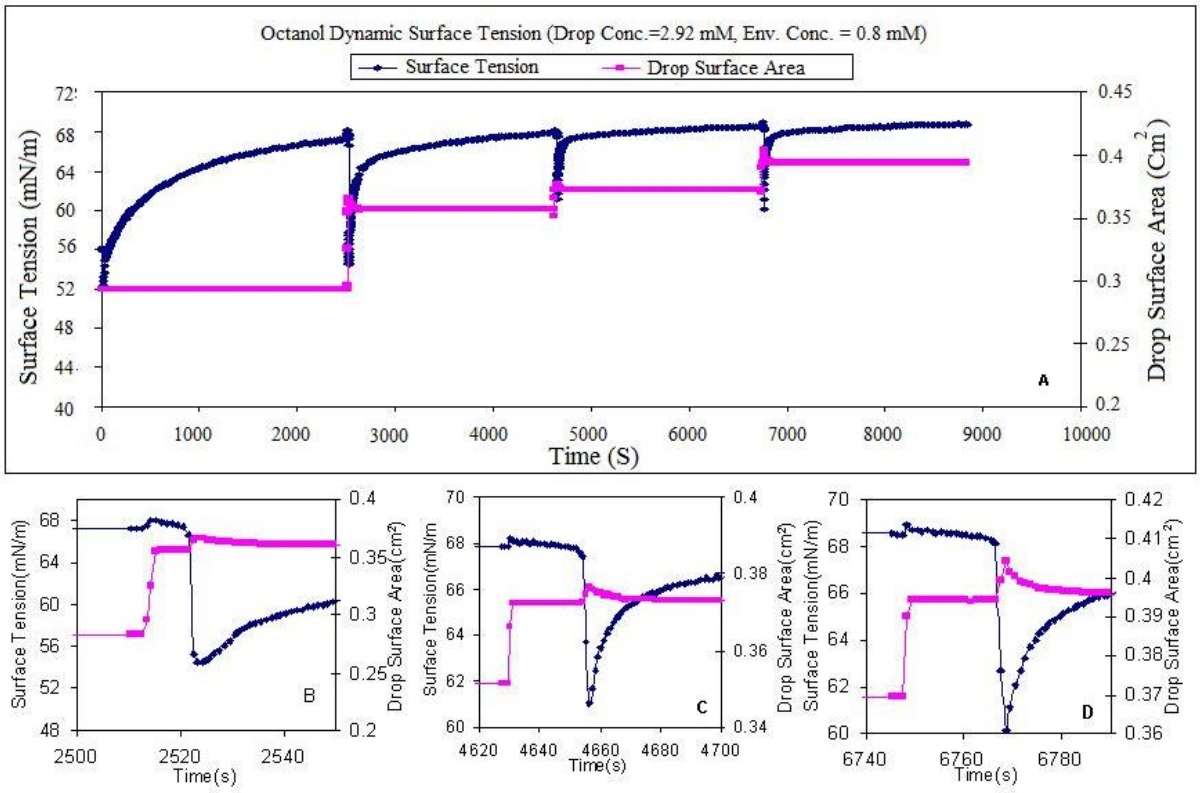

Figure 5.4: A:Effect of changes in surface area on dynamic surface tension of 1-octanol solution when drop concentration is much higher than environment concentration. B,C,D: Three sharp decreases of surface tension due to three increases of surface area ($C_{drop} = 2.92mM$ and $C_{env} = 0.8mM$).

Where K=0.0008s, with $R^2 = 0.8225$

From equation 5.1

$$\Delta t = [\frac{M\Delta C(\Delta S)^{3/2}}{\Delta\gamma}]^{1/2} F^{1/2} \tag{5.3}$$

From equation 5.3 we can conclude that

$$K = [\frac{M\Delta C(\Delta S)^{3/2}}{\Delta\gamma}]^{1/2} = 0.0008 \tag{5.4}$$

or

$$K^2 = \frac{M\Delta C(\Delta S)^{3/2}}{\Delta\gamma} = 64 \times 10^{-8} \tag{5.5}$$

or

$$\Delta\gamma = \frac{M\Delta C(\Delta S)^{3/2}}{64 \times 10^{-8}} \tag{5.6}$$

Using equation 5.6 , one can predict the surface tension response to changes in surface area for a specific molecular weight, concentration difference and change in surface area.

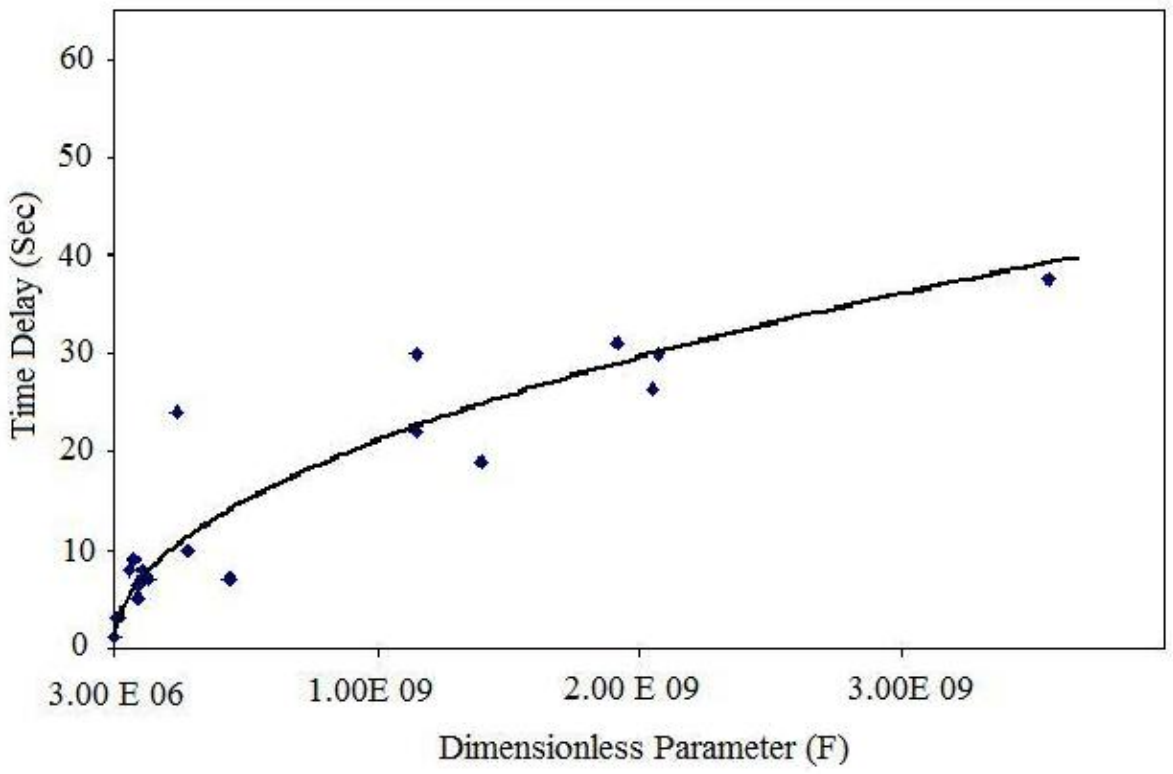

Figure 5.5: Response time versus dimensionless parameter F.

5.3 Summary

The surface tension response of 1-octanol solutions in surface compression and expansion was investigated. The dynamic surface tension was measured under the condition where both liquid and vapor phase adsorption were present. In compression, the surface tension decreased followed by a gradual increase back to the value prior to compression. In expansion, two categories of surface tension response were observed: First, when the change in surface area was smaller than 5%, the behavior similar to that of conventional surfactants was observed. The surface tension increased followed by a gradual decrease back to the value prior to expansion. Second, when the changes in surface area was greater than 5%, and the drop concentration was sufficiently larger than the environment concentration. In this case, the surface tension initially slightly increased; after a time delay, it sharply decreased, which followed by a gradual increase back to the value prior to expansion. For this second category, using the Buckingham Π theorem, a dimensionless parameter for predicting the surface tension response to changes in surface area was derived and the regression model for time delay versus dimensionless parameter F was fitted to the experimental data.

Chapter 6

Screening Experimental Design

In chapter 4 the effects of drop and environment concentrations on the dynamic and steady-state surface tension of 1-octanol, 1-hexanol and 1-butanol aqueous solutions were studied. In chapter 5 the effect of surface perturbations on the dynamic and steady-state surface tension of 1-octanol aqueous solutions was studied. In order to investigate if there is any other significant factor that may affect the steady-state surface tension of 1-octanol solutions, a screening experiment is designed. In this design, the effects of six relevant factors such as: concentration of the environment solution (Factor A), concentration of the sample drop solution (Factor B), the volume of the environment solution (Factor C), the distance between the drop and the environment solution (Factor D), the area of the environment solution (Factor E), and the saturation time —(Factor F), on the steady-state surface tension of 1-octanol solutions are examined.

6.1 Factorial Experimental Design

In this section, the aforementioned factors and their levels, the defining relations, the confounding patterns, the required number of runs, and the steady state surface tension response for each run are addressed. Each factor is considered at two levels. The factors and their levels are illustrated in Table 6.1. Two observations for each possible combination of factors are examined. For full factorial experimental design with six factors and two replications 128 experiments should be performed. In this research only one quarter of 2^6 factorial experiments are considered. Thus, the number of required experiments with two replications is decreased to 32, and the resolution of this design could be equal to four, which is the recommended resolution for good accuracy and minimum number of experiments [58]. The generators for this design are as follows:

E=ABC, and F=BCD

Thus, the defining relations and confounding patterns can be derived as follows:

I= ABCE = BCDF = ADEF

[A] = A + BCE + DEF + ABCDF

[B] = B + ACE + CDF + ABDEF

[C] = C + ABE + BDF + ACDEF

[D] = D + AEF + BCF + ABCDE

[E] = E + ABC + ADF + BCDEF

[F] = F + ADE + BCD + ABCEF

[AB] = AB + CE + ACDF + BDEF

[AC] = AC + BE + ABDF + CDEF

[AD] = AD + EF + BCDE + ABCF

[AE] = AE + BC + DF + ABCDEF

[AF] = AF + DE + BCEF + ABCD

[BD] = BD + CF + ACDE + ABEF

[BF] = BF + CD + ACEF + ABDE

[ABD] = ABD + ACF + BEF + CDE

[ABF] = ABF + ACD + BDE + CEF

The actual and coded values of six factors are illustrated in Table 6.1.

Table 6.1: Actual and coded value of six factors involved in the experimental design

	Actual Value Low	Actual Value High	Coded Value Low	Coded Value High
Factor A	$2 \times 10^{-7} mol/mlit$	$2.92 \times 10^{-6} mol/mlit$	-1	1
Factor B	$4 \times 10^{-7} mol/mlit$	$1 \times 10^{-6} mol/mlit$	-1	1
Factor C	$1 mlit$	$3 mlit$	-1	1
Factor D	$6 mm$	$10 mm$	-1	1
Factor E	$1 cm^2$	$5 cm^2$	-1	1
Factor F	$15 min$	$30 min$	-1	1

Table 6.2 shows the steady state surface tension for 32 experiments at different combinations of factors A-F.

Table 6.2: The steady state surface tension results for 32 experiments at different coded value

Run Number	A	B	C	D	E=ABC	F=BCD	γ_1 mN/m	γ_2 mN/m
1,2	-1	-1	-1	-1	-1	-1	66.07	68.07
3,4	1	-1	-1	-1	1	-1	38.15	35.88
5,6	-1	1	-1	-1	1	1	65.11	67.30
7,8	1	1	-1	-1	-1	1	37.59	36.07
9,10	-1	-1	1	-1	1	1	67.72	68.00
11,12	1	-1	1	-1	-1	1	35.80	36.00
13,14	-1	1	1	-1	-1	-1	68.53	67.65
15,16	1	1	1	-1	1	-1	35.00	36.50
17,18	-1	-1	-1	1	-1	1	68.00	67.19
19,20	1	-1	-1	1	1	1	36.39	35.95
21,22	-1	1	-1	1	1	-1	65.42	67.40
23,24	1	1	-1	1	-1	-1	36.63	36.02
25,26	-1	-1	1	1	1	-1	68.86	68.10
27,28	1	-1	1	1	-1	-1	35.76	35.40
29,30	-1	1	1	1	-1	1	65.01	67.10
31,32	1	1	1	1	1	1	36.40	36.10

6.2 Analysis of One-Quarter Fraction of the 2^6 Experimental Design

Normal probability plot of effects which is a graphical tool to assess whether the effects are significant is illustrated in Figure 6.1. The negligible effects are normally distributed, with mean zero and variance σ^2 and will lie along a straight line on this plot, whereas the significant effects will have non zero means and departure from the line. Based on this plot, only factor A (environment concentration) departures from the line and it does not follow the normal distribution and can be judged as a significant factor. All other factors, which follow the straight line, are not significant. The Analysis Of Variance (ANOVA) statistics for these results are tabulated in Table 6.3. The high value of $F_{observed}$ of factor A supports the idea that only this factor is significant. Thus, only factor A is considered in the model, and the other factors are considered as the error.

Using regression analysis, based on the coded and actual values of factor A, the final equations for predicted value of steady state surface tension for 1-octanol system are as follows:

For coded value of factor A:

$$\gamma = 51.73 - 15.50 \times A \tag{6.1}$$

For real value of factor A:

$$\gamma = 69.49939 - 1.13938 \times 10^7 \times A \tag{6.2}$$

Examining of residuals is a key part of all statistical modelling. Residuals are the elements of variation unexplained by the fitted model. In this set of experiments, the difference between the observation value of the steady state surface tension, and the predicted value based on equation 6.2 can be assessed as the residuals.

The residuals should have the four characters of the random error, if the predicted model is reliable. The random error usually normally distributed, independent, with mean zero and constant variance. The normal probability plot of residuals (Figure 6.2A) is an extremely useful tool for judging whether or not the residuals are randomly distributed. If the data points in the normal probability plot approximately resemble a straight line (Figure 6.2A), it can be concluded that the residuals have a normal distribution. If the model is correct, and if the assumptions are satisfied, the residuals should not reveal any pattern, and they should be structureless and independent. Particularly, they have to be unrelated to the predicted value. Figure 6.2B shows the residuals versus the predicted values for the steady state surface tension data. In this plot no unusual structure is

Table 6.3: The ANOVA table for the steady state surface tension of 1-octanol solutions.

Source	Sum of Square	D.F.	M.S.	$F_{observed}$
Model	7683.66	1	7683.66	7616.99
A	7683.66	1	7683.66	7616.99
Error	30.26	30	1.01	
Lack of Fit	15.42	14	1.10	1.19
Pure Error	14.84	16	0.93	
Total Error	7713.92	31		

apparent. Plot of residuals versus number of runs (Figure 6.2C) is a helpful tool in detecting correlation between the residuals. No correlation can be observed in this graph. The plot of residuals versus the effect of different factors is a tool for assessing whether or not the residuals are independent of the variables. Any pattern in such residual plot imply that the variable affects the response. This suggests that the variable should be either controlled in the next experiments, or included in the analysis. Figure 6.2D-I show the residuals versus the effect of factors A-F. No pattern can be observed in these plots. This imply that the residuals cannot be affected by any factor. From nine different plots of Figure 6.2 it can be concluded that residuals have four characters of a random error, and the predicted model is reliable. Thus, it can be judged that between six relevant factors such as: concentration of the environment solution (Factor A), concentration of the drop solution (Factor B), the volume of the environment solution (Factor C), the distance between the drop and the environment solution (Factor D), the area of the environment solution (Factor E), and the saturation time (Factor F), included in the analysis, only factor A (concentration of the environment solution) has significant effect on the steady state surface tension of 1-octanol aqueous solutions, and the effect of other five factors can be considered as the error. This result supports the previous results on chapters 4 and 5 that steady-state surface tension of volatile organic amphiphiles in aqueous solution is only affected by the adsorption/desorption from the vapor side of the surface.

6.3 Summary

In this chapter the effect of six different factors such as: concentration of the environment solution (Factor A), concentration of the sample drop solution (Factor B), the volume of the environment solution (Factor C), the distance between the drop and the environment solution (Factor D), the area of the environment solution (Factor E), and the saturation

time (Factor F) was investigated on the steady-state surface tension of 1-octanol aqueous solutions. Using an experimental design, it was found that only concentration of the environment solution (Factor A) had significant effect on the steady-state surface tension of 1-octanol aqueous solution. This result was supported by the analysis of variance and normal probability plot. No unusual structure was observed in the residual plots, which proved that the experimental results were reliable and only concentration of the environment solution had significant effect on the steady-state surface tension of 1-octanol aqueous solutions.

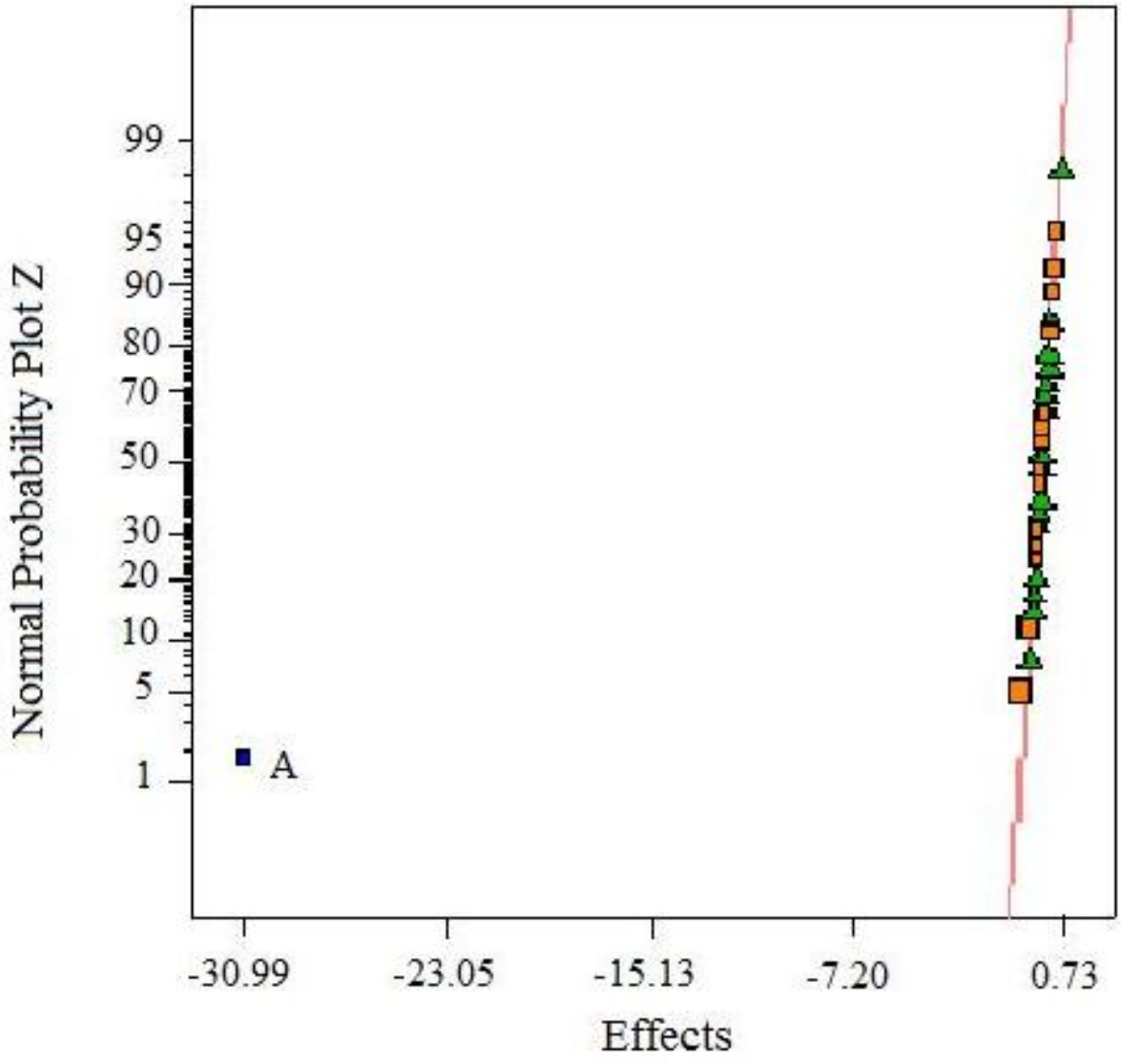

Figure 6.1: Normal probability plot of effects for the steady state surface tension of 1-octanol aqueous solutions

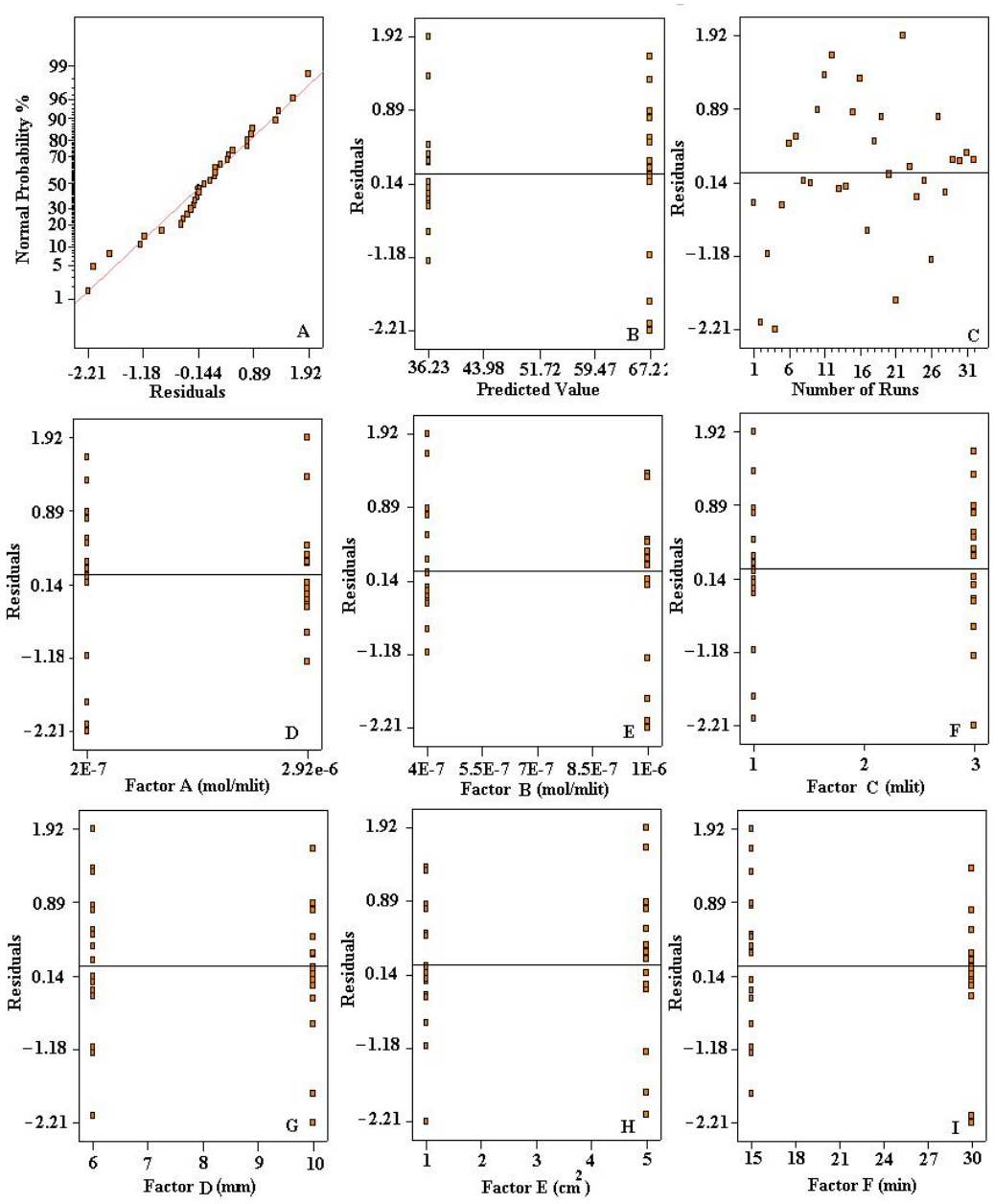

Figure 6.2: (A) Normal probability plot of residuals, (B) Residuals versus predicted value based on equation (6.1), (C) Residuals versus number of runs, (D) Residuals versus factor A, (E) Residuals versus factor B, (F) Residuals versus factor C, (G) Residuals versus factor D, (H) Residuals versus factor E, (I) Residuals versus factor F.

Chapter 7

Effect of Temperature on the Surface Tension of 1-Octanol, 1-Hexanol and 1-Butanol Aqueous Solutions

This chapter describes the effect of temperature on the surface tension and adsorption kinetics of 1-octanol, 1-hexanol and 1-butanol aqueous solutions. The experiments are performed in a closed chamber where both liquid and vapor phases co-existed, and the surface tension is influenced by a combination of liquid and vapor phase adsorption. The steady-state and dynamic surface tension of the aqueous solutions of these chemicals are measured at temperature ranging from 10 to 35 °C. The modified Langmuir equation of state and the modified kinetic transfer equation are used to model the experimental data of the steady-state and dynamic (time-dependent) surface tension, respectively. The equilibrium constants and adsorption rate constants are evaluated through non-linear regression for temperatures ranging from 10 to 35 °C.

7.1 Introduction

Previous studies showed that the dynamic adsorption behavior of normal alcohols with short carbon chains is controlled by the transfer of surfactant molecules from the subsurface to the surface [14, 32]. When an interface is formed between two bulk phases, physical properties like the density vary rapidly and continuously from one bulk to another. However, because the interface region is very thin, this effect is limited and does not extend beyond several molecule diameters to each side of the interface. The subsurface denotes the position inside the bulk phase with a few molecular diameters thick. Previous studies also showed that the diffusion from the bulk to the subsurface is very fast compared to the

transfer of molecules from the subsurface to the surface. In chapters 4-6, it was illustrated that when a volatile surfactant, such as 1-octanol, 1-hexanol and 1-butanol, is dissolved in a liquid, it presents a finite partial pressure in the vapor phase, and the surface tension of the solution can be affected by surfactant adsorption from both sides of the vapor/liquid interface[25, 59, 60, 61]. In chapters 4-6 it was shown that at initial condition the effect of adsorption from liquid side is important and the surface tension profile starts at different point depending on the concentration of the drop solution. It was found that at the steady-state, the effect of adsorption from the vapor side is more significant than that from the liquid side [25, 59, 60, 61]. In the current chapter, the effect of adsorption from both sides of a vapour/liquid interface was considered simultaneously. In practice, temperature is an important parameter and may have a significant effect on the surface tension and its applications [28, 29, 30]. The main goal of this chapter is to investigate the effect of temperature on the surface tension and adsorption dynamics of 1-octanol, 1-hexanol and 1-butanol in aqueous solutions. These chemicals are used as the ingredient in foods, wines, flavors, perfumes and as a substitute for gasoline and diesel fuel [102, 103, 104, 105]. 1-hexanol is also used as the promoter of mRNA release in the presence of Ttgv protein [27]. In all cases, the temperature can change the surface tension of these chemicals, hence the efficiency of the applications [27, 28, 29, 30, 31]. In this chapter, dynamic and steady-state surface tensions are measured using an Axisymmetric Drop Shape Analysis-Profile (ADSA-P) method for a temperature range from 10 °C to 35 °C. The concentration of 1-octanol aqueous solutions changes from 0.2 mM to 2.92 mM (about 70% of 1-octanol solubility in water). The concentration of 1-hexanol aqueous solutions varies from 2.0 mM to 30.0 mM (about 52% of 1-hexanol solubility in water). The concentration of 1-butanol aqueous solutions changes from 20 mM to 400 mM (about 38% of 1-butanol solubility in water).

7.2 Experimental Section

7.2.1 Materials

The chemical 1-octanol, 1-hexanol and 1-butanol with purity greater than 99% , was purchased from Sigma-Aldrich (Oakville, Ontario, Canada). The water used was purified by an ultra-pure water system (Millipore Ltd., Mississauga, Ontario, Canada), with resistivity of 18.2 MW. The relative humidity of the environment during the experiments was around 80%. Four different concentrations: 0.2, 0.6, 1 , and 2.92 mM for 1-octanol, four different concentrations: 2.0, 5.0, 9.0, and 30.0 mM for 1-hexanol and four different concentrations: 20, 40, 100, and 400 mM for 1-butanol were prepared. They were used in preparation of both the sample drop solution (C_{drop}) and the environment solution (C_{env}).

The sample with the highest concentration was prepared as the stock solution, and the lower concentration samples were made by diluting the stock solution.

7.2.2 Surface Tension Measurement

Different methods have been used for measuring surface tension[46, 47]. Among them, drop shape methods are distinguished by the fact that the surface tension of a solution is obtained based on the shape of a liquid drop (or a bubble formed inside the liquid) [48]. In this research, Axisymmetric Drop Shape Analysis-Profile (ADSA-P) method was used for surface tension measurements. The temperature of the chamber containing environment solution was controlled using a RTE 111 NesLab circulating bath. At each combination of the concentrations of the drop and environment solutions, the dynamic surface tension was measured at six different temperatures (10 °C, 15 °C, 20 °C, 25 °C, 30 °C and 35 °C).

7.3 Theoretical Framework: Kinetic Transfer Equation

The change in surface concentration over time can be expressed as the net rate of adsorption minus the net rate of desorption:

$$\frac{d\Gamma}{dt} = (r_a^g + r_a^l) - (r_d^g + r_d^l) \tag{7.1}$$

Where r_a^g and r_a^l are the rates of adsorption from the vapor and the liquid phase, respectively, and r_d^g and r_d^l are the rates of desorption to the vapor and the liquid phase, respectively. The developed model assumed to follow the Langmuir kinetics [27] where the rate of desorption is proportional to the surface coverage (Γ). The rate of adsorption from the vapor phase is proportional to the vapor pressure (P) and the number of vacant adsorption sites at the interface ($\Gamma_\infty - \Gamma$), where Γ_∞ is the maximum surface concentration. The rate of adsorption from the liquid phase is proportional to the surfactant concentration in the liquid phase (C_{drop}) and the number of vacant adsorption sites at the interface ($\Gamma_\infty - \Gamma$). Substituting in the appropriate expressions for the rates of adsorption and desorption gives the following equations:

$$r_a^g = k_a^g P\,(\Gamma_\infty - \Gamma) \tag{7.2}$$

$$r_a^l = k_a^l C_{drop}\,(\Gamma_\infty - \Gamma) \tag{7.3}$$

$$r_d^g = k_d^g \Gamma \tag{7.4}$$

$$r_d^l = k_d^l \Gamma \tag{7.5}$$

Where k_a^g and k_a^l are the adsorption rate constant from the vapor phase and liquid phase, respectively. k_d^g and k_d^l are the desorption rate constant to the vapor phase and liquid phase, respectively. Using equations 7.2 to 7.5, equation 7.1 is simplified as follows:

$$\frac{d\Gamma}{dt} = k_a^g P(\Gamma_\infty - \Gamma) + k_a^l C_{drop}(\Gamma_\infty - \Gamma) - (k_d^g + k_d^l)\Gamma \tag{7.6}$$

For the rate of adsorption from the vapor phase, the partial pressure of surfactant (P) is related to the concentration of the environment solution (C_{env}) through Henry′s Law ($P = HC_{env}$). It should be noted that the Henry′s law constant has been incorporated into k_a^g so that the units of the adsorption rates constants are uniform. For solution purposes, it is desirable to reduce the number of unknown constants in equation 7.6 using the equilibrium adsorption constants for adsorption from the vapor phase (K_1) and the liquid phase (K_2). From their definitions, the following simplifications can be made:

$$K_1 = \frac{k_a^g}{k_d^g + k_d^l} \tag{7.7}$$

$$K_2 = \frac{k_a^l}{k_d^g + k_d^l} \tag{7.8}$$

Substitution into equation 6 eliminates all but one of the kinetic rate constants:

$$\frac{d\Gamma}{dt} = k_a^g \left(C_{env} + \frac{K_2}{K_1} C_{drop} \right) (\Gamma_\infty - \Gamma) - \frac{k_a^g}{K_1 + K_2} \left(1 + \frac{K_2}{K_1} \right) \Gamma \tag{7.9}$$

Equation 7.9 is a first order ordinary differential equation and can be solved to give the surface concentration of the surfactant as a function of time (7.10).

$$\Gamma = \frac{b}{a} + \left(\Gamma_{min} - \frac{b}{a} \right) exp(-at) \tag{7.10}$$

$$a = \left(C_{env} + \left(\frac{K_2}{K_1} \right) C_{drop} + \frac{1}{K_1} \right) k_a^g \tag{7.11}$$

$$b = \left(C_{env} + \left(\frac{K_2}{K_1} \right) C_{drop} \right) k_a^g \Gamma_\infty \tag{7.12}$$

Where Γ_{min} is the minimum surface concentration (at the beginning of each experiment). The surface concentration can be related to the surface tension through Frumkin equation (7.13), which is consistent with the Langmuir-type adsorption kinetics [37]:

$$\gamma = \gamma_0 + RT\Gamma_\infty ln \left(1 - \frac{\Gamma}{\Gamma_\infty} \right) \tag{7.13}$$

where γ is the dynamic surface tension of solution, γ_0 is the surface tension of pure solvent (water), and R is the universal gas constant. Substitution equation 7.10 into equation 7.13 eliminates the surface concentration Γ:

$$\gamma = \gamma_0 + RT\Gamma_\infty ln \left(1 - \frac{\frac{b}{a} + (\Gamma_{min} - \frac{b}{a}) exp(-at)}{\Gamma_\infty} \right) \tag{7.14}$$

A theoretical prediction of dynamic surface tension can be achieved from equation 7.14 , and the fitting parameters including the adsorption rate constant from the vapor phase (k_a^g), the maximum surface concentration (Γ_∞), and the initial surface concentration (Γ_{min}) can be evaluated through nonlinear regression with experimental data of $\gamma(t)$. The equilibrium constant for adsorption from the vapor phase (K_1) and the equilibrium constant for adsorption from the liquid phase (K_2) are evaluated through nonlinear regression with experimental data of the steady-state surface tension. In the next section the kinetic transfer equation (7.14) will be fitted to the experimental data for 1-octanol, 1-hexanol and 1-butanol solutions at temperatures ranging from 10 °C to 35 °C and a wide variety of concentrations of drop (C_{drop}) and environment solutions (C_{env}).

Under the steady-state condition, the overall rate of adsorption is equal to the overall rate of desorption. Equating the expressions for the rates of adsorption and desorption and simplifying the equation using the Frumkin equation (7.13) leads to the modified Langmuir equation of state:

$$\gamma = \gamma_0 - RT\Gamma_\infty ln \left(1 + K_1 C_{env} + K_2 C_{drop} \right) \tag{7.15}$$

Equation 7.15 can also be evaluated from equation 7.14 when $t \longrightarrow \infty$. The modified Langmuir equation of state (7.15) can be used for predicting the steady-state surface tension of an aqueous surfactant solution. The maximum surface concentration (Γ_∞), the equilibrium constant for adsorption from the vapor phase (K_1) and the equilibrium

constant for adsorption from the liquid phase (K_2) can be evaluated through nonlinear regression with experimental data of the steady-state surface tension.

7.4 Effect of Temperature on the Steady-State and Dynamic Surface Tension

Using the outlined experimental procedure, the dynamic and steady-state surface tension of 1-octanol, 1-hexanol and 1-butanol aqueous solutions was measured at the six different temperatures and four different concentrations for the environment solutions and drop solutions of each chemical. Each experiment repeated three times to ensure that the results are reproducible. The reproducibility test of the surface tension values showed that the results were reproducible with the 95% confidence intervals less than 0.2 mN/m. A total of 96 profiles were collected for each chemical and divided into four different categories based on the concentrations of the environment solution. The concentrations of the environment solutions for 1-octanol were: 0.2mM (Figure 7.1), 0.6mM (Figure 7.2), 1mM (Figure 7.3) and 2.92mM (Figure 7.4). The concentration of the environment solutions for 1-hexanol were: 2mM (Figure 7.5), 5mM (Figure 7.6), 9mM (Figure 7.7) and 30mM (Figure 7.8). The concentrations of the environment solutions for 1-butanol were: 20mM (Figure 7.9), 60mM (Figure 7.10), 100mM (Figure 7.11) and 400mM (Figure 7.12). Each figure divided into six charts based on the environment temperature during the experiments. Four different profiles can be observed in each figure. These profiles are related to different drop concentrations. In all of these 288 profiles, the dynamic surface tension initially increases if the concentration of the environment solution is less than that of the drop solution, eventually reaching a plateau value. The dynamic surface tension initially decreases if the concentration of the environment solution is greater than that of the drop solution. The surface tension essentially remains constant when the concentration of the drop solution is as same as the concentration of the environment solution. At a specific temperature, the final steady-state surface tension for each component is almost identical for all profiles with the same environment concentration regardless of the drop concentration. Similar experimental results have been observed in chapter 4. In Figures 7.1-7.12, the reduction of the steady-state surface tension can be observed when temperature increases from 10 °C (A) to 35 °C (F). In all profiles, solid lines represent the theoretical predictions from the kinetic transfer equation (equation 7.14). In the next section the effect of temperature on the steady-state surface tension and adsorption kinetics of 1-octanol, 1-hexanol and 1-butanol is studied.

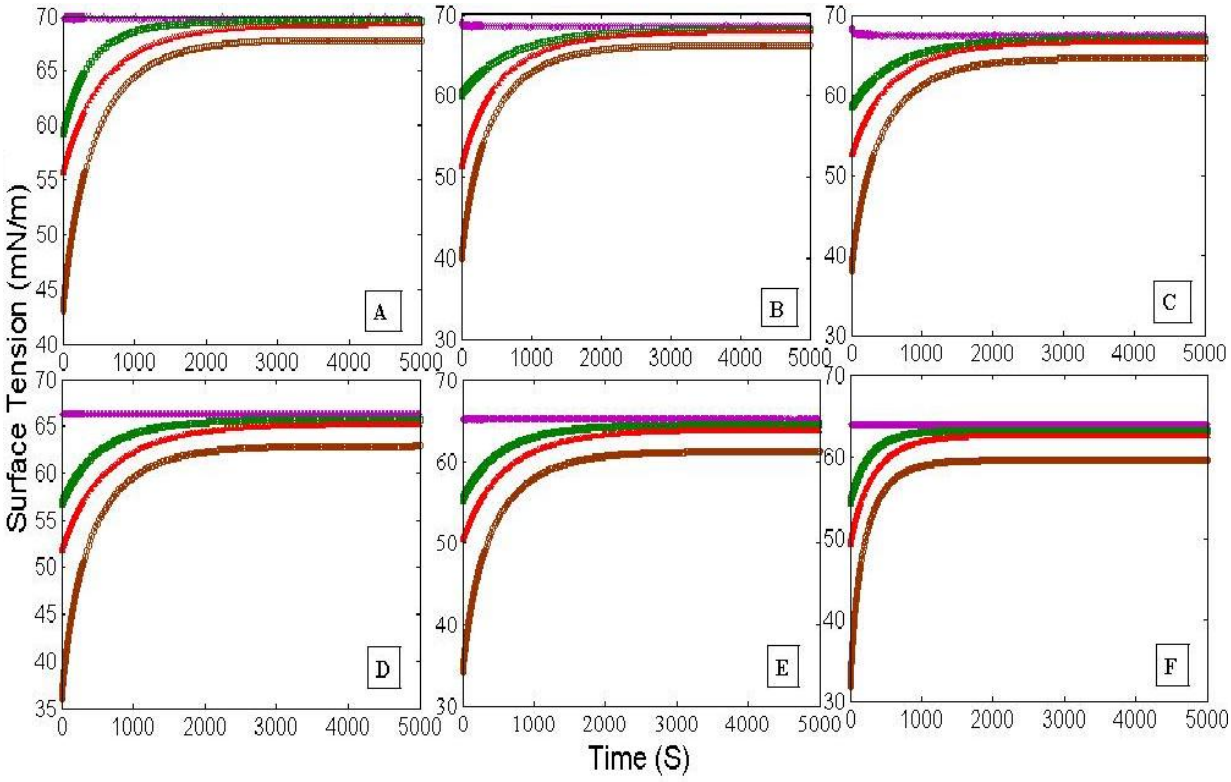

Figure 7.1: Effect of temperature on the surface tension of 1-octanol solution [Concentration of the environment solution (C_{env}) is 0.2mM in all experiments, and Concentrations of the drop solutions (C_{drop}) are 0.2mM (purple), 0.6mM (green), 1mM (red), and 2.92mM (brown)]. Each graph represents a different temperature; (A) 10 °C, (B) 15 °C, (C) 20 °C, (D) 25 °C, (E) 30 °C, (F) 35 °C. Solid lines represent theoretical predictions from the kinetic transfer equation (equation 7.14).

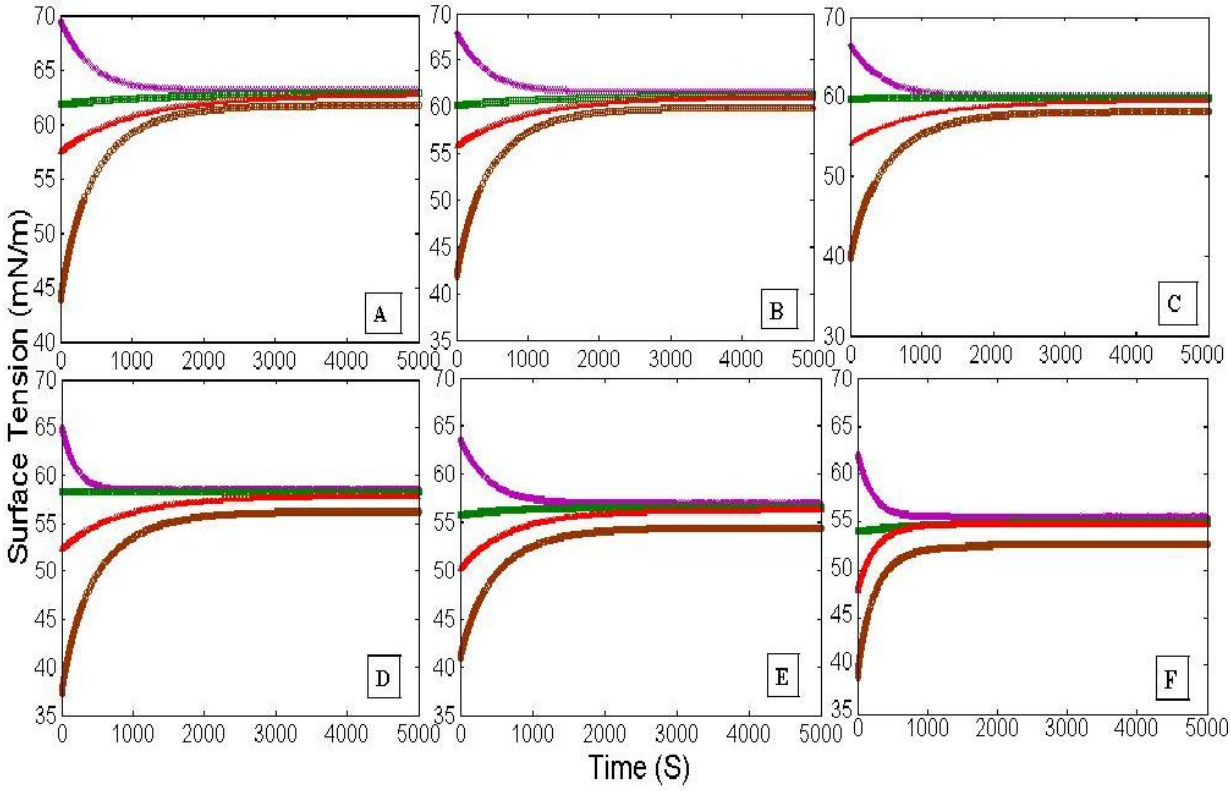

Figure 7.2: Effect of temperature on the surface tension of 1-octanol solution [Concentration of the environment solution (C_{env}) is 0.6mM in all experiments, and Concentrations of the drop solutions (C_{drop}) are 0.2mM (purple), 0.6mM (green), 1mM (red), and 2.92mM (brown)]. Each graph represents a different temperature; (A) 10 °C, (B) 15 °C, (C) 20 °C, (D) 25 °C, (E) 30 °C, (F) 35 °C. Solid lines represent theoretical predictions from the kinetic transfer equation (equation 7.14).

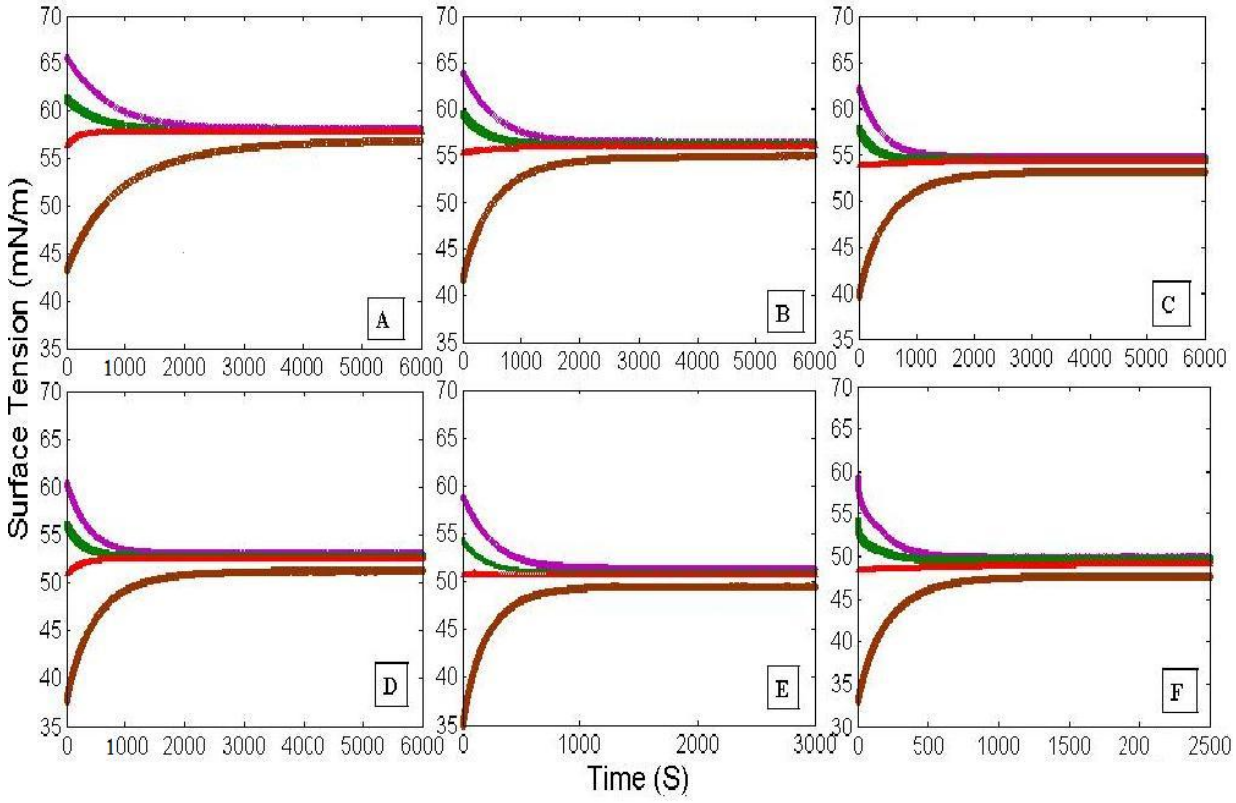

Figure 7.3: Effect of temperature on the surface tension of 1-octanol solution [Concentration of the environment solution (C_{env}) is 1mM in all experiments, and Concentrations of the drop solutions (C_{drop}) are 0.2mM (purple), 0.6mM (green), 1mM (red), and 2.92mM (brown)]. Each graph represents a different temperature; (A) 10 °C, (B) 15 °C, (C) 20 °C, (D) 25 °C, (E) 30 °C, (F) 35 °C. Solid lines represent theoretical predictions from the kinetic transfer equation (equation 7.14).

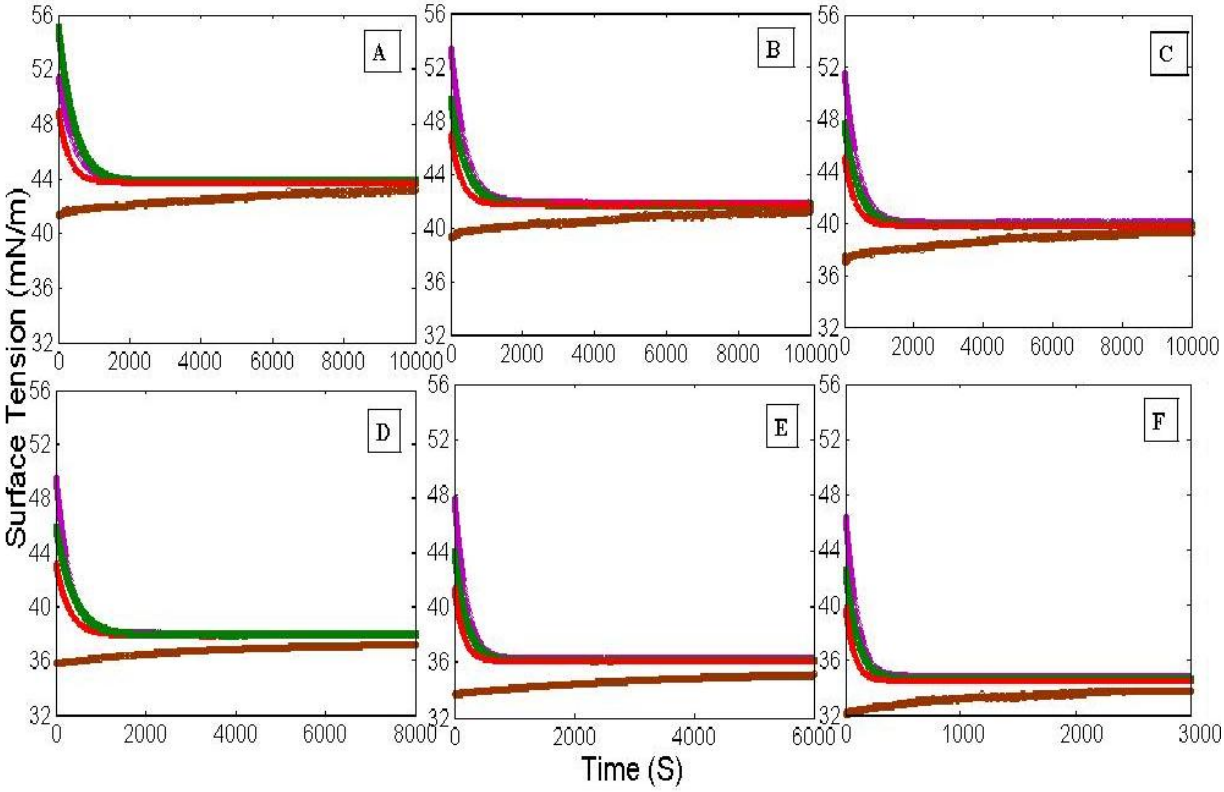

Figure 7.4: Effect of temperature on the surface tension of 1-octanol solution [Concentration of the environment solution (C_{env}) is 2.92mM in all experiments, and Concentrations of the drop solutions (C_{drop}) are 0.2mM (purple), 0.6mM (green), 1mM (red), and 2.92mM (brown)]. Each graph represents a different temperature; (A) 10 °C, (B) 15 °C, (C) 20 °C, (D) 25 °C, (E) 30 °C, (F) 35 °C. Solid lines represent theoretical predictions from the kinetic transfer equation (equation 7.14).

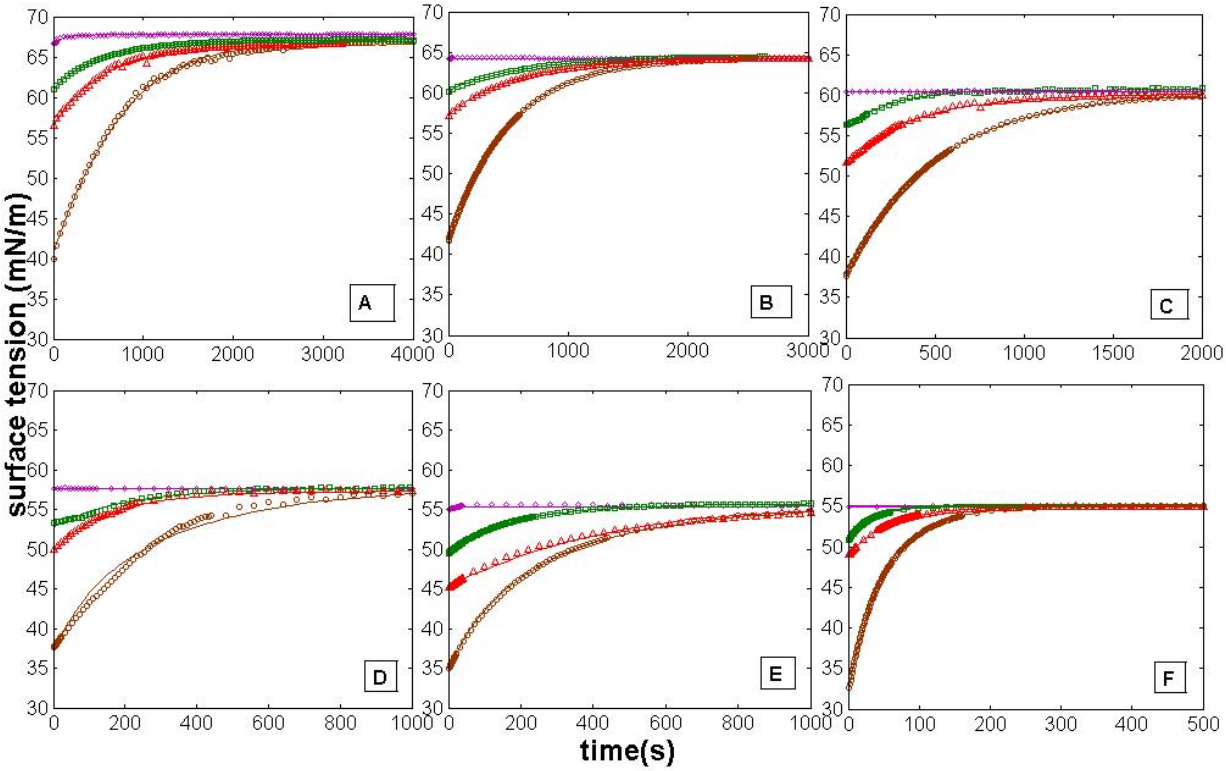

Figure 7.5: Effect of temperature on the surface tension of 1-hexanol solution [Concentration of the environment solution (C_{env}) is 2mM in all experiments, and Concentrations of the drop solutions (C_{drop}) are 2mM (purple), 5mM (green), 9mM (red), and 30mM (brown)]. Each graph represents a different temperature; (A) 10 °C, (B) 15 °C, (C) 20 °C, (D) 25 °C, (E) 30 °C, (F) 35 °C. Solid lines represent theoretical predictions from the kinetic transfer equation (equation 7.14).

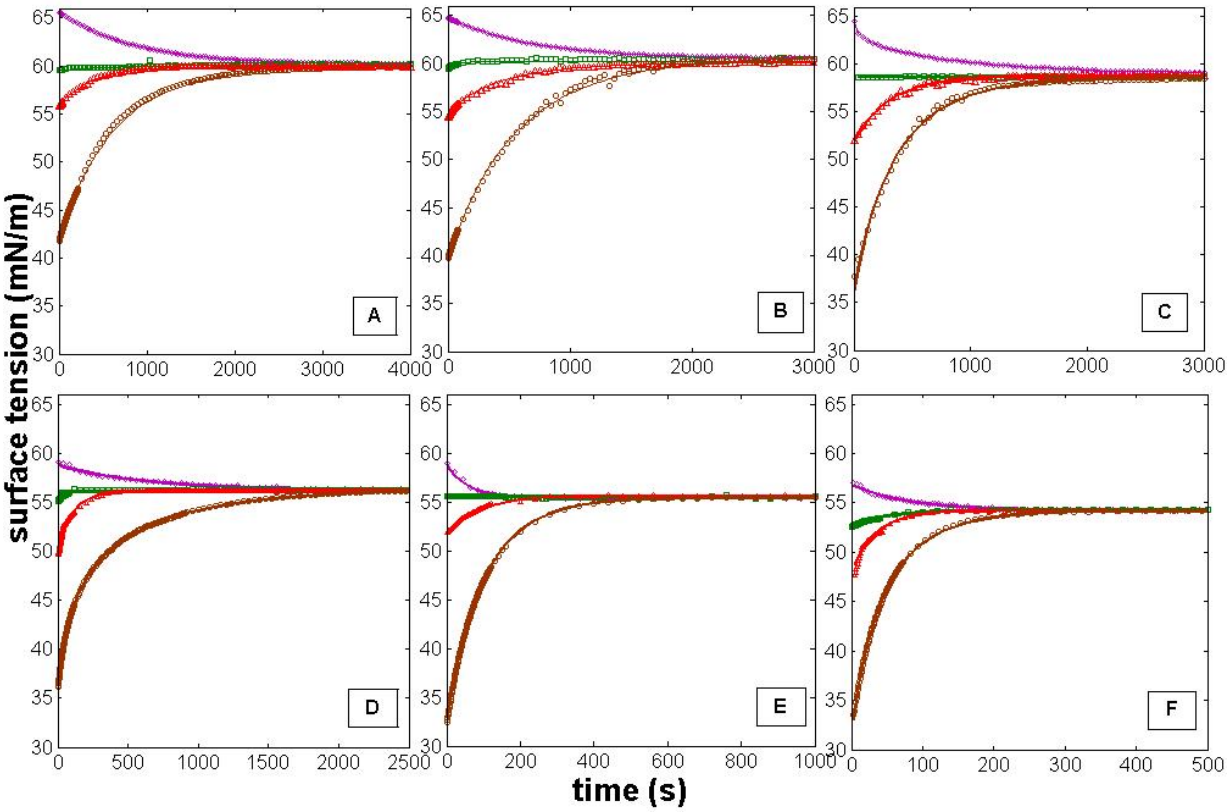

Figure 7.6: Effect of temperature on the surface tension of 1-hexanol solution [Concentration of the environment solution (C_{env}) is 5mM in all experiments, and Concentrations of the drop solutions (C_{drop}) are 2mM (purple), 5mM (green), 9mM (red), and 30mM (brown)]. Each graph represents a different temperature; (A) 10 °C, (B) 15 °C, (C) 20 °C, (D) 25 °C, (E) 30 °C, (F) 35 °C. Solid lines represent theoretical predictions from the kinetic transfer equation (equation 7.14).

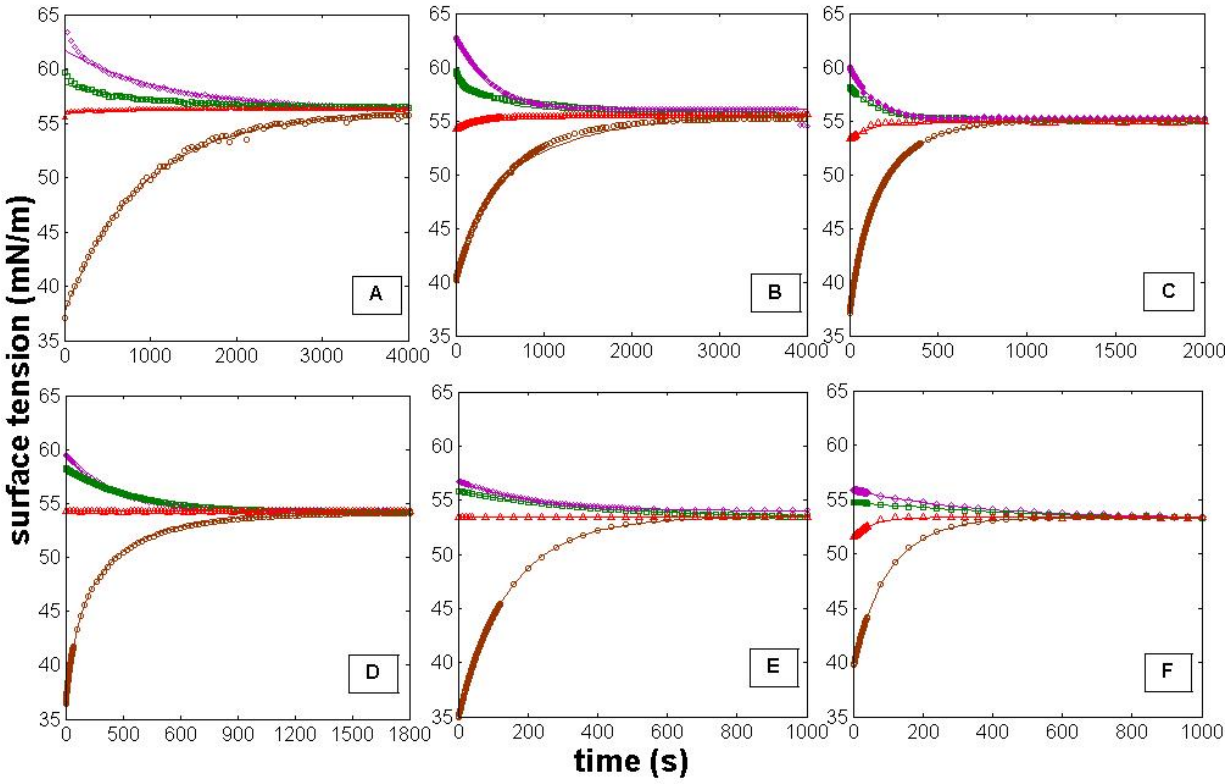

Figure 7.7: Effect of temperature on the surface tension of 1-hexanol solution [Concentration of the environment solution (C_{env}) is 9mM in all experiments, and Concentrations of the drop solutions (C_{drop}) are 2mM (purple), 5mM (green), 9mM (red), and 30mM (brown)]. Each graph represents a different temperature; (A) 10 °C, (B) 15 °C, (C) 20 °C, (D) 25 °C, (E) 30 °C, (F) 35 °C. Solid lines represent theoretical predictions from the kinetic transfer equation (equation 7.14).

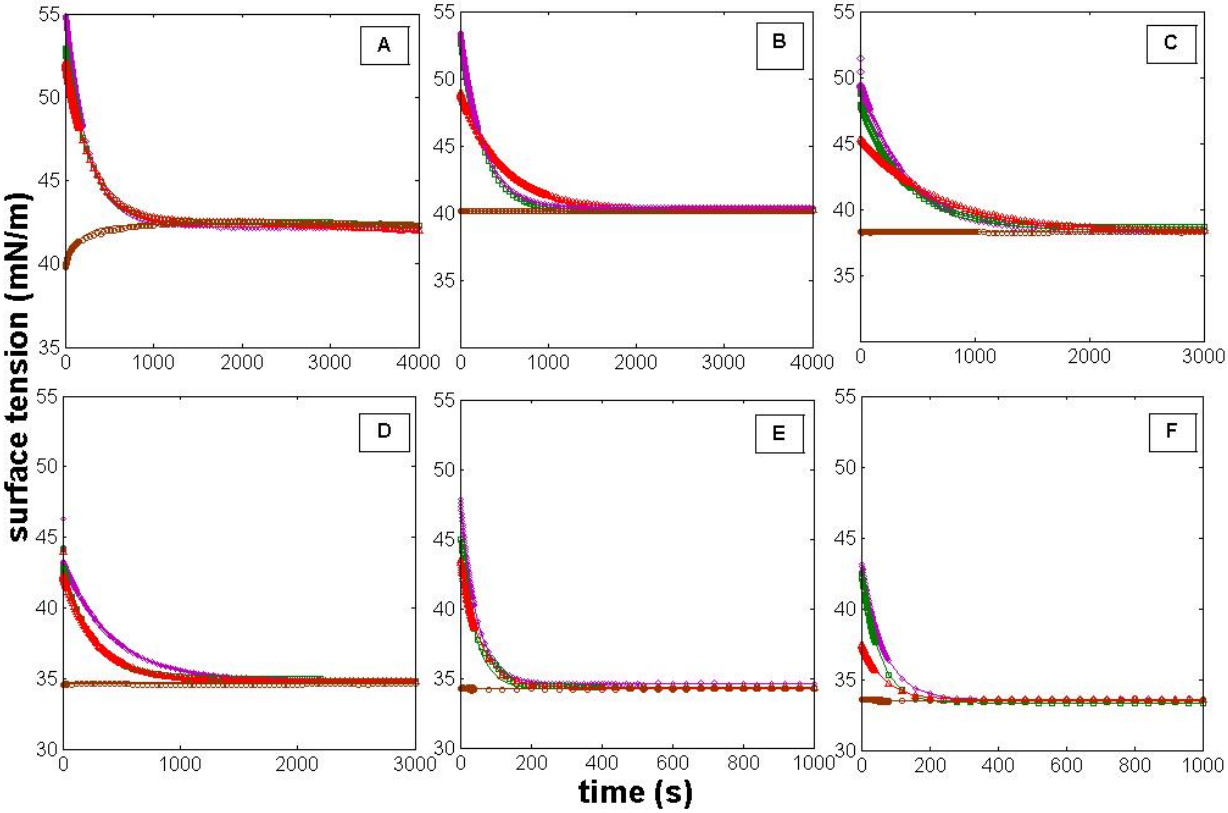

Figure 7.8: Effect of temperature on the surface tension of 1-hexanol solution [Concentration of the environment solution (C_{env}) is 30mM in all experiments, and Concentrations of the drop solutions (C_{drop}) are 2mM (purple), 5mM (green), 9mM (red), and 30mM (brown)]. Each graph represents a different temperature; (A) 10 °C, (B) 15 °C, (C) 20 °C, (D) 25 °C, (E) 30 °C, (F) 35 °C. Solid lines represent theoretical predictions from the kinetic transfer equation (equation 7.14).

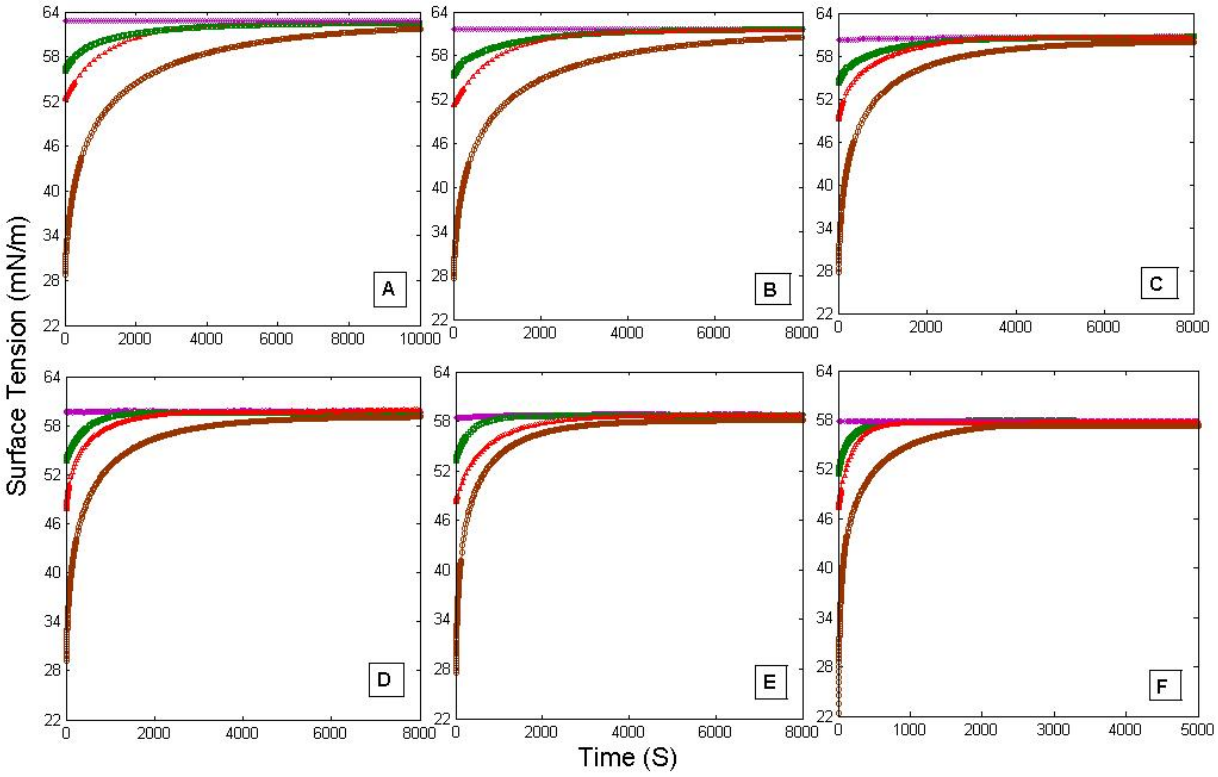

Figure 7.9: Effect of temperature on the surface tension of 1-butanol solution [Concentration of the environment solution (C_{env}) is 20mM in all experiments, and Concentrations of the drop solutions (C_{drop}) are 20mM (purple), 60mM (green), 100mM (red), and 400mM (brown)]. Each graph represents a different temperature; (A) 10 °C, (B) 15 °C, (C) 20 °C, (D) 25 °C, (E) 30 °C, (F) 35 °C. Solid lines represent theoretical predictions from the kinetic transfer equation (equation 7.14).

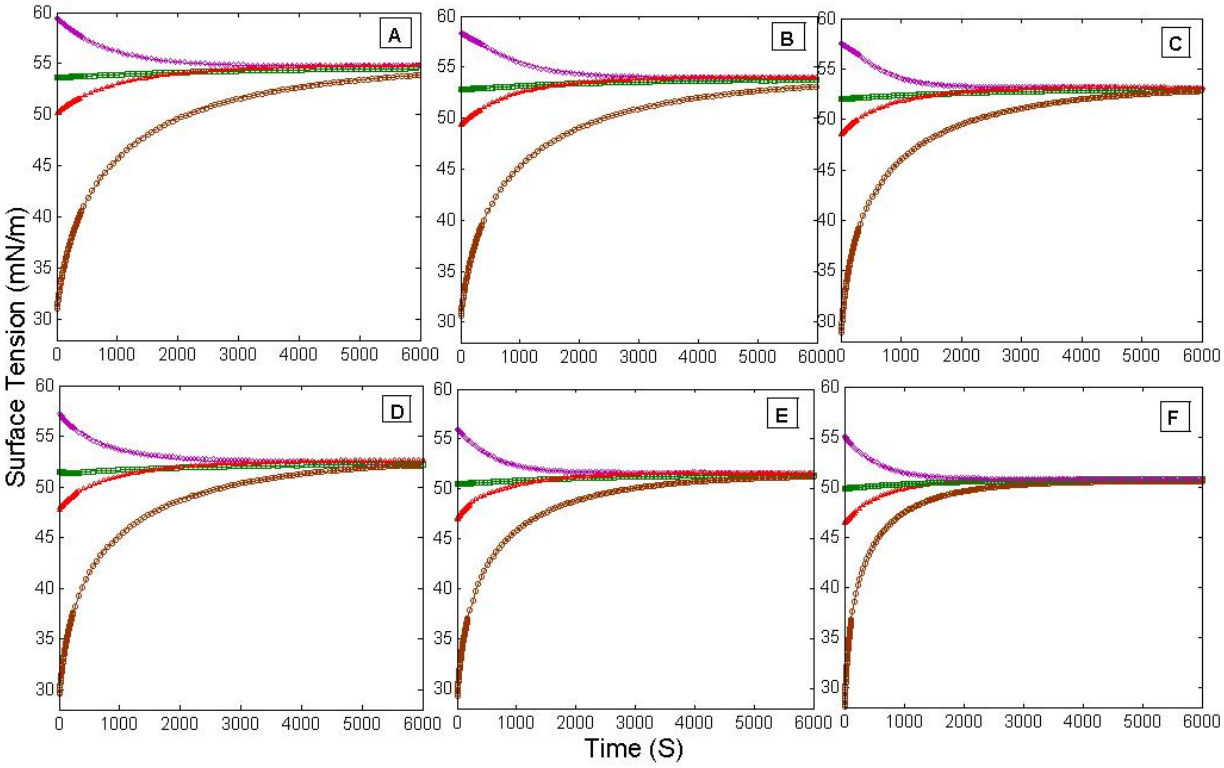

Figure 7.10: Effect of temperature on the surface tension of 1-butanol solution [Concentration of the environment solution (C_{env}) is 60mM in all experiments, and Concentrations of the drop solutions (C_{drop}) are 20mM (purple), 60mM (green), 100mM (red), and 400mM (brown)]. Each graph represents a different temperature; (A) 10 °C, (B) 15 °C, (C) 20 °C, (D) 25 °C, (E) 30 °C, (F) 35 °C. Solid lines represent theoretical predictions from the kinetic transfer equation (equation 7.14).

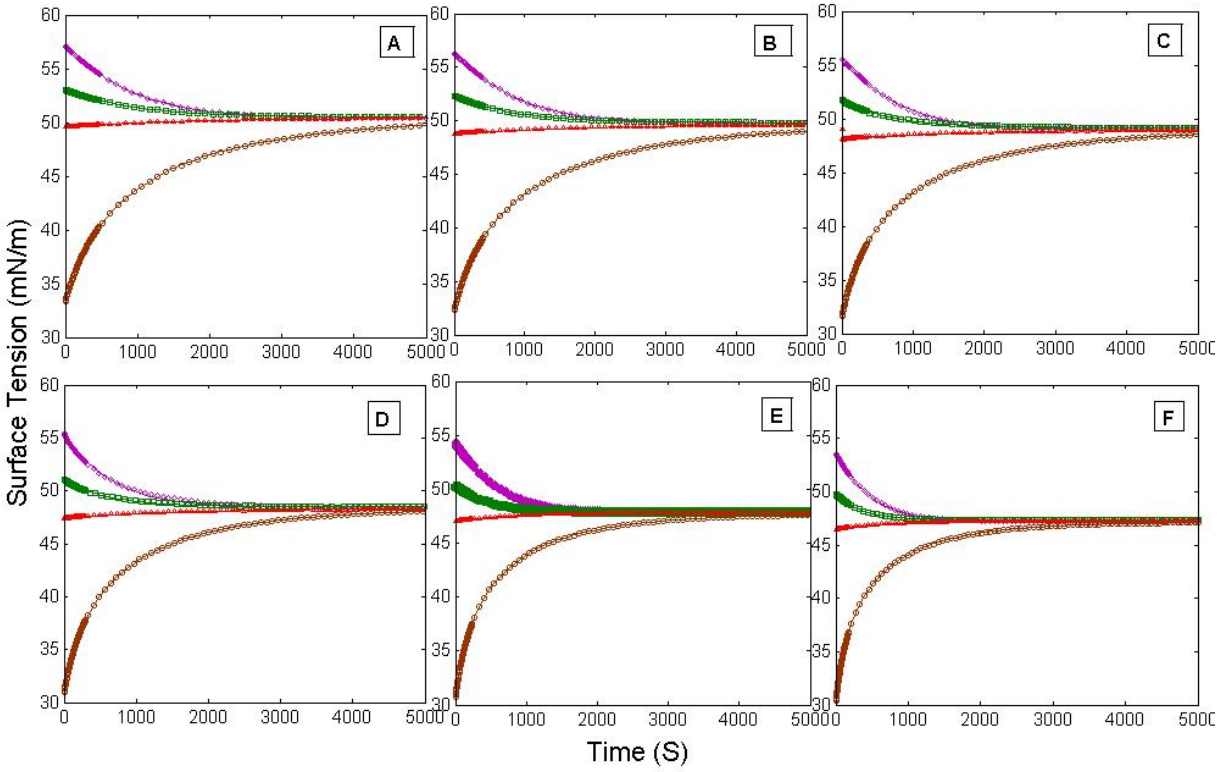

Figure 7.11: Effect of temperature on the surface tension of 1-butanol solution [Concentration of the environment solution (C_{env}) is 100mM in all experiments, and Concentrations of the drop solutions (C_{drop}) are 20mM (purple), 60mM (green), 100mM (red), and 400mM (brown)]. Each graph represents a different temperature; (A) 10 °C, (B) 15 °C, (C) 20 °C, (D) 25 °C, (E) 30 °C, (F) 35 °C. Solid lines represent theoretical predictions from the kinetic transfer equation (equation 7.14).

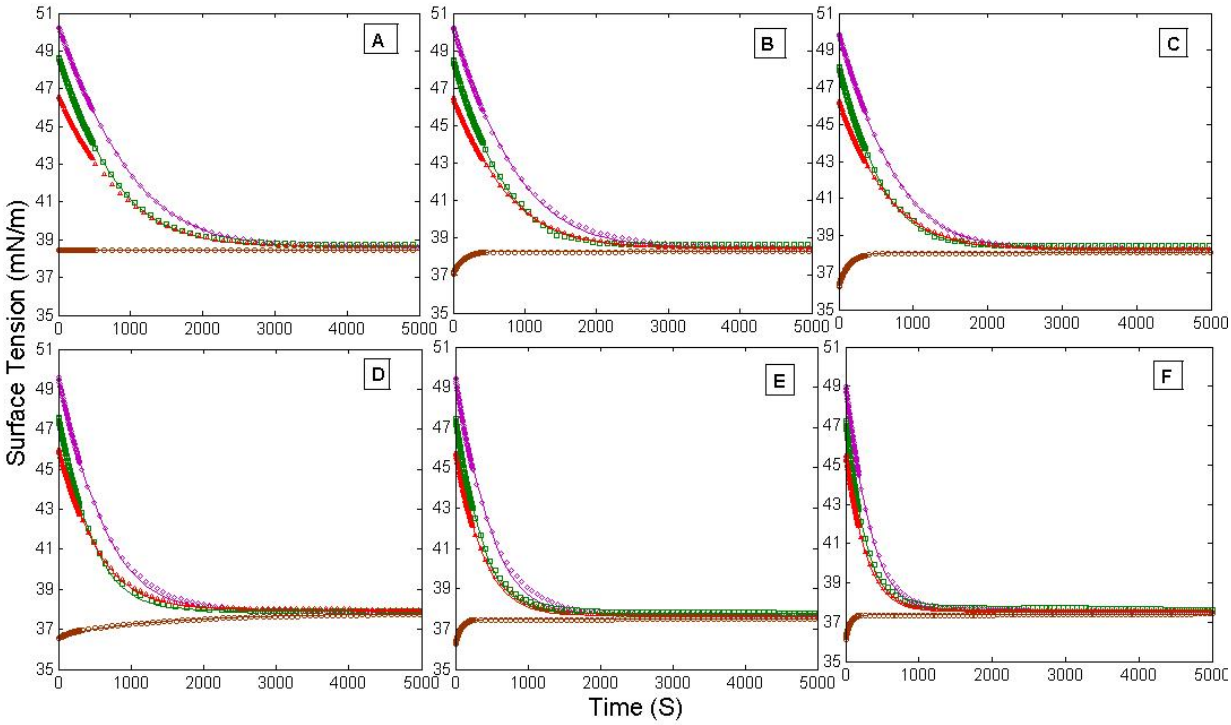

Figure 7.12: Effect of temperature on the surface tension of 1-butanol solution [Concentration of the environment solution (C_{env}) is 400mM in all experiments, and Concentrations of the drop solutions (C_{drop}) are 20mM (purple), 60mM (green), 100mM (red), and 400mM (brown)]. Each graph represents a different temperature; (A) 10 °C, (B) 15 °C, (C) 20 °C, (D) 25 °C, (E) 30 °C, (F) 35 °C. Solid lines represent theoretical predictions from the kinetic transfer equation (equation 7.14).

7.4.1 Effect of Temperature on the Steady-State Surface Tension of 1-octanol, 1-hexanol and 1-butanol Aqueous Solutions

The modified Langmuir equation of state (equation 7.15) was applied for correlating the steady-state surface tension of 1-octanol, 1-hexanol and 1-butanol aqueous solutions in all profiles of Figures 7.1-7.12. The optimization routine was implemented in MATLAB, and the fitting parameters including the maximum surface concentration (Γ_∞), the equilibrium constant for adsorption from the vapor phase (K_1) and the equilibrium constant for adsorption from the liquid phase (K_2) were obtained by minimizing the residual sum of squares between the model prediction (based on equation 7.15) and the experimental data of the steady-state surface tension of the chemicals under study. The minimization procedure was repeated for six different temperatures. The values of fitting parameters for 1-octanol, 1-hexanol and 1-butanol are illustrated in Table 7.1 to 7.3, respectively. The steady-state modelling results show that the predicted maximum surface concentration is very close to the maximum surface coverage which can be calculated based on the molecular size. For example, the area of a 1-hexanol molecule at the surface is $20.23A^2/molecule$ at the saturation condition or full surface coverage [62]. Thus, the surface concentration of such chemical species under the condition is $8.21 \times 10^{-6} mol/m^2$; such value is in qualitative agreement with the values presented in Table 7.2. It should be noted that there is always repulsion/attraction between the adjacent polar molecules at the surface that may change the distance between adjacent molecules.

The equilibrium constants for a surfactant are often used to describe the tendency of surfactant molecules to adsorb at the interface and reduce the surface tension [23]. The main consideration in the modified Langmuir equation of state (equation 7.15) is the fact that the adsorption from both sides of a vapour/liquid interface should be considered simultaneously. The values obtained for the equilibrium constants (Tables 7.1- 7.3) show that at the final steady-state condition the equilibrium constant for adsorption from the vapor phase is much greater than that from the liquid phase ($K_1 > K_2$). This behavior is much more important in the short chain alcohol (1-butanol) than that of the long chain alcohol (1-octanol). From equation 7.7 and 7.8 it implies that adsorption rate constant from the vapor phase is much greater than that from the liquid phase ($k_a^g > k_a^l$), specially for short chain alcohols. Tables 7.1- 7.3 show that the contribution to adsorption (equilibrium constants) from both sides of the vapor/liquid interface increases with temperature. The contribution to adsorption from both sides of vapor /liquid interface show an increase with chain length from 1-butanol to 1-octanol.

In statistics, the best tools to identify if the model is fitted to the experimental results are the F test and residual plots. The ANOVA table, the F test and the residual plots for the steady-state modelling of 1-octanol, 1-hexanol and 1-butanol are illustrated in Tables 7.4, 7.5, 7.6, and Figures 7.13 , 7.14 and 7.15 respectively. No trend or unusual behavior

Table 7.1: The equilibrium constant for adsorption from the vapor phase (K_1) and from the liquid phase (K_2) and the maximum surface concentration (Γ_∞) obtained from fitting the experimental data of 1-octanol steady-state surface tension to the modified Langmuir equation of state (7.15).

T	K_1	K_2	$\Gamma_\infty \times 10^6$	K_1/K_2
°C	m^3/mol	m^3/mol	mol/m^2	
10	1.27	0.048	8.37	26.46
15	1.41	0.061	8.12	23.11
20	1.56	0.077	7.87	20.26
25	1.73	0.096	7.63	18.02
30	1.91	0.118	7.4	16.19
35	2.07	0.144	7.17	14.08

Table 7.2: The equilibrium constant for adsorption from the vapor phase (K_1) and from the liquid phase (K_2) and the maximum surface concentration (Γ_∞) obtained from fitting the experimental data of 1-hexanol steady-state surface tension to the modified Langmuir equation of state (7.15).

T	K_1	K_2	$\Gamma_\infty \times 10^6$	K_1/K_2
°C	m^3/mol	m^3/mol	mol/m^2	
10	0.262	0.008	6.32	32.75
15	0.280	0.009	6.39	31.11
20	0.292	0.011	6.16	26.45
25	0.319	0.013	6.24	24.54
30	0.340	0.015	5.97	22.67
35	0.360	0.017	5.71	22.18

Table 7.3: The equilibrium constant for adsorption from the vapor phase (K_1) and from the liquid phase (K_2) and the maximum surface concentration (Γ_∞) obtained from fitting the experimental data of 1-butanol steady-state surface tension to the modified Langmuir equation of state (7.15).

T	K_1	K_2	$\Gamma_\infty \times 10^6$	K_1/K_2
°C	m^3/mol	m^3/mol	mol/m^2	
10	0.13	0.0005	3.84	260
15	0.15	0.0007	3.58	214
20	0.17	0.0009	3.36	189
25	0.19	0.0011	3.18	173
30	0.21	0.0013	3.02	162
35	0.24	0.0014	2.88	171

Table 7.4: ANOVA table for the steady-state modelling of 1-octanol data based on Langmuir equation

Source	Sum of Square	Degree of Freedom	Mean Square	$F_{observed}$
Regression	SSR=105.68	p-1=3-1=2	MSR=52.84	MSR/MSE=582579
Error	SSE=0.01	n-p=96-3=93	MSE=9.07×10^{-5}	R^2=1-SSE/SST= 0.9999
Total	SST=105.61	n-1=96-1=95		

Table 7.5: ANOVA table for the steady-state modelling of 1-hexanol based on Langmuir equation

Source	Sum of Square	Degree of Freedom	Mean Square	$F_{observed}$
Regression	SSR=10003.66	p-1=3-1=2	MSR=5001.83	MSR/MSE=570.33
Error	SSE=815.67	n-p=96-3=93	MSE=8.77	R^2=1-SSE/SST= 0.91
Total	SST=8807.91	n-1=96-1=95		

Table 7.6: ANOVA table for the steady-state modelling of 1-butanol based on Langmuir equation

Source	Sum of Square	Degree of Freedom	Mean Square	$F_{observed}$
Regression	SSR=6286.06	p-1=3-1=2	MSR=3143.03	MSR/MSE=7665.9
Error	SSE=3.80	n-p=96-3=93	MSE=0.41	R^2=1-SSE/SST= 0.9999
Total	SST=6267.00	n-1=96-1=95		

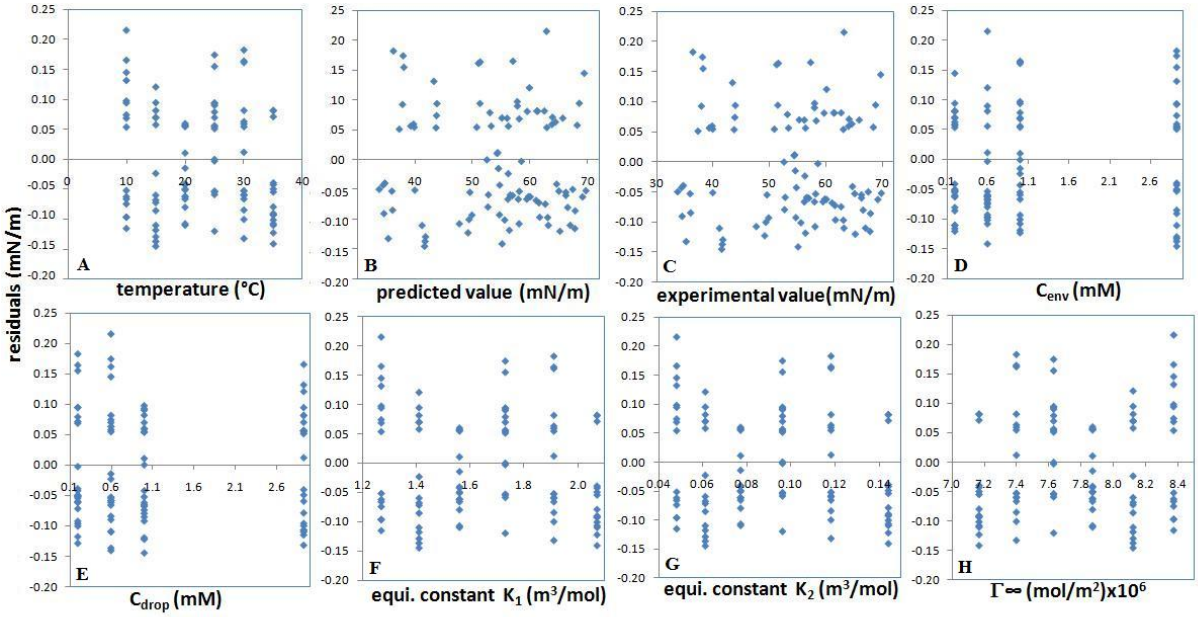

Figure 7.13: Residual plots based on the experimental and modeling results of the steady-state surface tension of 1-octanol in aqueous solution: (A) Residuals versus temperature, (B) Residuals versus predicted values based on equation (7.14) (C) Residuals versus experimental values, (D) Residuals versus C_{env}, (E) Residuals versus C_{drop}, (F) Residuals versus equilibrium constant (K_1), (G) Residuals versus equilibrium constant (K_2), (H) Residuals versus maximum surface concentration (Γ_∞)

can be observed in the residual plots. Residual plots and the ANOVA tables show that the model is significant. In Table 7.4 to 7.6, SSR, SSE and SST represents the regression sum of square, error sum of square and total sum of square, respectively. They were determined using the following equations:

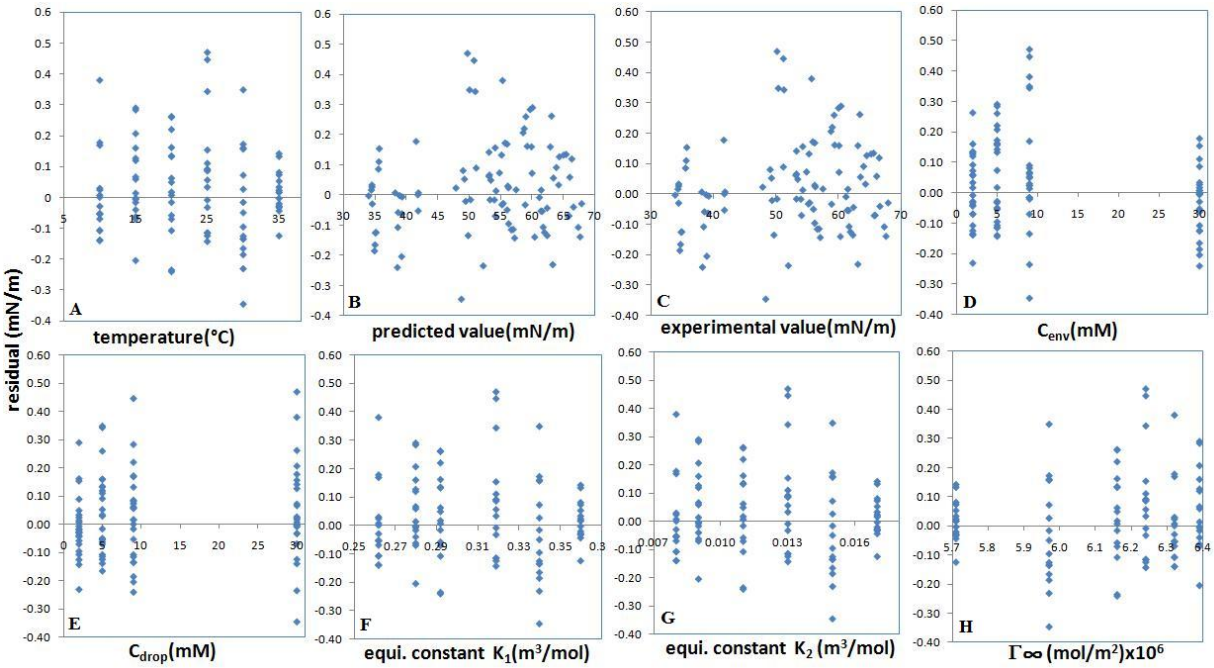

Figure 7.14: Residual plots based on the experimental and modeling results of the steady-state surface tension of 1-hexanol in aqueous solution: (A) Residuals versus temperature, (B) Residuals versus predicted values based on equation (7.14), (C) Residuals versus experimental values, (D) Residuals versus C_{env}, (E) Residuals versus C_{drop}, (F) Residuals versus equilibrium constant (K_1), (G) Residuals versus equilibrium constant (K_2), (H) Residuals versus maximum surface concentration (Γ_∞)

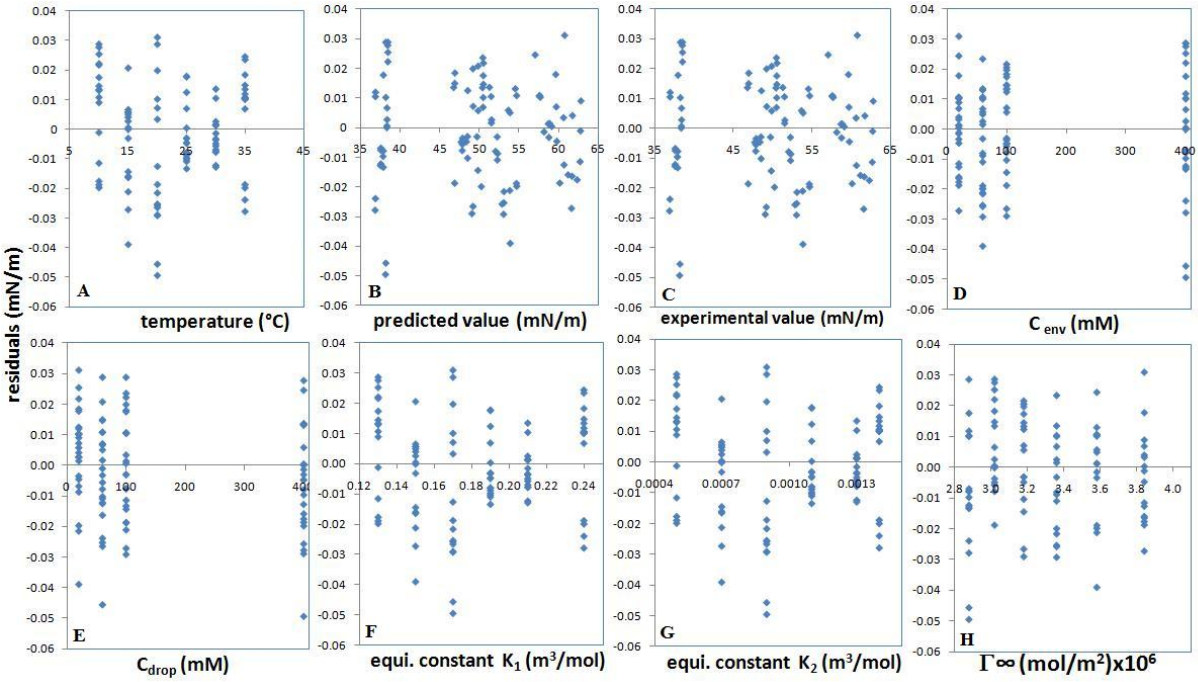

Figure 7.15: Residual plots based on the experimental and modeling results of the steady-state surface tension of 1-butanol in aqueous solution: (A) Residuals versus temperature, (B) Residuals versus predicted values based on equation (7.14) (C) Residuals versus experimental values, (D) Residuals versus C_{env}, (E) Residuals versus C_{drop}, (F) Residuals versus equilibrium constant (K_1), (G) Residuals versus equilibrium constant (K_2), (H) Residuals versus maximum surface concentration (Γ_∞)

$$SSR = (\gamma_p - \gamma_{avr})^2 \tag{7.16}$$

$$SSE = (\gamma - \gamma_p)^2 \tag{7.17}$$

$$SST = (\gamma - \gamma_{avr})^2 \tag{7.18}$$

where γ_p is the predicted steady-state surface tension based on the modified Langmuir equation of state (equation 7.15), γ_{avr} is the average steady-state surface tension based on experimental results, and γ is the experimental steady-state surface tension. P in tables 7.4 to 7.6 represents the number of fitting parameters and n is the number of experimental points. MSR and MSE are regression mean square and error mean square, respectively. The $F_{observed}$ value is the ratio of the regression mean square to the error mean square and represents the significance of the fit. The large $F_{observed}$ compare to the tabulated value ($F_{tabulated} = F_{2,93,0.05} = 3.11$)shows that $F_{observed} > F_{tabulated}$ and the overall regression is significant in all cases.

The experimental data for the steady-state surface tension of 1-octanol, 1-hexanol and 1-butanol (obtained from Figures 7.1 to 7.12) is plotted against temperature in Figures 7.16- 7.19, 7.20-7.23 and 7.24-7.27, respectively. In all cases the steady-state surface tension showed a linear relation with temperature. Thus, the following linear regression model fitted to the experimental data.

$$\gamma = r_1 T + r_2 \tag{7.19}$$

In this equation γ represents the steady-state surface tension. T is temperature in °C, and r_1 and r_2 are two constants. The values of C_{env}, C_{drop}, r_1, r_2 and the coefficient of determination (R^2) related to each regression model for 1-octanol, 1-hexanol and 1-butanol are illustrated in Tables 7.7, 7.8 and 7.9, respectively. The values of the coefficients of determination show that the linear regression is a good candidate for investigating the effect of temperature on the steady-state surface tension of 1-octanol, 1-hexanol and 1-butanol aqueous solutions at temperature ranging from 10 °C to 35 °C.

Figures 7.16- 7.27 and Tables 7.7- 7.9 show that the values of r_1 and r_2 for a system immersed in a same environment ($C_{env} = constant$) with different drop concentrations are not so much different and the steady-state surface tension is mostly dependant on the concentration of the environment solution (C_{env}), and not on the drop concentration (C_{drop}). This results support our previous discussion that for the chemicals under study the effect of adsorption/desorption from/to the vapor phase is more important than that of the liquid phase. This behavior can be observed at different concentrations of drop and environment solutions and at temperatures ranging from 10 to 35 °C.

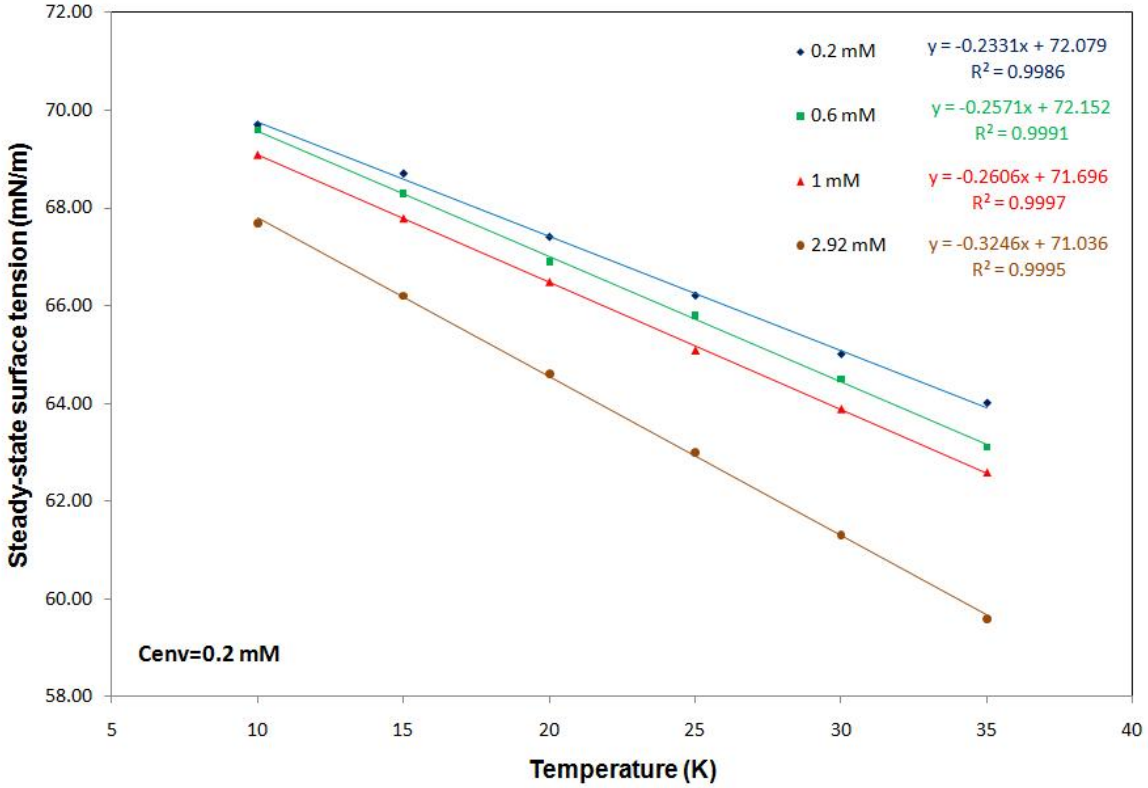

Figure 7.16: Steady state surface tension of 1-octanol at different temperatures. Concentration of the environment solution is 0.2 mM ($C_{env} = 0.2mM$); Experiments were performed at four different drop concentrations (C_{drop}) illustrated in the legend of each figure; Lines represent linear regression model (quation 7.19) to the experimental data.

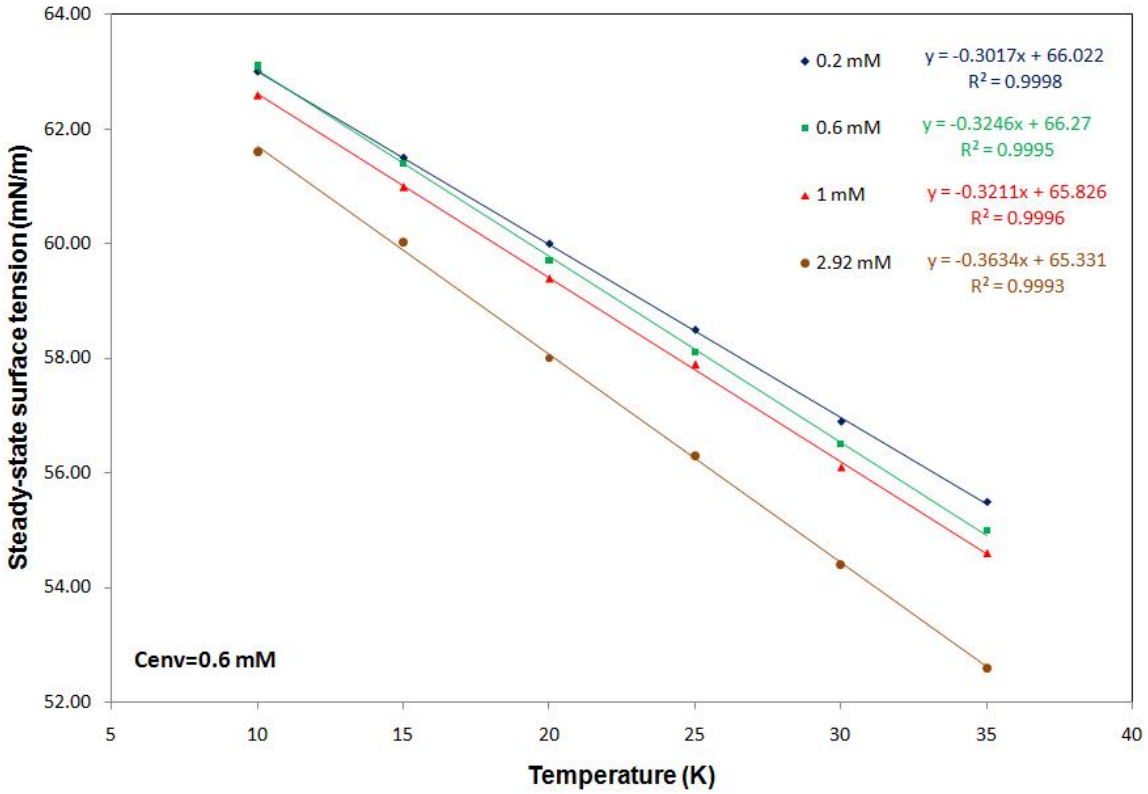

Figure 7.17: Steady state surface tension of 1-octanol at different temperatures. Concentration of the environment solution is 0.6 mM ($C_{env} = 0.6mM$); Experiments were performed at four different drop concentrations (C_{drop}) illustrated in the legend of each figure; Lines represent linear regression model (quation 7.19) to the experimental data.

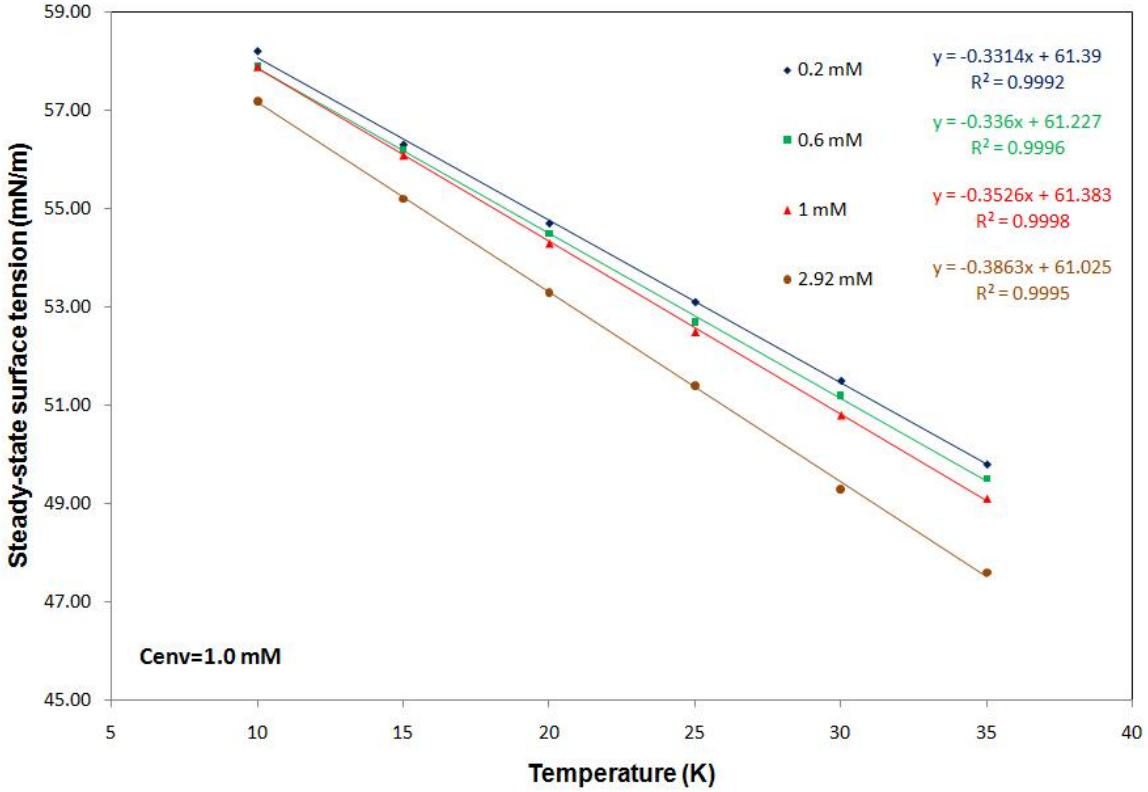

Figure 7.18: Steady state surface tension of 1-octanol at different temperatures. Concentration of the environment solution is 1 mM ($C_{env} = 1mM$); Experiments were performed at four different drop concentrations (C_{drop}) illustrated in the legend of each figure; Lines represent linear regression model (quation 7.19) to the experimental data.

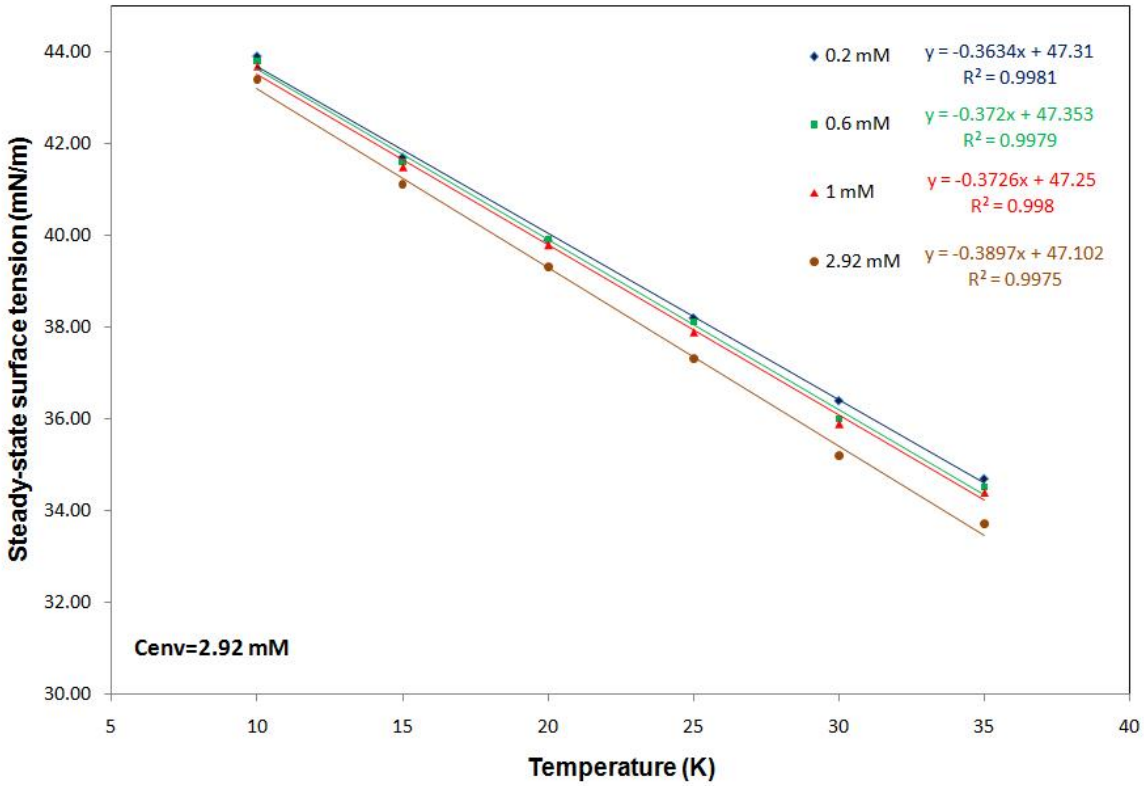

Figure 7.19: Steady state surface tension of 1-octanol at different temperatures. Concentration of the environment solution is 2.92 mM ($C_{env} = 2.92mM$); Experiments were performed at four different drop concentrations (C_{drop}) illustrated in the legend of each figure; Lines represent linear regression model (quation 7.19) to the experimental data.

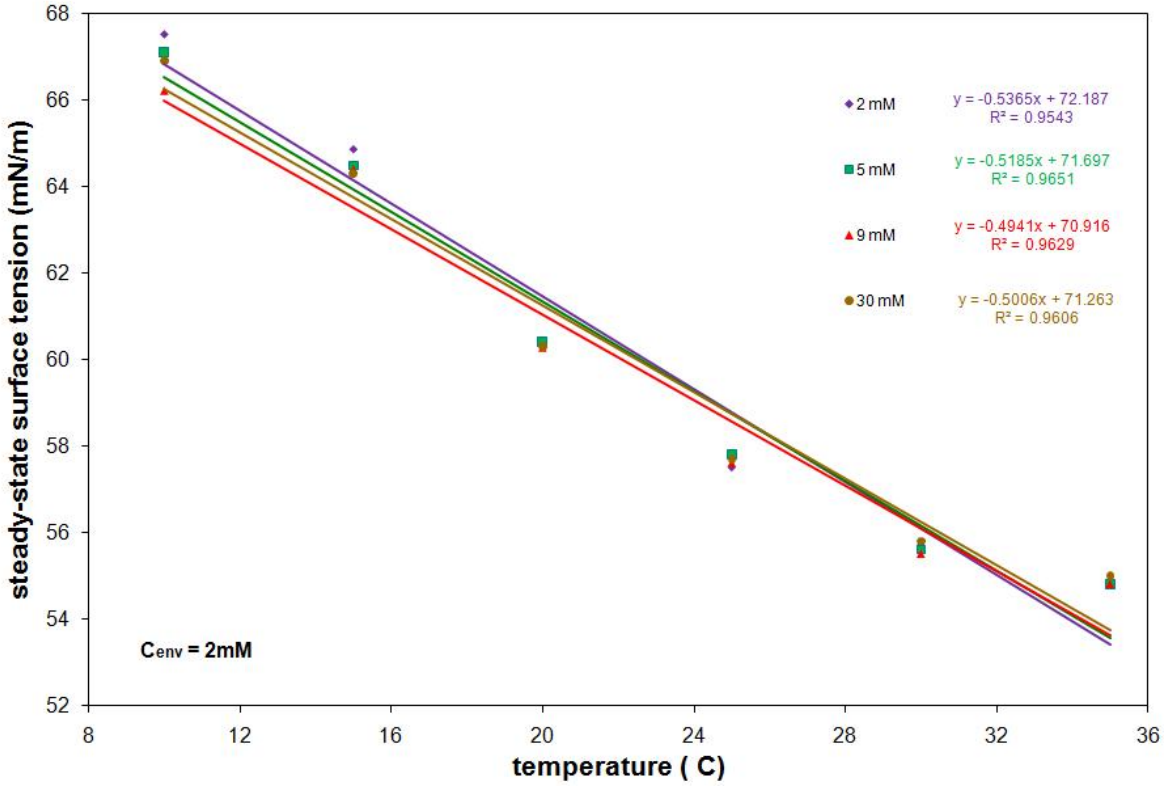

Figure 7.20: Steady state surface tension of 1-hexanol at different temperatures. Concentration of the environment solution is 2 mM ($C_{env} = 2mM$); Experiments were performed at four different drop concentrations (C_{drop}) illustrated in the legend of each figure; Lines represent linear regression model (quation 7.19) to the experimental data.

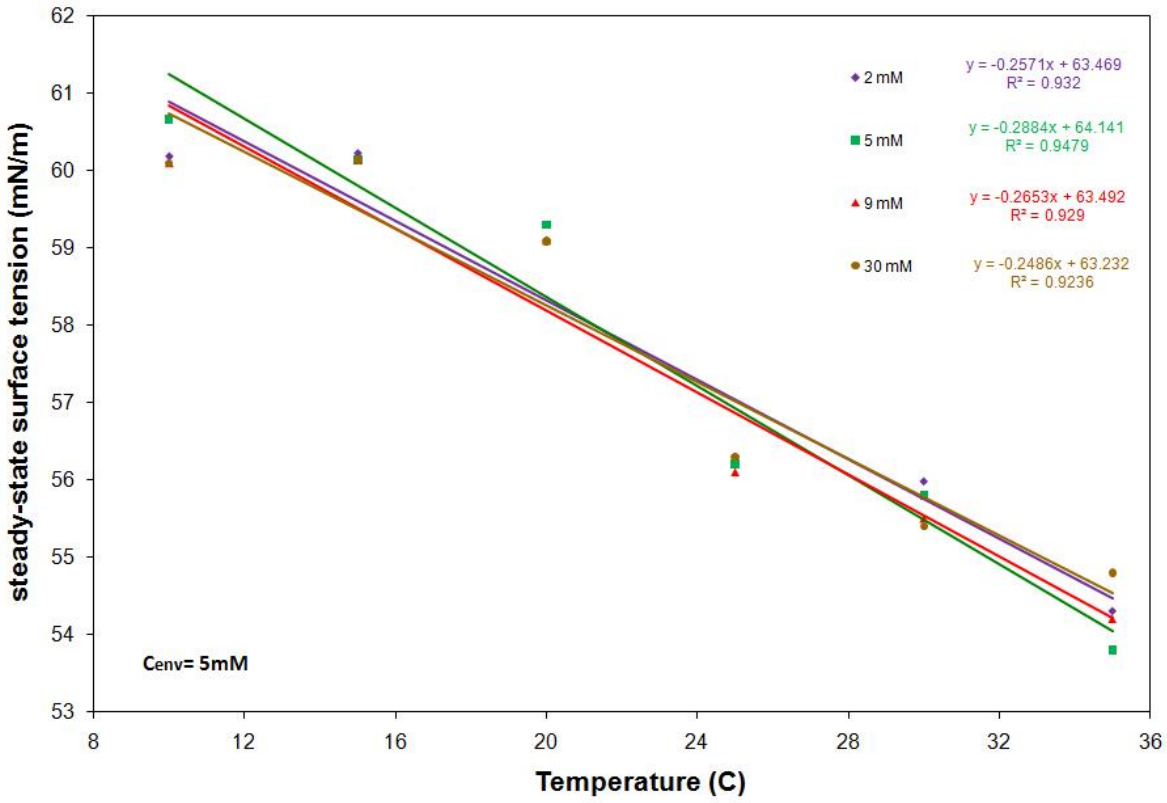

Figure 7.21: Steady state surface tension of 1-hexanol at different temperatures. Concentration of the environment solution is 5 mM ($C_{env} = 5mM$); Experiments were performed at four different drop concentrations (C_{drop}) illustrated in the legend of each figure; Lines represent linear regression model (quation 7.19) to the experimental data.

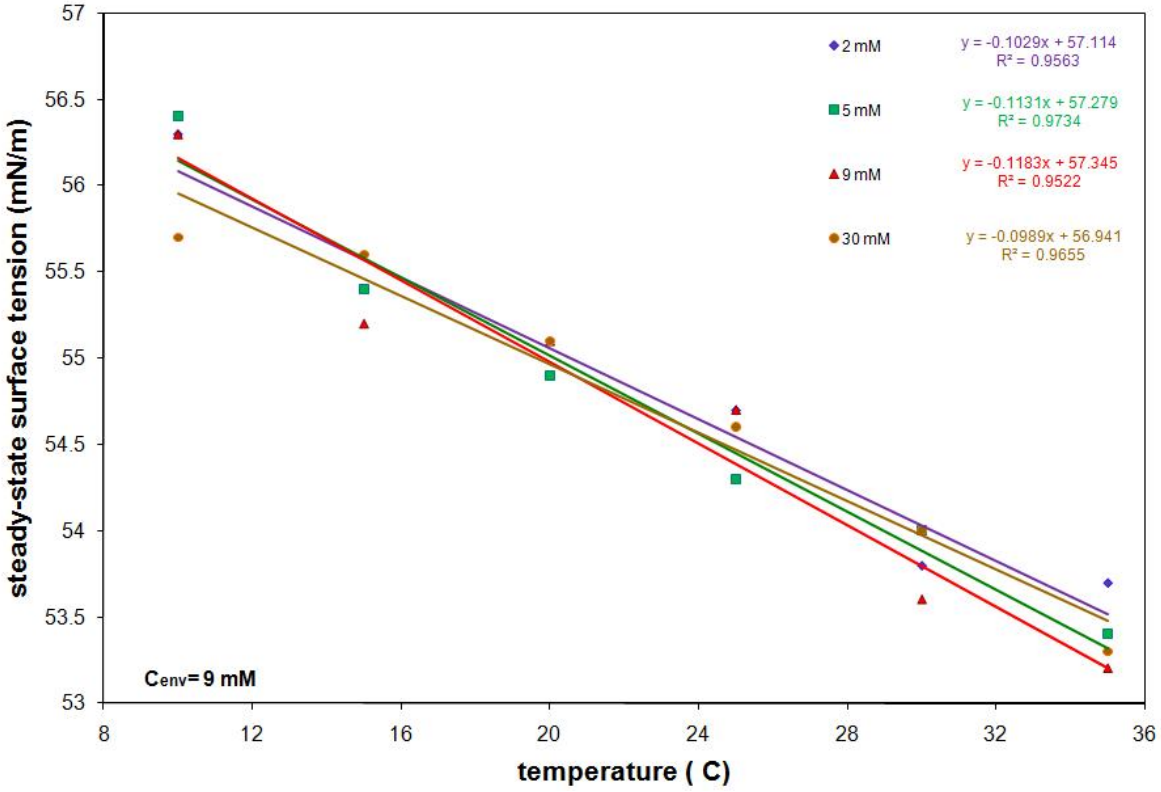

Figure 7.22: Steady state surface tension of 1-hexanol at different temperatures. Concentration of the environment solution is 9 mM ($C_{env} = 9mM$); Experiments were performed at four different drop concentrations (C_{drop}) illustrated in the legend of each figure; Lines represent linear regression model (quation 7.19) to the experimental data.

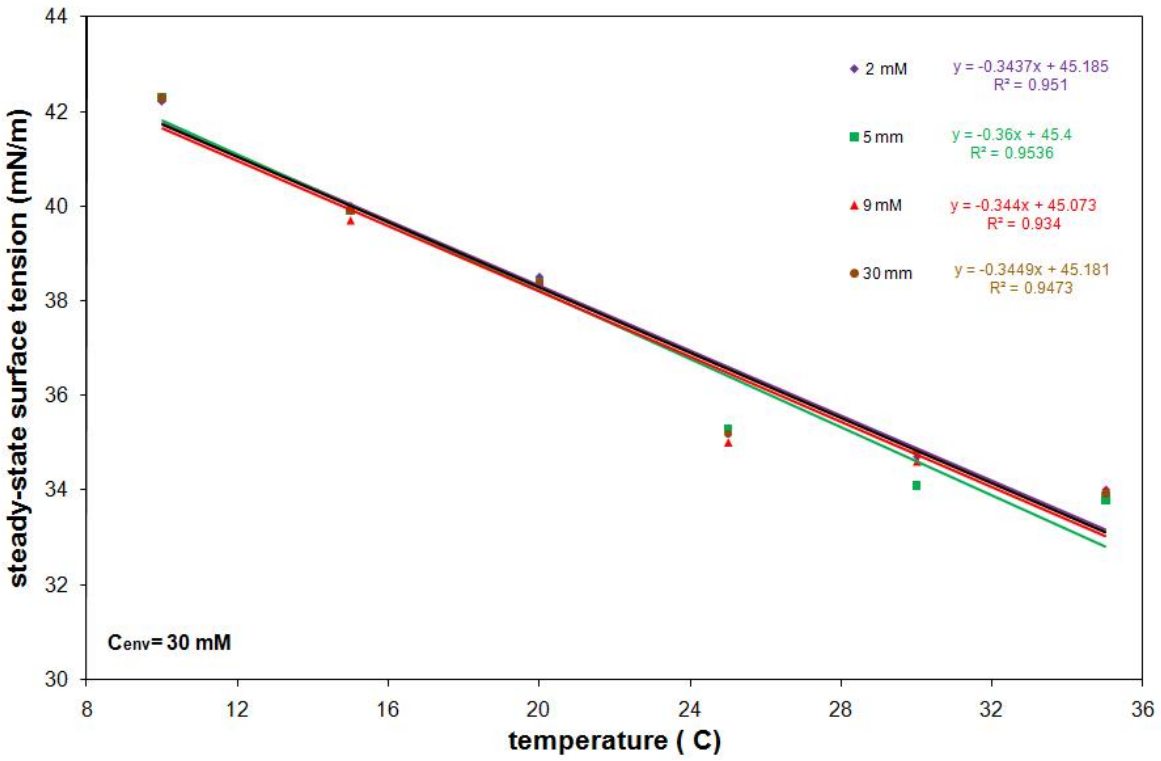

Figure 7.23: Steady state surface tension of 1-hexanol at different temperatures. Concentration of the environment solution is 30 mM ($C_{env} = 30mM$); Experiments were performed at four different drop concentrations (C_{drop}) illustrated in the legend of each figure; Lines represent linear regression model (quation 7.19) to the experimental data.

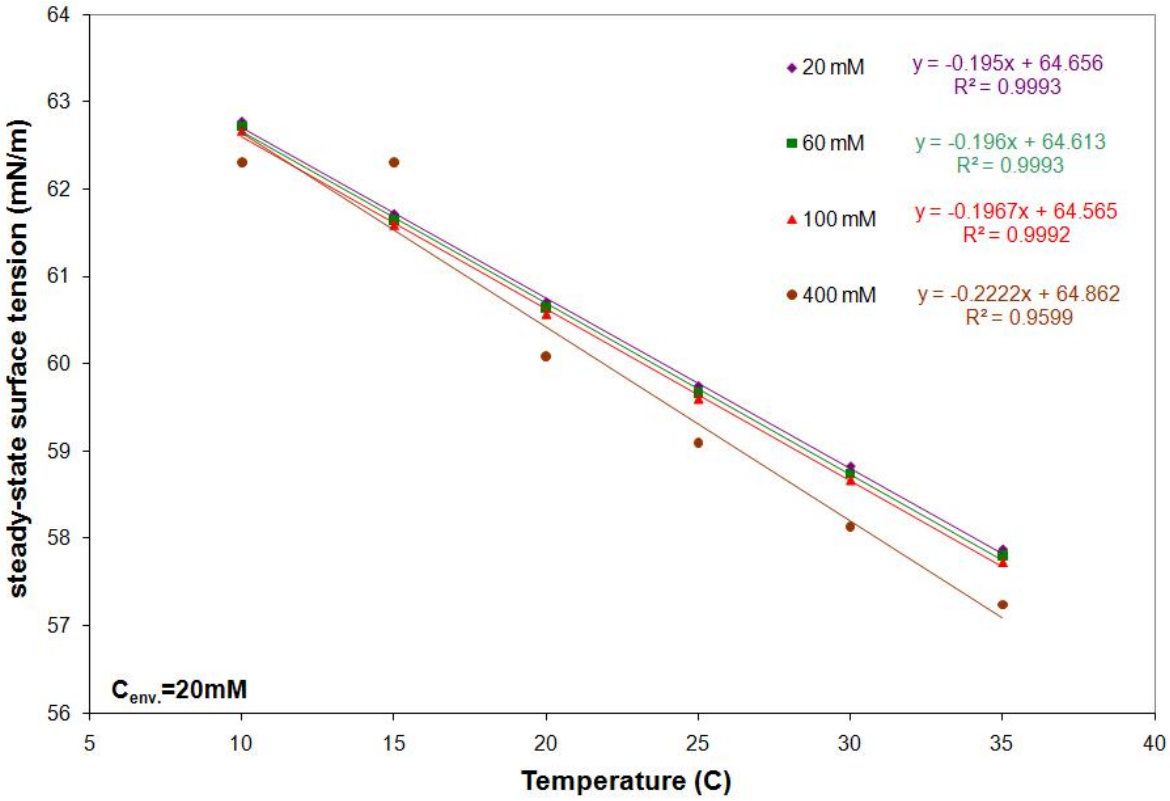

Figure 7.24: Steady state surface tension of 1-butanol at different temperatures. Concentration of the environment solution is 20 mM ($C_{env} = 20mM$); Experiments were performed at four different drop concentrations (C_{drop}) illustrated in the legend of each figure; Lines represent linear regression model (quation 7.19) to the experimental data.

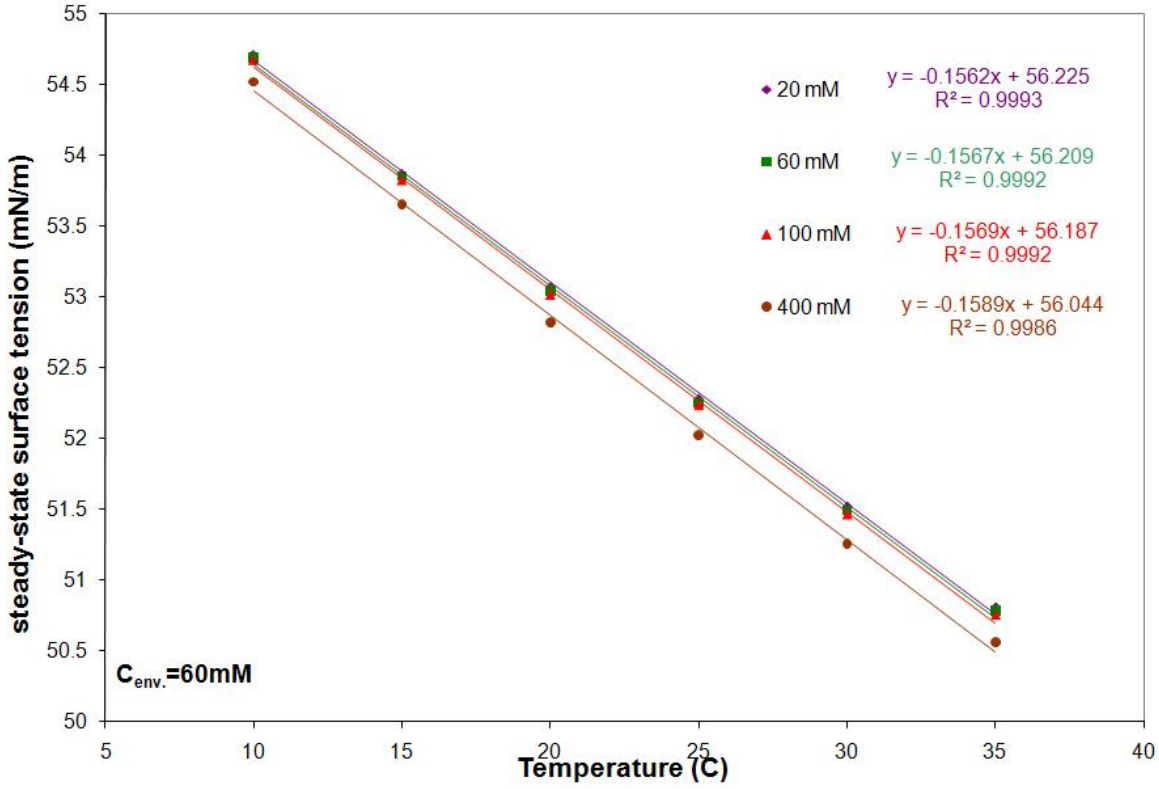

Figure 7.25: Steady state surface tension of 1-butanol at different temperatures. Concentration of the environment solution is 60 mM ($C_{env} = 60mM$); Experiments were performed at four different drop concentrations (C_{drop}) illustrated in the legend of each figure; Lines represent linear regression model (quation 7.19) to the experimental data.

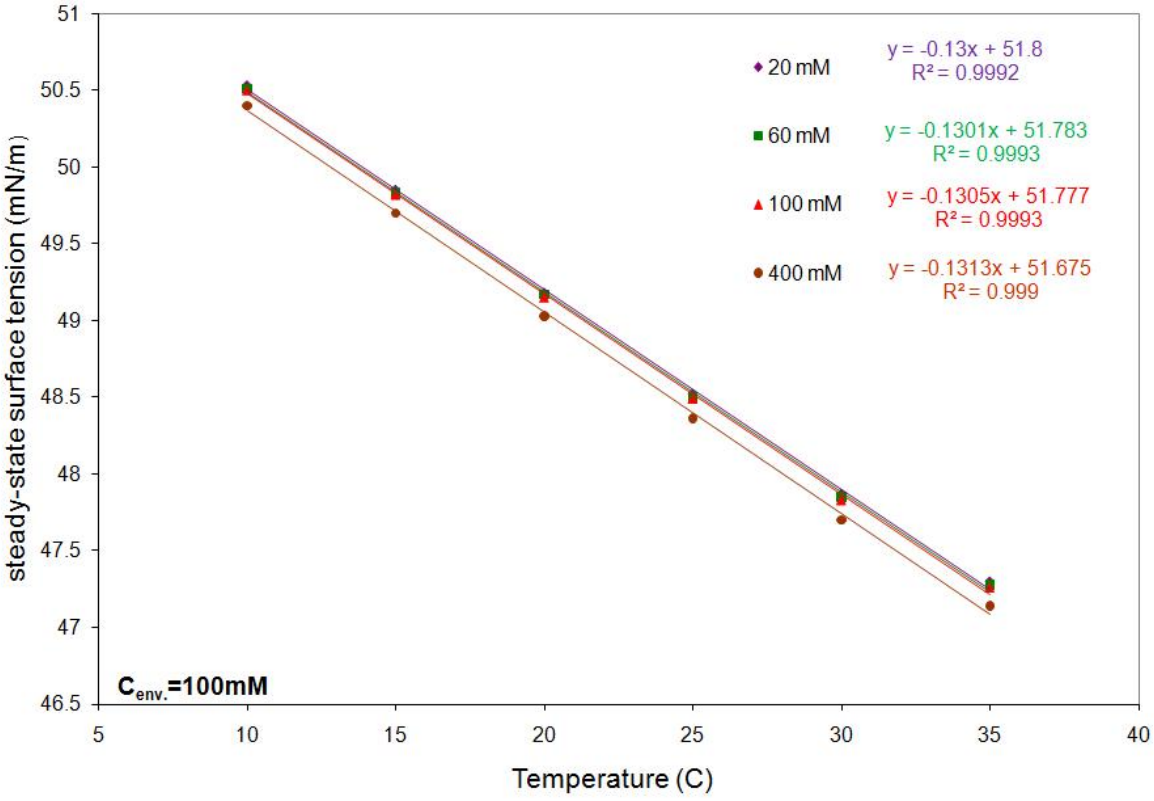

Figure 7.26: Steady state surface tension of 1-butanol at different temperatures. Concentration of the environment solution is 100 mM ($C_{env} = 100mM$); Experiments were performed at four different drop concentrations (C_{drop}) illustrated in the legend of each figure; Lines represent linear regression model (quation 7.19) to the experimental data.

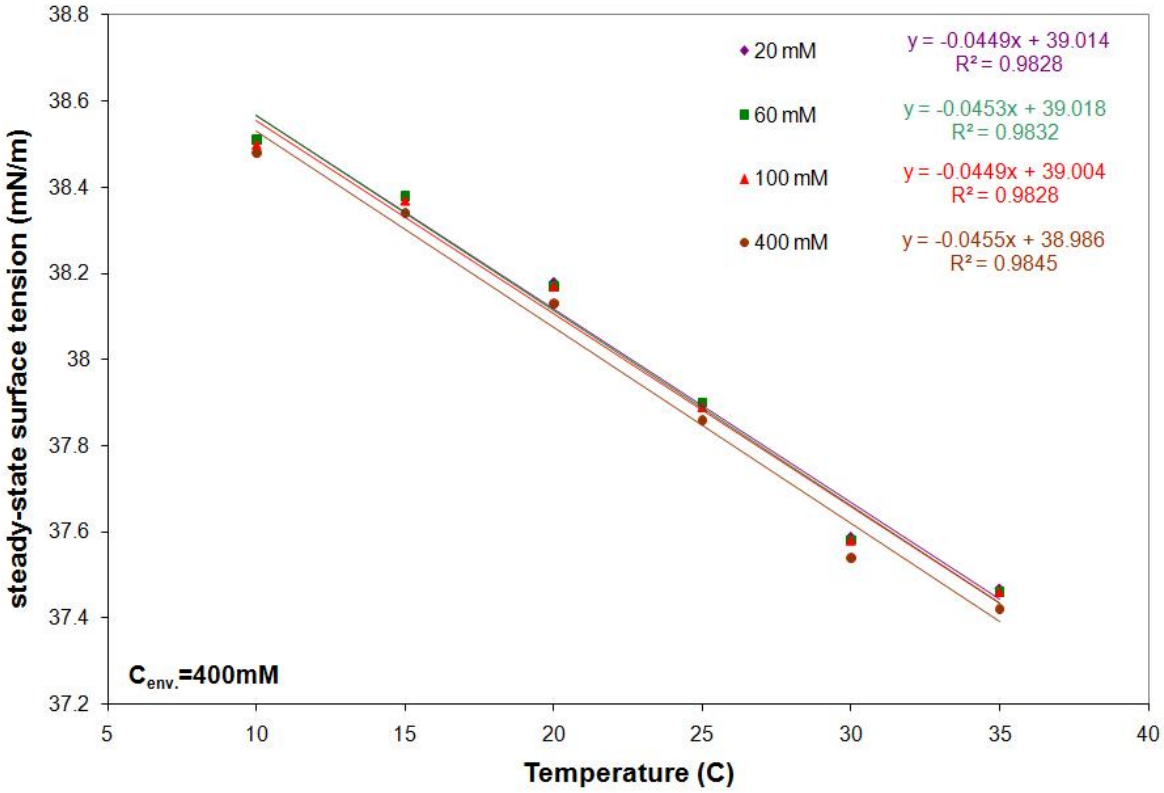

Figure 7.27: Steady state surface tension of 1-butanol at different temperatures. Concentration of the environment solution is 400 mM ($C_{env} = 400mM$); Experiments were performed at four different drop concentrations (C_{drop}) illustrated in the legend of each figure; Lines represent linear regression model (quation 7.19) to the experimental data.

Table 7.7: Concentration of the environment solution (C_{env}), concentration of the drop solution (C_{drop}), slope (r_1), Surface tension intercept (r_2), and the coefficient of determination (R^2) of a linear regression model (equation 7.19) fitted to the experimental results in Figures 7.16- 7.19

$C_{env}(mM)$	$C_{drop}(mM)$	$r_1(mN/m\,^{\circ}\mathrm{C})$	$r_2(mN/m)$	R^2
0.2	0.2	-0.23	72.08	0.9986
0.2	0.6	-0.26	72.16	0.9991
0.2	1.0	-0.26	71.70	0.9997
0.2	2.92	-0.32	71.04	0.9995
0.6	0.2	-0.30	66.02	0.9998
0.6	0.6	-0.32	66.27	0.9995
0.6	1.0	-0.32	65.83	0.9996
0.6	2.92	-0.36	65.33	0.9993
1.0	0.2	-0.33	61.39	0.9992
1.0	0.6	-0.34	61.23	0.9996
1.0	1.0	-0.35	61.38	0.9998
1.0	2.92	-0.39	61.03	0.9995
2.92	0.2	-0.36	47.31	0.9981
2.92	0.6	-0.37	47.36	0.9979
2.92	1.0	-0.37	47.25	0.9980
2.92	2.92	-0.39	47.10	0.9975

7.4.2 Effect of Temperature on the Dynamic Surface Tension of 1-octanol, 1-hexanol and 1-butanol Aqueous Solutions

The kinetic transfer equation, equation 7.14, was applied for modeling the dynamic surface tension of 1-octanol, 1-hexanol and 1-butanol solutions at all examined temperatures (Figures 7.1- 7.12). The fitting parameters ($k_a^g, \Gamma_\infty, \Gamma_{min}$) of equation 7.14 were obtained by minimizing the residual sum of squares between the model prediction and the experimental data for each profile in Figures 7.1- 7.12. Totally 96 fitting procedures were performed for each chemical at four concentrations of the environment solution, four concentrations of the drop solution, and six temperatures. In the dynamic modelling, the equilibrium constant for adsorption from the vapor phase (K_1), and the equilibrium constant for adsorption from the liquid phase (K_2) were considered constant and they were obtained from the steady-state modelling (Tables 7.1-7.3).

The theoretical prediction from the kinetic transfer equation is plotted along with

Table 7.8: Concentration of the environment solution (C_{env}), concentration of the drop solution (C_{drop}), slope (r_1), Surface tension intercept (r_2), and the coefficient of determination (R^2) of a linear regression model (equation 7.19) fitted to the experimental results in Figures 7.20- 7.23

$C_{env}(mM)$	$C_{drop}(mM)$	$r_1(mN/m\,^{\circ}\mathrm{C})$	$r_2(mN/m)$	R^2
2	2	-0.54	72.2	0.9543
2	5	-0.52	71.7	0.9651
2	9	-0.50	70.9	0.9629
2	30	-0.5046	71.3	0.9606
5	2	-0.26	63.5	0.9320
5	5	-0.29	64.1	0.9479
5	9	-0.27	63.5	0.9290
5	30	-0.25	63.2	0.9236
9	2	-0.10	57.1	0.9563
9	5	-0.11	57.3	0.9734
9	9	-0.12	57.3	0.9522
9	30	-0.10	56.9	0.9655
30	2	-0.34	45.2	0.9510
30	5	-0.36	45.4	0.9536
30	9	-0.34	45.1	0.9340
30	30	-0.35	45.2	0.9473

Table 7.9: Concentration of the environment solution (C_{env}), concentration of the drop solution (C_{drop}), slope (r_1), Surface tension intercept (r_2), and the coefficient of determination (R^2) of a linear regression model (equation 7.19) fitted to the experimental results in Figures 7.24- 7.27.

$C_{env}(mM)$	$C_{drop}(mM)$	$r_1(mN/m\,^{\circ}\mathrm{C})$	$r_2(mN/m)$	R^2
20	20	-0.20	64.6	0.9993
20	60	-0.20	64.6	0.9993
20	100	-0.20	64.6	0.9992
20	400	-0.22	64.9	0.9599
60	20	-0.16	56.2	0.9993
60	60	-0.16	56.2	0.9992
60	100	-0.16	56.2	0.9992
60	400	-0.16	56.0	0.9986
100	20	-0.13	51.8	0.9992
100	60	-0.13	51.8	0.9993
100	100	-0.13	51.8	0.9993
100	400	-0.13	51.7	0.9990
400	20	-0.045	39.0	0.9828
400	60	-0.045	39.0	0.9832
400	100	-0.045	39.0	0.9828
400	400	-0.046	39.0	0.9845

Table 7.10: 95% confidence intervals for Γ_∞, k_a^g, Γ_{min} and k_a^l obtained from fitting the experimental data of 1-octanol surface tension to the kinetic transfer equation (equation 7.14) at temperature ranging from 10 °C to 35 °C.

T	Γ_∞	k_a^g	Γ_{min}	k_a^l
°C	mol/m^2	$m^3/mol.s$	mol/m^2	$m^3/mol.s$
10	$8.35 \times 10^{-6} \pm 1.74 \times 10^{-8}$	$8.94 \times 10^{-4} \pm 2.88 \times 10^{-4}$	$4.86 \times 10^{-6} \pm 8.01 \times 10^{-7}$	$3.38 \times 10^{-5} \pm 1.09 \times 10^{-5}$
15	$8.12 \times 10^{-6} \pm 1.39 \times 10^{-8}$	$9.87 \times 10^{-4} \pm 2.48 \times 10^{-4}$	$4.89 \times 10^{-6} \pm 7.71 \times 10^{-7}$	$4.20 \times 10^{-5} \pm 1.05 \times 10^{-5}$
20	$7.87 \times 10^{-6} \pm 1.34 \times 10^{-8}$	$1.12 \times 10^{-3} \pm 3.41 \times 10^{-4}$	$4.89 \times 10^{-6} \pm 7.39 \times 10^{-7}$	$5.72 \times 10^{-5} \pm 1.75 \times 10^{-5}$
25	$7.63 \times 10^{-6} \pm 1.24 \times 10^{-8}$	$1.38 \times 10^{-3} \pm 5.53 \times 10^{-4}$	$4.91 \times 10^{-6} \pm 6.94 \times 10^{-7}$	$7.63 \times 10^{-5} \pm 3.07 \times 10^{-5}$
30	$7.39 \times 10^{-6} \pm 1.04 \times 10^{-8}$	$2.08 \times 10^{-3} \pm 7.41 \times 10^{-4}$	$4.89 \times 10^{-6} \pm 6.41 \times 10^{-7}$	$1.28 \times 10^{-4} \pm 4.58 \times 10^{-5}$
35	$7.17 \times 10^{-6} \pm 5.21 \times 10^{-8}$	$3.39 \times 10^{-3} \pm 9.63 \times 10^{-4}$	$4.88 \times 10^{-6} \pm 6.09 \times 10^{-7}$	$2.36 \times 10^{-4} \pm 6.70 \times 10^{-5}$

the experimental data in Figures 7.1- 7.12. For all profiles, the kinetic transfer equation fits the experimental data very well. At each temperature, the three fitting parameters ($k_a^g, \Gamma_\infty, \Gamma_{min}$) along with k_a^l (calculated from equation 7.3) are tabulated in Tables 7.10, 7.11 and 7.12 for 1-octanol, 1-hexanol and 1-butanol, respectively. For example, the values presented at 10 °C for 1-octanol solutions are the 95% confidence interval of the fitting parameters obtained at 16 different fitting procedures of 16 profiles presented in figures 7.1A, 7.2A, 7.3A, and 7.4A.

The adsorption rate constant from the vapor phase (k_a^g) and the maximum surface concentration (Γ_∞), according to the theory, should be constant regardless of the surfactant concentrations. However, small variations in them were observed at different concentrations. These variations may be due to the measurement and experimental errors or due to the limitations of the model. 95% confidence intervals in Tables 7.10 to 7.12 are the consequence of such variations.

The goodness of fit for some dynamic surface tension results of 1-hexanol is presented on 7.13-7.16. The large $F_{observed}$ compared to the tabulated one ($F_{tabulated}$) shows the significance of the model.

The limitation of this type of model is the variation in the fitting parameters. An obvious limitation is that material properties and their corresponding constants or fit-

Table 7.11: 95% confidence intervals for Γ_∞, k_a^g, Γ_{min} and k_a^l obtained from fitting the experimental data of 1-hexanol surface tension to the kinetic transfer equation (equation 7.14) at temperature ranging from 10 °C to 35 °C.

T	Γ_∞	k_a^g	Γ_{min}	k_a^l
°C	mol/m^2	$m^3/mol.s$	mol/m^2	$m^3/mol.s$
10	$6.49 \times 10^{-6} \pm 2.20 \times 10^{-7}$	$1.52 \times 10^{-4} \pm 3.55 \times 10^{-5}$	$4.30 \times 10^{-6} \pm 4.67 \times 10^{-7}$	$4.66 \times 10^{-6} \pm 1.09 \times 10^{-6}$
15	$6.37 \times 10^{-6} \pm 3.39 \times 10^{-7}$	$1.61 \times 10^{-4} \pm 4.30 \times 10^{-5}$	$4.41 \times 10^{-6} \pm 4.27 \times 10^{-7}$	$5.16 \times 10^{-6} \pm 1.38 \times 10^{-6}$
20	$6.67 \times 10^{-6} \pm 6.86 \times 10^{-7}$	$2.48 \times 10^{-4} \pm 1.08 \times 10^{-4}$	$4.69 \times 10^{-6} \pm 4.80 \times 10^{-7}$	$9.33 \times 10^{-6} \pm 4.02 \times 10^{-6}$
25	$6.72 \times 10^{-6} \pm 8.72 \times 10^{-7}$	$4.29 \times 10^{-4} \pm 2.41 \times 10^{-4}$	$4.88 \times 10^{-6} \pm 5.24 \times 10^{-7}$	$1.74 \times 10^{-5} \pm 9.80 \times 10^{-6}$
30	$6.63 \times 10^{-6} \pm 1.01 \times 10^{-6}$	$5.95 \times 10^{-4} \pm 3.06 \times 10^{-4}$	$4.81 \times 10^{-6} \pm 6.08 \times 10^{-7}$	$2.62 \times 10^{-5} \pm 1.35 \times 10^{-5}$
35	$6.31 \times 10^{-6} \pm 8.72 \times 10^{-7}$	$1.21 \times 10^{-3} \pm 5.34 \times 10^{-4}$	$4.67 \times 10^{-6} \pm 4.68 \times 10^{-7}$	$5.72 \times 10^{-5} \pm 2.52 \times 10^{-5}$

ting parameters are varying with time. Thus, these parameters may have different values between the initial and the final stages of the experiment. Discrepancies would occur depending on which set of fitting parameters is used in the model predictions over the entire time range. Improvements may be made when incorporating the varying nature of these fitting parameters. Of course, other experimental errors or factors may also contribute to the discrepancies, such as temperature fluctuations, the presence of impurities, and loss of surfactant due to vapor leakage that may distort the experimental results. Similar to any minimization procedure any imperfections in the experimental results will be reflected in the value obtained for the fitting parameters in Tables 7.10 to 7.12. Such variations can be observed in the values obtained for the maximum surface concentration (Γ_∞) based on the steady-state modelling (Table 7.1) and the values obtained based on dynamic modelling. In the steady-state modelling the modified Langmuir equation of state was applied to model the steady-state surface tension, while in the dynamic modelling the kinetic transfer equation was applied to model the entire duration of the dynamic surface tension results. The maximum surface concentration was used as a fitting parameter in both cases. Since the interface changes with time and surfactant adsorption, hence the value of this parameter may vary from the beginning to the end of the experiment. However, in all cases the values of maximum surface concentration in Tables 7.1 to 7.3 are in the 95% confidence intervals of Γ_∞ in Tables 7.10 to 7.12. As there is a finite rate of adsorption, the theoretical value of the

Table 7.12: 95% confidence intervals for Γ_∞, k_a^g, Γ_{min} and k_a^l obtained from fitting the experimental data of 1-butanol surface tension to the kinetic transfer equation (equation 7.14) at temperature ranging from 10 °C to 35 °C.

T	Γ_∞	k_a^g	Γ_{min}	k_a^l
°C	mol/m^2	$m^3/mol.s$	mol/m^2	$m^3/mol.s$
10	$3.83 \times 10^{-6} \pm 1.14 \times 10^{-8}$	$8.84 \times 10^{-6} \pm 3.17 \times 10^{-6}$	$3.50 \times 10^{-6} \pm 2.72 \times 10^{-7}$	$3.40 \times 10^{-8} \pm 2.48 \times 10^{-8}$
15	$3.57 \times 10^{-6} \pm 9.23 \times 10^{-9}$	$1.05 \times 10^{-5} \pm 3.70 \times 10^{-6}$	$3.30 \times 10^{-6} \pm 2.30 \times 10^{-7}$	$4.88 \times 10^{-8} \pm 3.56 \times 10^{-8}$
20	$3.36 \times 10^{-6} \pm 9.80 \times 10^{-9}$	$1.43 \times 10^{-5} \pm 4.75 \times 10^{-6}$	$3.13 \times 10^{-6} \pm 1.91 \times 10^{-7}$	$7.56 \times 10^{-8} \pm 5.14 \times 10^{-8}$
25	$3.17 \times 10^{-6} \pm 1.54 \times 10^{-8}$	$1.51 \times 10^{-5} \pm 6.87 \times 10^{-6}$	$2.97 \times 10^{-6} \pm 1.70 \times 10^{-7}$	$8.74 \times 10^{-8} \pm 8.12 \times 10^{-8}$
30	$3.02 \times 10^{-6} \pm 4.73 \times 10^{-9}$	$2.25 \times 10^{-5} \pm 1.10 \times 10^{-5}$	$2.84 \times 10^{-6} \pm 1.46 \times 10^{-7}$	$1.38 \times 10^{-7} \pm 1.39 \times 10^{-7}$
35	$2.83 \times 10^{-6} \pm 4.66 \times 10^{-9}$	$4.07 \times 10^{-5} \pm 2.61 \times 10^{-5}$	$2.69 \times 10^{-6} \pm 1.25 \times 10^{-7}$	$2.38 \times 10^{-7} \pm 3.11 \times 10^{-7}$

Table 7.13: ANOVA table for the dynamic modelling of 1-hexanol ($C_{drop} = 5mM, C_{env} = 2mM, T = 25\,°C$

Source	Sum of Square	Degree of Freedom	Mean Square	$F_{observed}$
Regression	SSR=2826.3	p-1=3-1=2	MSR=1413.2	MSR/MSE=94213
Error	SSE=10.9	n-p=722-3=719	MSE=0.015	R^2=1-SSE/SST= 0.996
Total	SST=2787.3	n-1=722-1=721		$F_{tabulated} = 3.0$

Table 7.14: ANOVA table for the dynamic modelling of 1-hexanol ($C_{drop} = 9mM, C_{env} = 2mM, T = 25\,°C$

Source	Sum of Square	Degree of Freedom	Mean Square	$F_{observed}$
Regression	SSR=434.4	p-1=3-1=2	MSR=217.2	MSR/MSE=28369
Error	SSE=4.9	n-p=722-3=640	MSE=0.0077	R^2=1-SSE/SST= 0.986
Total	SST=446.1	n-1=643-1=642		$F_{tabulated} = 3.0$

Table 7.15: ANOVA table for the dynamic modelling of 1-hexanol ($C_{drop} = 30mM, C_{env} = 2mM, T = 25\,^{\circ}C$

Source	Sum of Square	Degree of Freedom	Mean Square	$F_{observed}$
Regression	SSR=11366.1	p-1=3-1=2	MSR=5683.1	MSR/MSE=87432.3
Error	SSE=43.5	n-p=722-3=674	MSE=0.065	R^2=1-SSE/SST= 0.996
Total	SST=11276.7	n-1=677-1=676		$F_{tabulated} = 3.0$

Table 7.16: ANOVA table for the dynamic modelling of 1-hexanol ($C_{drop} = 2mM, C_{env} = 5mM, T = 10\,^{\circ}C$

Source	Sum of Square	Degree of Freedom	Mean Square	$F_{observed}$
Regression	SSR=1147.5	p-1=3-1=2	MSR=573.3	MSR/MSE=1960000
Error	SSE=0.12	n-p=413-3=410	MSE=0.0003	R^2=1-SSE/SST= 0.9999
Total	SST=1147.4	n-1=413-1=412		$F_{tabulated} = 3.0$

minimum surface concentration should be zero. Since the image acquisitions were started a few seconds after the drop was formed, the predicted minimum surface concentrations (Γ_{min}) in Tables 7.10 to 7.12 have the values larger than zero.

The temperature dependency of the equilibrium constants (K_1, K_2) and the rate constants of adsorption (k_a^g, k_a^l) for 1-octanol, 1-hexanol and 1-butanol systems are illustrated in Figures 7.28, 7.29 and 7.30. According to these figures, the equilibrium constants (K_1, K_2) and the rate constants for adsorption from both sides of the vapor/liquid interface (k_a^g, k_a^l) increase with temperature in all three systems. Also, the rate of adsorption from the vapor phase (k_a^g) is much greater than that from the liquid phase (k_a^l). The results show that the rate constant for adsorption from the vapor phase increases when the chain length is increased from 1-butanol to 1-octanol.

The Arrhenius expression (equation 7.20) is one of the most often used formulas for the temperature dependency of the adsorption rate constants.

$$k = A_f exp(\frac{-E}{RT}) \tag{7.20}$$

In this equation, A_f is the frequency factor or pre-exponential factor. It varies slightly with temperature, but is often taken as a constant across a small temperature range. R is the universal gas constant, and T is the temperature (K). E is the fitting parameter

related to the energy barrier (activation energy or minimum energy required) for adsorption to occur. Based on the Van't Hoff equation (7.21, E is equal to the change in enthalpy if Arrhenius equation is used for equilibrium constants.

$$\frac{d(ln(K))}{d(1/T)} = \frac{-\Delta H_{ad}}{R} \tag{7.21}$$

Thus, a plot of $ln(k)$ versus T^{-1} gives a straight line, whose slope and intercept can be used to determine E and A_f. Figures 7.31, 7.32 and 7.33 show these plots for the rate constants of adsorption (k_a^g, k_a^l) as well as the equilibrium constants (K_1, K_2) for 1-octanol, 1-hexanol and 1-butanol, respectively. Good agreement between the predicted and the experimental data is illustrated by the coefficient of determination (R^2) value being near 1 in all cases. The frequency factor (A_f) and the fitting parameter (E) obtained from fitting the experimental data to the Arrhenius expression 7.20 are illustrated in Tables 7.17, 7.18 and 7.19 for 1-octanol, 1-hexanol and 1-butanol, respectively.

Figures 7.1- 7.12 also shows that when the temperature is increased from 10 °C to 35 °C, the slopes of the profiles increase, and the time required reaching to the steady-state surface tension decreases dramatically. For instance when the concentration of 1-hexanol in the environment solution is 2mM (Figure 7.5) and concentration of the drop solution is 30 mM, the time required to reach to the steady-state surface tension is 2500 second at 10 °C (Figure 7.5A), while it is 200 second at 35 °C (Figure 7.5F). The time required reaching to 95% of the steady-state surface tension (t_{95}) is chosen to show how fast the surface tension reaches the steady-state value. Figures 7.34, 7.35 and 7.36 show that t_{95} decreases with temperature for 1-octanol, 1-hexanol and 1-butanol, respectively. Thus, the time required reaching to the steady-state surface tension decreases with temperature. This trend can be observed in various systems (1-octanol, 1-hexanol and 1-butanol) and in all different concentrations of the drop and environment solutions. This is due to the fact that the adsorption rate constant from the vapor phase (k_a^g) and the adsorption rate constant from the liquid phase (k_a^l) increases dramatically with temperature (Tables 7.10 to 7.12 and Figures 7.28 to 7.30). According to Figures 7.34- 7.36, t_{95} is zero when there is no concentration difference between drop and environment solutions because there is no driving force for molecular exchange across the interface. Figures 7.34- 7.36 also show that t_{95} increases when the concentration difference between drop and environment solutions is increased. This may be due to the fact that at higher concentration difference, a larger number of molecules should be adsorbed/desorbed from/to the surface to reach to the steady-state condition.

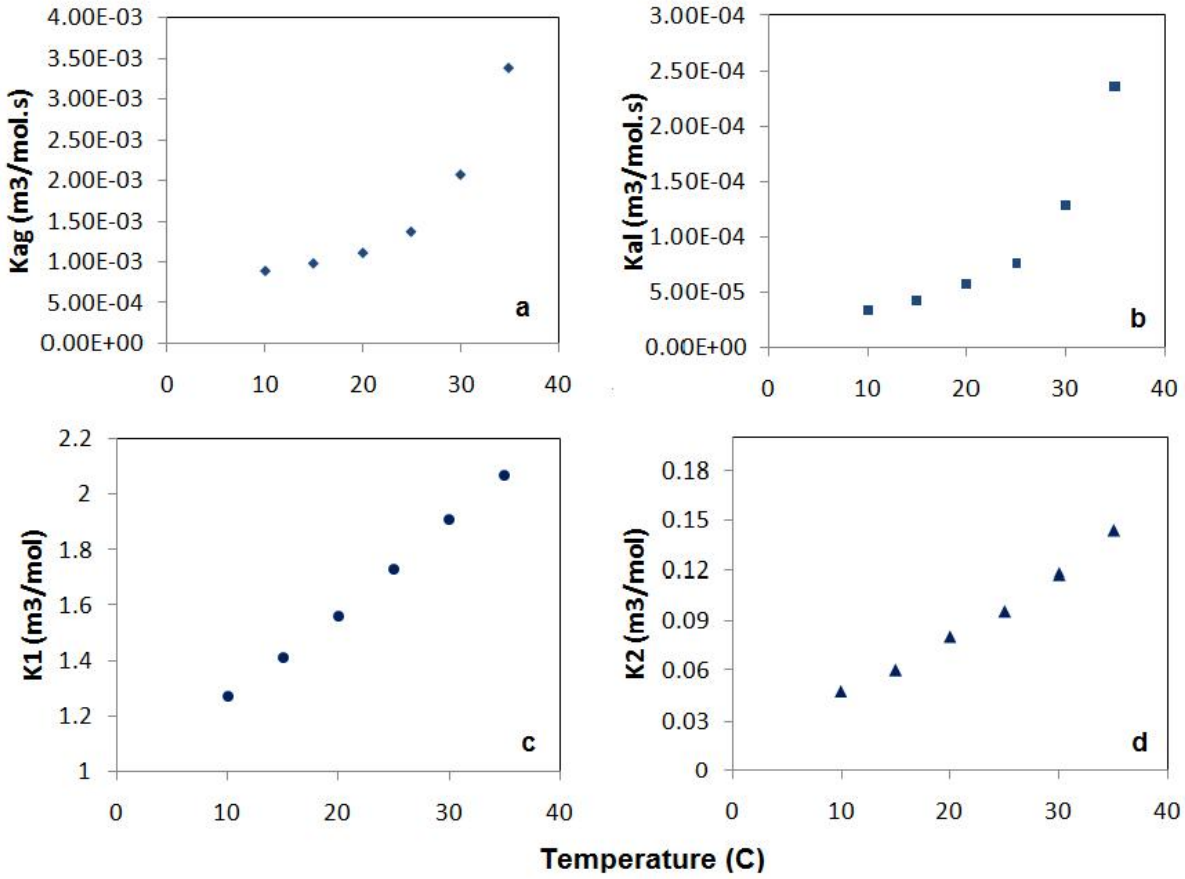

Figure 7.28: Adsorption constants for 1-octanol: (a) Average adsorption rate constant for adsorption from the vapor phase (k_a^g) versus temperature. (b) Average adsorption rate constant for adsorption from the liquid phase (k_a^l) versus temperature. (c) Equilibrium constant for adsorption from the vapor phase (K_1) versus temperature. (d) Equilibrium constant for adsorption from the liquid phase (K_2) versus temperature.

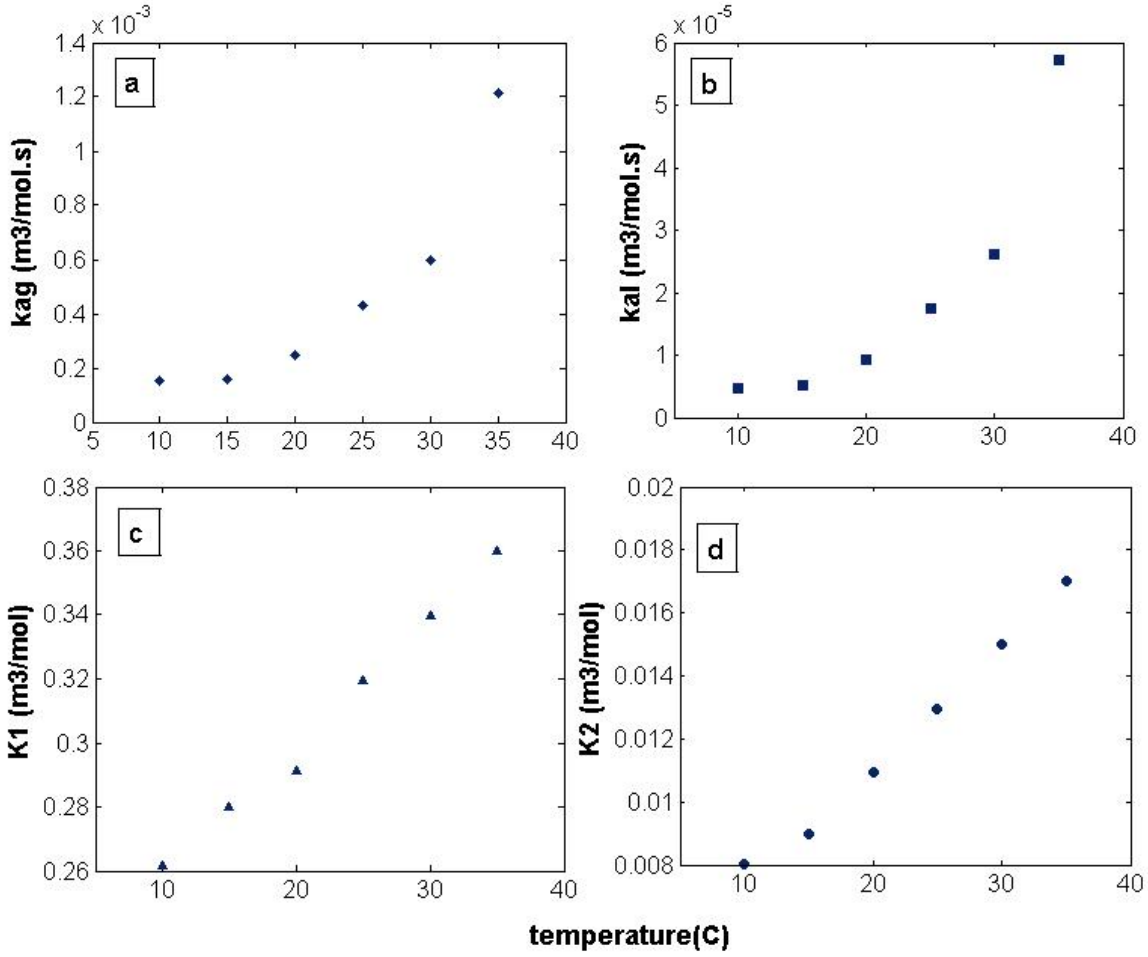

Figure 7.29: Adsorption constants for 1-hexanol: (a) Average adsorption rate constant for adsorption from the vapor phase (k_a^g) versus temperature. (b) Average adsorption rate constant for adsorption from the liquid phase (k_a^l) versus temperature. (c) Equilibrium constant for adsorption from the vapor phase (K_1) versus temperature. (d) Equilibrium constant for adsorption from the liquid phase (K_2) versus temperature.

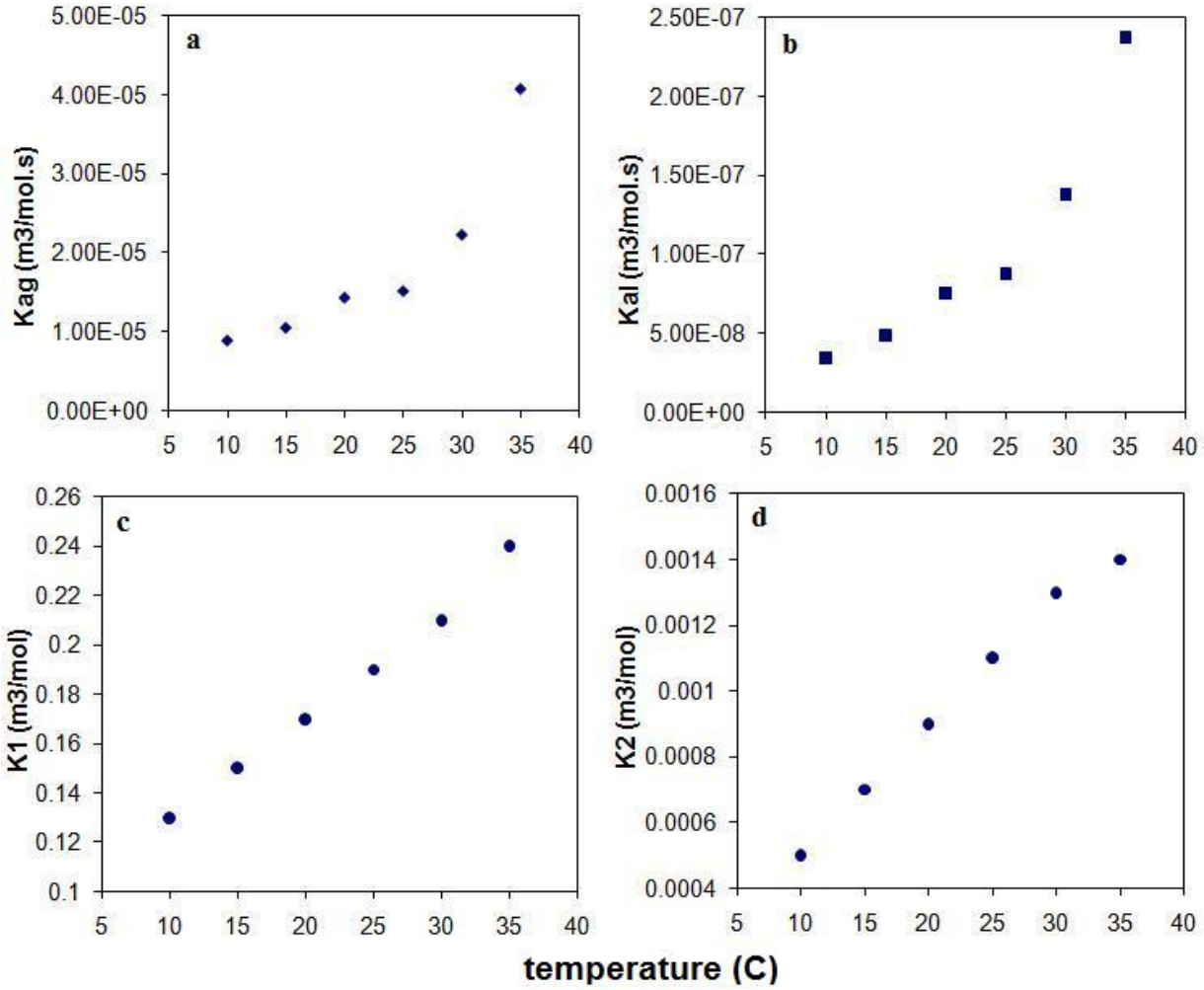

Figure 7.30: Adsorption constants for 1-butanol: (a) Average adsorption rate constant for adsorption from the vapor phase (k_a^g) versus temperature. (b) Average adsorption rate constant for adsorption from the liquid phase (k_a^l) versus temperature. (c) Equilibrium constant for adsorption from the vapor phase (K_1) versus temperature. (d) Equilibrium constant for adsorption from the liquid phase (K_2) versus temperature.

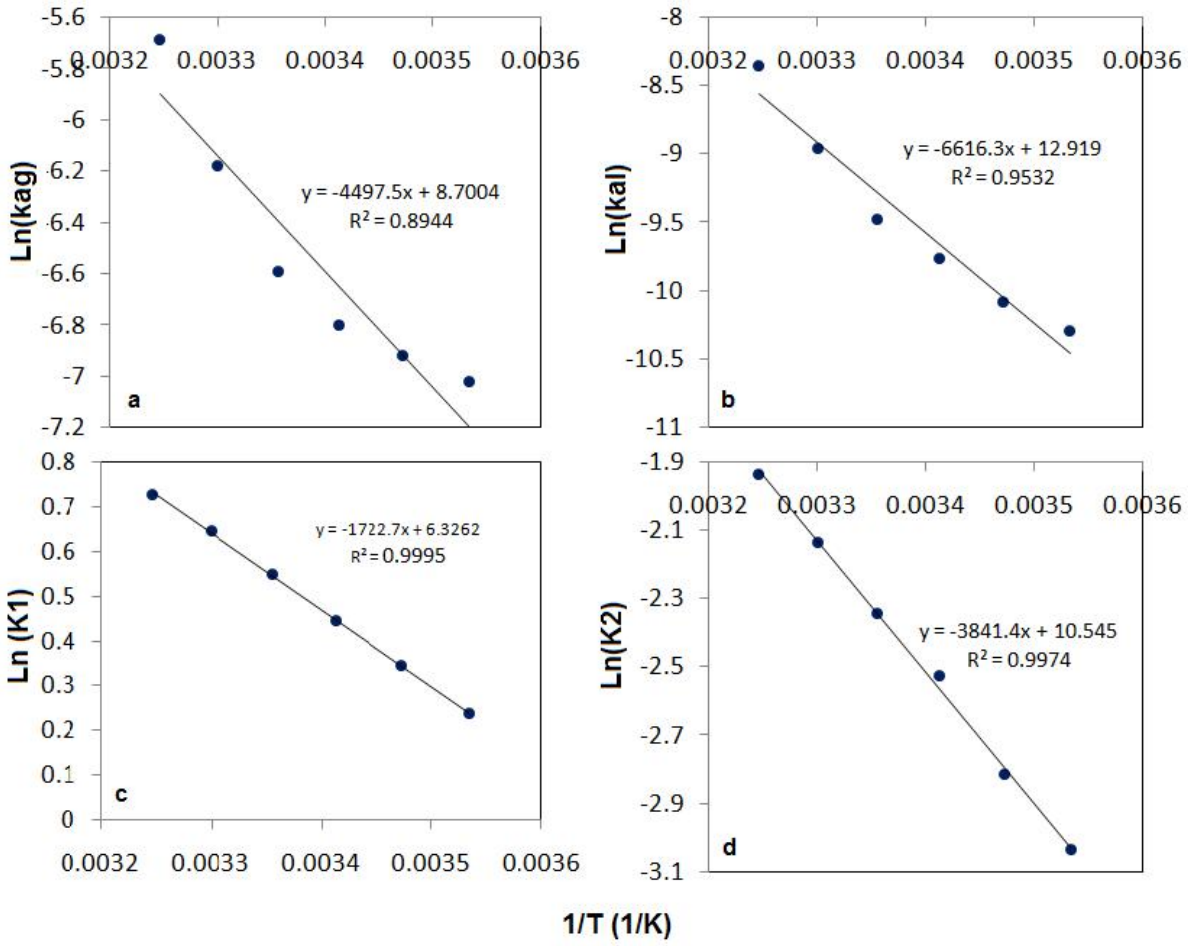

Figure 7.31: For 1-octanol system: (a) $ln(k_a^g)$ versus $1/T$. (b) $ln(k_a^l)$ versus$1/T$. (c) $ln(K_1)$ versus $1/T$. (d) $ln(K_2)$ versus $1/T$. Lines represent the regression models based on the Arrhenius expression.

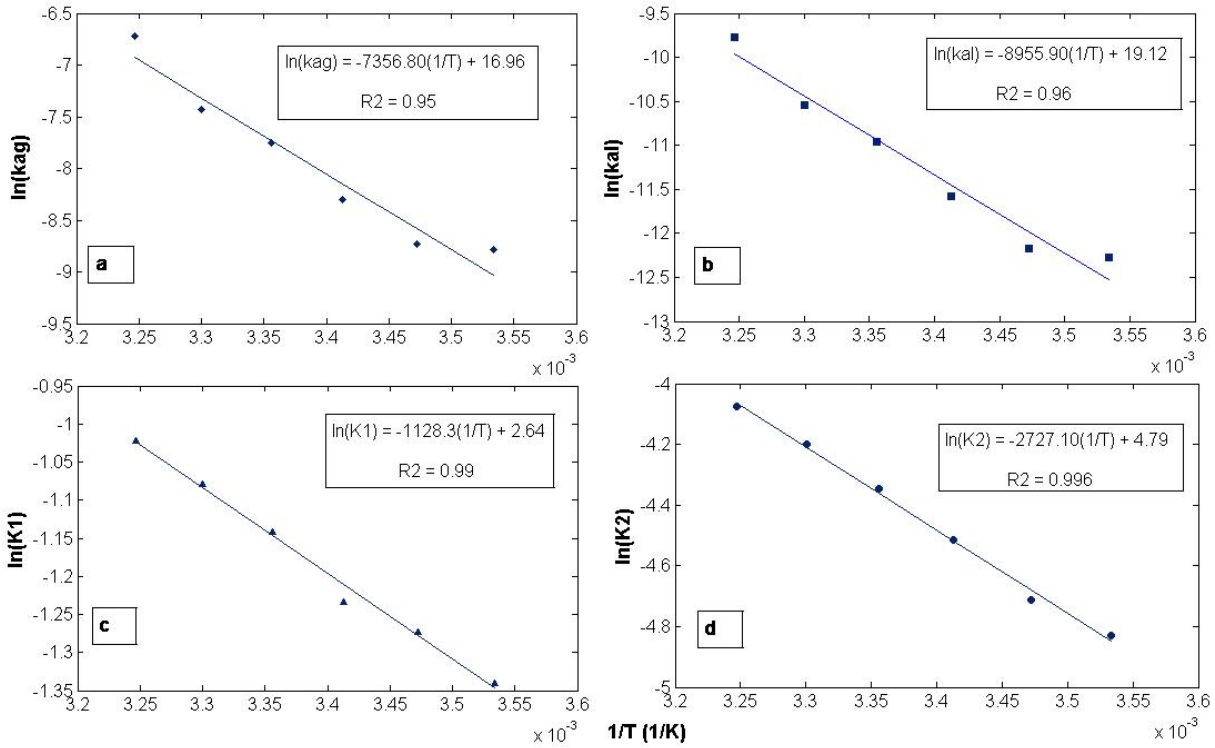

Figure 7.32: For 1-hexanol system: (a) $ln(k_a^g)$ versus $1/T$. (b) $ln(k_a^l)$ versus $1/T$. (c) $ln(K_1)$ versus $1/T$. (d) $ln(K_2)$ versus $1/T$. Lines represent the regression models based on the Arrhenius expression.

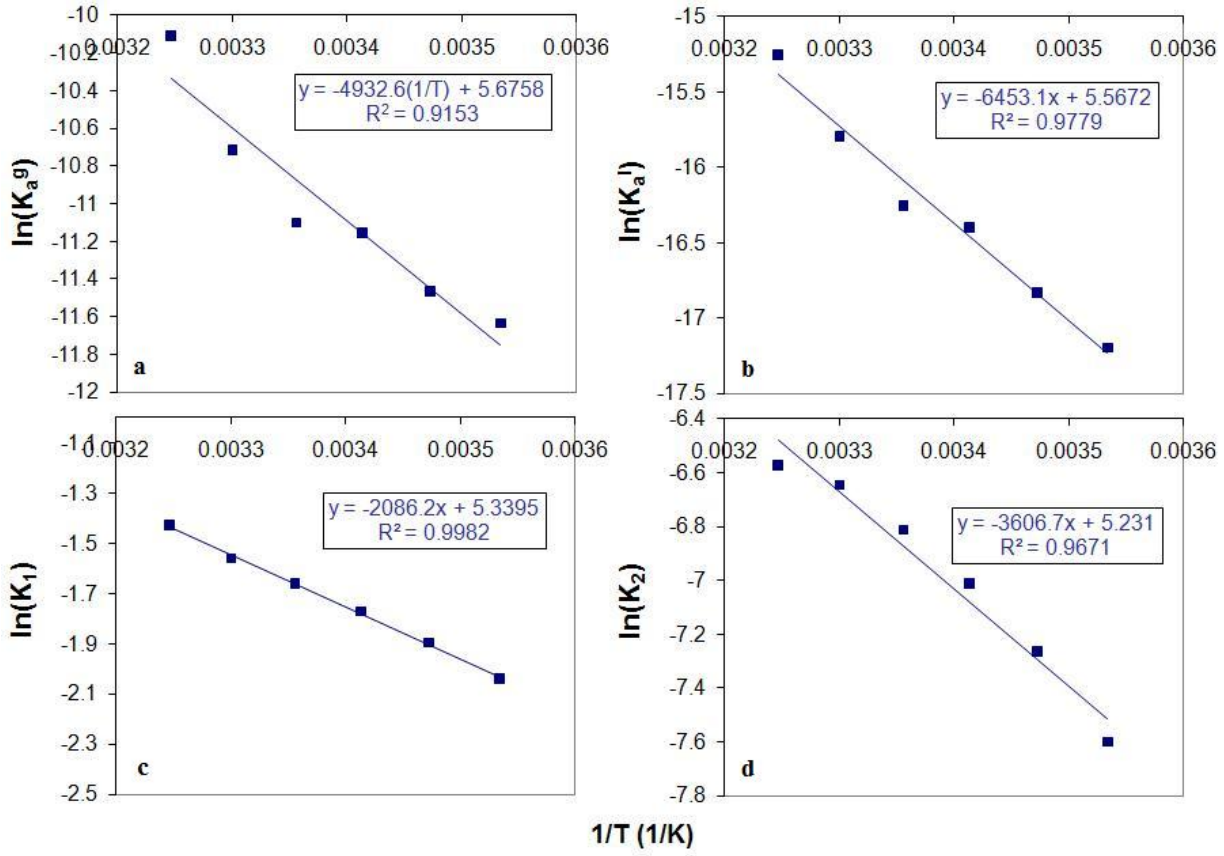

Figure 7.33: For 1-butanol system: (a) $ln(k_a^g)$ versus $1/T$. (b) $ln(k_a^l)$ versus $1/T$. (c) $ln(K_1)$ versus $1/T$. (d) $ln(K_2)$ versus $1/T$. Lines represent the regression models based on the Arrhenius expression.

Table 7.17: Frequency factor (A_f) and the fitting parameter related to energy barrier (E) obtained from fitting the experimental data of the adsorption rate constants (k_a^g, k_a^l) and equilibrium constants (K_1, K_2) for 1-octanol system to the Arrhenius expression (equation 7.20).

Parameter	A_f	E(j/mol)
k_a^g	$6.01 \times 10^3 m^3/mol.s$	3.74×10^4
k_a^l	$4.08 \times 10^5 m^3/mol.s$	5.50×10^4
K_1	$5.59 \times 10^2 m^3/mol$	1.43×10^4
K_2	$3.80 \times 10^4 m^3/mol$	3.19×10^4

Table 7.18: Frequency factor (A_f) and the fitting parameter related to energy barrier (E) obtained from fitting the experimental data of the adsorption rate constants (k_a^g, k_a^l) and equilibrium constants (K_1, K_2) for 1-hexanol system to the Arrhenius expression (equation 7.20).

Parameter	A_f	E(j/mol)
k_a^g	$2.33 \times 10^7 m^3/mol.s$	6.12×10^4
k_a^l	$2.00 \times 10^8 m^3/mol.s$	7.45×10^4
K_1	$1.40 \times 10^1 m^3/mol$	9.38×10^3
K_2	$1.20 \times 10^2 m^3/mol$	2.27×10^4

Table 7.19: Frequency factor (A_f) and the fitting parameter related to energy barrier (E) obtained from fitting the experimental data of the adsorption rate constants (k_a^g, k_a^l) and equilibrium constants (K_1, K_2) for 1-butanol system to the Arrhenius expression (equation 7.20).

Parameter	A_f	E(j/mol)
k_a^g	$4.10 \times 10^4 m^3/mol.s$	1.87×10^2
k_a^l	$5.37 \times 10^4 m^3/mol.s$	2.08×10^2
K_1	$1.73 \times 10^4 m^3/mol$	2.62×10^2
K_2	$3.00 \times 10^4 m^3/mol$	2.92×10^2

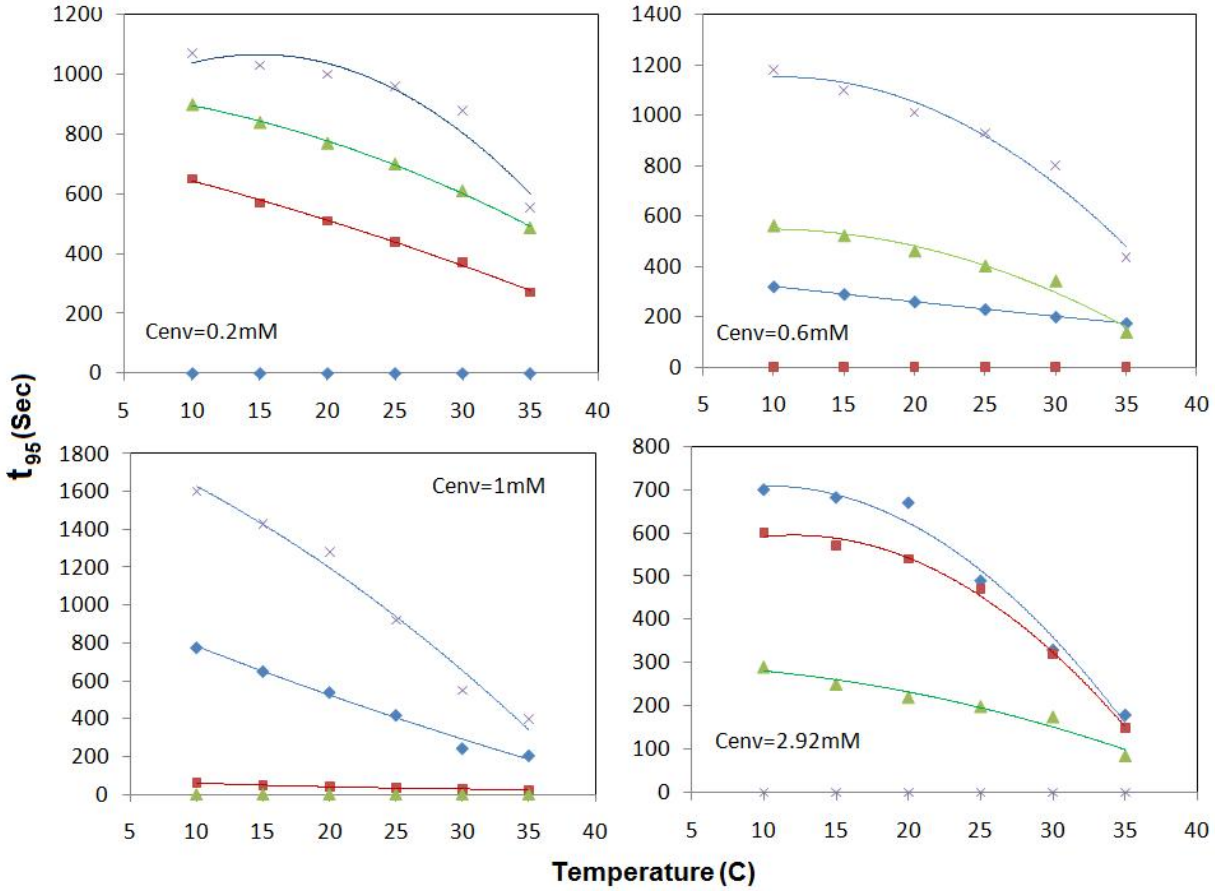

Figure 7.34: t_{95} versus temperature for 1-octanol aqueous solutions. Concentration of the environment solution is indicated in each graph. Experiments were performed at four different drop concentrations (C_{drop}): 0.2mM (blue diamond), 0.6mM (red square), 1mM (green triangle), 2.92mM (blue cross); Lines represent the best quadratic regression model to the experimental data.

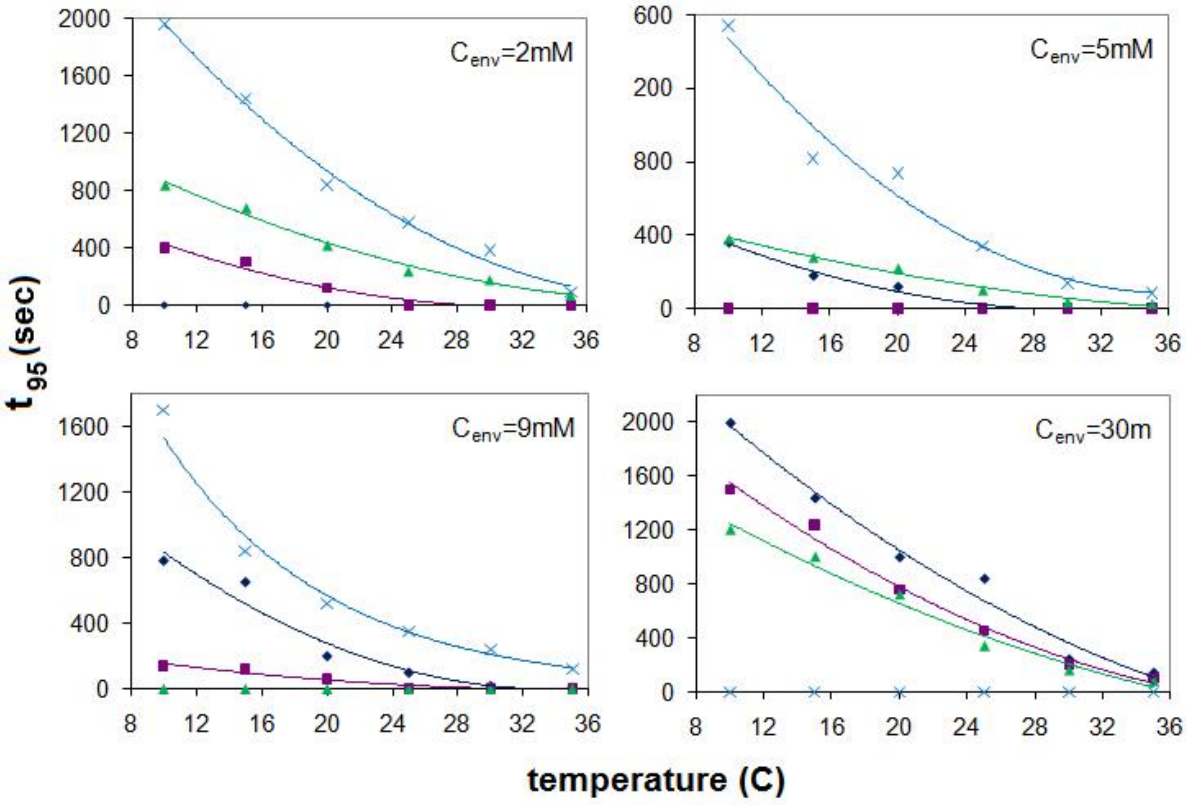

Figure 7.35: t_{95} versus temperature for 1-hexanol aqueous solutions. Concentration of the environment solution is indicated in each graph. Experiments were performed at four different drop concentrations (C_{drop}): 2mM (blue diamond), 5mM (red square), 9mM (green triangle), 30mM (blue cross); Lines represent the best quadratic regression model to the experimental data.

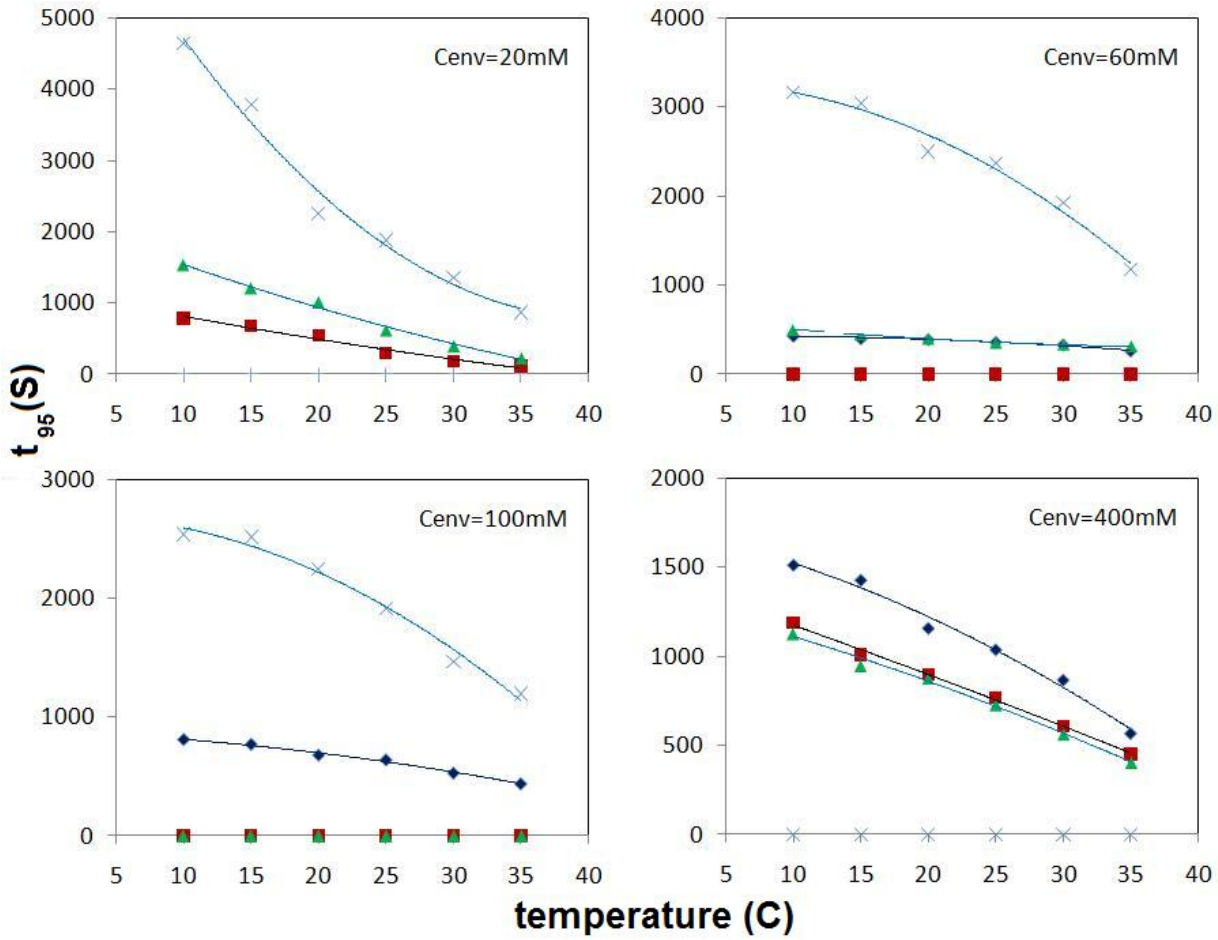

Figure 7.36: t_{95} versus temperature for 1-butanol aqueous solutions. Concentration of the environment solution is indicated in each graph. Experiments were performed at four different drop concentrations (C_{drop}): 20mM (blue diamond), 60 mM (red square), 100mM (green triangle), 400mM (blue cross); Lines represent the best quadratic regression model to the experimental data.

7.5 Summary

The effect of temperature on adsorption kinetics and surface tension of 1-octanol, 1-hexanol and 1-butanol aqueous solutions was investigated in this chapter. Experiments were performed in a closed chamber where the effect of adsorption/desorption from both sides of the liquid/vapor interface could be considered simultaneously. The modified Langmuir equation of state was used to correlate the steady-state surface tension as a function of temperature and concentration. The fitting parameters for this modelling were: the equilibrium constant for adsorption from the vapor phase (K_1), the equilibrium constant for adsorption from the liquid phase (K_2) and the maximum surface concentration (Γ_∞). The experimental results showed that the steady-state surface tension decreased linearly with temperature for all three chemicals at different concentrations of the drop and environment solutions and at temperature ranging from 10 °C to 35 °C. It was shown that $K_1 \gg K_2$ and hence the contribution to adsorption from the vapor side was more important than that from the liquid side. This behavior was much more important in the short chain alcohol (1-butanol) than that of the long chain alcohol (1-octanol). It was found that the contribution to adsorption from both sides of the vapor/liquid interface increased with temperature. The contribution to adsorption from vapor phase (K_1) and liquid phase (K_2) showed an increase with chain length from 1-butanol to 1-octanol. Furthermore, the adsorption kinetics for 1-octanol, 1-hexanol and 1-butanol was modelled using a kinetic transfer equation. The fitting parameters for this modelling were: the maximum surface concentration (Γ_∞), minimum surface concentration (Γ_{min}) and the adsorption rate constant from the vapor phase (k_a^g). Results showed that the rate constants for adsorption from both sides of the vapor/ liquid interface increased with temperature in all three systems of 1-octanol, 1-hexanol and 1-butanol. The modelling results also showed that the rate constant for adsorption from the vapor phase increased when the chain length was increased from 1-butanol to 1-octanol.

Chapter 8

Effect of Carbon Dioxide Pressure on the Surface Tension of 1-octanol, 1-hexanol and 1-butanol Aqueous Solutions

The effect of carbon dioxide pressure on the surface tension and adsorption kinetics of 1-octanol,1-hexanol and 1-butanol aqueous solutions is investigated in this chapter. For each chemical, the experiments performed at four different drop concentrations, four different environment concentrations and five different carbon dioxide pressures. To consider the effect of adsorption/desorption of the two species (surfactant and carbon dioxide) from both sides of a vapor/ liquid interface on the surface tension, the modified Langmuir equation of state and the modified kinetic transfer equation were derived. The steady-state and dynamic (time-dependent) surface tension data were modelled using the modified Langmuir equation of state and the modified kinetic transfer equation, respectively. The equilibrium constants and adsorption rate constants of the surfactants and carbon dioxide were evaluated through a minimization procedure for CO_2 pressures ranging from 0 to 690 KPa.

8.1 Introduction

For over a century, the effect of compressed gases, such as carbon dioxide, nitrogen and hydrogen, on the surface tension of water has been one of the most intriguing research subjects in interfacial phenomena and surface science [29, 63, 64, 65, 66, 67, 68, 69]. Jho et al. showed that an increase in the pressure of gases, such as carbon dioxide, methane,

ethane, ethylene, normal butane, and isobutene, over gas-water systems can produce marked changes in surface tension by virtue of enhanced adsorption of the gas component at the interface [65]. The surface tension of ethanol-carbon dioxide and ethanol-nitrogen systems showed a decrease with the pressure of carbon dioxide and nitrogen, respectively [68]. Massoudi et al. showed that the surface tension of aqueous solutions of sodium chloride and tetra-n-butylammonium bromide decreased with the pressure of sourrounding gases, such as CH_4 , C_2H_4 , C_2H_6 C_4H_{10}, and CO_2 [64]. It has been shown that the interfacial tension of fish oil triglycerides (TG) and fatty acid ethyl esters (FAEE) in contact with carbon dioxide decreased substantially with the CO_2 pressure [70]. Georgiadis et al. showed that the surface tension of water and n-alkane mixtures in contact with carbon dioxide decreased with the pressure of carbon dioxide [71].

In chapters 4-7 we showed that when a volatile surfactant, such as 1-octanol, 1-hexanol and 1-butanol, is dissolved in a liquid, it presents a finite partial pressure in the vapor phase, and the surface tension of the solution can be affected by surfactant adsorption from both sides of the vapor/liquid interface [25, 59, 60, 61, 72]. It was shown that at steady-state, the effect of adsorption from the vapor side is more important than that from the liquid side [25, 59, 60, 61, 72]. The main objective and the unique approach of the current research is to investigate the effect of carbon dioxide pressure on the surface tension and adsorption kinetics of 1-octanol, 1-hexanol and 1-butanol aqueous solutions when adsorption/desorption of two species (carbon dioxide and surfactant) from both sides of a vapor-liquid surface is considered simultaneously. 1-octanol, 1-hexanol and 1-butanol were chosen because of their applications in flavors and essences. They are used as an intermediate solvent in the pharmaceutical and perfume industry [27]. Also, they are used in the production of plasticizers and fatty alcohols.

8.2 Experimental Section

8.2.1 Materials

The chemical 1-octanol, 1-hexanol and 1-butanol with purity greater than 99% , was purchased from Sigma-Aldrich (Oakville, Ontario, Canada). The water used was purified by an ultra-pure water system (Millipore Ltd., Mississauga, Ontario, Canada), with resistivity of 18.2 $m\Omega$. The relative humidity of the environment during the experiments was around 80%. Four different concentrations: 0.2, 0.6, 1 , and 2.92 mM for 1-octanol, four different concentrations: 2.0, 6.0, 10.0, and 25.0 mM for 1-hexanol and four different concentrations: 20, 40, 100, and 400 mM for 1-butanol were prepared. They were used in preparation of both the sample drop solution (C_{drop}) and the environment solution (C_{env}). The sample with the highest concentration was prepared as the stock solution, and the lower concentration samples were made by diluting this stock solution.

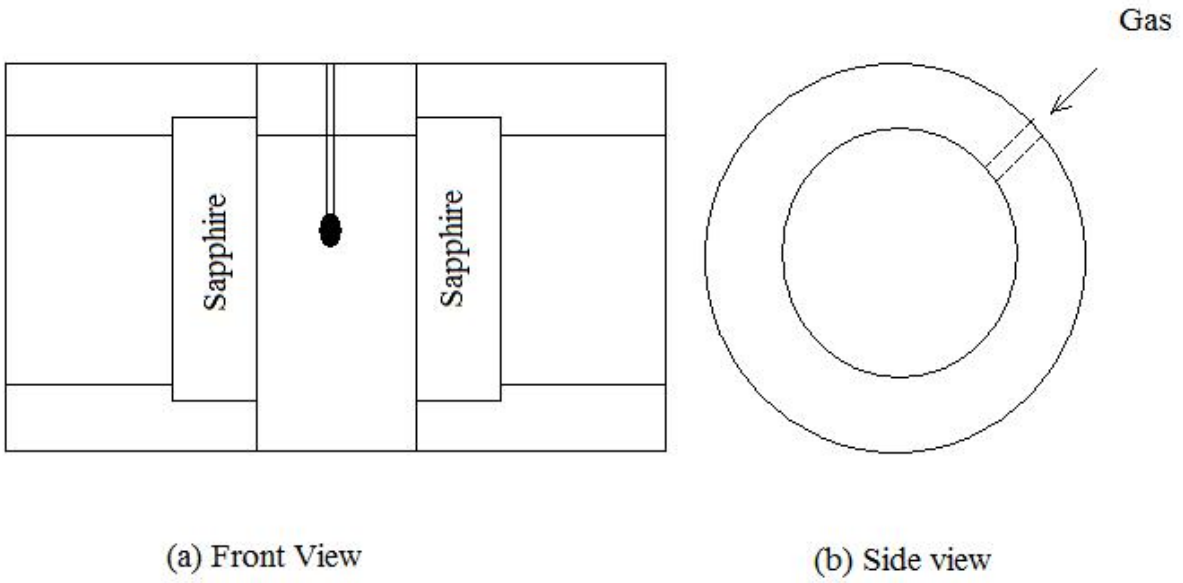

Figure 8.1: Schematic of the environment chamber: (a) front view and (b) side view.

8.2.2 Surface Tension Measurement

In this chapter the ADSA-P method was used for measuring the surface tension of 1-octanol, 1-hexanol and 1-butanol aqueous solutions in different pressures of carbon dioxide. The theoretical, numerical and experimental procedures for surface tension measurements using this method were explained in chapter 3-7. Figure 3.1B shows the experimental set-up of ADSA-P used in this work. For surface tension measurements at high carbon dioxide pressure a new environment chamber was designed and fabricated. The new environment chamber, used to hold the pendant drop, had two sapphire windows mounted perpendicular to the chamber axis (Figure 8.1). The inside of the chamber was cylindrical in shape, with dimensions of 30 mm (diameter) by 25 mm (length). Two flat optical-quality sapphire windows (Meller Optics, Inc.), sandwiched between Brass and Teflon gaskets within the chamber, permitted illumination and viewing of the drop.

A pressure gage was attached to the chamber (Figure 8.2) to measure the pressure inside the chamber. In the case of de-pressurizing the chamber, the pressure inside the chamber was relieved from an exhaust valve connected to the pressure gage. In order to protect the chamber from being subjected to a pressure exceeded from the designed limit, a pressure relief valve was connected to the chamber to open at a predetermined set pressure. A high pressure syringe was attached to the chamber to form a pendant drop within the

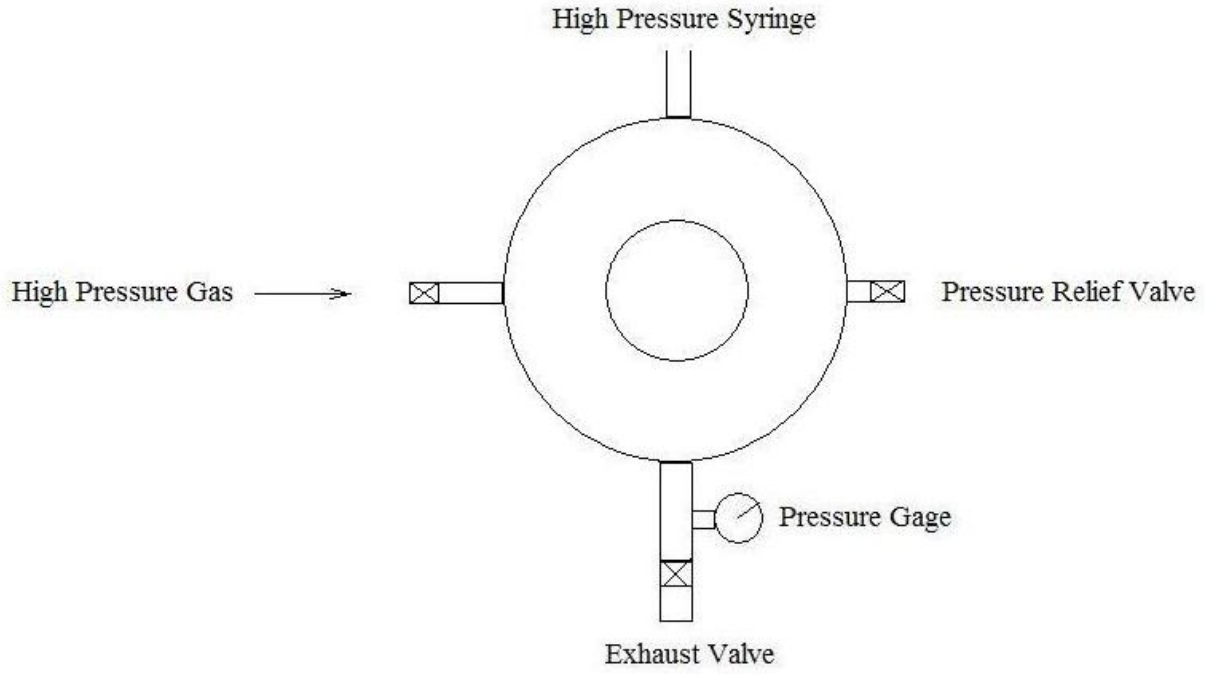

Figure 8.2: Schematic of the environment chamber: (a) front view and (b) side view.

cell.

In the experimental approach, at each combination of the prescribed concentrations of the drop and environment solutions, the dynamic surface tension of 1-octanol, 1-hexanol and 1-butanol aqueous solutions was measured at five different pressures of carbon dioxide (0 psi (0Kpa),10 psi (69KPa), 20 psi (138KPa), 50 psi (345KPa) and 100psi (690KPa)).

8.3 Theoretical Framework: Kinetic Transfer Equation

8.3.1 The Gibbs Equation and the Thermodynamic of Surface Adsorption

In Gibbs's treatment, a column containing two bulk phases α and β is considered (Figure 8.3) in which they are separated by a surface region ($AA^{'}BB^{'}$). Gibbs realized that the

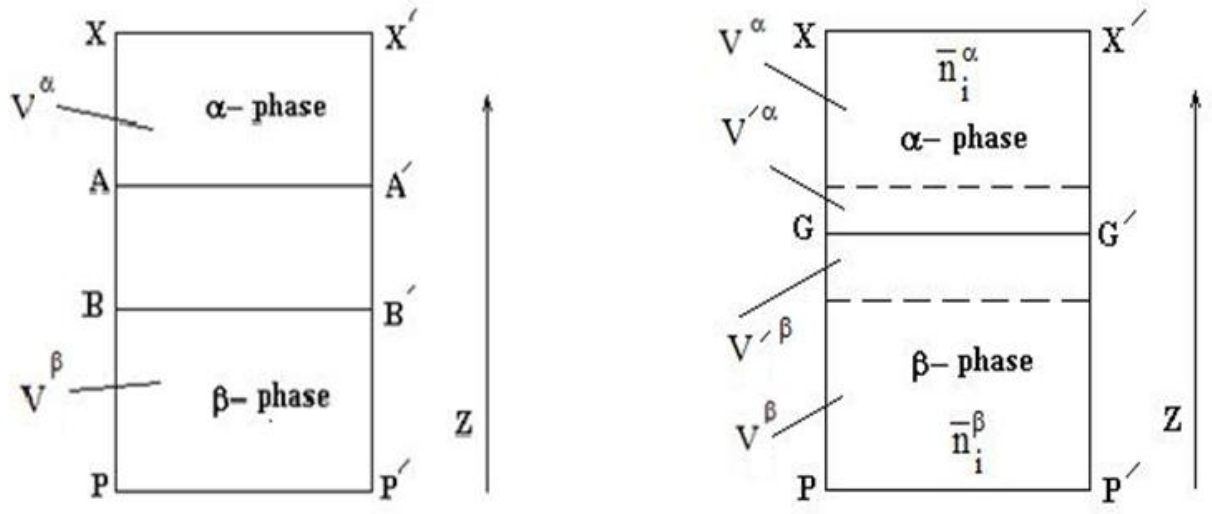

Figure 8.3: (left)The phase column in the real system (left) and in the idealized system (right).

actual surface region is inhomogeneous and hard to define. Thus, he considered a mathematical plane $GG^{'}$, called dividing surface, parallel to $AA^{'}$ and $BB^{'}$ (Figure 8.3). The two phases α and β are separated by this dividing surface. In the actual system, the bulk concentration of the i^{th} component in α and β phases are C_i^{α} and C_i^{β} , respectively, and n_i^t stands for the total number of moles of the i^{th} component in all three regions. In the idealized system, the chemical compositions of α and β phases are assumed to remain constant right up to the dividing surface.

In the real system, the total number of moles can be defined as follows:

$$n_i^t = n_i^{\alpha} + n_i^{\beta} + n_i^s = C_i^{\alpha} V^{\alpha} + C_i^{\beta} V^{\beta} + n_i^s \tag{8.1}$$

where n_i^{α} , $n_i^{\beta}$and n_i^s are the number of moles of component i^{th} in phase α , β and in the surface region of the real system, respectively. V^{α} and V^{β} are the volumes of phase α and β in the real system, respectively. In the idealized system, the total number of moles can be defined as follows:

$$n_i^t = \overline{n}_i^{\alpha} + \overline{n}_i^{\beta} + n_i^x = C_i^{\alpha}(V^{\alpha} + V^{'\alpha}) + C_i^{\beta}(V^{\beta} + V^{'\beta}) + n_i^x \tag{8.2}$$

where$V^{'\alpha}$ and $V^{'\beta}$ are the volumes added to phase α and β because of the position of

dividing plane $GG^{'}$ in the idealized system. Substituting equation 8.2 into equation 8.1 yield:

$$n_i^x = n_i^s - C_i^{\alpha} V^{'\alpha} - C_i^{\beta} V^{'\beta} \tag{8.3}$$

Because the mathematical plane $GG^{'}$ is arbitrary (theoretically for flat surfaces), it can be so chosen that the n_i^x for one component i^{th} would be zero. In constant temperature, the 2-D Gibbs-Duhem relation among changes in intensive parameters at the interface can be reduced to:

$$d\gamma + \Sigma \Gamma_i d\mu_i = 0 \tag{8.4}$$

Where the surface concentration equals to the number of moles per unit area of the surface:

$$\Gamma_i = \frac{n_i}{A} \tag{8.5}$$

For three component systems, equation 8.4 can be written as:

$$d\gamma + \Gamma_w d\mu_w + \Gamma_1 d\mu_1 + \Gamma_2 d\mu_2 = 0 \tag{8.6}$$

where Γ_w , Γ_1 and Γ_2 are the surface concentrations of solvent (water), solutes 1 and 2, respectively, and μ_w, μ_1 and μ_2 are the chemical potentials of solvent and solutes 1 and 2, respectively. Based on the aforementioned discussion, if plane $GG^{'}$ is chosen properly, it is possible to set the number of excess molecules of the solvent (n_w^x) on the surface $GG^{'}$ equal to zero ($\Gamma_w = 0$), so that equation 8.6 can be reduced to equation 8.7

$$-d\gamma = \Gamma_1 d\mu_1 + \Gamma_2 d\mu_2 = 0 \tag{8.7}$$

At equilibrium, chemical potential is uniform throughout the interface, and two adjacent bulk phases:

$$\mu_1 = \mu_1^0 + RTln(f_1 x_1) \tag{8.8}$$

$$\mu_1 = \mu_2^0 + RTln(f_2 x_2) \tag{8.9}$$

where μ_1^0 and μ_2^0 are the reference chemical potentials, f_1 and f_2 are the activity coefficients, x_1 and x_2 are the mole fraction of the two solutes, R is the universal gas constant,

and T is the absolute temperature. For dilute solution, the activity coefficients can be considered as one (equation 8.10). If the mole fractions are replaced by concentrations (equation 8.11 and 8.12), then the Gibbs adsorption equation (equation 8.13), which relates the changes in the surface concentrations (for solute 1 and 2) to the surface tension, will be derived:

$$f_1 = f_2 = 1 \tag{8.10}$$

$$x_1 = C_1 \tag{8.11}$$

$$x_2 = C_2 \tag{8.12}$$

$$-d\gamma = \Gamma_1 RTd(ln(C_1)) + \Gamma_2 RTd(ln(C_2)) \tag{8.13}$$

C_1 and C_2 are the concentrations of the solutes in the bulk liquid phases.

8.4 Modified Langmuir Adsorption Isotherm

In the derivation of the classic Langmuir isotherm, just adsorption from the liquid phase was considered. In the previously derived modified adsorption equation, adsorption from the liquid phase and the vapor phase was considered simultaneously [25]. As a result, the modified Langmuir adsorption isotherm is a relation between the surface concentration and either the concentration in the bulk liquid phase or the partial pressure of the vapor phase. In the current system the simultaneous contribution to adsorption of two solutes from the two sides of a vapor/liquid interface will be considered. The derivation will follow the same rationales and level of assumptions as the classic Langmuir isotherm. The first step in the derivation is to write expressions for the rates of adsorption and desorption to and from either side of the vapor/liquid interface [75]:

$$r_{a1}^g = k_{a1}^g P_1 (S_{m1} - S_1 - S_2 \frac{\Gamma_{\infty 1}}{\Gamma_{\infty 2}}) \tag{8.14}$$

$$r_{a1}^l = k_{a1}^l C_1 (S_{m1} - S_1 - S_2 \frac{\Gamma_{\infty 1}}{\Gamma_{\infty 2}}) \tag{8.15}$$

$$r_{a2}^g = k_{a2}^g P_2 (S_{m2} - S_2 - S_1 \frac{\Gamma_{\infty 2}}{\Gamma_{\infty 1}}) \tag{8.16}$$

$$r_{a2}^{l} = k_{a2}^{l} C_2 (S_{m2} - S_2 - S_1 \frac{\Gamma_{\infty 2}}{\Gamma_{\infty 1}}) \tag{8.17}$$

$$r_{d1}^{g} = k_{d1}^{g} S_1 \tag{8.18}$$

$$r_{d1}^{l} = k_{d1}^{l} S_1 \tag{8.19}$$

$$r_{d2}^{g} = k_{d2}^{g} S_2 \tag{8.20}$$

$$r_{d2}^{l} = k_{d2}^{l} S_2 \tag{8.21}$$

where $r_{a1}^{g}, r_{d1}^{g}, r_{a1}^{l}$ and r_{d1}^{l} are the rates of adsorption and desorption for species 1 from the vapor (g) and liquid (l) phase, respectively. $r_{a2}^{g}, r_{d2}^{g}, r_{a2}^{l}$ and r_{d2}^{l} are the rates of adsorption and desorption for species 2 from the vapor (g) and liquid (l) phase, respectively. $k_{a1}^{g}, k_{d1}^{g}, k_{a1}^{l}$ and k_{d1}^{l} are the kinetic rate constants of adsorption and desorption for species 1 from the vapor phase(g) and liquid phase (l), respectively. $k_{a2}^{g}, k_{d2}^{g}, k_{a2}^{l}$ and k_{d2}^{l} are the kinetic rate constants of adsorption and desorption for species 2 from the vapor phase(g) and liquid phase (l), respectively. P_1 and P_2 are the partial pressures of species 1 and 2, respectively. C_1 and C_2 are the concentrations of species 1 and 2 in the liquid phase, respectively. S_{m1} and S_{m2} are the total number of adsorption sites per unit area of the interface if surface is occupied only by species 1 or 2, respectively. S_1 and S_2 are the number of occupied adsorption sites per unit area of the surface by species 1and 2, respectively. $\Gamma_{\infty 1}$ and $\Gamma_{\infty 2}$ are the maximum surface concentrations of species 1 and 2, respectively. The model follows Langmuir kinetics where the rates of adsorption minus the rates of desorption is equal to the change of surface concentration over time. Equations 8.22 and 8.23 show these relations for species 1 and 2, respectively:

$$\frac{d\Gamma_1}{dt} = (r_{a1}^{g} + r_{a1}^{l}) - (r_{d1}^{g} + r_{d1}^{l}) \tag{8.22}$$

$$\frac{d\Gamma_2}{dt} = (r_{a2}^{g} + r_{a2}^{l}) - (r_{d2}^{g} + r_{d2}^{l}) \tag{8.23}$$

For the steady-state condition, the change in surface concentrations versus time should be equal to zero:

$$\frac{d\Gamma_1}{dt} = \frac{d\Gamma_2}{dt} = 0 \tag{8.24}$$

For this condition, equation 8.25 can be achieved for species 1 if equations 8.14 , 8.15 , 8.18 and 8.19 substitute into equation 8.22:

$$k_{a1}^{g} P_1 (S_{m1} - S_1 - S_2 \frac{\Gamma_{\infty 1}}{\Gamma_{\infty 2}}) + k_{a1}^{l} C_1 (S_{m1} - S_1 - S_2 \frac{\Gamma_{\infty 1}}{\Gamma_{\infty 2}}) = k_{d1}^{g} S_1 + k_{d1}^{l} S_1 \tag{8.25}$$

Relations 8.26 can be applied if we consider that the number of occupied sites at the surface is proportional to surface concentration:

$$S_1 \propto \Gamma_1, S_2 \propto \Gamma_2, S_{m1} \propto \Gamma_{\infty 1}, S_{m2} \propto \Gamma_{\infty 2} \tag{8.26}$$

Equation 8.27 can be derived if relations 8.26 are applied into equation 8.25:

$$k_{a1}^{g} P_1 (1 - \frac{\Gamma_1}{\Gamma_{\infty 1}} - \frac{\Gamma_2}{\Gamma_{\infty 2}}) + k_{a1}^{l} C_1 (1 - \frac{\Gamma_1}{\Gamma_{\infty 1}} - \frac{\Gamma_2}{\Gamma_{\infty 2}}) = (k_{d1}^{g} + k_{d1}^{l}) \frac{\Gamma_1}{\Gamma_{\infty 1}} \tag{8.27}$$

After rearranging equation 8.27, equation 8.28 can be achieved:

$$(k_{a1}^{g} P_1 + k_{a1}^{l} C_1) = (k_{a1}^{g} P_1 + k_{a1}^{l} C_1 + k_{d1}^{g} + k_{d1}^{l}) \frac{\Gamma_1}{\Gamma_{\infty 1}} + (k_{a1}^{g} P_1 + k_{a1}^{l} C_1) \frac{\Gamma_2}{\Gamma_{\infty 2}} \tag{8.28}$$

In a similar way, equation 8.29 can be derived if the net rate of adsorption and desorption for the second species equate to zero:

$$(k_{a2}^{g} P_2 + k_{a2}^{l} C_2) = (k_{a2}^{g} P_2 + k_{a2}^{l} C_2 + k_{d2}^{g} + k_{d2}^{l}) \frac{\Gamma_2}{\Gamma_{\infty 2}} + (k_{a2}^{g} P_2 + k_{a2}^{l} C_2) \frac{\Gamma_1}{\Gamma_{\infty 1}} \tag{8.29}$$

Solving equations 8.28 and 8.29 for $\frac{\Gamma_1}{\Gamma_{\infty 1}}$ and $\frac{\Gamma_2}{\Gamma_{\infty 2}}$ yields the following results for the new modified adsorption isotherms:

$$\frac{\Gamma_1}{\Gamma_{\infty 1}} = \frac{K_1 P_1 + K_2 C_1}{1 + K_1 P_1 + K_2 C_1 + K_3 P_2 + K_4 C_2} \tag{8.30}$$

$$\frac{\Gamma_2}{\Gamma_{\infty 2}} = \frac{K_3 P_2 + K_4 C_2}{1 + K_1 P_1 + K_2 C_1 + K_3 P_2 + K_4 C_2} \tag{8.31}$$

where K_1 and K_2 are the equilibrium constants for adsorption from the gas phase and liquid phase of species 1, respectively. K_3 and K_4 are the equilibrium constants for

adsorption from the gas phase and liquid phase of species 2, respectively. The equilibrium constants represent the contribution to adsorption from each side of a vapor/liquid interface:

$$K_1 = \frac{k_{a1}^g}{k_{d1}^g + k_{d1}^l} \tag{8.32}$$

$$K_2 = \frac{k_{a1}^l}{k_{d1}^g + k_{d1}^l} \tag{8.33}$$

$$K_3 = \frac{k_{a2}^g}{k_{d2}^g + k_{d2}^l} \tag{8.34}$$

$$K_4 = \frac{k_{a2}^l}{k_{d2}^g + k_{d2}^l} \tag{8.35}$$

8.4.1 Modified Frumkin Equation

Equation 8.36 can be derived if equations 8.30 and 8.31 substitute into the Gibbs adsorption equation (equation 8.13):

$$-d\gamma = \Gamma_{\infty 1}\frac{K_1P_1 + K_2C_1}{1 + K_1P_1 + K_2C_1 + K_3P_2 + K_4C_2}RTd(lnC_1) +$$

$$\Gamma_{\infty 2}\frac{K_3P_2 + K_4C_2}{1 + K_1P_1 + K_2C_1 + K_3P_2 + K_4C_2}RTd(lnC_2) \tag{8.36}$$

For integrating purposes, the partial pressures P_1 and P_2 can be related to the concentrations of species 1 and 2 in the liquid bulk phases C_1 and C_2 through Henry's law ($P_1 = H_1C_1$ and $P_2 = H_2C_2$):

$$-d\gamma = \Gamma_{\infty 1}\frac{K_1P_1 + K_2^{'}P_1}{1 + K_1P_1 + K_2^{'}P_1 + K_3^{'}C_2 + K_4C_2}RTd(lnP_1) +$$

$$\Gamma_{\infty 2}\frac{K_3^{'}C_2 + K_4C_2}{1 + K_1P_1 + K_2^{'}P_1 + K_3^{'}C_2 + K_4C_2}RTd(lnC_2) \tag{8.37}$$

Where $K_2^{'} = K_2/H_1$ and $K_3^{'} = K_3/H_2$. The new modified kinetic transfer equation (equation 8.38) can be derived if the first expression in the right hand side of equation 8.37 is integrated from $P_1 = 0$ to P_1 and the second expression is integrated from $C_2 = 0$ to C_2. The expression in the left hand side is integrated from γ_w (pure water surface tension) to γ (surface tension at specific condition of P, T, C_1 and C_2):

$$\gamma - \gamma_w = RT\left[\Gamma_{\infty 1} ln\left(\frac{1 + K_3^{'}C_2 + K_4C_2}{1 + K_1P_1 + K_2^{'}P_1 + K_3^{'}C_2 + K_4C_2}\right)\right] + RT\left[\Gamma_{\infty 2} ln\left(\frac{1 + K_1P_1 + K_2^{'}P_1}{1 + K_1P_1 + K_2^{'}P_1 + K_3^{'}C_2 + K_4C_2}\right)\right] \tag{8.38}$$

Using the new modified adsorption isotherms (equations 8.30 and 8.31), equation 8.38 can be simplified as the modified Frumkin equation (equation 8.39):

$$\gamma = \gamma_w + RT\left[\Gamma_{\infty 1} ln\left(1 - \frac{\Gamma_1}{\Gamma_{\infty 1}}\right) + \Gamma_{\infty 2} ln\left(1 - \frac{\Gamma_2}{\Gamma_{\infty 2}}\right)\right] \tag{8.39}$$

The second term in the right hand side of equation 8.39 represents the effect of adsorption of first species (i.e., carbon dioxide) on the steady-state surface tension (γ), and the third term represents the effect of adsorption of the second species (i.e., 1-hexanol) on the steady-state surface tension.

8.4.2 Modified Langmuir Equation of State

Since the source of the surfactant vapor pressure inside the chamber is the environment solution, the partial pressure of the surfactant in the vapor phase (P_2) can be related to the concentration of the environment solution (C_{env2}) through Henry's law. For more clarity the concentration of surfactant in the liquid bulk phase (C_2) can be replaced by C_{drop2}. It should be noted that the Henry's law constant has been incorporated into K_2 and K_3 so the units of the equilibrium constants for each species are uniform. In this case, equation 8.38 can be simplified as the modified Langmuir equation of state (equation 8.40):

$$\gamma = \gamma_w + RT\left[\Gamma_{\infty 1} ln\left(\frac{1 + K_3C_{env2} + K_4C_{drop2}}{1 + K_1P_1 + K_2P_1 + K_3C_{env2} + K_4C_{drop2}}\right)\right] + RT\left[\Gamma_{\infty 2} ln\left(\frac{1 + K_1P_1 + K_2P_1}{1 + K_1P_1 + K_2P_1 + K_3C_{env2} + K_4C_{drop2}}\right)\right] \tag{8.40}$$

The modified Langmuir equation of state (equation 8.40) can be applied for modelling the experimental data of the steady-state surface tension when the effect of adsorption/desorption of two species from/to the both sides of an interface is considered simultaneously. Equation 8.40 can be simplified to equation 8.41 if carbon dioxide pressure would be zero. Equation 8.41 was applied in chapter 7 for modelling the steady-state surface tension of 1-octanol, 1-hexanol and 1-butanol aqueous solutions.

$$\gamma = \gamma_w - RT\Gamma_{\infty 2} ln\left(1 + K_3 C_{env2} + K_4 C_{drop2}\right) \tag{8.41}$$

Equation 8.40 can be simplified to equation 8.42 if the surfactant concentrations in the environment solution and in the drop solution would be zero ($C_{env} = C_{drop} = 0$).

$$\gamma = \gamma_w - RT\Gamma_{\infty 1} ln\left(1 + K_a P_1\right) \tag{8.42}$$

where $K_a = K_1 + K_2$. In section 8.5.1, equation 8.42 is applied for modelling the steady-state surface tension data of water/carbon dioxide system. Two fitting parameters including $\Gamma_{\infty 1}$ and K_a are evaluated by minimization residual sum of squares between the experimental data and theoretical prediction of the steady-state surface tension of water/carbon dioxide system. In chapter 7 the three groups of fitting parameters including $\Gamma_{\infty 2}, K_3$ and K_4 were evaluated from modelling the steady-state surface tension data of 1-octanol, 1-hexanol and 1-butanol aqueous solutions (at different temperatures) using equation 8.41. In section 8.5.1, the two groups of fitting parameters ($\Gamma_{\infty 1}$, K_a, $\Gamma_{\infty 2}$ K_3 and K_4) evaluated from minimizing the residual sum of squares between the theoretical predictions and experimental data of the two systems (water-CO_2 and surfactant in aqueous solutions) substitute in equation 8.40. The significance of fit of the theoretical prediction (from equation 8.40) to the experimental data of a the surfactant aqueous solutions surrounded by carbon dioxide is evaluated through the analysis of variance (ANOVA table).

The theoretical prediction of the dynamic surface concentrations can be achieved if equations 8.22 and 8.23 are simplified based on equations 8.14- 8.21 and 8.32 - 8.35:

$$\frac{d\Gamma 1}{dt} = k_{a1}^{g}\Gamma_{\infty 1}\left(P_1 + \frac{K_2}{K_1}C_{drop1}\right) - k_{a1}^{g}\Gamma_1\left(P_1 + \frac{K_2}{K_1}C_{drop1} + \frac{1}{K_1}\right) - k_{a1}^{g}\Gamma_2\frac{\Gamma_{\infty 1}}{\Gamma_{\infty 2}}\left(P_1 + \frac{K_2}{K_1}C_{drop1}\right) \tag{8.43}$$

$$\frac{d\Gamma 2}{dt} = k_{a2}^{g}\Gamma_{\infty 2}\left(C_{env2} + \frac{K_4}{K_3}C_{drop2}\right) - k_{a2}^{g}\Gamma_2\left(C_{env2} + \frac{K_4}{K_3}C_{drop2} + \frac{1}{K_3}\right) -$$

$$k_{a2}^{g}\Gamma_1\frac{\Gamma_{\infty 2}}{\Gamma_{\infty 1}}\left(C_{env2} + \frac{K_4}{K_3}C_{drop2}\right) \tag{8.44}$$

If the concentration of species 1 (carbon dioxide) in the liquid phase (C_{drop1}) is related to the partial pressure of species 1 (P_1) through Henry's law ($P_1 = H_1 C_{drop1}$), the equation 8.43 can be simplified as equation 8.45:

$$\frac{d\Gamma 1}{dt} = k_{a1}^{g}K_b P_1\Gamma_{\infty 1} - k_{a1}^{g}\Gamma_1\left(K_b P_1 + \frac{K_b}{K_a}\right) - k_{a1}^{g}K_b P_1\Gamma_2\frac{\Gamma_{\infty 1}}{\Gamma_{\infty 2}} \tag{8.45}$$

where $K_b = 1 + \frac{K_2}{K_1}$. It should be noted that the Henry's law constant has been incorporated into K_2 so the units of the equilibrium constants are uniform. Equations 8.44 and 8.45 are first order ordinary differential equations and can be solved to give the surface concentrations of the two species as a function of time. A theoretical prediction of dynamic surface tension can be achieved from the modified Frumkin equation 8.39 and the two solutions for Γ_1 and Γ_2 calculated from equations 8.44 and 8.45. Using a minimization procedure, fitting parameters including the adsorption rate constants from the vapor phase for two species (k_{a1}^{g}, k_{a2}^{g}) and constant K_b can be evaluated by minimizing the residual sum of squares between the model prediction (using equations 8.39, 8.44 and 8.45) and the experimental data of the dynamic surface tension.

8.5 Results and Discussion

Using the outlined experimental procedure, the dynamic and steady-state surface tension of 1-octanol,1-hexanol and 1-butanol aqueous solutions were measured at 25 °C and at five different pressures of carbon dioxide and four different concentrations of the drop and environment solutions. Each experiment repeated three times to ensure that the results are reproducible. The reproducibility test of the surface tension values showed that the results were reproducible with the 95% confidence intervals less than 0.2 mN/m. A total of 80 profiles were collected for each chemical and divided into four different categories based on the concentrations of the environment solution. The concentrations of the environment solution for 1-octanol were: 0.2 mM (Figure 8.4), 0.6 mM (Figure 8.5), 1 mM (Figure 8.6) and 2.92 mM (Figure 8.7). The concentrations of the environment solution for 1-hexanol were: 1mM (Figure 8.8), 6mM (Figure 8.9), 10mM (Figure 8.10) and 25mM (Figure

8.11). The concentrations of the environment solution for 1-butanol were: 20 mM (Figure 8.12), 60 mM (Figure 8.13), 100 mM (Figure 8.14) and 400 mM (Figure 8.15). In profiles of Figures 8.4-8.15, the dynamic surface tension initially increases if the concentration of the environment solution is less than that of the drop solution, eventually reaching a plateau value. The dynamic surface tension initially decreases if the concentration of the environment solution is greater than that of the drop solution. The surface tension essentially remains constant when the concentration of the drop solution is as same as the concentration of the environment solution. In Figures 8.4-8.15, the reduction of the steady-state surface tension can be observed when pressure increases from 0 to 690 KPa. Furthermore, in Figures 8.4-8.15 the time required to reach to the steady-state surface tension increases if the pressure is increased. For instance for 1-hexanol aqueous solution, when the concentration of the environment solution is 6mM and concentration of the drop solution is 25mM (Figure 8.9D), the time required to reach to the steady-state surface tension is 7000 second when the carbon dioxide pressure is 690 KPa, while it is 3000 second at 0 KPa of carbon dioxide pressure.

8.5.1 Steady-State Surface Tension

In chapter 7 three groups of fitting parameters ($\Gamma_{\infty 2}, K_3,$ andK_4) were evaluated from modelling the steady-state surface tension data of 1-octanol, 1-hexanol and 1-butanol aqueous solutions using equation 8.41. Equation 8.42 was applied for correlating the steady-state surface tension of water surrounded by carbon dioxide. Two fitting parameters ($\Gamma_{\infty 1}$ and K_a) were evaluated by minimization residual sum of squares between the experimental data and theoretical prediction of the steady-state surface tension. The theoretical prediction from equation 8.42 and the experimental data of the steady-state surface tension of water in the presence of carbon dioxide at different pressure of carbon dioxide and at 25 °C are illustrated in Figure 8.16. Table 8.2 shows the fitting parameters obtained from fitting equaton 8.41 to the steady-state surface tension data for water surrounded by carbon dioxide at 25 °C . Table 8.1 shows the ANOVA table and the F test for the experimental and modeling results of the steady-state surface tension of water at different pressures of carbon dioxide. The large $F_{observed}$ value compare to the tabulated value of F shows the significance of the model and goodness of fit. Table 8.3 shows the fitting parameters obtained from minimization procedures for 1-octanol, 1-hexanol and 1-butanol aqueous solutions at 25 °C (obtained from chapter 7).

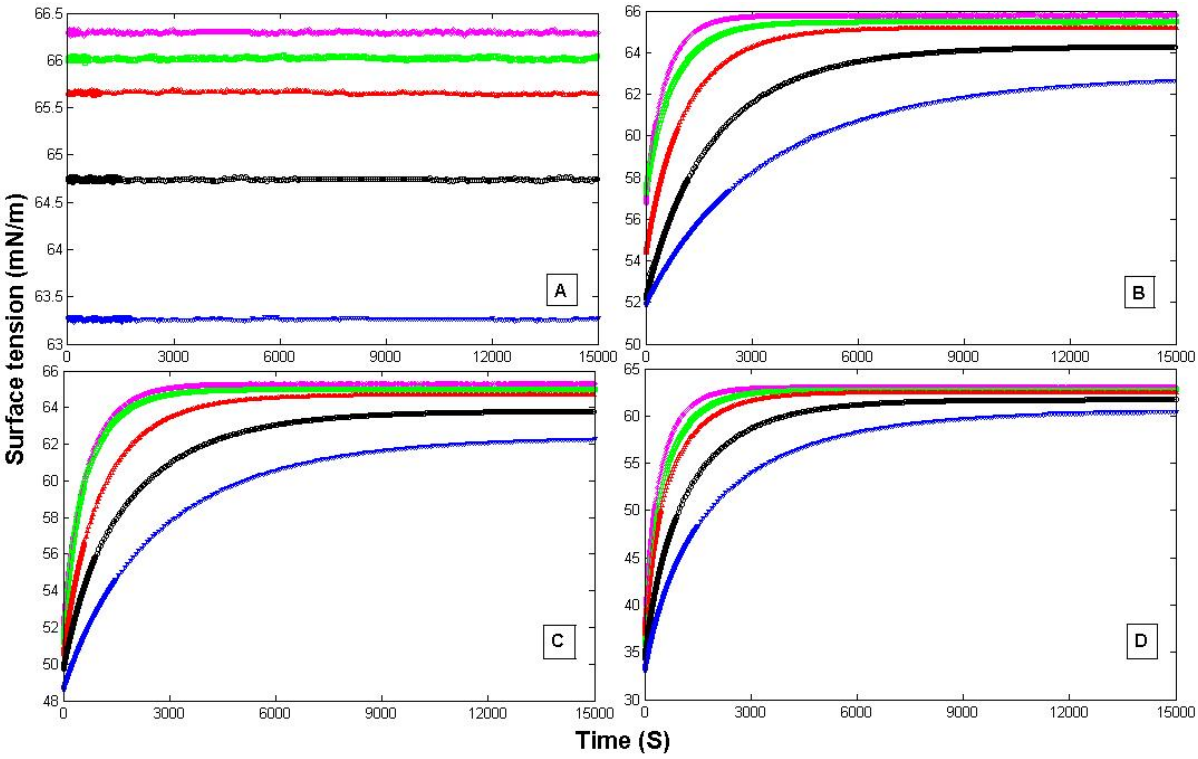

Figure 8.4: Effect of pressure on the surface tension of 1-octanol aqueous solution [Concentration of the environment solution (C_{env}) is 0.2 mM in all experiments, and A: Concentration of the drop solutions (C_{drop}) is 0.2 mM, B: C_{drop}=0.6 mM, C: C_{drop}=1 mM and D: C_{drop}=2.92 mM. Each graph represents a different pressures : 0 KPa (pink diamond), 69 KPa, (green square), 138 KPa (red triangle), 345 KPa (black circle), 690 KPa (blue triangle). Solid lines represent theoretical predictions from the dynamic modelling.

Table 8.1: ANOVA table and the F test for experimental and modeling results of the steady-state surface tension of water at different pressure of carbon dioxide based on the Langmuir equation (equation 8.42)

Source	Sum of Square	Degree of Freedom	Mean Square	
Regression	SSR=11.8	p-1=2-1=1	MSR=11.8	$F_{observed}$ =MSR/MSE =898
Error	SSE=0.0394	n-p=5-2=3	MSE=0.0131	R^2=1-SSE/SST= 0.997
Total	SST=11.7	n-1=5-1=4	$F_{tabulated}$ = 10.13	$F_{observed} \gg F_{tabulated}$

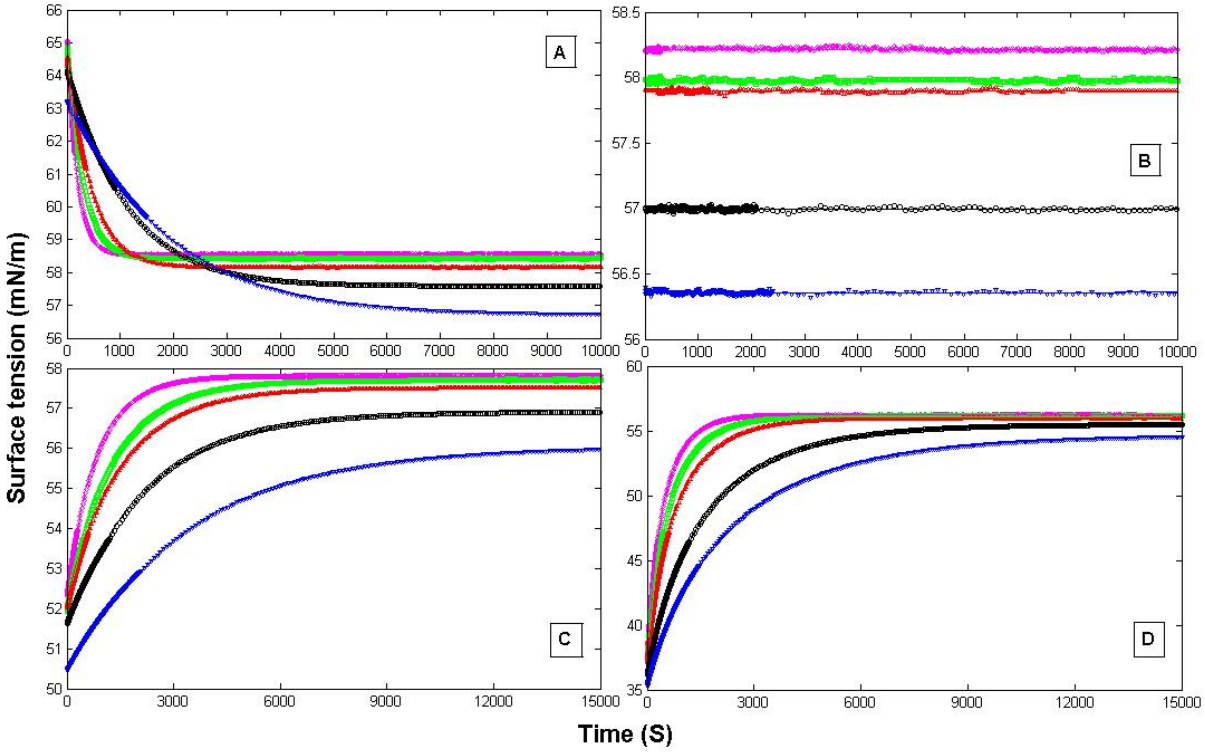

Figure 8.5: Effect of pressure on the surface tension of 1-octanol aqueous solution [Concentration of the environment solution (C_{env}) is 0.6 mM in all experiments, and A: Concentration of the drop solutions (C_{drop}) is 0.2 mM, B: C_{drop}=0.6 mM, C: C_{drop}=1 mM and D: C_{drop}=2.92 mM. Each graph represents a different pressures : 0 KPa (pink diamond), 69 KPa, (green square), 138 KPa (red triangle), 345 KPa (black circle), 690 KPa (blue triangle). Solid lines represent theoretical predictions from the dynamic modelling.

Table 8.2: The equilibrium constant for carbon dioxide adsorption ($K_a = K_1 + K_2$) and the maximum surface concentration for carbon dioxide ($\Gamma_{\infty 1}$) obtained from fitting the experimental data to the modified Langmuir equations of state (equations 8.42).

$K_a \times 10^5$	$\Gamma_{\infty 1} \times 10^5$
m^3/mol	mol/m^2
3.31	7.56

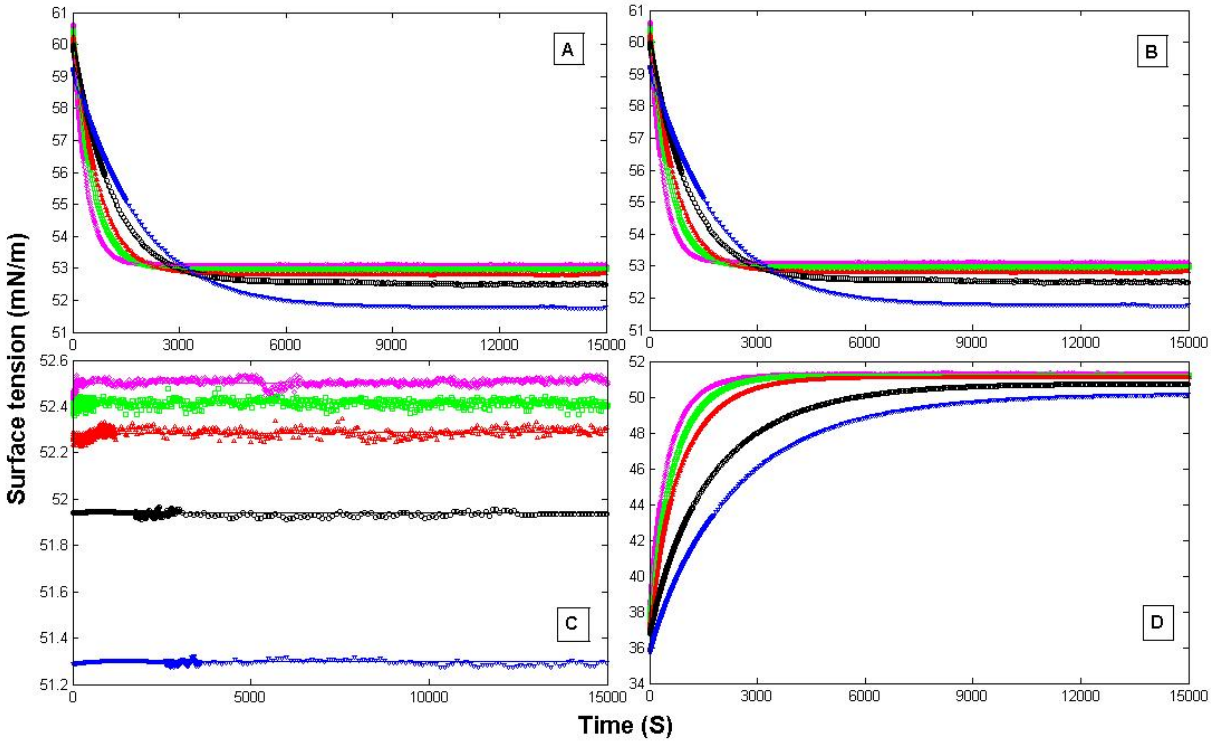

Figure 8.6: Effect of pressure on the surface tension of 1-octanol aqueous solution [Concentration of the environment solution (C_{env}) is 1 mM in all experiments, and A: Concentration of the drop solutions (C_{drop}) is 0.2 mM, B: C_{drop}=0.6 mM, C: C_{drop}=1 mM and D: C_{drop}=2.92 mM. Each graph represents a different pressures : 0 KPa (pink diamond), 69 KPa, (green square), 138 KPa (red triangle), 345 KPa (black circle), 690 KPa (blue triangle). Solid lines represent theoretical predictions from the dynamic modelling.

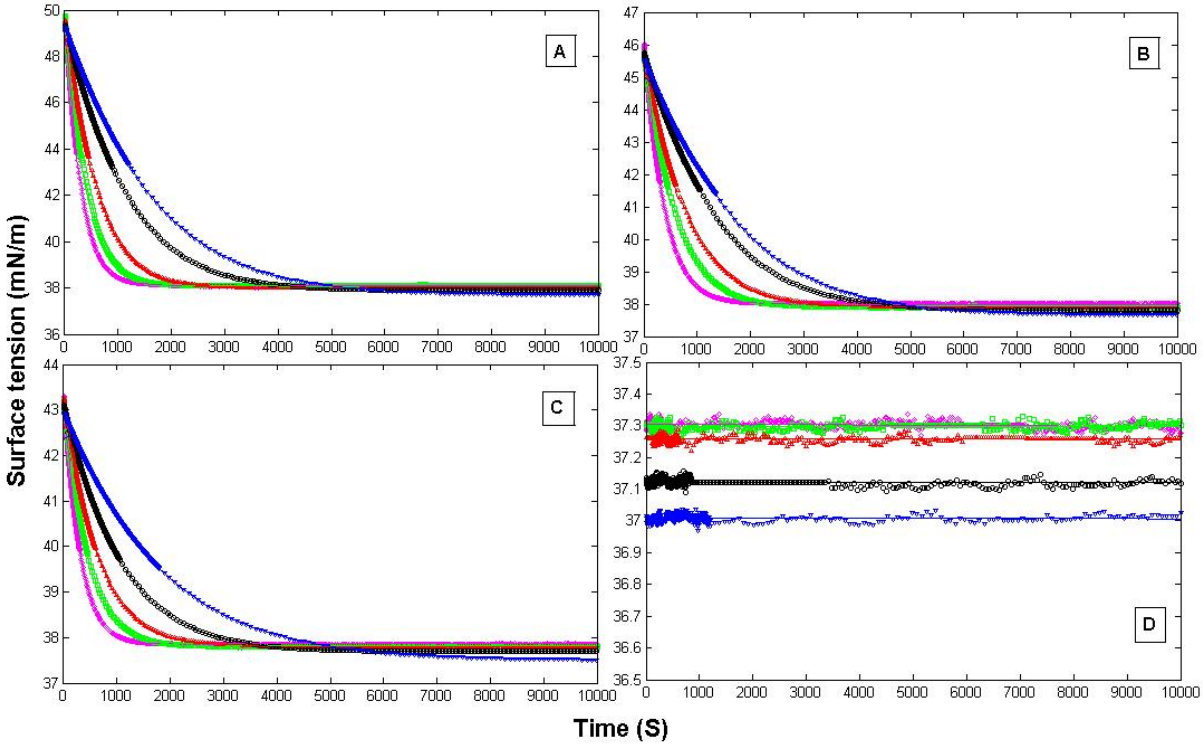

Figure 8.7: Effect of pressure on the surface tension of 1-octanol aqueous solution [Concentration of the environment solution (C_{env}) is 2.92 mM in all experiments, and A: Concentration of the drop solutions (C_{drop}) is 0.2 mM, B: C_{drop}=0.6 mM, C: C_{drop}=1 mM and D: C_{drop}=2.92 mM. Each graph represents a different pressures : 0 KPa (pink diamond), 69 KPa, (green square), 138 KPa (red triangle), 345 KPa (black circle), 690 KPa (blue triangle). Solid lines represent theoretical predictions from the dynamic modelling.

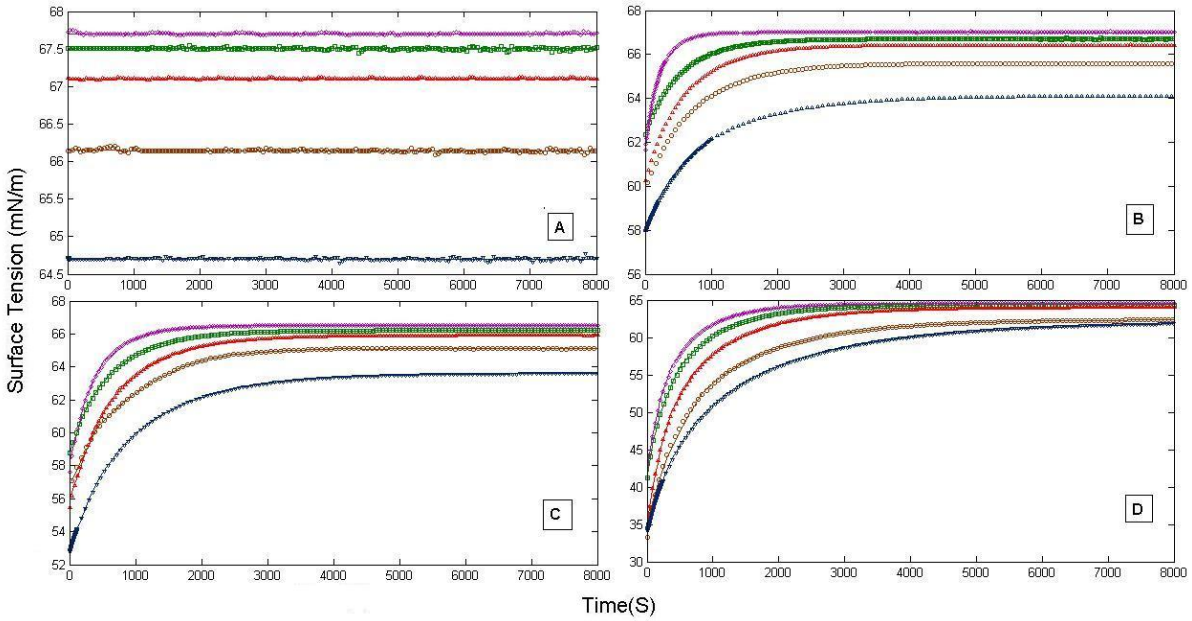

Figure 8.8: Effect of pressure on the surface tension of 1-hexanol aqueous solution [Concentration of the environment solution (C_{env}) is 1 mM in all experiments, and A: Concentration of the drop solutions (C_{drop}) is 1 mM, B: C_{drop}=6 mM, C: C_{drop}=10 mM and D: C_{drop}=25 mM. Each graph represents a different pressures : 0 KPa (pink diamond), 69 KPa, (green square), 138 KPa (red triangle), 345 KPa (black circle), 690 KPa (blue triangle). Solid lines represent theoretical predictions from the dynamic modelling.

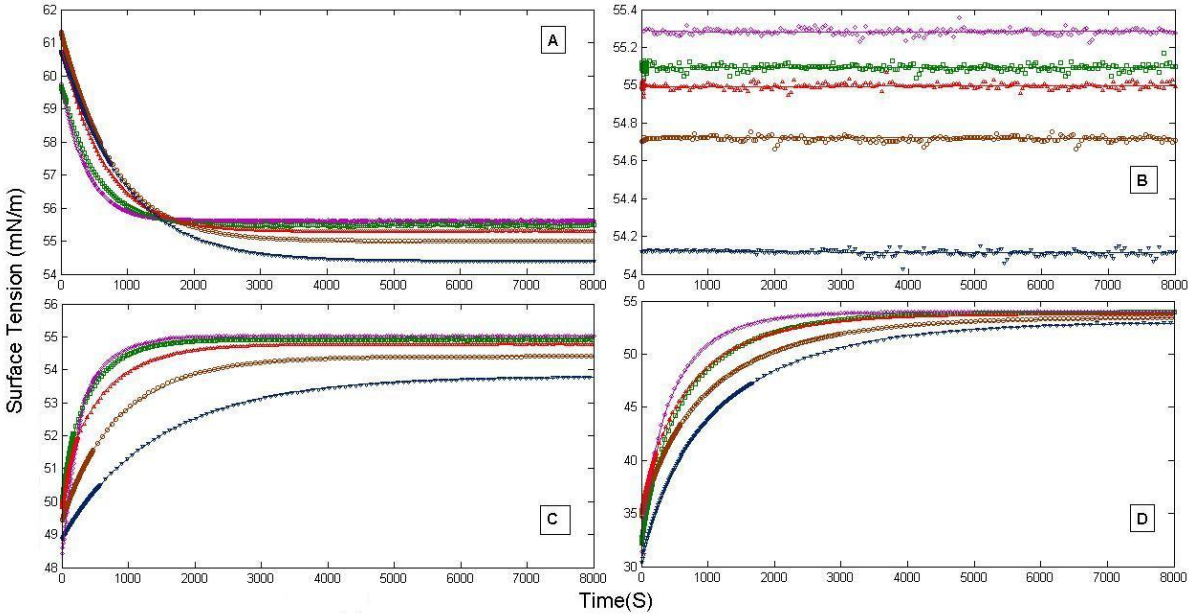

Figure 8.9: Effect of pressure on the surface tension of 1-hexanol aqueous solution [Concentration of the environment solution (C_{env}) is 6 mM in all experiments, and A: Concentration of the drop solutions (C_{drop}) is 1 mM, B: C_{drop}=6 mM, C: C_{drop}=10 mM and D: C_{drop}=25 mM. Each graph represents a different pressures : 0 KPa (pink diamond), 69 KPa, (green square), 138 KPa (red triangle), 345 KPa (black circle), 690 KPa (blue triangle). Solid lines represent theoretical predictions from the dynamic modelling.

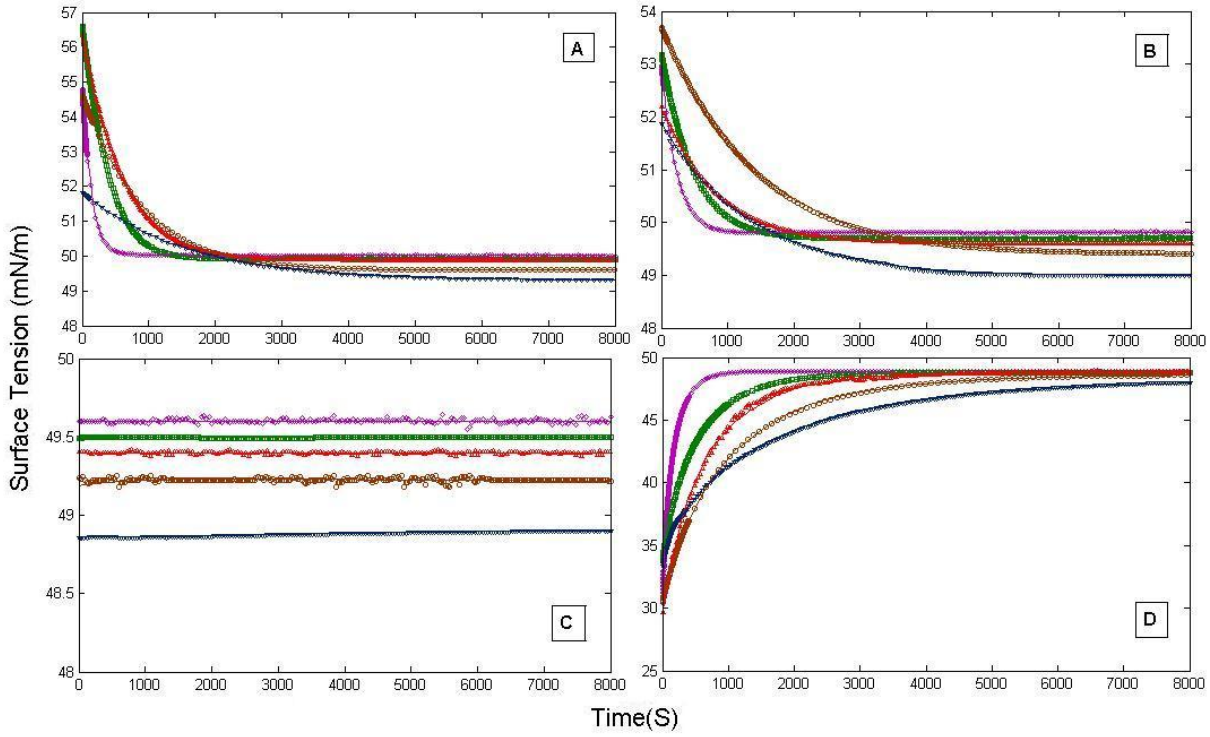

Figure 8.10: Effect of pressure on the surface tension of 1-hexanol aqueous solution [Concentration of the environment solution (C_{env}) is 10 mM in all experiments, and A: Concentration of the drop solutions (C_{drop}) is 1 mM, B: C_{drop}=6 mM, C: C_{drop}=10 mM and D: C_{drop}=25 mM. Each graph represents a different pressures : 0 KPa (pink diamond), 69 KPa, (green square), 138 KPa (red triangle), 345 KPa (black circle), 690 KPa (blue triangle). Solid lines represent theoretical predictions from the dynamic modelling.

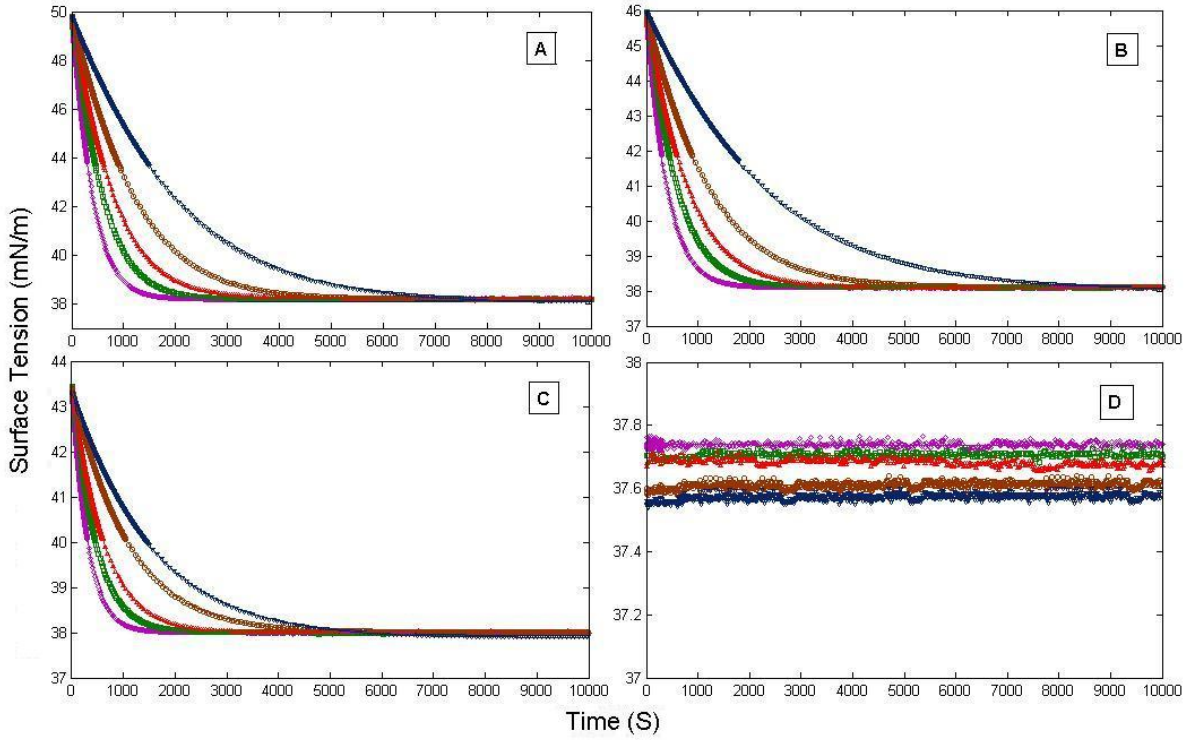

Figure 8.11: Effect of pressure on the surface tension of 1-hexanol aqueous solution [Concentration of the environment solution (C_{env}) is 25 mM in all experiments, and A: Concentration of the drop solutions (C_{drop}) is 1 mM, B: C_{drop}=6 mM, C: C_{drop}=10 mM and D: C_{drop}=25 mM. Each graph represents a different pressures : 0 KPa (pink diamond), 69 KPa, (green square), 138 KPa (red triangle), 345 KPa (black circle), 690 KPa (blue triangle). Solid lines represent theoretical predictions from the dynamic modelling.

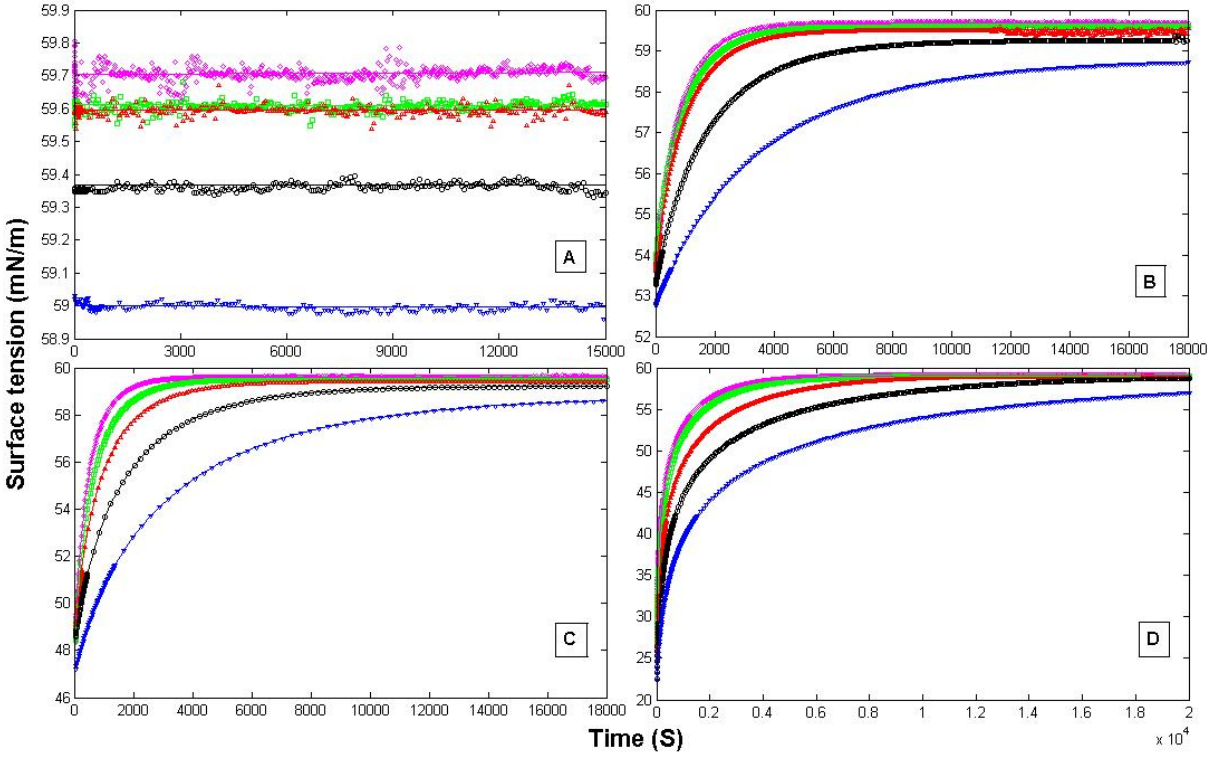

Figure 8.12: Effect of pressure on the surface tension of 1-butanol aqueous solution [Concentration of the environment solution (C_{env}) is 20 mM in all experiments, and A: Concentration of the drop solutions (C_{drop}) is 20 mM, B: C_{drop}=60 mM, C: C_{drop}=100 mM and D:C_{drop}=400 mM. Each graph represents a different pressures : 0 KPa (pink diamond), 69 KPa, (green square), 138 KPa (red triangle), 345 KPa (black circle), 690 KPa (blue triangle). Solid lines represent theoretical predictions from the dynamic modelling.

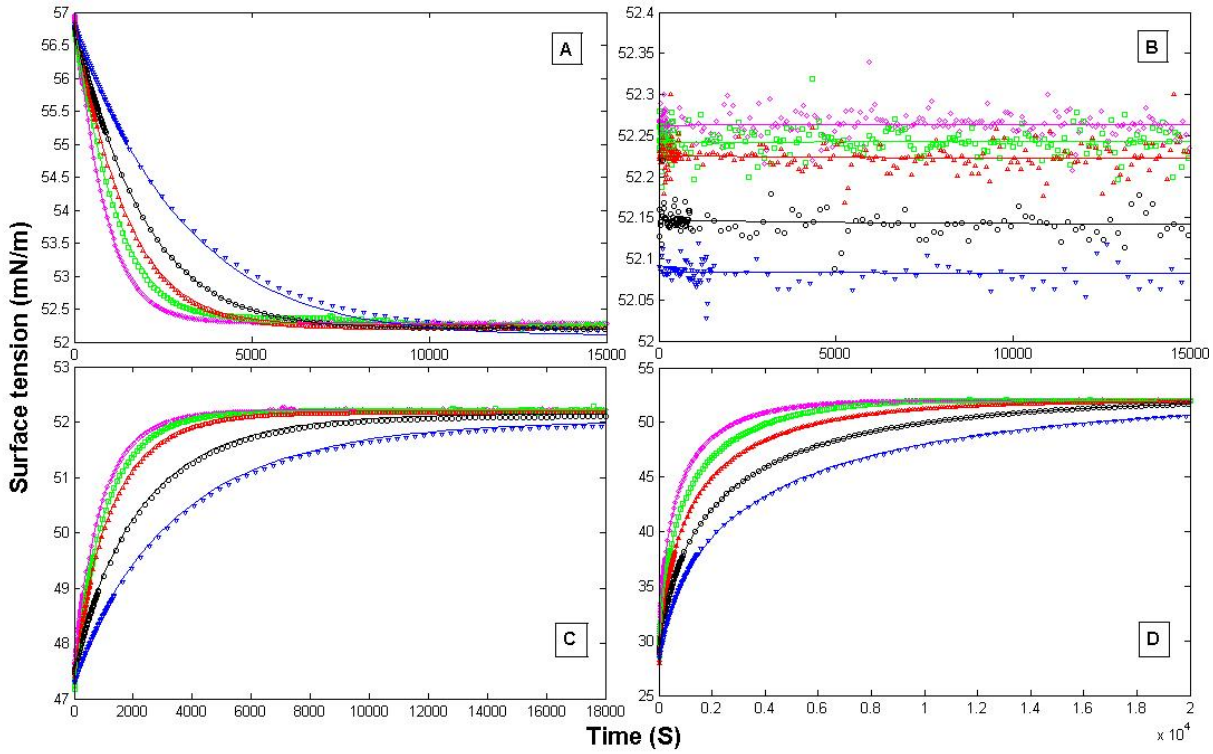

Figure 8.13: Effect of pressure on the surface tension of 1-butanol aqueous solution [Concentration of the environment solution (C_{env}) is 20 mM in all experiments, and A: Concentration of the drop solutions (C_{drop}) is 20 mM, B: C_{drop}=60 mM, C: C_{drop}=100 mM and D:C_{drop}=400 mM. Each graph represents a different pressures : 0 KPa (pink diamond), 69 KPa, (green square), 138 KPa (red triangle), 345 KPa (black circle), 690 KPa (blue triangle). Solid lines represent theoretical predictions from the dynamic modelling.

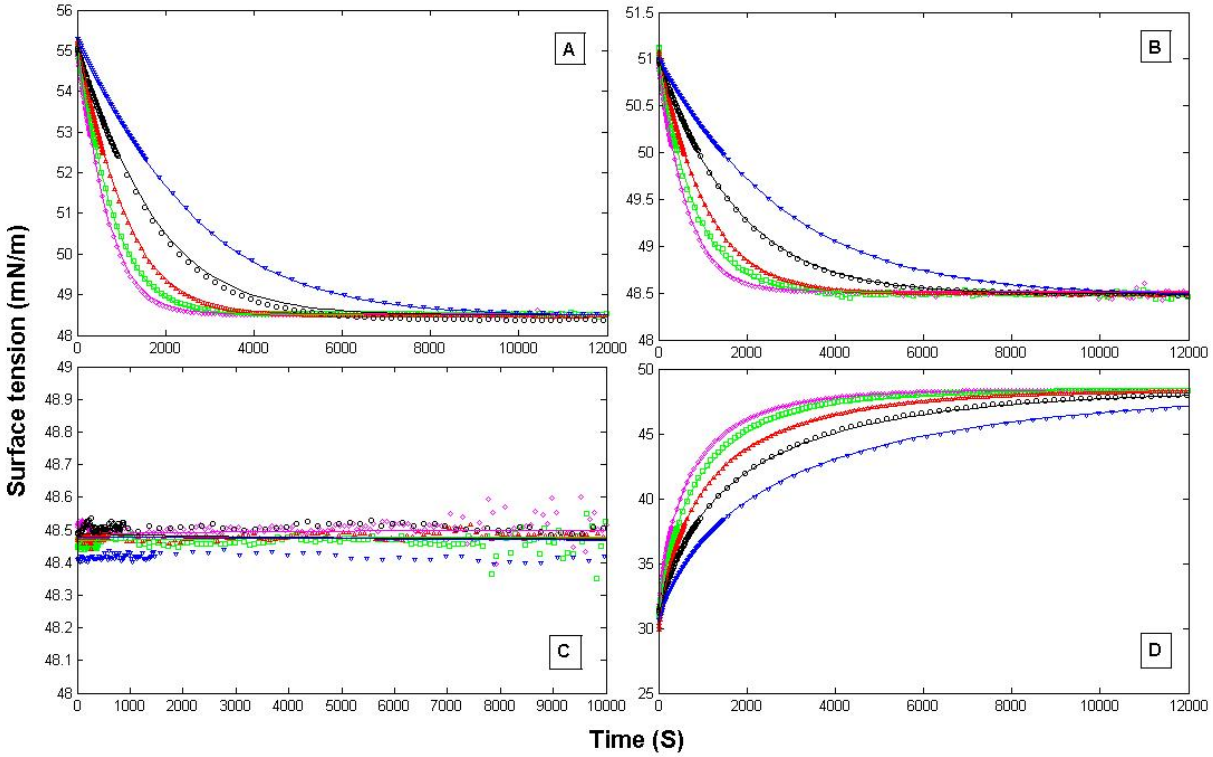

Figure 8.14: Effect of pressure on the surface tension of 1-butanol aqueous solution [Concentration of the environment solution (C_{env}) is 20 mM in all experiments, and A: Concentration of the drop solutions (C_{drop}) is 20 mM, B: C_{drop}=60 mM, C: C_{drop}=100 mM and D:C_{drop}=400 mM. Each graph represents a different pressures : 0 KPa (pink diamond), 69 KPa, (green square), 138 KPa (red triangle), 345 KPa (black circle), 690 KPa (blue triangle). Solid lines represent theoretical predictions from the dynamic modelling.

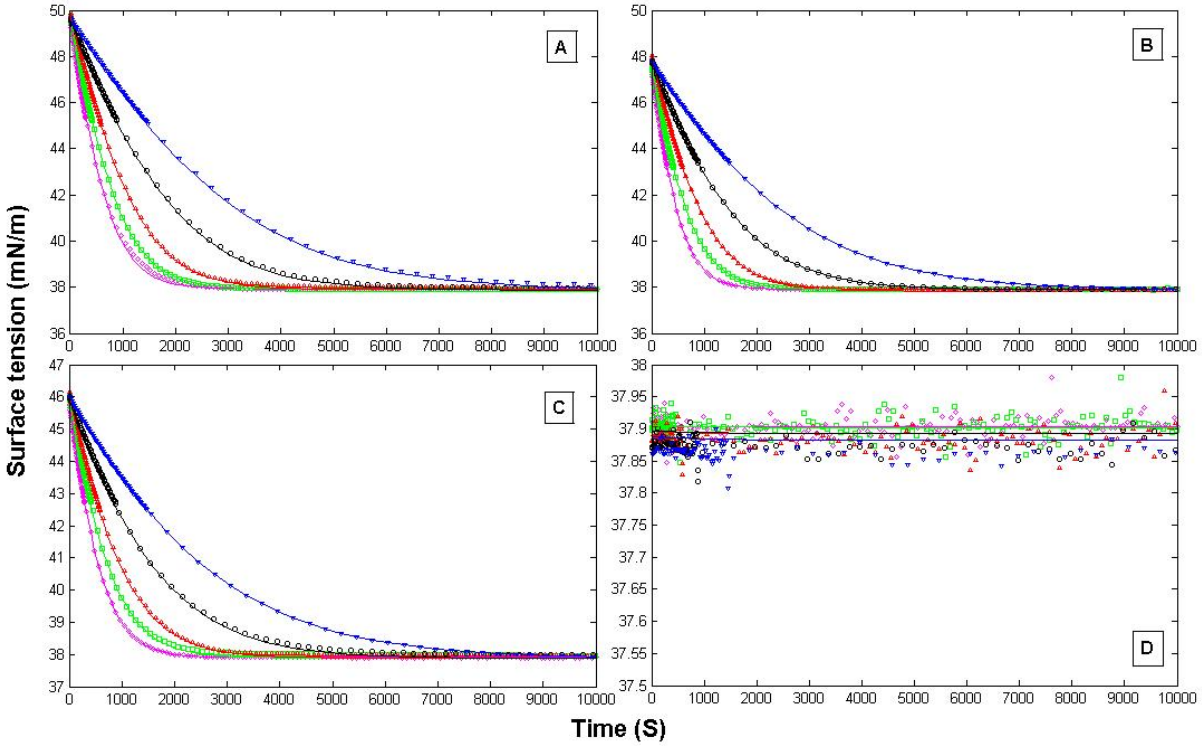

Figure 8.15: Effect of pressure on the surface tension of 1-butanol aqueous solution [Concentration of the environment solution (C_{env}) is 20 mM in all experiments, and A: Concentration of the drop solutions (C_{drop}) is 20 mM, B: C_{drop}=60 mM, C: C_{drop}=100 mM and D:C_{drop}=400 mM. Each graph represents a different pressures : 0 KPa (pink diamond), 69 KPa, (green square), 138 KPa (red triangle), 345 KPa (black circle), 690 KPa (blue triangle). Solid lines represent theoretical predictions from the dynamic modelling.

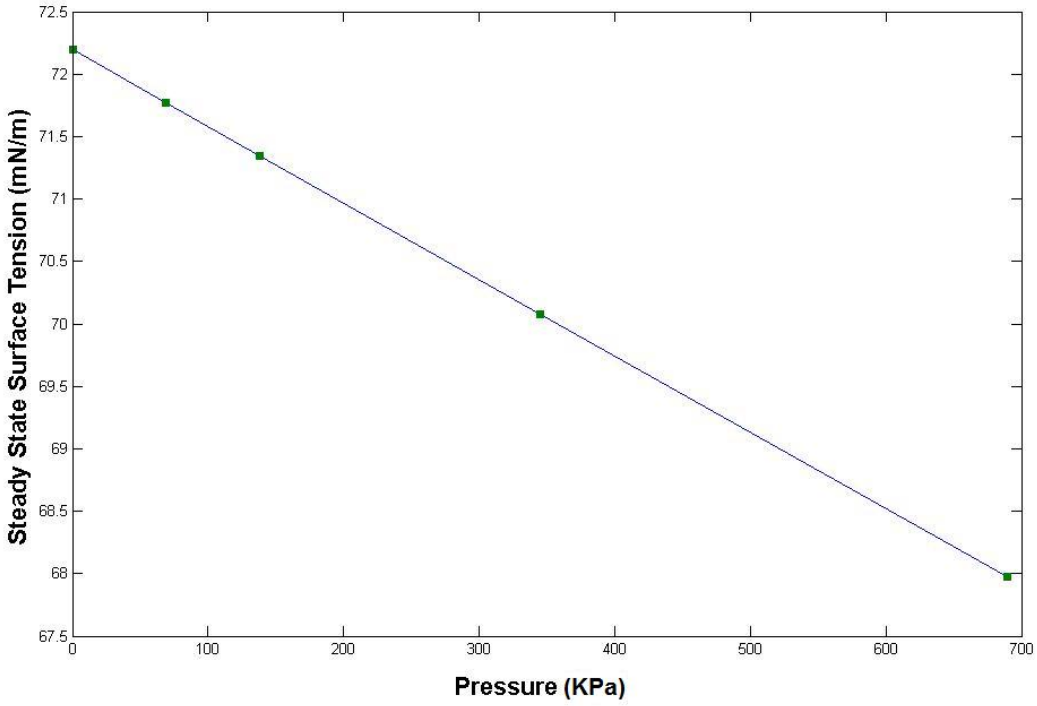

Figure 8.16: Effect of carbon dioxide pressure on the steady-state surface tension of water.

Table 8.3: The equilibrium constant for adsorption from the vapor phase (K_3) and from the liquid phase (K_4) and the maximum surface concentration ($\Gamma_{\infty 2}$) obtained from fitting the steady-state surface tension of 1-octanol, 1-hexanol and 1-butanol to the modified Langmuir equation of state (equation 8.41).

	K_3	K_4	$\Gamma_{\infty 2} \times 10^6$
	m^3/mol	m^3/mol	mol/m^2
1-octanol	1.73	0.096	7.63
1-hexanol	0.319	0.013	6.24
1-butanol	0.19	0.0011	3.18

A theoretical prediction for the steady-state surface tension of 1-octanol, 1-hexaol and 1-butanol aqueous solutions surrounded by carbon dioxide was achieved when the fitting parameters ($\Gamma_{\infty 1}, K_a, \Gamma_{\infty 2}, K_3$ and K_3) evaluated from two minimizing procedures of the two systems (water surrounded by carbon dioxide and surfactant aqueous solutions) substituted in equation 8.40.

In statistics, one of the best tools to identify if the model is fitted to the experimental results is the F test. The ANOVA table and the F test for the steady-state modelling of 1-octanol, 1-hexanol and 1-butanol are illustrated in Tables 8.4, 8.5 and 8.6, respectively. The definition of parameters introduced in Tables 8.4-8.6 was described in chapter 7. The large $F_{observed}$ compare to the tabulated value shows the overall regression for all three systems is significant. The results in Tables 8.4-8.6 support the idea that the equilibrium constant for adsorption a species from each side of an interface is not dependent to the other species involved in the adsorption. Tables 8.4-8.6 show that the equilibrium constants obtained based on fitting equations 8.41 or 8.42 to the experimental data of the steady-state surface tension (when adsorption of just one species is involved) can be applied for fitting equation 8.40 to the experimental data of the steady-state surface tension of the surfactant aqueous solutions surrounded by carbon dioxide (when simultaneous adsorption of two species is involved). These results show that, at a constant temperature, the equilibrium constants and maximum surface concentration for a species are always constant regardless of the number of species involved in the adsorption process.

The equilibrium constants are often used to describe the tendency of surfactant molecules to adsorb at the interface and reduce the surface tension ([23]). The values obtained for the equilibrium constants (Table 8.3) show that at the final steady-state condition the equilibrium constant for 1-octanol, 1-hexanol and 1-butanol adsorption from the vapor phase (K_3) is much greater than that from the liquid phase (K_4). From equation 13-16 it implies that adsorption rate constant from the vapor phase is much greater than that from the

Table 8.4: ANOVA table for the steady-state modelling of 1-octanol data based on Langmuir equation (equation 8.40)

Source	Sum of Square	Degree of Freedom	Mean Square	
Regression	SSR=7579.90	p-1=5-1=4	MSR=1895.0	$F_{observed}$ =MSR/MSE =130987
Error	SSE=1.09	n-p=80-5=75	MSE=0.014	R^2=1-SSE/SST= 0.9998
Total	SST=7595.08	n-1=80-1=79	$F_{tabulated} = 2.53$	$F_{observed} \gg F_{tabulated}$

Table 8.5: ANOVA table for the steady-state modelling of 1-hexanol data based on Langmuir equation (equation 8.40)

Source	Sum of Square	Degree of Freedom	Mean Square	
Regression	SSR=7870	p-1=5-1=4	MSR=1967.5	$F_{observed}$ =MSR/MSE =1970000
Error	SSE=0.083	n-p=80-5=75	MSE=0.001	R^2=1-SSE/SST= 0.9999
Total	SST=7870	n-1=80-1=79	$F_{tabulated} = 2.53$	$F_{observed} \gg F_{tabulated}$

Table 8.6: ANOVA table for the steady-state modelling of 1-butanol data based on Langmuir equation (equation 8.40)

Source	Sum of Square	Degree of Freedom	Mean Square	
Regression	SSR=4744.2	p-1=5-1=4	MSR=1186.1	$F_{observed}$ =MSR/MSE =401685
Error	SSE=0.2	n-p=80-5=75	MSE=0.003	R^2=1-SSE/SST= 0.9999
Total	SST=4757.0	n-1=80-1=79	$F_{tabulated} = 2.53$	$F_{observed} \gg F_{tabulated}$

liquid phase ($k_a^g \gg k_a^l$). The values presented in Tables 8.2 and 8.3 also show that the contribution to adsorption for 1-octanol, 1-hexanol and 1-butanol is much greater than that for carbon dioxide ($K_3 \gg K_a$ and $K_4 \gg K_a$). This may be due to the amphiphilic behavior of 1-octanol, 1-hexanol and 1-butanol molecules. Both hydrophobicity and hydrophilicty characters of these amphiphiles can be satisfied when they adsorb at the interface.

The experimental data for the steady-state surface tension of these surfactant aqueous solutions surrounded by carbon dioxide (obtained from Figures 8.4- 8.12) showed a decrease with carbon dioxide pressure (Figure 8.17-8.19). A linear relation was observed between the steady-state surface tension and carbon dioxide surrounding pressure. Thus, the following linear regression model fitted to the experimental data of the steady-state surface tension at different concentrations of drop and environment solution and different pressures of carbon dioxide.

$$\gamma = r_1 P + r_2 \tag{8.46}$$

In this equation γ represents the steady-state surface tension. P is carbon dioxide pressure in KPa, and r_1 and r_2 are two constants. The values of C_{env}, C_{drop}, r_1, r_2 and the coefficient of determination (R^2) related to each regression model for 1-octanol, 1-hexanol and 1-butanol are illustrated in Tables 8.7, 8.8 and 8.9, respectively. The values of the coefficients of determination show that the linear regression is a good candidate for investigating the effect of carbon dioxide pressure on the steady-state surface tension of 1-octanol, 1-hexanol and 1-butanol aqueous solutions at pressure ranging from 0 KPa to 690 KPa.

The values presented in Figures 8.17- 8.19 and Tables 8.7- 8.9 show that the dependency of the steady-state surface tension on carbon dioxide pressure (slope of the lines) decreases as the concentration of 1-octanol, 1-hexanol and 1-butanol in the environment solution is increased. It shows that the effect of carbon dioxide pressure on the steady-state surface tension of these aqueous solutions is almost negligible at high concentration of these surfactants in the environment solutions. This behavior is probably due to the higher tendency of adsorption for surfactants than that for carbon dioxide (especially at high concentration of surfactants in the vapour phase). The higher tendency for adsorption of surfactants than carbon dioxide can be observed by the higher values of equilibrium constants for surfactants adsorption (especially from the vapour phase) than that for carbon dioxide adsorption ($K_3 \gg K_a$).

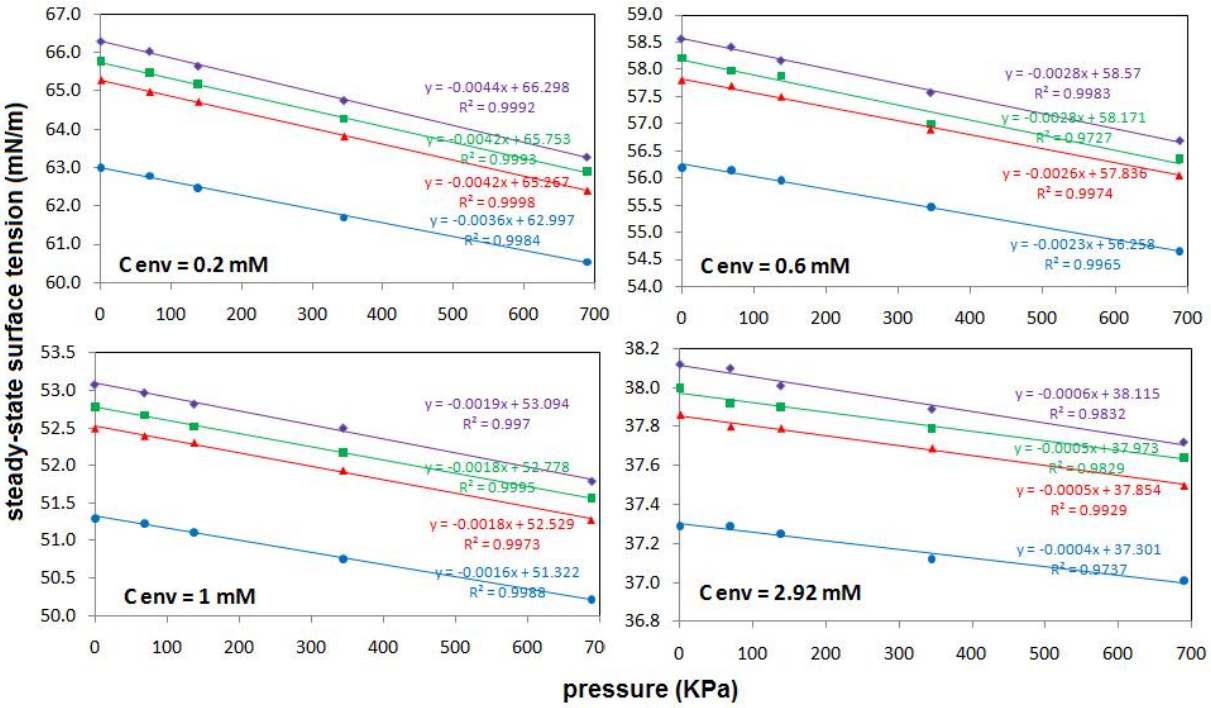

Figure 8.17: Steady state surface tension of 1-octanol at different pressures of carbon dioxide. Concentration of the environment solution (C_{env}) is indicated in each graph; Experiments were performed at four different drop concentrations (C_{drop}): 0.2 mM (purple diamond), 0.6 mM (green square), 1 mM (red triangle), 2.92 mM (blue circle); Lines represent linear regression model to the experimental data.

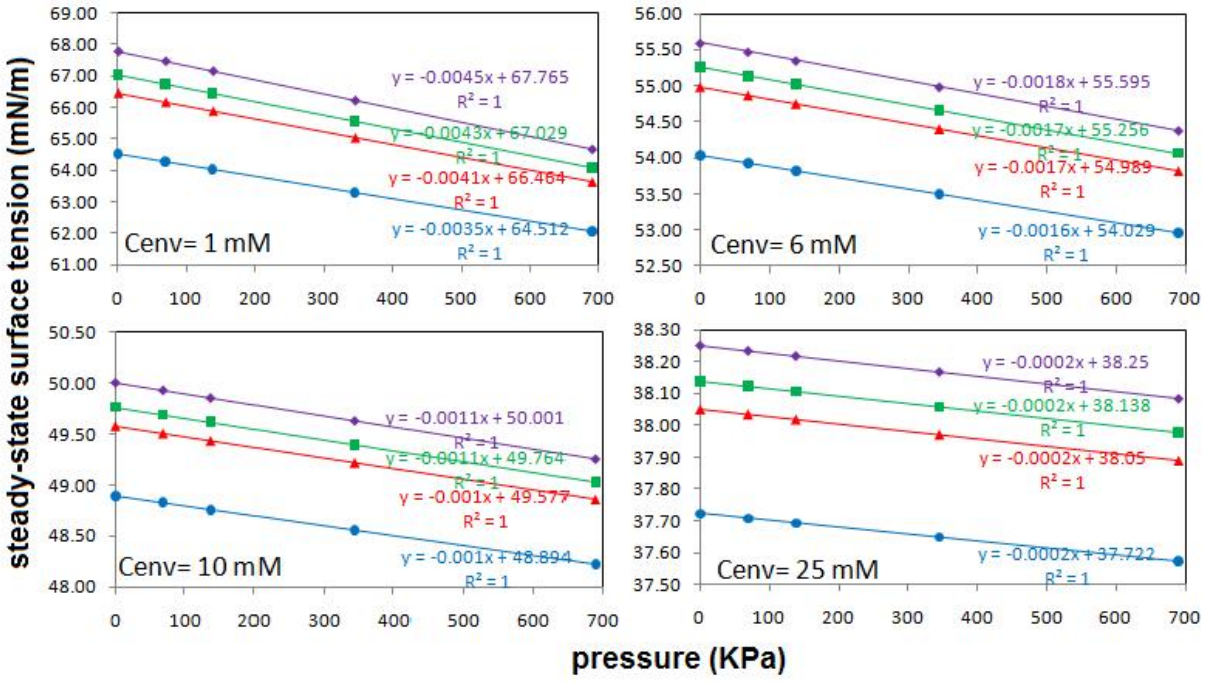

Figure 8.18: Steady state surface tension of 1-hexanol at different pressures of carbon dioxide. Concentration of the environment solution (C_{env}) is indicated in each graph; Experiments were performed at four different drop concentrations (C_{drop}): 1 mM (purple diamond), 6 mM (green square), 10 mM (red triangle), 25 mM (blue circle); Lines represent linear regression model to the experimental data.

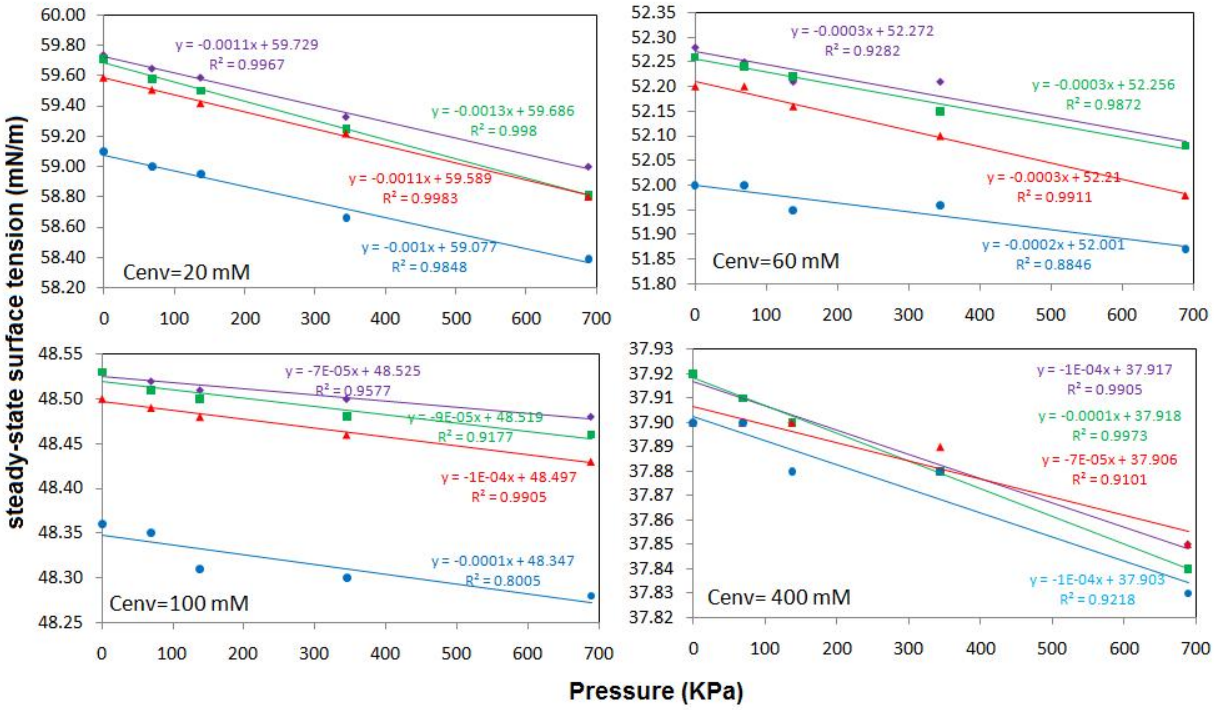

Figure 8.19: Steady state surface tension of 1-butanol at different pressures of carbon dioxide. Concentration of the environment solution (C_{env}) is indicated in each graph; Experiments were performed at four different drop concentrations (C_{drop}): 20 mM (purple diamond), 60 mM (green square), 100 mM (red triangle), 400 mM (blue circle); Lines represent linear regression model to the experimental data.

Table 8.7: Concentration of the environment solution (C_{env}), concentration of the drop solution (C_{drop}), slope (r_1), Surface tension intercept (r_2), and the coefficient of determination (R^2) of a linear regression model (equation 8.46) fitted to the steady-state surface tension of 1-octanol at different pressures of carbon dioxide (Figures 8.17)

$C_{env}(mM)$	$C_{drop}(mM)$	$r_1(mN/mKPa)$	$r_2(mN/m)$	R^2
0.2	0.2	-0.0044	66.30	0.99
0.2	0.6	-0.0042	65.75	0.99
0.2	1.0	-0.0042	65.27	0.99
0.2	2.92	-0.0036	63.00	0.99
0.6	0.2	-0.0028	58.57	0.97
0.6	0.6	-0.0028	58.17	0.99
0.6	1.0	-0.0026	57.84	0.99
0.6	2.92	-0.0023	56.26	0.99
1.0	0.2	-0.0019	53.09	0.99
1.0	0.6	-0.0018	52.78	0.99
1.0	1.0	-0.0018	52.53	0.99
1.0	2.92	-0.0016	51.32	0.99
2.92	0.2	-0.0006	38.12	0.98
2.92	0.6	-0.0005	37.97	0.98
2.92	1.0	-0.0005	37.85	0.99
2.92	2.92	-0.0004	37.30	0.97

It also can be observed that the slopes of the lines are almost independent to the drop concentration of 1-octanol, 1-hexanol and 1-butanol solutions. These results support our previous finding that the effect of adsorption from vapour phase is more important than liquid phase for a group of short carbon chain alcohols [25, 59, 60, 61, 72].

8.5.2 Dynamic Surface Tension

A theoretical prediction of dynamic surface tension was achieved from the modified Frumkin equation (equation 8.39) and the two solutions for Γ_1 and Γ_2 calculated from equations 8.44 and 8.45. Using a minimization procedure, fitting parameters including kinetic rate constant for adsorption from the vapor phase for species 1 and species 2 (k^g_{a1} and k^g_{a2}) and constant K_b were evaluated by minimizing the residual sum of squares between the model predictions and the experimental data of the dynamic surface tension. For each chemical, 80 fitting procedures were performed at four concentrations of the environment solution,

Table 8.8: Concentration of the environment solution (C_{env}), concentration of the drop solution (C_{drop}), slope (r_1), Surface tension intercept (r_2), and the coefficient of determination (R^2) of a linear regression model (equation 8.46) fitted to the steady-state surface tension of 1-hexanol at different pressures of carbon dioxide (Figures 8.18)

$C_{env}(mM)$	$C_{drop}(mM)$	$r_1(mN/mKPa)$	$r_2(mN/m)$	R^2
2	2	-0.0045	67.8	1
2	5	-0.0043	67.0	1
2	9	-0.0041	66.5	1
2	30	-0.0035	64.5	1
5	2	-0.0018	55.6	1
5	5	-0.0017	55.3	1
5	9	-0.0017	55.0	1
5	30	-0.0016	54.0	1
9	2	-0.0011	50.0	1
9	5	-0.0011	49.8	1
9	9	-0.0010	49.6	1
9	30	-0.0010	48.9	1
30	2	-0.0002	38.3	1
30	5	-0.0002	38.1	1
30	9	-0.0002	38.1	1
30	30	-0.0002	37.7	1

Table 8.9: Concentration of the environment solution (C_{env}), concentration of the drop solution (C_{drop}), slope (r_1), Surface tension intercept (r_2), and the coefficient of determination (R^2) of a linear regression model (equation 8.46) fitted to the steady-state surface tension of 1-butanol at different pressures of carbon dioxide (Figures 8.19)

$C_{env}(mM)$	$C_{drop}(mM)$	$r_1(mN/mKPa)$	$r_2(mN/m)$	R^2
20	20	-0.0011	59.73	1
20	60	-0.0013	59.69	1
20	100	-0.0011	59.59	1
20	400	-0.0010	59.08	0.98
60	20	-0.0003	52.27	0.93
60	60	-0.0003	52.26	0.99
60	100	-0.0003	52.21	0.99
60	400	-0.0002	52.00	0.88
100	20	-0.00007	48.53	0.96
100	60	-0.00009	48.52	0.92
100	100	-0.0001	48.5	0.99
100	400	-0.00009	48.35	0.80
400	20	-0.0001	37.92	0.99
400	60	-0.0001	37.92	1
400	100	-0.00007	37.91	0.91
400	400	-0.0001	37.90	0.92

Table 8.10: 95% confidence intervals for k_{a1}^g, k_{a2}^g, $k_{a1}^l, k_{a2}^l, K_b, K_1$ and K_2 obtained from fitting the experimental data of 1-octanol surface tension to the kinetic transfer equation (equation 8.39) at pressure ranging from 0 KPa to 690 KPa.

P	k_{a1}^g	k_{a2}^g	k_{a1}^l	k_{a2}^l	K_b	K_1	K_2
KPa	$m^3/mol.s$	$m^3/mol.s$	$m^3/mol.s$	$m^3/mol.s$		$1/KPa$	$1/KPa$
0	$9.15 \times 10^{-8} \pm 2.36 \times 10^{-8}$	$2.93 \times 10^{-3} \pm 7.86 \times 10^{-4}$	$3.27 \times 10^{-10} \pm 8.42 \times 10^{-11}$	$1.63 \times 10^{-4} \pm 4.36 \times 10^{-5}$	1.004	3.30×10^{-5}	1.30×10^{-7}
68.93	$6.45 \times 10^{-8} \pm 1.61 \times 10^{-8}$	$2.02 \times 10^{-3} \pm 5.32 \times 10^{-4}$	$2.30 \times 10^{-10} \pm 5.75 \times 10^{-11}$	$1.12 \times 10^{-4} \pm 2.95 \times 10^{-5}$	1.004	3.30×10^{-5}	1.30×10^{-7}
137.86	$4.54 \times 10^{-8} \pm 9.40 \times 10^{-9}$	$1.39 \times 10^{-3} \pm 3.19 \times 10^{-4}$	$1.62 \times 10^{-10} \pm 3.35 \times 10^{-11}$	$7.74 \times 10^{-5} \pm 1.77 \times 10^{-5}$	1.004	3.30×10^{-5}	1.30×10^{-7}
344.65	$2.42 \times 10^{-8} \pm 4.25 \times 10^{-9}$	$7.07 \times 10^{-4} \pm 1.48 \times 10^{-4}$	$8.63 \times 10^{-11} \pm 1.52 \times 10^{-11}$	$3.92 \times 10^{-5} \pm 8.23 \times 10^{-6}$	1.004	3.30×10^{-5}	1.30×10^{-7}
689.3	$1.66 \times 10^{-8} \pm 3.23 \times 10^{-9}$	$5.33 \times 10^{-4} \pm 1.80 \times 10^{-4}$	$5.93 \times 10^{-11} \pm 1.15 \times 10^{-11}$	$2.96 \times 10^{-5} \pm 1.00 \times 10^{-5}$	1.004	3.30×10^{-5}	1.30×10^{-7}

four concentrations of the drop solution and five pressures of carbon dioxide. The theoretical prediction from the kinetic transfer equation (equation 8.39) is plotted along with the experimental data in Figures 8.4- 8.15. For all profiles, the kinetic transfer equation fits the experimental data very well. At each pressure, the three fitting parameters (k_{a1}^g and k_{a2}^g , and K_b) along with k_{a1}^l, k_{a2}^l (calculated from equation 8.32-8.35), K_1 and K_2 (calculated from equations 8.47 and 8.48) are tabulated in Tables 8.10-8.12 for 1-octanol, 1-hexanol and 1-butanol aqueous solution surrounded by carbon dioxide.

$$K_1 = \frac{K_a}{K_b} \tag{8.47}$$

$$K_2 = K_a - K_1 \tag{8.48}$$

The results show that the equilibrium constants for carbon dioxide adsorption from both sides of a vapor/liquid interface (K_1 and K_2) similar to equilibrium constants for 1-octanol, 1-hexanol and 1-butanol adsorption from both sides of a vapor/liquid interface (K_3 and K_4 presented in tables 8.3) do not change with carbon dioxide pressure.

The limitation of this type of model is the variation in the fitting parameters (Tables 8.10-8.12). An obvious limitation is that material properties and their corresponding constants or fitting parameters are varying with time. Thus, these parameters may have

Table 8.11: 95% confidence intervals for k_{a1}^g, k_{a2}^g, $k_{a1}^l, k_{a2}^l, K_b, K_1$ and K_2 obtained from fitting the experimental data of 1-hexanol surface tension to the kinetic transfer equation (equation 8.39) at pressure ranging from 0 KPa to 690 KPa.

P	k_{a1}^g	k_{a2}^g	k_{a1}^l	k_{a2}^l	K_b	K_1	K_2
KPa	$m^3/mol.s$	$m^3/mol.s$	$m^3/mol.s$	$m^3/mol.s$		$1/KPa$	$1/KPa$
0	$1.22 \times 10^{-7} \pm 4.11 \times 10^{-8}$	$8.25 \times 10^{-4} \pm 4.73 \times 10^{-4}$	$4.37 \times 10^{-10} \pm 1.47 \times 10^{-10}$	$3.36 \times 10^{-5} \pm 1.93 \times 10^{-5}$	1.004	3.30×10^{-5}	1.30×10^{-7}
68.93	$6.08 \times 10^{-8} \pm 9.40 \times 10^{-9}$	$2.90 \times 10^{-4} \pm 5.97 \times 10^{-5}$	$2.17 \times 10^{-10} \pm 3.36 \times 10^{-11}$	$1.18 \times 10^{-5} \pm 2.43 \times 10^{-6}$	1.004	3.30×10^{-5}	1.30×10^{-7}
137.86	$4.67 \times 10^{-8} \pm 7.79 \times 10^{-9}$	$2.33 \times 10^{-4} \pm 7.11 \times 10^{-5}$	$1.67 \times 10^{-10} \pm 2.78 \times 10^{-11}$	$9.48 \times 10^{-6} \pm 2.90 \times 10^{-6}$	1.004	3.30×10^{-5}	1.30×10^{-7}
344.65	$3.32 \times 10^{-8} \pm 7.10 \times 10^{-9}$	$1.56 \times 10^{-4} \pm 4.66 \times 10^{-5}$	$1.18 \times 10^{-10} \pm 2.53 \times 10^{-11}$	$6.34 \times 10^{-6} \pm 1.90 \times 10^{-6}$	1.004	3.30×10^{-5}	1.30×10^{-7}
689.3	$2.86 \times 10^{-8} \pm 5.63 \times 10^{-9}$	$1.30 \times 10^{-4} \pm 3.85 \times 10^{-5}$	$1.02 \times 10^{-10} \pm 2.01 \times 10^{-11}$	$5.31 \times 10^{-6} \pm 1.57 \times 10^{-6}$	1.004	3.30×10^{-5}	1.30×10^{-7}

Table 8.12: 95% confidence intervals for k_{a1}^g, k_{a2}^g, $k_{a1}^l, k_{a2}^l, K_b, K_1$ and K_2 obtained from fitting the experimental data of 1-butanol surface tension to the kinetic transfer equation (equation 8.39) at pressure ranging from 0 KPa to 690 KPa.

P	k_{a1}^g	k_{a2}^g	k_{a1}^l	k_{a2}^l	K_b	K_1	K_2
KPa	$m^3/mol.s$	$m^3/mol.s$	$m^3/mol.s$	$m^3/mol.s$		$1/KPa$	$1/KPa$
0	$6.98 \times 10^{-8} \pm 2.98 \times 10^{-8}$	$5.49 \times 10^{-5} \pm 1.33 \times 10^{-5}$	$2.49 \times 10^{-10} \pm 1.06 \times 10^{-10}$	$2.24 \times 10^{-6} \pm 5.41 \times 10^{-7}$	1.004	3.30×10^{-5}	1.30×10^{-7}
68.93	$5.53 \times 10^{-8} \pm 2.25 \times 10^{-8}$	$5.27 \times 10^{-5} \pm 2.24 \times 10^{-5}$	$1.97 \times 10^{-10} \pm 8.03 \times 10^{-11}$	$2.15 \times 10^{-6} \pm 9.15 \times 10^{-7}$	1.004	3.30×10^{-5}	1.30×10^{-7}
137.86	$3.97 \times 10^{-8} \pm 1.67 \times 10^{-8}$	$2.96 \times 10^{-5} \pm 6.66 \times 10^{-6}$	$1.42 \times 10^{-10} \pm 5.95 \times 10^{-11}$	$1.21 \times 10^{-6} \pm 2.71 \times 10^{-7}$	1.004	3.30×10^{-5}	1.30×10^{-7}
344.65	$2.49 \times 10^{-8} \pm 1.07 \times 10^{-9}$	$1.95 \times 10^{-5} \pm 5.20 \times 10^{-6}$	$8.90 \times 10^{-11} \pm 3.80 \times 10^{-11}$	$7.94 \times 10^{-7} \pm 2.12 \times 10^{-7}$	1.004	3.30×10^{-5}	1.30×10^{-7}
689.3	$1.72 \times 10^{-8} \pm 6.66 \times 10^{-9}$	$1.67 \times 10^{-5} \pm 5.42 \times 10^{-6}$	$6.15 \times 10^{-11} \pm 2.38 \times 10^{-11}$	$6.81 \times 10^{-7} \pm 2.21 \times 10^{-7}$	1.004	3.30×10^{-5}	1.30×10^{-7}

different values between the initial and the final stages of the experiment. Discrepancies would occur depending on which set of data points is used in the model predictions over the entire time range. Improvements may be made when incorporating the varying nature of these fitting parameters.

Of course, other experimental errors or factors may also contribute to the discrepancies, such as temperature and pressure fluctuations, the changes in surface area and volume of drop during the experiments, the presence of impurities and loss of surfactant due to vapor leakage that may distort the experimental results. Similar to any minimization procedure any imperfections in the experimental results will be reflected in the value obtained for the fitting parameters in Tables 8.10 to 8.12.

Figures 8.7-8.12 also show that when the pressure is increased from 0 KPa to 689 KPa, the slopes of the profiles decrease, and the time required reaching to the steady-state surface tension increases dramatically. For instance for 1-hexanol, when the concentration of the environment solution is 6mM and concentration of the drop solution is 25mM (Figure 8.9D), the time required to reach to the steady-state surface tension is 3000 second at 0 KPa, while it is 7000 second at 689 KPa. The time required reaching to 95% of the steady-state surface tension (t_{95}) is chosen to show how fast the surface tension reaches the steady-state value. Figures 8.20 -8.22 show that t_{95} increases with carbon dioxide pressure for all three systems. Thus, the time required reaching to the steady-state surface tension increases with carbon dioxide pressure. This trend can be observed in all different concentrations of the drop and environment solutions. This is due to the fact that the adsorption rate constants from the vapor phase (k^g_{a1}, k^g_{a2}) and the adsorption rate constants from the liquid phase (k^l_{a1}, k^l_{a2}) decreases with carbon dioxide pressure (Tables 8.10-8.12). According to Figures 8.20 -8.22, t_{95} is zero when there is no concentration difference between drop and environment solutions because there is no driving force for molecular exchange across the interface. Figures 8.20 -8.22 also shows that t_{95} increases when the concentration difference between drop and environment solutions is increased. This may be due to the fact that at higher concentration difference, a larger number of molecules should be adsorbed/desorbed from/to the surface to reach to the steady-state condition.

8.6 Summary

This chapter reported the effect of carbon dioxide pressure on adsorption kinetics and surface tension of 1-octanol, 1-hexanol and 1-butanol aqueous solutions. Experiments were performed in a closed chamber where the effect of adsorption/desorption from both sides of the liquid/vapor interface could be considered simultaneously. The experimental results showed that the steady-state surface tension of the surfactants (1-octanol, 1-hexanol and 1-butanol) aqueous solutions surrounded by carbon dioxide decreased linearly with carbon

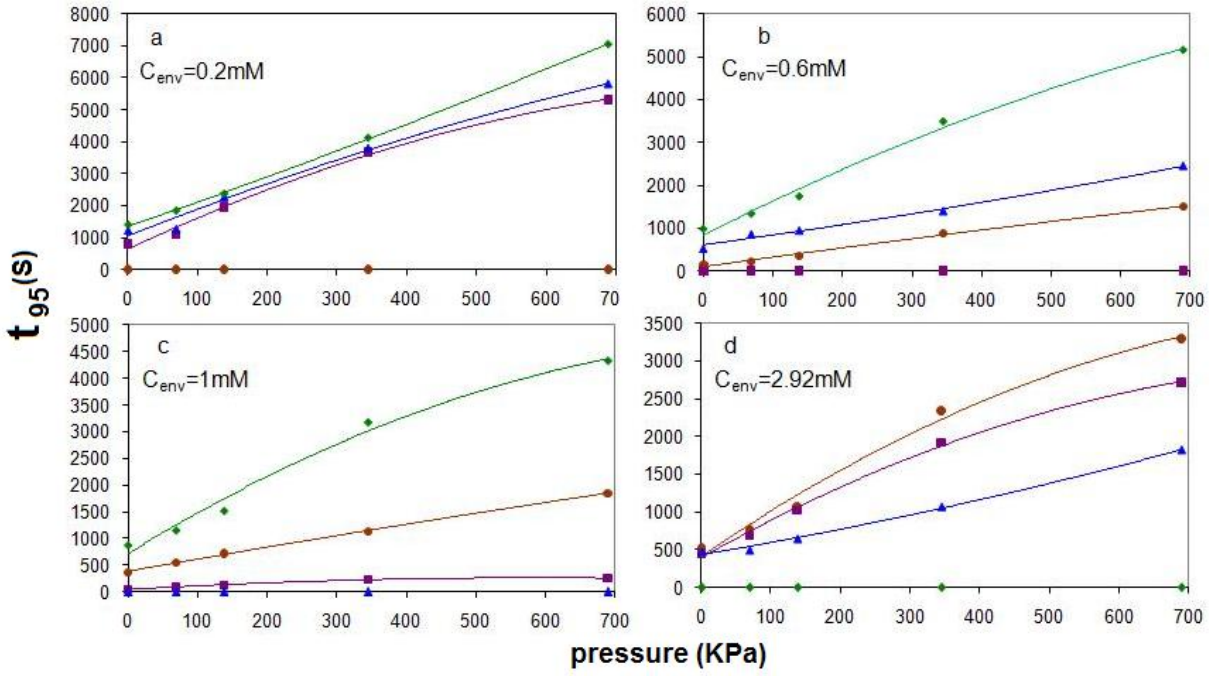

Figure 8.20: t_{95} versus carbon dioxide pressure for 1-octanol aqueous solutions. Concentration of the environment solution is indicated in each graph. Experiments were performed at four different drop concentrations (C_{drop}): 0.2 mM (brown circle), 0.6 mM (purple square), 1 mM (blue triangle), 2.92 mM (green diamond); Lines represent the best quadratic regression model to the experimental data.

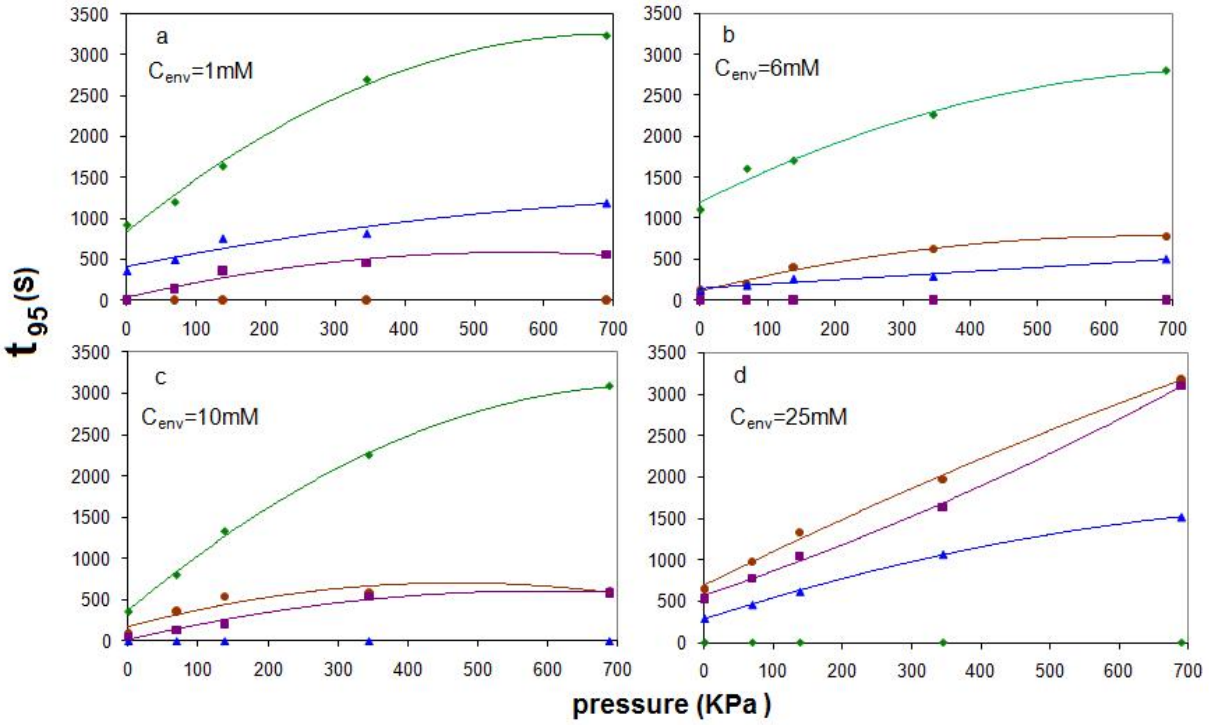

Figure 8.21: t_{95} versus carbon dioxide pressure for 1-hexanol aqueous solutions. Concentration of the environment solution is indicated in each graph. Experiments were performed at four different drop concentrations (C_{drop}): 2 mM (brown circle), 5 mM (purple square), 9 mM (blue triangle), 30 mM (green diamond); Lines represent the best quadratic regression model to the experimental data.

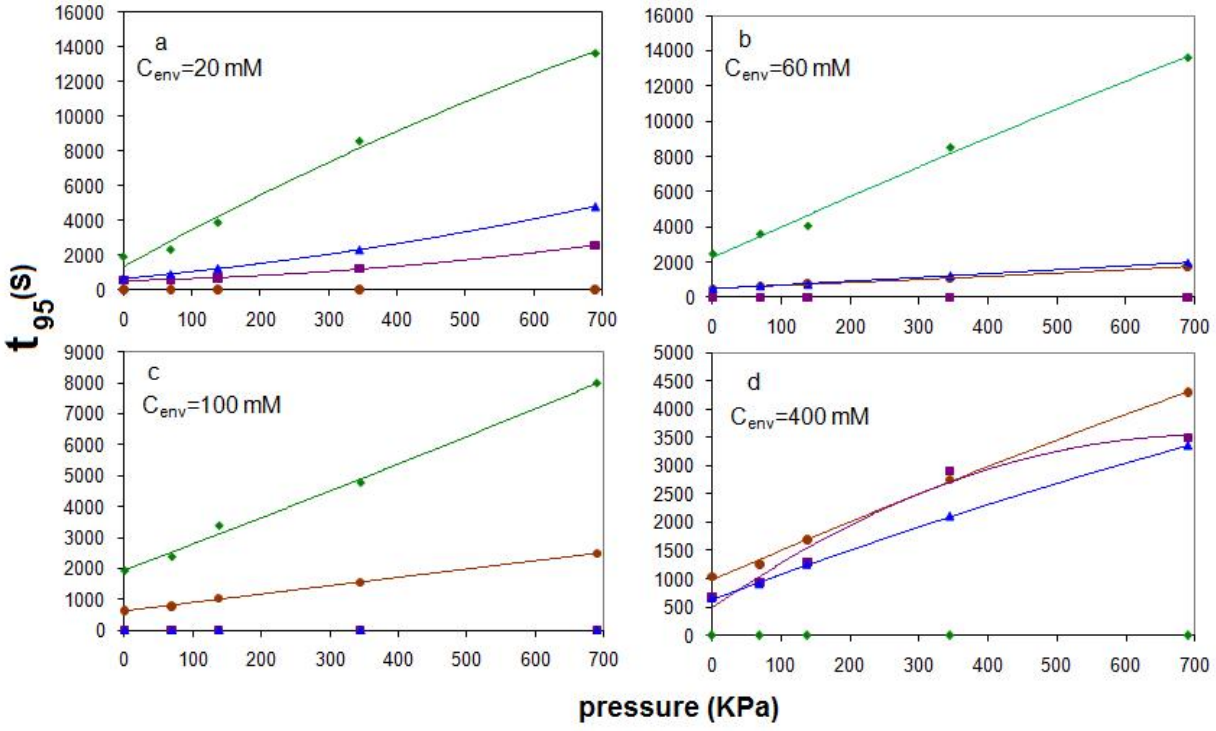

Figure 8.22: t_{95} versus carbon dioxide pressure for 1-butanol aqueous solutions. Concentration of the environment solution is indicated in each graph. Experiments were performed at four different drop concentrations (C_{drop}): 20 mM (brown circle), 60 mM(purple square), 100 mM (blue triangle), 400 mM (green diamond); Lines represent the best quadratic regression model to the experimental data.

dioxide pressure. The modified Langmuir equation of state was applied to correlate the steady-state surface tension of two systems: water surrounded by carbon dioxide and surfactant aqueous solutions. The fitting parameters including the equilibrium constant for carbon dioxide adsorption from the vapor and liquid phase (K_a) and the maximum surface concentration of carbon dioxide ($\Gamma_{\infty 1}$) were evaluated in a minimization procedure using the steady-state surface tension data of water surrounded by carbon dioxide. The fitting parameters for surfactants aqueous solutions including the equilibrium constant for adsorption from the vapor phase and liquid phase (K_3 and K_4) and the maximum surface concentration of the surfactants ($\Gamma_{\infty 2}$) were obtained from chapter 7. The results showed that the theoretical prediction of the steady-state surface tension obtained from modified Langmuir equation of state (based on the fitting parameters obtained from two systems: water surrounded by carbon dioxide and surfactants aqueous solutions) can satisfy the experimental results of surfactants aqueous solutions surrounded by carbon dioxide. It was shown that equilibrium constants from vapor phase were much greater than that from the liquid phase for carbon dioxide and three surfactants; hence the contribution to adsorption from the vapor side is more important than that from the liquid side. The experimental and modelling results showed that the effect of surfactant adsorption is much greater than that of carbon dioxide adsorption in the steady-state surface tension. In the dynamic simulation, the adsorption kinetics for 1-octanol, 1-hexanol and 1-butanol aqueous solutions surrounded by carbon dioxide was modelled using a kinetic transfer equation. The fitting parameters for this modelling were: The constant K_b, the kinetic rate constant for adsorption of carbon dioxide from the vapor phase (K^g_{a1}) and the kinetic rate constant for adsorption of surfactant from the vapor phase (K^g_{a2}). It was found that the adsorption rate constants ($K^g_{a1}, K^g_{a2}, K^l_{a1}$ and K^l_{a2}) decreased with carbon dioxide pressure. Thus, the time required to reach to the steady-state surface tension increased with carbon dioxide pressure. Because of the measurement and experimental errors or more likely due to limitations of the proposed model, some variations were observed in the values obtained for the fitting parameters (K^g_{a1} and K^g_{a2}). A major limitation of the model is due to large differences in adsorption/desorption between initial and final stages of the process, and a single set of property parameters cannot describe both initial and final states of the system. Variations may occur depending on which set of data, of initial or final states, is used in the model predictions over the entire time range.

Chapter 9

The Role of Carbon Chain Length in Adsorption Kinetics of Amphiphiles in Aqueous Solutions

The effect of carbon chain length on adsorption kinetics and surface tension of amphiphiles (1-octanol, 1-hexanol and 1-butanol) in aqueous solutions is studied in this chapter. The effect of carbon chain length in adsorption parameters including the equilibrium constant for adsorption from the vapor phase, the equilibrium constant for adsorption from the liquid phase, the adsorption rate constant for adsorption from the vapor phase, the adsorption rate constant for adsorption from the liquid phase and the maximum surface concentrations is investigated. All experiments and modelling (based on equations presented in chapters 7 and 8) are repeated for four concentrations of the drop solutions, four concentrations of the environment solutions, six temperatures and five carbon dioxide pressures.

9.1 Introduction

Amphiphiles in aqueous solution that possess a dual character (hydrophobic and hydrophilic) are employed in many chemical, pharmaceutical and biological applications [76, 77, 78, 79, 80]. An amphiphile molecule that includes a hydrophilic head and a hydrophobic tail can easily adsorb at a liquid/vapour interface to reach to the minimum free energy and hence the most thermodynamically stable state. Surface tension is a key parameter for understanding the behavior of an amphiphile (or a surfactant) in many physiological and industrial applications [81, 82, 83, 84, 85]. For example, surface tension of pulmonary surfactant that influences alveolar capillary shape and oxygenation, plays a vital rule in proper breathing [85]. In the foam industries, surface tension of a polymer

foam at the polymer/bubble interface is a key parameter in the efficiency of the foaming [86].

Effect of temperature and carbon dioxide pressure on the surface tension and adsorption kinetics of surfactants in aqueous solutions is an important factor affecting their applications [87, 88, 89, 72]. In chapter 7 and 8, we showed that temperature and carbon dioxide pressure have significant effect on the dynamic and steady-state surface tension of amphiphiles in aqueous solution. We showed that the equilibrium and kinetic rate constants could be affected by temperature and carbon dioxide pressures.

Carbon chain length of many chemicals in aqueous solutions can alter their surface behavior and hence their applications. Basketter et al. found a biphasic relationship between the skin sensitization potential and the bromoalkane carbon chain length [90]. It was also found that the toxicokinetics of perfluorocarboxylic acids was changed with carbon chain length [91]. M. F. Cox observed that the surface activity, viscosity, foaming and detergency abilities in a series of linear alcohol ether sulphates could be affected by changing the alkyl carbon chain length and ethylene oxide content [92]. It was shown that the thermodynamic properties including transition temperature, phase change enthalpies and heat capacities in the solid or liquid state of n-alkanes could be varied as a function of carbon chain length [93]. Flora et al. observed the importance of carbon chain length with regard to the hepatic effects associated with perfluoro-n-carboxylic acids [94]. In another research a series of individual fatty acids (caprylic, capric, lauric, myristic, palmitic, and steric acids) and their mixtures present in vegetable oils, namely, coconut oil, ground nut oil, olive oil, and soybean oil, were selected for esterification with methanol at different reaction temperatures. The esterification reactivity was found to be inversely proportional to alkyl chain length of the acid [95]. Grundke et al. found that the contact angle and surface tension of maleimide copolymers with two different backbones, poly(propene-alt-N-(n-alkyl)maleimides) (PAlkMI) and poly(styrene-alt-N-(n-alkyl) maleimides) (SAlkMI) could be changed with lengths of n-alkyl side chains (methyl, ethyl, propyl, butyl, pentyl, hexyl, octyl, and dodecyl) [96]. Hamdorf et al. realized that the surface tension and shear stress at the surface of polystyreneis was dependant on the chain length [97]. Surface tension studies of copper soap solution in benzene plus methanol mixture confirmed that CMC values decrease with increase in chain length of the soap anion [98]. Surface tension measurements for three ternary mixtures containing alkanes (hexane + cyclohexane + benzene, pentane + hexane + benzene and cyclohexane + heptane + toluene at 298K) revealed that the surface tension depend ultimately upon the chain length of the component of the mixtures [99]. Diaz et al. observed that an increase in the alkyl chain length of tetradecyl and octadecyl trimethyl ammonium bromide decreased the critical micelle concentration [100]. In another research, the foaming properties and dynamic surface tension of aqueous solutions of a series of sodium 2,4,5-trialkyl benzene sulfonates and sodium 2,5-dialkyl benzene sulfonates were determined. It was found that with increasing

the chain length, foam stability decreases [101].

In previous chapters, it was observed that when a volatile surfactant such as 1-octanol, 1-hexanol and 1-butanol was dissolved in water, it exerted a partial pressure in the vapor phase and the surface tension could be affected by adsorption/desorption from both sides of a vapour/liquid interface [72, 25, 59, 60, 61, 73]. The experimental results showed that the effect of adsorption from vapor phase is more important than that from liquid phase especially at the final steady-state condition [72, 25, 59, 60, 61, 73]. The unique approach and main objective of this chapter is to investigate the effect of carbon chain length on the dynamic and steady-state surface tension of 1-octanol, 1-hexanol and 1-butanol aqueous solutions. In addition, the effect of carbon chain length on the adsorption kinetics of these chemicals is also studied. These chemicals have many applications in perfume, wine and food industries [102, 103, 104]. In addition, the mixture of these chemicals and vegetable oils are used as an alternative to diesel fuel [105].

9.2 Experimental Section

9.2.1 Materials

The chemicals 1-octanol, 1-hexanol and 1-butanol with purity greater than 99%, were purchased from Sigma-Aldrich (Oakville, Ontario, Canada). The molecular weight, vapour pressure, water solubility and specific gravity of these chemicals were listed in chapter 3. Four different concentrations: 0.2, 0.6, 1 and 2.92 mM were prepared for 1-octanol aqueous solutions and four concentrations: 20, 60, 100, and 400 mM were prepared for 1-butanol aqueous solutions. For temperature experiments four concentrations: 2, 5, 9 and 30 mM were prepared for 1-hexanol aqueous solutions. For pressure experiments four different concentrations: 1, 6, 10 and 25 mM were prepared for 1-hexanol aqueous solutions. The sample with the highest concentration was prepared as the stock solution and lower concentration samples were made by diluting the stock solution. The relative humidity of the environment during the experiments was around 80%. The effect of carbon chain length on the dynamic and steady-state surface tension of the systems was investigated at six various temperatures (10, 15, 20, 25, 30 and 35C) and five different pressures of carbon dioxide (0, 69, 138, 354 and 689 KPa)

9.2.2 Apparatus and Procedure

Dynamic surface tension, 95% confidence interval of the surface tension, surface area and volume of the pendant drop were determined using the ADSA-P software as it was explained in chapter 3.

9.3 Theoretical Framework

The theoretical framework followed the same rationales and level of assumptions that was explained in chapters 7 and 8.

9.4 Results and Discussions

The dynamic and steady-state surface tension of 1-octanol, 1-hexanol and 1-butanol aqueous solutions were measured at six different temperatures and five different pressures of carbon dioxide. To ensure about the reproducibility of the data, each experiment repeated three times. The reproducibility test of the surface tension values showed that the results were reproducible with the 95% confidence intervals less than 0.2 mN/m. For each chemical, a total of 96 profiles were collected at different temperatures and 80 profiles at different carbon dioxide pressures. Experimental results were divided into four different categories based on the concentrations of the environment solution. The experimental results at different temperatures were illustrated in chapter 7. The experimental results at different pressures of carbon dioxide were presented in chapter 8.

9.4.1 Modelling Results

The modified Langmuir equations of state (presented in chapters 7 and 8) were applied for correlating the steady-state surface tension of 1-octanol 1-hexanol and 1-butanol aqueous solutions. For each chemical, the optimization routine was implemented in MATLAB, and the fitting parameters including the maximum surface concentration (Γ_∞), the equilibrium constant for adsorption from the vapor phase and the equilibrium constant for adsorption from the liquid phase were obtained by minimizing the residual sum of squares between the model prediction and the experimental data of the steady-state surface tension. The minimization procedure was repeated for six different temperatures and five different pressures. The values of fitting parameters for 1-octanol, 1-hexanol and 1-butanol at different temperatures were illustrated in Tables 7.1-7.3, respectively. For the effect of carbon dioxide pressure on the steady-state surface tension of our three systems, the modified Langmuir equation of state fitted to the experimental data and the fitting parameters, which are not dependant on the carbon dioxide pressures, were presented in Tables 8.2. The kinetic transfer equation was applied for modelling the dynamic surface tension of the three systems at all examined temperatures and carbon dioxide pressures. The fitting parameters for temperature effect of the three systems were presented in Tables 7.10-7.12. The fitting parameters for the effect of carbon dioxide pressure of the three systems were illustrated in Tables 8.9 -8.11.

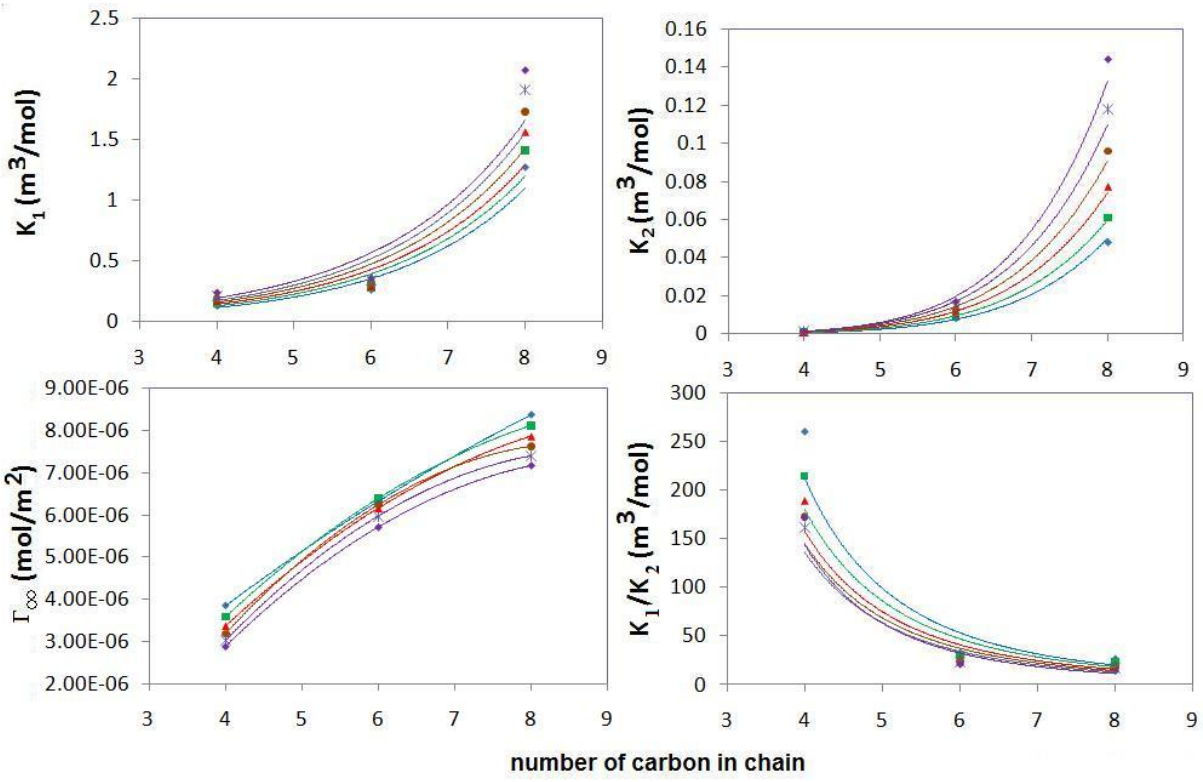

Figure 9.1: Effect of carbon chain length on the equilibrium constant for adsorption from the vapor phase (K_1), equilibrium constant for adsorption from the liquid phase (K_2), the maximum surface concentration (Γ_∞) and the ratio of K_1/K_2. Results presented at six different temperatures: 10 °C(blue diamond), 15 °C(green rectangle), 20 °C(red triangle), 25 °C(brown circle), 30 °C(blue star) and 35 °C(purple rectangle).

Carbon chain length of the surfactants in aqueous solutions can change their surface tension and hence the adsorption parameters. Figures 9.1 shows the effect of carbon chain length in the equilibrium constant for adsorption from the vapor phase (K_1), the equilibrium constant for adsorption from the liquid phase (K_2), the maximum surface concentration (Γ_∞) and the ratio of K_1/K_2 obtained from fitting the experimental data of steady-state surface tension into the modified Langmuir equation of state.

Figure 9.1 shows that the equilibrium constants from vapor phase and liquid phase (K_1 and K_2) increase with carbon chain length from 1-butanol to 1-octanol. Figure 9.1 show that the equilibrium constants also increase with temperature from 10 °C to 35 °C. Results show that the effect of carbon chain length in equilibrium constants is much more important than the effect of temperature. These results show that the tendency of surfactant

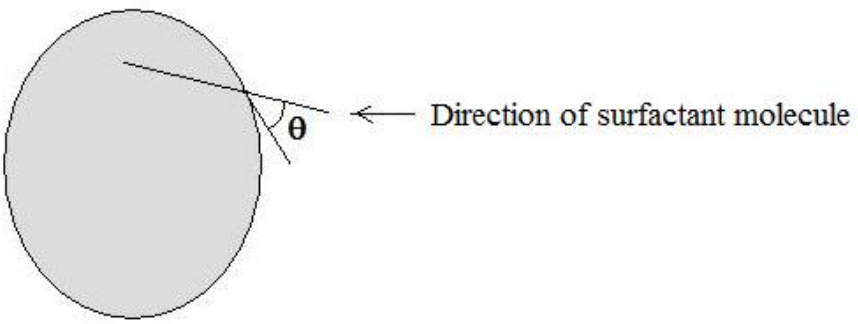

Figure 9.2: Direction of surfactant molecules at vapor/liquid interface

molecules to adsorb at the interface from both sides of a vapor/liquid interface increases with carbon chain length from 1-butanol to 1-octanol. Figure 9.1 shows that the maximum surface concentration (Γ_∞) increases with carbon chain length. However, one may expect that the maximum surface concentration, which is proportional to the inverse of the area occupied by the surfactant molecules at the vapor/liquid interface, would decrease with carbon chain length. This unexpected result may be due to the value of the angle Θ ($0^\circ \leq \Theta \leq 90^\circ$) between the direction of surfactant molecules at the surface and the plane of vapor/liquid interface (Figure 9.2). Angle Θ is zero when surfactant molecules lay down the surface, and angle Θ is 90° if surfactant molecules are perpendicular to the surface. The values of maximum surface concentrations (Γ_∞) for 1-octanol, 1-hexanol and 1-butanol support the idea that the angle Θ increases as the number of carbon in the carbon chain of this group of surfactants is increased. As expected, results show that the maximum surface concentration (Γ_∞) decreased with temperature at temperature ranging from 10 to 35 °C.

Figure 9.1 also shows that the contribution to adsorption from vapor side is more important than that of liquid phase ($K_1/K_2 >> 1$). The ratio of equilibrium constant from vapor phase to equilibrium constant from liquid phase (K_1/K_2) shows a decrease with carbon chain length. The modelling results showed that this ratio declined from 260 to 26 as the chain length was increased from 1-butanol to 1-octanol. This result supports our previous discussion that the effect of adsorption from vapor side is more important than that of liquid side, especially for short carbon chain alcohols [72, 25, 59, 60, 61, 73]. Previous results showed that this behavior was not quite observed for higher carbon chain length surfactants such as 1-decanol ($C_{10}H_{22}O$) [25]. The results showed that the steady-state surface tensions of 1-decanol for different drop concentrations with the same environment concentration were not exactly identical [25].

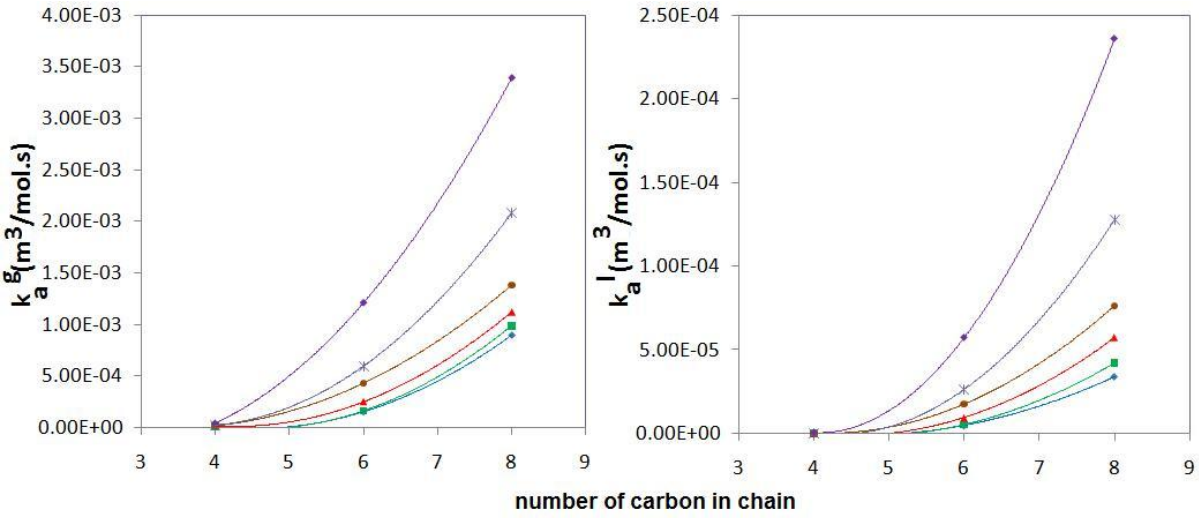

Figure 9.3: Effect of carbon chain length and temperature on adsorption rate constant from vapor phase (k_a^g) and adsorption rate constant from liquid phase (k_a^l). Results presented at six different temperatures: 10 °C(blue diamond), 15 °C(green rectangle), 20 °C(red triangle), 25 °C(brown circle), 30 °C(blue star) and 35 °C(purple rectangle).

Modelling results presented in chapter 8 showed that equilibrium constants for adsorption from vapor phase and liquid phase and also maximum surface concentration remained unchanged when carbon dioxide pressure was increased from 0 to 690 KPa.

Figures 9.3 shows that the effect of carbon chain length and temperature on the adsorption rate constants (k_a^g and k_a^l) obtained from fitting the experimental results of dynamic surface tension to the kinetic transfer equation (equation 7.14). Figures 9.4 shows that the effect of carbon chain length and carbon dioxide pressure on the adsorption rate constants (k_a^g and k_a^l) obtained from fitting the experimental results of dynamic surface tension to the kinetic transfer equation (equation 8.39 and the two solutions of equations 8.44 and 8.45).

Tables 7.10-7.12, 8.9-8.11 and Figures 9.3 and 9.4 show that the adsorption rates constants from vapor phase and liquid phase increase with carbon chain length from 1-butanol to 1-octanol. Results show that the adsorption rate constant from the vapor phase (k_a^g) is much greater than that from the liquid phase (k_a^l). Based on equations 7.7 and 7.8, this is the reason why equilibrium constant from the vapor phase is much greater than that from the liquid phase ($K_1 >> K_2$). Results also demonstrate that the rates of adsorption from both sides of vapor/liquid interface increase with temperature for temperature ranging from 10 °C to 35 °C, but the effect of carbon chain length on adsorption rates is

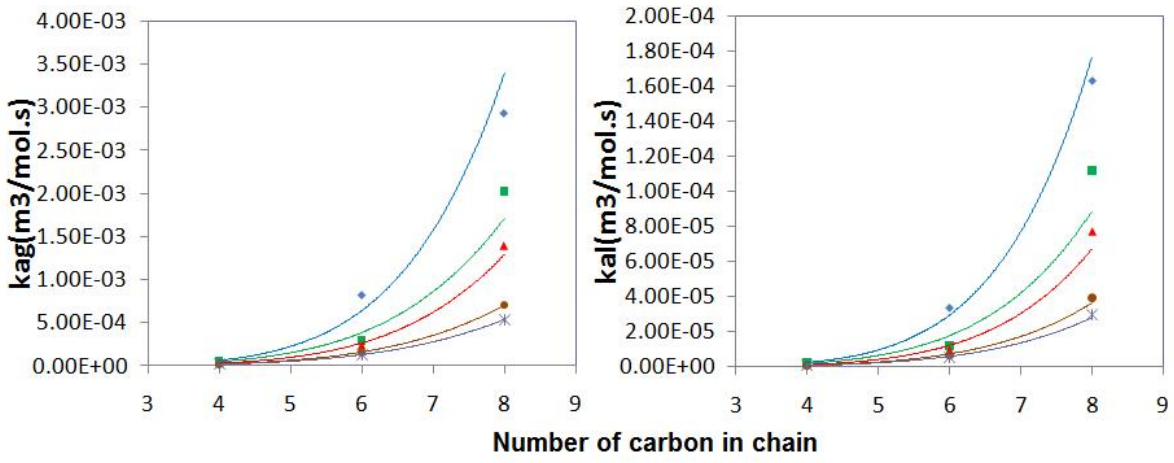

Figure 9.4: Effect of carbon chain length and carbon dioxide pressure on adsorption rate constant from vapor phase (k_a^g) and adsorption rate constant from liquid phase (k_a^l). Results presented at five different pressures: 0 KPa (blue diamond), 69 KPa (green rectangle) , 138 KPa (red triangle), 354 KPa (brown circle) and 689 KPa (blue star).

more important than the effect of temperature on that. Figure 9.4 show that the rates of adsorption from both sides of vapor/liquid interface decrease with carbon dioxide pressure for pressure ranging from 0 KPa to 690 KPa.

9.5 Summary

The role of carbon chain length on adsorption kinetics and surface tension of a group of short carbon chain surfactants (1-octanol, 1-hexanol and 1-butanol) was studied in this chapter. Experiments were performed at six temperatures and five carbon dioxide pressures. Using a designed sealed chamber, effect of adsorption/desorption from both sides of the liquid/vapor interface was considered simultaneously. The modified Langmuir equation of state was fitted to the experimental data of the steady-state surface tension. The effect of carbon chain length on the equilibrium constant for adsorption from the vapor phase, equilibrium constant for adsorption from the liquid phase and the maximum surface concentration was investigated. It was illustrated that the equilibrium constants for adsorption from both sides of a vapor/liquid interface increased with carbon chain length. It was shown that the ratio of K_1/K_2 is much larger than 1, hence the contribution to adsorption from the vapor side is much more important than that from the liquid side. The modelling results showed that this ratio declined from 260 to 26 as the chain length

was increased from 1-butanol to 1-octanol. Therefore, the contribution to adsorption from liquid phase augmented as the chain length was increased. The adsorption kinetics for this group of short carbon chain surfactants was modelled using a kinetic transfer equation. The modelling results showed that the adsorption rate constants from vapor phase and liquid phase (k_a^g and k_a^l) increased with carbon chain length. Steady-state and dynamic modelling also revealed that the maximum surface concentration increased with carbon chain length. This unexpected results may be related to the increased contact angle (Θ) between the carbon chain at the surface and the plane of vapor/liquid interface when the chain length is increased.

Chapter 10

Conclusions and Future work

This thesis represents a comprehensive study on surfactant adsorption and surface tension of slightly volatile, organic amphiphiles in aqueous solution. The research illustrates the influence of concentration, temperature, carbon dioxide pressure and carbon chain length on the interfacial properties of a liquid solution, particularly the surface tension. The simultaneous adsorption/desorption from both sides of a vapor/liquid interface is considered. The following sections highlight some of the main conclusions based on the experimental and theoretical approaches.

10.1 Conclusions

The Axisymmetric Drop Shape Analysis-Profile (ADSA-P) method was used to measure the dynamic surface tension of a number of organic amphiphiles in aqueous solution. The results showed that when 1-octanol, 1-hexanol or 1-butanol was dissolved in water, it presented a finite partial pressure in the vapor phase, and the surface tension of the solution could be affected by surfactant adsorption from both sides of the vapor/liquid interface.These results also showed that at the steady-state, the effect of adsorption from the vapor side is more important than that from the liquid side. These results for 1-octanol, 1-hexanol and 1-butanol were in stark contrast to the surface tension behavior of conventional surfactants such as aqueous octaethelene glycol monododecyl ether ($C_{12}E_8$) and aqueous Igepal CO-720 (Figure 4.4) [25].

The surface tension response of 1-octanol solutions to surface compression and expansion was investigated. The dynamic surface tension was measured under the condition where both liquid and vapor phase adsorption were present. In compression, the surface tension decreased followed by a gradual increase back to the value prior to compression. In expansion, two categories of surface tension response were observed: First, when the

change in surface area was smaller than 5%, the behavior similar to that of conventional surfactants was observed. The surface tension increased followed by a gradual decrease back to the value prior to expansion. Second, when the changes in surface area was greater than 5%, and the drop concentration was sufficiently larger than the environment concentration. In this case, the surface tension initially slightly increased; after a time delay, it sharply decreased, which followed by a gradual increase back to the value prior to expansion. For this second category, using the Buckingham Π theorem, a dimensionless parameter for predicting the surface tension response to changes in surface area was derived and the regression model for time delay versus dimensionless parameter F was fitted to the experimental data.

The effect of six different factors such as: concentration of the environment solution (Factor A), concentration of the sample drop solution (Factor B), the volume of the environment solution (Factor C), the distance between the drop and the environment solution (Factor D), the area of the environment solution (Factor E), and the saturation time (Factor F) was investigated on the steady-state surface tension of 1-octanol aqueous solutions. Using an experimental design, it was found that only concentration of the environment solution (Factor A) had significant effect on the steady-state surface tension of 1-octanol aqueous solution. This result was supported by Analysis of variance and normal probability plot. No unusual structure was observed in the residual plots, which proved that the experimental results were reliable and only concentration of the environment solution had significant effect on the steady-state surface tension of 1-octanol aqueous solutions.

The experimental results showed that the steady-state surface tension decreased linearly with temperature for all three chemicals at different concentrations of the drop and environment solutions and at temperature ranging from 10 °C to 35 °C. It was shown that $K_1 \gg K_2$ and hence the contribution to adsorption from the vapor side was more important than that from the liquid side. This behavior was much more important in the short chain alcohol (1-butanol) than that of the long chain alcohol (1-octanol). It was found that the contribution to adsorption from both sides of the vapor/liquid interface increased with temperature. The contribution to adsorption from vapor phase and liquid phase showed an increase with chain length from 1-butanol to 1-octanol. Furthermore, the adsorption kinetics for 1-octanol, 1-hexanol and 1-butanol was modelled using a kinetic transfer equation. Results showed that the rate constants for adsorption from both sides of the vapor/liquid interface increased with temperature in all three systems of 1-octanol, 1-hexanol and 1-butanol. The modelling results also showed that the rate constant for adsorption from the vapor phase increased when the chain length was increased from 1-butanol to 1-octanol.

The experimental results showed that the steady-state surface tension of the surfactants (1-octanol, 1-hexanol and 1-butanol) aqueous solutions surrounded by carbon dioxide decreased linearly with carbon dioxide pressure. The modified Langmuir equation of state

was applied to correlate the steady-state surface tension of two systems: water surrounded by carbon dioxide and surfactant aqueous solutions. The fitting parameters including the equilibrium constant for carbon dioxide adsorption from the vapor and liquid phase (K_a) and the maximum surface concentration of carbon dioxide ($\Gamma_{\infty 1}$) were evaluated in a minimization procedure using the steady-state surface tension data of water surrounded by carbon dioxide. The fitting parameters for surfactants aqueous solutions including the equilibrium constant for adsorption from the vapor phase and liquid phase (K_3 and K_4) and the maximum surface concentration of the surfactants ($\Gamma_{\infty 2}$) were obtained from chapter 7. The results showed that the theoretical prediction of the steady-state surface tension obtained from modified Langmuir equation of state (based on the fitting parameters obtained from two systems: water surrounded by carbon dioxide and surfactants aqueous solutions) can satisfy the experimental results of surfactants aqueous solutions surrounded by carbon dioxide. It was shown that equilibrium constants from vapor phase were much greater than that from the liquid phase for carbon dioxide and three surfactants; hence the contribution to adsorption from the vapor side is more important than that from the liquid side. The experimental and modelling results showed that the effect of surfactant adsorption is much greater than that of carbon dioxide adsorption in the steady-state surface tension. In the dynamic simulation, the adsorption kinetics for 1-octanol, 1-hexanol and 1-butanol aqueous solutions surrounded by carbon dioxide was modelled using a kinetic transfer equation. The fitting parameters for this modelling were: The constant K_b, the kinetic rate constant for adsorption of carbon dioxide from the vapor phase (k^g_{a1}) and the kinetic rate constant for adsorption of surfactant from the vapor phase (k^g_{a2}). It was found that the adsorption rate constants ($k^g_{a1}, k^g_{a2}, k^l_{a1}$ and k^l_{a2}) decreased with carbon dioxide pressure. Thus, the time required to reach to the steady-state surface tension increased with carbon dioxide pressure.

It was illustrated that the equilibrium constants for adsorption from both sides of a vapor/liquid interface increased with carbon chain length. It was shown that the ratio of K_1/K_2 was much larger than 1, hence the contribution to adsorption from the vapor side was much more important than that from the liquid side. The modelling results showed that this ratio declined from 260 to 26 as the chain length was increased from 1-butanol to 1-octanol. Therefore, the contribution to adsorption from liquid phase augmented as the chain length was increased. The adsorption kinetics for this group of short carbon chain surfactants was modelled using a kinetic transfer equation. The modelling results showed that the adsorption rate constants from vapor phase and liquid phase (k^g_a and k^l_a) increased with carbon chain length. Steady-state and dynamic modelling also revealed that the maximum surface concentration increased with carbon chain length. This unexpected results may be related to the increased contact angle (Θ) between the carbon chain at the surface and the plane of vapor/liquid interface when the chain length is increased.

Because of the measurement and experimental errors or more likely due to limitations

of the proposed model, some variations were observed in the values obtained for the fitting parameters of the dynamic modelling. These discrepancies may be due to the measurement and experimental errors or due to the restrictions of the model used. The measurement errors can be related to temperature and pressure instabilities, variations of surface area and volume of the drop during the experiments, the occurrence of impurities, and loss of surfactant due to vapor leakage that may alter the experimental results. The restriction of the model is that the adsorption parameters are changed during the adsorption process and they may have different values at various steps of the adsorption process. Discrepancies would occur depending on different time intervals in the experimental results and different set of experimental results (based on different time required to reach to the steady-state condition) is used in the model predictions over the entire time range.

10.2 Recommendations for Future Work

The following are some recommendations for future work based on the results and conclusions of the current research.

a. The surfactants studied in this thesis are all similar in structure (i.e., linear hydrocarbon chain with a polar group attached at the first carbon position). Thus, it would be of interest to investigate other volatile organic amphiphiles with different structures. Some possible suggestions may include: components with multiple polar groups, polar group displaced towards the interior of the hydrocarbon chain, branched chain amphiphiles as opposed to linear, and amphiphiles with other polar groups.

b. Surface tension study of amphiphiles aqueous solutions under the pressure of different gasses such as nitrogen, helium, hydrogen, carbon monoxide and argon is suggested. This study can reveal a possible relation between the gasses molecular structure and their competitions with surfactant molecules for adsorption at vapor/liquid interface.

c. Additional surface characterization techniques should be used to further the understanding of this unique phenomenon. Although this research represents a significant advance in surface science research, there are still many questions remaining. Exploring different experimental techniques may shed some light on these areas of interest. A technique such as Infrared Reflection Adsorption Spectroscopy (IRRAS), or Horizontal Neutron Reflectometry could be utilized to help characterize the structure, orientation, and composition of surfactant at the interface. This information would vastly develop the understanding of the behavior of the surfactants at the interface and possibly confirm or disprove the energy barrier hypothesis as an explanation to the diminish of molecular exchange from the liquid phase at steady-state conditions.

d. The equilibrium adsorption isotherm, the modified Langmuir equation of state and the modified kinetic transfer equation should be improved to account for molecular inter-

actions between surfactant molecules at the interface. It has been reported that alcohol molecules exhibit a cooperative effect for adsorption especially at high surfactant concentrations due to intermolecular attraction. The cohesive forces among the adsorbed molecules strengthen the energy barrier for desorption into the bulk and thus, decreases the rate of desorption. Including an activation energy-type concept which incorporates the effect of increasing surface concentration on the net rate of adsorption at the interface may modify the equations and improve the accuracy of the model predictions. It is possible that some of the discrepancies between the experimental results and the theoretical predictions (from the adsorption isotherm, the modified Langmuir equation of state or the modified transfer equation) may be caused by the failure to account for such interactions.

e. The limitation of the dynamic model is the variation in the fitting parameters. An obvious limitation is that material properties and their corresponding constants or fitting parameters are varying with time. Thus, these parameters may have different values between the initial and the final stages of the experiment. Discrepancies would occur depending on which set of data points is used in the model predictions over the entire time range. Improvements may be made when incorporating the varying nature of these fitting parameters. The kinetic transfer equation should be modified considering the varying nature of the adsorption rate constants.

f. The dynamic surface tension model should be improved to allow for the simulation of mixed diffusion/transfer-controlled adsorption. Although in this research a new kinetic transfer equation was developed and solved independently to model transfer-controlled adsorption, it may also be coupled with the diffusion equation to describe mixed control systems. This requires the simultaneous solution of the diffusion equation to describe the transport of molecules from the bulk to the subsurface, and the transfer equation to describe the adsorption/desorption step. This improvement would greatly increase the applicability of the model. However, it would also significantly enhance the complexity and require the knowledge of additional surfactant properties such as the vapor and liquid phase diffusion coefficients. Possible applications of the advanced model would include alcohols and other similar amphiphiles with longer carbon chains where diffusion effects become more important.

Bibliography

[1] Franklin, B. *Philos. Trans. R. Soc.* **1774**, 64, 445. 1

[2] Rayleigh L. *Proc. R. Soc.* **1890**, 47,364. 1

[3] Langmuir, I. J. *American Chem. Soc.* **1917**, 39,1848. 1

[4] Hong, Y.; Pritzker, M. D.; Legg, R. L.; Chen P. *Colloids and Surfaces B: Biointerfaces* **2005**, 46, 152. 1

[5] Hyder, M. N.; Huang R. Y. M.; Chen, P. *J. of Membranes Sci.* **2006**, 283, 281. 1

[6] Scatena, L. F.; Brown, M. G.; Richmond, G. L. *Science* **2001**, 292, 908. 1

[7] Serrano, A. G.; Perez-Gill, J. *Chem. Phys. Lipids* **2006**, 141(1-2), 105. 1

[8] Young, P. S.; Hannemann, R. E.; Franses, E. I. *Colloids and Surfaces B (Biointerfaces)* **1999**, 15 (3-4), 325. 1

[9] Neumann, A. W.; Good, R. J.; Stromberg, R. R. *Experimental Methods in Surface and Colloid Science* **1979**, 11, 31. 1

[10] Adamson, A. D.; Gast, A. P. *Physical Chemistry of Surfaces, 6 ed.* **1997**, New York, N Y, John Wiley Sons Inc. 1, 15

[11] Chattoraj, D. K.; Birdi, K. S. *Adsorption and the Gibbs Surface Excess, 1ed.* **1984**, New York, N Y, Plenum Press. 1, 10

[12] MacLeaod, C. A.; Radke, C. *Phys. Chem.* **1985**, 89(6), 1027. 1

[13] Hommelen, J. R. *Colloid Sci.* **1959**, 14(4), 385. 1, 35

[14] Bleys, G.; Joos, P. *J. Phys. Chem.* **1985**, 89(6), 1027. 1, 2, 15, 50

[15] Chang, C. H.; Franses, E. I. *J. Colloids Surf.* **1992**, 69(2-3), 189. 1

[16] Chang, C. H.; Franses, E. I. *Chem. Eng. Sci.* **1994**, 49(3), 313. 1

[17] Fainerman, V. B.; Miller, R. *J. Colloid Interface Sci.* **1996**, 178(1), 168. 1, 23

[18] Kuffner, R. J. *J. Colloid Sci.* **1961**, 16(5), 497. 1

[19] Lin, S. Y.; lu, T. L.; Hwang, W. B. *Langmuir* **1995**, 11(2), 555. 1

[20] Lin, S. Y.; McKeigue, K.; Maldarelli, C. *Langmuir* **1991**, 7(6), 1055. 1

[21] Lin, S. Y.; Wang, W. J.; Hsu, C. T. *Langmuir* **1997**, 13(23), 6211. 1

[22] Miller, R.; Lunkenheimer, K. *Colloid Polym. Sci.* **1986**, 264(4), 357. 1

[23] Chang, C. H.; Franses, E. I. *J. Colloids Surf. A* **1995**, 100, 1. 1, 12, 14, 68, 133

[24] Eastoe, J.; Dalton, J. S. *Adv. Colloid Interface Sci.* **2000**, 85,103. 1, 12, 14

[25] Prpich, A. M.; Biswas, M. E.; Chen, P. *J. Phys. Chem. C* **2008**, 112(7), 2522. 2, 13, 14, 51, 107, 112, 139, 151, 154, 158

[26] Lyon, R. C.; McComb, J. A.; Schreurs, J.; Goldstein, D. B. *J. Pharmacol Exp. Ther.* **1981**, 218(3), 669. 2

[27] Guazzaroni, M. E.; Teran, W.; Zhang, X.; Gallegos, M. T.; Ramos, J. L. *J. of Bacteriology* **2004**, 2921, 10, 186. 2, 51, 52, 107

[28] Donaldson, G.C.; Seemungal, T.; Jeffries, D.J.; Wedzicha, J. A. *ERS Journals Ltd.* **1999**. 2, 51

[29] Phongikaroon, S.; Hoffmaster, R.; Judd, K. P.; Smith, G. B.; Handler, R. A. *J. Chem. Eng. Data* **2005**, 50, 1602. 2, 51, 106

[30] Romero, C. M.; Jimnez, E.; Surez, F. *J. Chem. Thermodynamics* **2009**, 41, 513. 2, 51

[31] Sathiyagnanam, A. P.; Saravanan, C. G.; Gopalakrishnan, M. *Proceedings of the World Congress on Engineering 2010 Vol II WCE 2010* **June 30-July 2, 2010**, London, U. K. 2, 51

[32] Joos, P.; Serrien, G. *J. Colloid Interface Sci.* **1989**, 127, 97. 2, 50

[33] Guggenheim, E. A.; Adam, N. K. *Proc. R. Soc. A* **1933**, 139, 231. 11

[34] Gibbs, J. W.; *The Collected Works of J.W. Gibbs* **1931**, 1, New York, N Y, Longmans, Green. 12

[35] Guggenheim, E. A.; Adam, N. K. *Proc. R. Soc. A* **1933**, 139, 231. 11

[36] Castellan, G. W. *Physical Chemistry. 3 ed.* **1983**, Menlo Park, CA: Benjamin/ Cummings, Inc. 13, 14

[37] Biswas, M. E. *Ph.D. Thesis in Chemical Engineering* **2005**, University of Waterloo, Waterloo, ON. 15, 54

[38] Mysels, K. J. *Colloids Surf.* **1990**, 43 (2-3), 241. 15, 19

[39] Harkins, W. D.; Brown, F. E. *J. Am. Chem. Soc.* **1919**, 41, 499. 20

[40] Ambrose, D.; Ghiassee, N. B. *The Journal of Chemical Thermodynamics* **1987**, 19 (5), 505. 22

[41] Munday, E. B.; Mullins, J. C.; Edie, D. D. *J. Chem. Eng. Data* **1980**, 25 (3), 191. 22

[42] Nasirzadeh, K.; Neueder, R.; Kunz, W. *J. Chem. Eng. Data* **2006**, 51 (1), 7. 22

[43] Steele, W. V.; Chirico, R. D.; Knipmeyer, S. E.; Nguyen, A.; Smith, N. K.; Tasker, I. R. *J. Chem. Eng. Data* **1996**, 41 (6), 1269. 22

[44] Abraham, M. H.; Le, J. *J. Pharm. Sci.* **1999**, 88 (9), 868. 22

[45] Yaws, C. L.; Hopper, J. R.; Sheth, S. D.; Han, M.; Pike, R. W. *Waste Management* **1998**, 17 (8), 541. 22

[46] Padday, J. F.; In: Matijevic (ed.) *Surface and Colloid Science* **1968**, Wiley, New York, 1, 101. 23, 52

[47] Jennings Jr., J. W.; Pallas, N. R. *Langmuir* **1999**, 4, 959. 23, 52

[48] Lahooti, S.; del Rio, Cheng, P.; Neumann, A. W.; Spelt, J. K. (Eds.) *Applied Surface Thermodynamics* **1996**, Marcel Dekker Inc., New York, 1, 441. 23, 52

[49] Neumann, A. W.; Spelt, J. K. *Applied Surface Thermodynamics. Surfactant Science Series* **1996**, Marcel Dekker, Inc., New York, 63. 23

[50] Rotenberg, Y.; Boruvka, L.; Neumann, A. W. *Colloid Interface Sci.* **1983**, 93 (1), 169. 23

[51] Gao, J.; Jorgenson, W. L. *J. Phys. Chem.* **1988**, 92, 5813. 36

[52] Matsumoto, M.; Kataoka, Y. *J. Che. Phys.* **1993**, 98, 1464. 36

[53] Tarek, M.; Tobias, D. J.; Klein, M. L. *J. Chem. Soc., Faraday Trans.* **1996**, 92, 559. 36

[54] Tarek, M.; Bandyopadhyay , S. J.; Klein, M. L. *J. of Mol. Liq.* **1998**, 78, 1. 36

[55] Sokhan, V. P.; Tidesley, D. J. *Faraday Discuss* **1959**, 104, 193. 36

[56] Wilson, M. A.; Pohorille, A. *J. Phys. Chem. B* **1997**, 101 (16), 3130. 36

[57] Debolt, S. E.; Kollman, P. A. *J. Am. Chem. Soc.* **1995**, 117 (19), 5316. 36

[58] Montgomery, D. C.; Runger, G. C. *Applied Statistics and Probability for Engineers, 3rd ed.* **2003**, Arizona State University, John Wiley Sons, Inc. 42

[59] Prpich, A. M.; Sheng, Y.; Wang, W.; Biswas, M. E.; Chen, P. *PLoS ONE* **2009**, 4 (12), e8281. 51, 107, 139, 151, 154

[60] Firooz, A.; Chen, P. *Engineering Letter* **2008**, 16:4, EL-16-4-15. 51, 107, 139, 151, 154

[61] Firooz, A.; Chen, P. *IAENG Transactions on Engineering Technologies, American Institute of Physics* **2009**, 2, 50. 51, 107, 139, 151, 154

[62] Scott, R. P. W.; Kucera, P. *J. Chromatogr.* **1997**, 171, 37. 68

[63] Massoudi, R.; King, Jr. A. D. *The Journal of Physical Chemistry* **1974**, 78, 22. 106

[64] Massoudi, R.; King, Jr. A. D. *The Journal of Physical Chemistry* **1975**, 79, 16. 106, 107

[65] Jho, C.; Nealon, D.; Shogbola, S.; King, Jr. A. D. *Journal of Colloid and Interface Science* **1978**, 65, 1. 106, 107

[66] Escobedo, J.; Mansoori, G. A. *AIChE Journal* **1998**, 44, 10. 106

[67] Dittmar, D.; Fredenhagen, A.; Oei, S. B.; Eggers, R. *Chemical Engineering Science* **2003**, 58, 1223. 106

[68] Jayant, K.; Kofke, D. A. *Langmuir* **2005**, 21, 4218. 106, 107

[69] Kvamme, B.; Kuznetsova, T; Hebach, A.; Oberhof, A.; Lunde, E. *Computational Materials Science* **2007**, 38, 506. 106

[70] Seifried, B.; Temelli, F. *J. of Supercritical Fluids* **2010**, 52, 203. 107

[71] Georgiadis, A.; Llovell, F.; Bismarcka, A.; Blasb, F. J.; Galindoa, A.; Maitlanda, G. C.; Truslera, J. P. M.; Jacksona,G. *J. of Supercritical Fluids* **2010**, 55, 743. 107

[72] Firooz, A.; Chen, P. *Langmuir* **2011**, la-2010-040932. 107, 139, 150, 151, 154

[73] Firooz, A.; Chen, P. *Langmuir* **2011**, la-2011-01102v (submitted). 151, 154

[74] Del Rio O.J.; Neumann, A.W. *J. Colloid Interface Sci.* **1997**, 196 (2), 136.

[75] Prpich, A.M. *Master Thesis in Chemical Engineering* **2005**, University of Waterloo: Waterloo, ON. 30, 112

[76] Ojha, B.; Das, G. *Chemistry and Physics of Lipids* **2011**, 164, 144. 149

[77] Schwarz, G.; Bodenthin, Y.; Tomkowicz, Z.; Haase, W.; Geue,T.; Kohlbrecher, J.; Pietsch, U.; Kurth. D. G. *J. Am. Chem. Soc.* **2011**, 133, 547. 149

[78] Angeloni, N. L.; Bond, C. W.; Tang, Y.; Harrington, D. A.; Zhang, S.; Stupp, S. I.; McKenna, K. E.; Podlasek, C. A. *J. Am. Chem. Soc.* **2011**, 32, 1091. 149

[79] Kong, M.; Chen, X.; Park, H. *Carbohydrate Polymers* **2011**, 83, 462. 149

[80] Alexandru, M.; Cazacu, M.; Racles, C.; Grigoras *Polymer Eng. Sci.* **2011**, 51,78. 149

[81] Zhangshui, G.; Xufeng, N.; Liang, Zhenhua, L.; Zhiquan, S. *Chin. J. Chem.* **2010**, 28, 2049. 149

[82] Talanquer, V.; Oxtoby, D. W. J. *J. Chem. Phys.* **2003**, 118(28), 872. 149

[83] Bangham, A. D. *Nature* **1992**, 359, 110. 149

[84] Cui, Z. G.; Canselier, J. P. *Colloid Polym Sci* **2001**, 279, 259. 149

[85] Ikegami, M.; Weaver, T. E.; Grant, S. N.; Whitsett, J. A. *American J. of Respiratory Cell and Molecular Biology* **2009**, 41, 433. 149

[86] Tao, L.; Dachao, L.; Ling, Z.; Weikang, Y. *Particuology* **2010**, 8(6), 607. 150

[87] Domanska,U.; Krolikowska, M. *J. of Colloid and Interface Science* **2010**, 348, 661. 150

[88] Tariqa, M.; Serrob, A. P.; Matab, J. L.; Saramagob, B.; Esperanc J.M.S.S.; Lopesa, J. N. C.; Rebeloa, L.P. N. *Fluid Phase Equilibria* **2010**, 294, 131. 150

[89] Aqra, F.; Ayyad, A. *Materials Letters* **2010**, 65, 760. 150

[90] Basketter, D. A.; Lea, L. J.; Dickens, A.; Briggs, D.; Pate, I.; Dearman, R. J.; and Kimber, I. *J. Appl. Toxicol.* **1999**, 19(4), 261. 150

[91] Ohmori, K.; Kudo N.; Katayama, K.; Kawashima, Y. *Toxicology* **2003**, 184, 135. 150

[92] Cox, M. F. *JAOCS* **1989**, 66 (11), 1637. 150

[93] Briard, A. J.; Bouroukba, M.; Petitjean, D.; Dirand, M. *J. Chem. Eng. Data* **2003**, 48, 1508. 150

[94] Flora, C. M. G.; Reo, N. V. *Chem. Res. Toxicol.* **1996**, 9, 689. 150

[95] Srilatha, K.; Lingaiah, N.; Sai Prasad, P. S.; Prabhavathi Devi,B. L. A.; Prasad, R. B. N.; Venkateswar, S. *Ind. Eng. Chem. Res.* **2009**, 48, 10816. 150

[96] Grundke, K.; Zschoche, S.; Schel, K. P.; T. Gietzelt, T.; Michel, S.; Friedel,P.; Jehnichen, D.; Neumann, A. W. *Macromolecules* **2001**, 34, 6768. 150

[97] Hamdorf, M.; Johannsmann, D. J. *J. Chem. Phys.* **2000**, 112 (9), 4262. 150

[98] Mehta, V. P.; Talesara, P. R.; Gangwal A.; Bhutra, R. *Indian J. of Chemistry Section A-Inorganic Bio-Inorganic physical, Theoretical and Analytical Chemistry* **2002**, 41 (6), 1173. 150

[99] Panday, J. D.; Soni, N.K.; Sanguri, V.; Singh, V.K. *Physics and Chemistry of Liquids* **2001**, 39 (5), 763. 150

[100] Diaz, D. G.; Navaza, J M.; Sanjurjo, B. *J. Chem. Eng. Data* **2007**, 52, 2091. 150

[101] Wang, X.C.; Zhang, L.; Gong, Q.T.; Wang, L.; Zhang, L.; Li, Z.Q.; Zhao, S.; Yu, J.Y. *Chem. J. of Chinese Univ.* **2007**, 28 (11), 2118. 151

[102] Comuzzo, P.; Tat, L.; Fenzi, D.; Brotto, L.; Battistutta, F.; Zironi, R. *Food Chemistry* **2011**, 127(2) , 473. 2, 51, 151

[103] Magalhaes, K. T.; Dragone, G; Pereira, G. V. D.; Oliveira, J. M. ; Domingues, L. ; Teixeira, J. A.; Silva, J. B. A. E.; Schwan, R. F. *Food Chemistry* **2011**, 126(1), 249. 2, 51, 151

[104] Li, Y. H.; Wang, S. B.; Chang, L. P. *China Surfactant Detergent Cosmetics* **2007**, 37(2), 102. 2, 51, 151

[105] Laza, T.; Bereczky, A. *Fuel* **2011**, 90(2), 803. 2, 51, 151